Spectral and chemical characterization of hydrous sulphate-phyllosilicate association and banded iron formation in India: Probable implications for Mars

A thesis submitted
in partial fulfillment for the degree of

Doctor of Philosophy

by

MAHIMA SINGH

Department of Earth and Space Sciences
INDIAN INSTITUTE OF SPACE SCIENCE AND TECHNOLOGY
Thiruvananthapuram - 695547

June 2017

to my family and friends

CERTIFICATE

This is to certify that the thesis titled **Spectral and chemical characterization of hydrous sulphate-phyllosilicate association and banded iron formation in India: Probable implications for Mars**, submitted by **Mahima Singh**, to the Indian Institute of Space Science and Technology, Thiruvananthapuram, for the award of the degree of **Doctor of Philosophy**, is a *bona fide* record of the research work done by her under my supervision. The contents of this thesis, in full or in parts, have not been submitted to any other Institute or University for the award of any degree or diploma.

Dr. Rajesh VJ
Supervisor
Department of Earth and Space Sciences
IIST Trivandrum

Place: Thiruvananthapuram
June 2017
.

Counter signature of Head
Department of Earth and Space Sciences
with seal

DECLARATION

I declare that this thesis titled **Spectral and chemical characterization of hydrous sulphate-phyllosilicate association and banded iron formation in India: Probable implications for Mars** submitted in partial fulfillment of the Degree of Doctor of Philosophy is a record of original work carried out by me under the supervision of **Dr. Rajesh VJ**, and has not formed the basis for the award of any degree, diploma, associateship, fellowship or other titles in this or any other Institution or University of higher learning. In keeping with the ethical practice in reporting scientific information, due acknowledgements have been made wherever the findings of others have been cited.

Mahima Singh
SC12D007

Place: Thiruvananthapuram
June 2017

ACKNOWLEDGEMENTS

This work was carried out during 2012-2016 at Department of Earth and Space Sciences, Indian Institute of Space Science and Technology, Trivandrum, Kerala, India.

I am eager to thank many individuals for their help, guidance, and support throughout my PhD tenure. Firstly, I owe my deepest gratitude to my supervisor **Dr. Rajesh VJ** for providing me with the opportunity to get involved with such enthusiastic research, for support, motivation and many fruitful discussions over the years. I thank my doctoral committee members: Prof. Chandrasekar A., Dr. Anandmayee Tej, Dr. Prakash Chauhan, Dr. Sajeev Krishnan, Prof. S.N. Kumar, Dr. Gnanappazham L. and Dr. Prabhakaran K. for their insightful discussions which have immensely improved the quality of work over the time. Dr. Subramaniam's guidance for field work in Cauvery basin, and Velu Murugan and Banavath Suman's assistance during the fieldwork in Karai, Kunnam and Odiyam in the year-2013 are much appreciated. I thank to all who helped me during the acquisition of the analytical component of the work. I thank Dr. Sajeev Krishnan, Dr. Gnanappazham L. and Dr. Prabhakaran K. for providing their respective labs and other facilities to carry out the work efficiently. I thank Dr. Sajinkumar for the guidance in acquisition and analysis of the X-ray diffractometer data. Thanks also to Dr. Nandakumar V. for providing National Facility for Geofluids Research and Raman Analysis lab to work in and Jayanthi JL for her guidance with the use of the Micro-thermometry instrument and analysis. I also gratefully acknowledge the lab facilities provided under the guidance of Dr. Rajeev R. in Vikram Sarabhai Space Centre, Kerala, India. Thanks goes also to Ms. Nirmala Jain for her assistance during MRO-CRISM data analysis which allowed

me to work directly on the Martian surface. I thank anonymous reviewers and editorial board members of the journals for their helpful feedback and criticizing comments on the manuscripts to enhance the quality of presentation. I also gratefully acknowledge the financial support received from IIST-PhD Fellowship.

I am forever indebted to my parents- Mr. Nanhey Lal Verma and Mrs. Vijay Kumari, sisters- Garima and Neelima, and brother- Satish for their untiring support and encouragement. Without their prayers, this achievement couldn't have come true. I am blessed with a wonderful friend L.K. Srivastava, thanks to him for sacrificing his time to energize and cheer me on. Thanks especially to my friends Ruchi, Rahul, Arkan, Thejashree and Sam.

Mahima Singh

ABSTRACT

Earth records the prevalent features generated by geological, chemical and biological processes of nature. These processes involve the natural agencies of Earth's atmosphere, particularly water, ice and wind. The geomorphology of planetary bodies is controlled mainly by the atmospheric agents prevailing on surface/subsurface condition; Mars' geomorphology today is the result of stormy winds. Geological features generated by direct involvement of water are well established on Mars' surface, like sedimentary structures: flow channels/gullies, cross bedding, mud cracks etc. Water related activities are involving the occurrence of life on Earth, hence speculations generated to search for the extinct life on Mars knowing the fact that today's atmosphere is not habitable for life-activity. Our understanding about Mars is based on the results obtained from orbital spectroscopy, visual imagery, laser altimetry and of-course meteorites hailed from Mars. Much is known about the habitable sedimentary settings on Earth, inferring this knowledge to analogous counterparts on Mars must be crucial.

Three potential terrestrial sedimentary settings considering their established nature of habitability for life, are selected for the research and have been investigated for mineralogy with sophisticated instrumentation. First, gypsum-phyllosilicate association of Karai Formation, Cauvery Basin, Tamil Nadu, India which is deposited through precipitation from low temperature fluids in fractures developed due to fluid overpressure in phyllosilicate rich ground mass. Second, banded iron formations (BIFs) of Odisha, Singhbhum craton, India, which are chemically precipitated units in marine conditions and possesses huge extent over the surface. Third, jarosite deposit of Warkalli Formation, India, which is found in association with kaolinite in coastal cliff

setting, is formed in locally existing acidic conditions. These mineral assemblages possess signatures of life which is a well established fact in terrestrial environments. VNIR reflectance spectroscopy, X-ray diffraction (XRD), laser Raman and Fourier Transform Infra-red (FTIR) techniques are used for the characterization of mineralogy after systematic sampling from the sites. Spectrally, Karai Formation samples are identified as gypsum and kaolinite, and similar results have been obtained from other analytical techniques. Banded iron formations are spectrally identified as hematite with characteristic absorption bands due to Fe; silica is not identifiable in the EMR range used for the study. Varkala samples show primarily the composition of jarosite and kaolinite with reflectance spectroscopy; but the XRD analysis detected natro-jarosite, jarosite, kaolinite, hematite, pyrite etc. in the samples. VNIR reflectance spectroscopic results are compared with the spectral responses of the same minerals from Mars. Based on the comparative mineralogical results, *Homestake* (Cape York), layered hematite deposit (Meridiani Planum) and jarosite (Mawrth Vallis) from Mars are proposed as mineralogical analogues to gypsum deposits of Karai Shale Formation, banded iron formations of Oidsha and jarosite deposit of Warkalli Formation respectively. *Homestake* is proposed to be analyzed in future Mars missions for palaeo-climate estimation as it may contain ancient waters in the form of fluid-inclusions with which water-chemistry and related palaeo-environment could be established, and for evidences of astrobiology in the form of remnants of microbial colonies which might have preserved within the gypsum (if life has ever existed on the planet).

Keywords:

Gypsum, banded iron formations, mineralogy, natro-jarosite, reflectance spectroscopy, X-ray diffraction, water-chemistry, Mars

TABLE OF CONTENTS

LIST OF TABLES

LIST OF FIGURES

CHAPTER 1

Introduction and Literature Review

1.1 Introduction and research objectives

Planetary geosciences have gained significant importance in science for providing theoretical to analytical tools, and laboratory reference data to support the geomorphologic to mineralogic results obtained from different inter-planetary missions. The on-going development in the field enables us to provide better understanding about the origin and evolution of planetary surfaces. Earth has been extensively explored and successfully concluded from the view point of geology by the end of the 20^{th} century (Faure and Mensing, 2007). The very next move after exploring the Earth was to look through the space around the earth, of the Moon and Mars, where the scientists have shown their interest earlier for human colonization etc.. This leads to development of Space Technology, which resulted into the development of orbiters present around the potential planets and rovers moving on the surface of the planets like Mars, today.

Mars has always been the centre of interest as far as life activity is concerned elsewhere in the solar system from very ancient times, and thus being explored extensively with several orbiters and rovers by running and future-planned missions to answer the question related to any life-evidence on the planet. Needless to say about the confirmation of the presence of liquid water on the surface of Mars during the Noachian and early Hesperian time (4.5 to 3 Ga), which is the key to host life on a planetary surface (McKay and Stoker, 1989; McKay et al., 1998; Jakosky and Shock, 1998; Horneck and Baumstark-Khan, 2002). Surface soils are interpreted to be negative for the occurrence of

any life signature, but being a hydrous planet evidences for past life activity could be explored in the least-weathered geologic settings such as banded iron formations (BIFs) and crystalline gypsum if present (Mazur et al., 1978; Parnell et al., 2004). Layered hematite deposits has already been traced on Mars' surface using Odyssey Thermal Emission Imaging System (THEMIS), Mars Global Surveyor Thermal Emission Spectrometer (MGS-TES), Mars Orbiter Laser Altimeter (MOLA) and Mars Orbiter Camera (MOC) data (Christensen et al., 2004) with the evidences to be formed in standing water. Therefore, there are speculations for banded iron formation (BIFs) deposits on Mars' surface on regional scale, which could potentially be used for further exploration in future missions to locate any preserved signature indicating past life as it provides first life signature on Earth. Today, we are limited to the orbital spectroscopic data with coarser spatial and spectral resolutions preventing us to identify silica deposits in hematite rich regions on Mars. With this constraint, it will be of much use if we could provide with the data of additional more sensitive spectroscopic techniques to check for the mineralogical variations, which will help in locating the habitable entities on Mars. Gypsum and Fe/Mg phyllosilicates are identified on Mars' surface extensively, and gypsum is mainly found in Meridiani Planum (Squyres et al., 2004a), Juventae chasma (Gendrin et al., 2005), Olympia Undae sand sea in North Polar region (Fishbaugh et al., 2007) and Endeavour crater (Squyres et al., 2012). The probable mechanisms for the formation of gypsum and Fe/Mg phyllosilicates have also been discussed in detail: *Homestake* hydrous sulphate vein in Endeavour crater, Cape-York, Mars has been proposed to be formed by the movement of sulphate rich fluids in the fractures of the host rock (Squyres et al., 2012); gypsum in Olympia Undae sand sea in north polar region of Mars has been proposed to be formed as a result of evaporation and or by direct alteration of high Ca sand dune grains, Fe-rich pyroxene and sulphide (Fishbaugh et al., 2007); and the sulphate salts, underlained by the material of middle to late Noachian (Reider et al., 2004; Squyres et al., 2004a) in Meridiani Planum are hypothesized to be formed by evaporation of fluids involved with weathering of

basalts (Tosca et al., 2005). In terrestrial scenario, gypsum is one of the most promising candidates to preserve fluid inclusions with which water chemistry could be determined and is also one of the potential targets to be looked for preserved microbial activity due to its semi-transparent character which allows the light to pass through it, and enrichment of nutrients. Jarosite, a potassium iron hydrous sulphate is a key mineral indicating aqueous, acidic and oxidizing conditions on Earth (Bigham and Nordstrom, 2000) and has been detected in Eagle crater (Klingelhofer et al., 2004) and Meridiani Planum (Squyres and Knoll, 2005) by using the Mossbauer spectrometer data aboard Mars Exploration Rover (MER) *Opportunity*, and Mawrth Vallis by using MRO-CRISM data (Farrand et al., 2009). Mineralogy of Mars' surface varies greatly and is influenced by subsurface mineralogy, temperature, pH, salinity, dissolved gases in fluid media mainly groundwater, and environmental conditions. Few terrestrial sites have been thoroughly investigated in terms of their mineralogy and ancient water chemistry: these sites are Haughton impact crater hydrothermal vein deposits, modern iron rich environments such as Rio Tinto to older ones such as BIFs and saline alkaline Pliocene-Pleistocene jarosite palaeolake deposits of Olduvai Gorge, Tanzania (Hay, 1973) etc.. Morris et al. (2010) has suggested warmer and wetter past of Mars which has direct influence on life activity. But Fairén et al. (2010) has given compelling evidences and argued that the temperature may not have been significantly warmer than today. Hence, in order to make most of the ground truth data available, we must look towards the terrestrial examples, mainly the mineralogy and environmental settings to develop the idea regarding the role of water in Martial crustal evolution and life signatures (if at all the planet hosted any living organism). This study takes a conservative approach and looks at the gypsum phyllosilicate association of Karai, Tiruchirapalli (Chapter 2), banded iron formations in Odisha (Chapter 3), and jarosite deposit of Warkalli Formation in Varkala (Chapter 4). The present study mainly focuses on geochemical and spectroscopic characterization of the mineral assemblages from the above-mentioned three research sites.

The objectives of this thesis are as follows:

1. To geologically characterize three potential terrestrial analogue sites namely, hydrous sulphate-phyllosilicate association of Tiruchirapalli, banded iron formations of Singhbhum craton, and jarosite deposit on Varkala Cliff;

2. To determine the mineralogy of the above-mentioned sites using Electron Probe Microanalysis (EPMA) and laboratory based X-ray diffraction (XRD);

3. To check for the deployment of modern spectroscopic techniques (VIS/NIR, laser Raman and Fourier transform infrared spectroscopy) and their advantages and disadvantages for mineralogy detection;

4. To analyze and classify the fluid inclusions in gypsum using Raman and micro-thermometric techniques; and

5. To implement the acquired information to locate or interpret the similar deposits on Mars.

1.2 Proxies selected for the present study

1.2.1 Gypsum-phyllosilicate association, Tiruchirapalli, Karai,Tamil Nadu

Cauvery basin, also known as a peri-cratonic rift basin formed all along the eastern continental margin of Peninsular India during the fragmentation of Gondwana supercontinent (Jafer, 1996; Biswas et al., 1992). It contains thick sedimentary sequence underlained by Archean granitic gneissic basement and these exposures are limited to 5 separate areas namely, Pondicherry, Vridhachalam, Ariyalur, Tanjore and Sivaganga (Banerji, 1972; Rangaraju et al., 1993).

Our area of interest lies in Ariyalur region, where mainly sedimentary rocks are exposed. Moreover, numerous studies are available in the area by a wide spectrum of geological research ranging from stratigraphy/biostratigraphy, sequence stratigraphy, palaeontology, geochemical to depositional history modeling (Ramanathan, 1968; Banerji, 1970, 1972; Sastry et al., 1972; Sastri et al., 1973; Jain, 1978; Sundaram and Rao, 1986; Ramasamy and Banerji, 1991; Govindan et al., 1996; Madhavaraju and Ramasamy, 2001; Sundaram et al., 2001; Nagendra et al., 2002; Madhavaraju et al., 2002, 2006, 2009; Nagendra et al., 2011). In literature, the sedimentary rocks of Ariyalur area are classified into three distinct groups namely, Uttatur, Trichinopoly (also denoted as Tiruchirapalli) and Ariyalur (Blanford, 1862). These groups have been further subdivided into Formations, and for the present study Uttatur Group is selected, which comprised of four Formations, namely Terani, Arogyapuram, Dalmiapuram and Karai (Sundaram et al., 2001). Terani, Arogyapuram and Dalmiapuram Formations were deposited during early Cretaceous, and Karai Shale Formation was deposited in late Cretaceous, late Albian to early Turonian period (Ramasamy and Banerji, 1991). Near Karai village, marine gypsiferous clay and thin limestone bands are exposed in mine cuttings. The colour of the gypsiferous clay is white to yellow and this change in colour is attributed to change in the provenance. Karai Shale Formation, comprised of two Members Odiyam sandy clay and gypsiferous clay members, is well exposed as badland (terrains where sedimentary rocks/clay rich exposures are heavily eroded by fluvial or eolian activity with high drainage density) in an easterly draining catchment to the East of Karai village in Tiruchirapalli (Ramkumar et al., 2004). Sundaram and Rao. (1986) have divided Karai Shale Formation into two Members based on a type area Odiyam and Kunnam. Odiyam Member constitutes gypsiferous mudstone with distinctive thin inter beds of pink shale and siltstone, and sporadic lenticular beds of coquinite and sandstone comprising the lower part of the Formation (Sundaram et al., 2001). In the upper part of the Formation, gypsum is present in the form of regular to irregular veins in ferruginous clay along with the sporadic and inter-layered

occurrences. Kunnam member constitutes inter layered mudstone, siltstone and fine-grained sandstone with calcite and siderite cements.

In recent studies, Nagendra et al. (2011) has carried out the paleobathymetry studies in the rock record of Ariyalur area where paleobathymetry trends have been reconstructed for Albian to Maastrichtian resulting into identification of four Transgressive-Regressive cycles. Additionally, correlation with global sea level curves (Vail et al., 1977; Haq et al., 1987; Miller et al., 2005) and relative sea level curves (Watkinson et al., 2007; Sundaram et al., 2001; Raju et al., 1993; Govindan, 1993; Ramanathan, 1977) has been made for Cauvery basin (Nagendra et al., 2011). He has also concluded that the maximum regressive surfaces define the sequence boundaries in the basin.

Ramkumar et al. (2011) has examined geochemical properties of the Cauvery Basin for testing the potential of chemostratigraphic modeling and the need for high-resolution stratigraphic setup. Extensive work has been done to define the presence of barren rock sequences, patchy occurrence of fossils and occurrence of exotic blocks (older rocks in younger sequences) which have thwarted successful stratigraphic correlation and exploration through conventional methods in the basin (Ramkumar, 2008a and b; Ramkumar et al., 2004). It has also been shown that conventional observation of geochemical profiles gives insights into major geological events in terms of detrital influx, basin starvation and changes in depositional pattern (Ramkumar et al., 2011).

1.2.2 Banded iron formation, Singhbhum craton, Odisha

The Singhbhum-Odisha craton forms a triangular crustal block, bounded by Chotanagpur gneissic complex to the North, Eastern Ghat Granulite belt to the South and the Bastar craton to the West and by recent alluvium to the East (Saha and Ray, 1984; Misra, 2006). This craton consists mainly of granitoid rocks, metasedimentary (Iron Ore Group), meta-volcanic schists and granites (Mahalik, 1987; Saha, 1994; Mazumder, 2005; Misra, 2006; Mukhopadhyay et

al., 2006). The BIFs of north Odisha are extensively developed supracrustals encircling the Singhbhum granite complex and various views have been proposed on the evolution of these supracrustals and their relation to the granite intrusives. Jones (1934), Dunn (1940) and Saha (1994) believed that all the BIFs were formed as a single assemblage during the Archean, underlained and/or intruded by the different phases of Singhbhum granites. According to Saha (1994), the age of BIFs could be between 3.3 and 3.1 Ga. Iyengar and Banerjee (1971), Banerji (1974, 1975) and Iyengar and Murthy (1982) classified BIFs into two distinct age Groups; Older (Gorumahisani group) and Younger (Noamundi group). Prasad Rao et al. (1964) and Acharya (1976, 1984) has categorized the BIFs into three distinct stratigraphic Formations, the oldest around Pallahara and Gorumahisani, the intermediate at Daitari and the youngest at the Joda-Koida region. The youngest one contains rich deposits of iron and manganese ores and forms a horse-shoe shaped synclinal structure (Jones, 1934). Relatively younger metasedimentary deposits of banded iron formations of Joda and Daitari region have two types of mineral assemblages: first, banded hematite jasper and second, banded hematite quartzite. These BIFs are conspicuous by the presence of alternate bands composed predominantly of iron oxide and silica. Secondary hematite formed after metamorphism, is generally found in the form of bladed crystals, specular variety called specularite whereas silica is of cryptocrystalline type, admixed with iron oxide dust and granules in jasper to mega quartz. The extensive volcano-sedimentary sequences in the Simlipal and Keonjhar plateaus are considered equivalent to the Dhanjoris and younger to BIFs by Saha and his associates (1994) while others (Prasad Rao et al., 1964; Iyengar and Banerjee, 1971; Banerji, 1974) found them sandwiched between BIFs. The extensive lava flows designated as Malangtoli Lava, occur between Malangtoli and Pallahara, and underlie the undeformed Kolhan sequence of the area (Saha, 1994). The age of volcanics and the volcano-sedimentary sequences in the North Odisha craton is early Proterozoic (Saha, 1994). The age of the sequence volcanic-BIF-ultramafic in Singhbhum craton is estimated to be 3.51 Ga (Mukhopadhyay

et al., 2008).

1.2.3 Jarosite deposit, Varkala, Kerala

Jarosite deposit, Warkalli Formation, Kerala belongs to the coastal cliff edging the Arabian Sea near Varkala, which is situated about 55 km north-west of Thiruvananthapuram - the capital of Kerala state, India. These coastal cliffs are the type area for the Warkalli Formation of Mio-Pliocene resting unconformably over the Precambrian crystallines of Kerala Khondalite Belt (KKB). Coastal cliffs of Varkala are mainly comprised of arkosic sand, kaolinitic sandy clay, carbonaceous clay and peat with plant remains (Desikachar, 1976). The whole Cenozoic sediments of Kerala was divided into four units from the oldest: Unit I comprises pebbly sands and sandy clays with black clay and lignite; Unit II comprises limestone with sand and clay; Unit III comprises arkosic sandy clay with lignite and IIIA comprises laterite, ferruginous sandstone and clay; and Unit IV comprises beach sand and alluvial clay (Nair and Rao, 1980). Jarosite shows the grainy occurrence onto the clayey base with basic replacement texture. Jarosite also occurs in carbonaceous clay layer as encrustations due to diagenetic replacement process and depicts a typical efflorescence texture. Jarosite in this part was first reported and identified as a natrojarosite (Tassel, 1965). This mineral is periodically washed away by waves during high tide and hence cannot be seen throughout the year. Carbonaceous clay which hosts jarosite is black organic-rich clay bed consisting of variable amounts of silt and poorly-sorted sands, and is partly iron oxide-coated.

1.3 Assessment of sulphate-sheet silicates minerals

1.3.1 Gypsum and associated phyllosilicate minerals

Gypsum is a crystalline white translucent, moderately water-soluble (∼2.0 – 2.5 g/l at 25^{o}C) (Bock, 1961) mineral of chemical composition calcium sulphate dihydrate ($CaSO_4.2H_2O$). Mainly it occurs in evaporitic geological setting (Sinha and Raymahashay, 2004; Vysotskiy et al., 2004) but its occurrence in hydrothermal setting (Martinez-Frias et al., 2004) is also well established. Because of its softness (1.5-2 on the Mohs' scale), gypsum is easily susceptible to physical weathering. It is the hydration product of anhydrite and has optimum properties to be used as a habitat by other microorganisms as it provides shelter, light-penetration capacity, nutrients, moisture, etc. It commonly precipitates in evaporitic conditions generally in arid regions (García-Ruiz et al., 2007). Eh-pH phase diagram of the Fe-S-Ca-Na-HCO_3-H_2O system at 298 ^{o}K as given by Elwood Madden et al. (2004) is shown to look for the stability field of gypsum (Fig 1.1). Karai Shale Formation, Tiruchirapalli contains gypsum as one of the hydrated sulphate in the form of veins along with the phyllosilicate rich ground mass mainly containing kaolinite, montmorillonite and illite. These minerals are well identified by reflectance spectroscopy, but the variation in phyllosilicate compositions is cleared by XRD results. Gypsum is precipitated in the fractures developed in phyllosilicate rich groundmass in the area.

Gypsum is detected on Mars within the Amazonian-aged North Polar Olympia Undae sand sea by the Observatoire pour le Mineralogie, l'Eau, les Glaces et l'Activité (OMEGA) on Mars Express (Langevin et al., 2005a and b). Apart from north polar deposit of gypsum, OMEGA team has also identified gypsum in the layered deposit of Juventae chasma (Gendrin et al., 2005). The

MER *Opportunity* rover has detected concretions of sulphate salts at Meridiani Planum, which are overlying middle to late Noachian material (Reider et al., 2004; Squyres et al., 2004a and b) and they are proposed to be formed by evaporation of fluids involved with weathering of basalts (Tosca and McLennan, 2006). The MER *Opportunity* rover has also detected sulphates within the Hesperian-aged Columbia Hills outcrops, at concentrations of up to 40 wt% (Ming et al., 2006). In orbital reflectance spectroscopy, gypsum is a mineral which could be identified with at least three H–O–H bending fundamentals in the 6 μm region (Cloutis et al., 2006), due to asymmetry in the H_2O site, and different bond length in H–O–H. (Hunt et al., 1971). A triplet combination and overtone between 1.4 and 1.6 μm is also characteristic of gypsum in 0.35-2.5 μm region (Cloutis et al., 2006). Gypsum is potential target for the preservation of ancient waters in the form of fluid inclusions in crystals defects or the cleavage planes to construct the palaeo-water chemistry. In addition, gypsum is also of interest in the search for evidence of life as it is capable of permineralizing microfossils (Schopf et al., 2012). Observations from OMEGA imaging spectrometer on board Mars Express spacecraft has proved diverse phyllosilicates and other aqueous alteration products (Poulet et al., 2005). These minerals are associated with the Noachian outcrops related to early active hydrological system and their formation is suggested in an early Noachian Mars climatic episode, which was followed by a more acidic environment responsible for the formation of sulphates on Mars (Poulet et al., 2005). Fe/Mg phyllosilicates are common in Mawrth Vallis (Bishop et al., 2008). In Mawrth Vallis, phyllosilicates belongs to smectite family and the minerals identified are montmorillonite (Al-OH smectites) and nontronite (Fe-OH smectites) (Poulet et al., 2005).

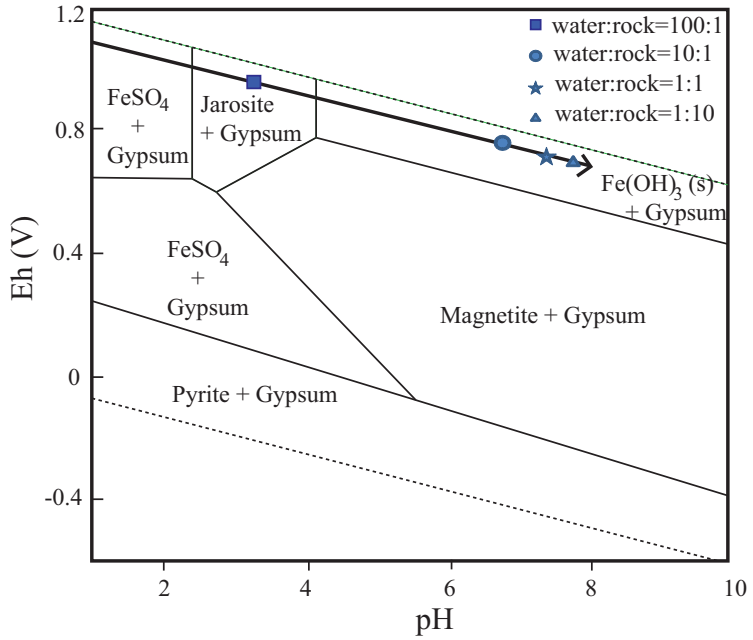

Figure 1.1: Eh-pH phase diagram of the Fe-S-Ca-Na-HCO_3-H_2O system at 298 ^oK (modified after Elwood Madden et al., 2004)

1.3.2 Jarosite and associated phyllosilicate minerals

Jarosite group of minerals with the general chemical formula $[AB_3(SO_4)_2(OH)_6$, where A represents K^+ and B represents Fe^{3+} for typical jarosite], are the key minerals indicating aqueous, acidic and oxidizing conditions on Earth (Bigham and Nordstrom, 2000). Jarosite is known to occur mainly in acid mine drainage. Alunite group has three main minerals jarosite ($KFe^{3+}3(SO_4)_2(OH)_6$), natrojarosite ($NaFe^{3+}$ $3(SO_4)_2(OH)_6$) and hydronium jarosite ($(H_3O)Fe^{3+}$ $3(SO_4)_2(OH)_6$) which could be distinguished by XRD analysis. All three minerals show extensive solid solution (Brophy and Sheridan, 1965; Basciano and Peterson, 2007). Jarosite and natrjarosite has been detected in the jarosite deposit of Kerala. Other minerals at jarosite deposit of Kerala include pyrite, quartz, feldspars, smectite and kaolinite. Jarosite require acidic environment for its formation which could be either generated in volcanic setting in the form of hot springs or caldera lakes with dissolved and oxidized gases including H_2S and SO_2 (Varekamp et al., 2000; Zolotov and Shock, 2005) or where iron-sulphide minerals are oxidized. The mineral also tells about the groundwater condi-

tions as it could be generated if groundwater circulate through Fe-sulphides at deeper level, and ejects out at the surface.

Jarosite is thermodynamically stable under the ranges of temperatures and pressures currently present on Mars (Navrotsky et al., 2005; Cloutis et al., 2008). Therefore, it might have preserved the palaeo-environment and any biological indicator in the form of chemistry or texture. Jarosite is reported from Meridiani Planum and Mawrth Vallis on Mars and has many strong absorption features to be identified from orbital spectroscopy. The absorptions at 2.26 and 2.46 μm, which are due to combinations of the overtones of OH stretching, adsorbed H_2O stretching and O–S–O bending fundamentals (Cloutis et al., 2006), are characteristic of mineral. Due to thermodynamic stability of jarosite on Mars, it does not show any change in absorption features (Navrotsky et al., 2005), which is generally shown by other minerals in the form of shifts by orbital spectroscopy adding to martian atmospheric conditions (Cloutis et al., 2008). Hence, laboratory spectra obtained with similar spectral and spatial resolutions can be directly compared with the reflectance spectra generated from the datasets such as CRISM.

1.4 Assessment of the oxide minerals

1.4.1 Hematite deposits in association with silica

Hematite iron(III) oxide (Fe_2O_3) crystallizes in trigonal system and have the same crystal structure as ilmenite and corundum (Dunlop and Ozdemir, 2001; Anthony et al., 2011). Hematite and ilmenite form a complete solid solution at temperature above 950^oC (Anthony et al., 2011). Hematite is found mainly as an alteration product in igneous, sedimentary and metamorphic rocks and most important hematite deposits are formed in sedimentary environments. Hematite is part of a complex solid solution oxyhydroxide system having wa-

ter, hydroxyl groups and vacancy substitutions that affects its magnetic and chemical properties (Dang et al., 1998). On Earth, huge deposits of hematite occur within the banded iron formations which are suggested to be precipitated from a column of stagnant water in the geological past. Goethite (FeO(OH)) is an iron bearing hydroxide mineral of diaspore group, crystallizes in orthorhombic system and mainly forms by the weathering/alteration of other iron rich minerals (Klein et al., 1993). Both of these minerals are widely identified in BIFs of Odisha and they are also reported from Mars in quite abundance.

Christensen et al. (2000) reported the presence of hematite-rich deposit on the surface in Meridiani Planum by using the data from the Thermal Emission Spectrometer (TES) boarded on the Mars Global Surveyor spacecraft. Deposits of crystalline gray hematite have been identified in thermal infrared mapping by Mars Global Surveyor-Thermal Emission Spectrometer (MGS-TES) on Mars; exposures at Martian surface are in Sinus Meridiani, Aram Chaos and some other locations throughout Valles Marineris (Christensen et al., 2001a). The mechanism of hematite formation is important as it may require involvement of water into the system making it a suitable candidate for the preservation of any evidence of past life on Mars (Newsom et al., 2003). Remains of microbes may have been preserved if life existed during or subsequent to hematite formation in aqueous or hydrothermal environments in Meridiani Planum (Newsom et al., 2003). Terrestrial evidences are available within banded iron formation deposits in the $\sim$2.0 Ga Gunflint iron formation where preservation of microbial communities has been documented within hematite (Barghoorn and Tyler, 1965; Tazaki et al., 1992; Allen et al., 2001) and these studies have reported coccoidal, filamentous, sheath-like bacterial remains and fossil extracellular polymeric substances (EPS).

Opaline silica deposits are found in association with volcanic materials on Mars as detected by *Spirit* rover.In some regions on Mars, the silica deposits are interpreted as coating on rocks (Kraft et al., 2003; Michalski et al., 2005) whereas results from *Opportunity* have shown that opaline silica could be

present within sulphate rich sedimentary rocks of Meridiani Planum (Glotch et al., 2006a). Silica deposits are indicative of hydrous activity in terrestrial scenario. Usually, opaline silica results as a consequence of high solubility of silica in aqueous systems under warm and alkaline conditions on Earth (Dove et al., 1994). High-purity opaline silica deposits on Mars, produced by hydrothermal processes could have led to locally habitable environments and are proposed to be a strong candidate for examination by future landed missions and one of the returned samples from Mars (Squyres et al., 2008).

1.5 Based on the selected proxies, earlier proposed analogue sites on Earth to Mars

1.5.1 Impact-generated hydrothermal sulphate deposits, Haughton impact structure, Canada

Impact craters, especially associated with hydrothermal systems are always of great importance in planetary exploration as they are the sites where primitive life could evolve (Farmer and Des Marais, 1999; Farmer, 2000; Newsom et al., 2001). Haughton impact crater of Miocene age, located in Devon Island, Canadian High Arctic, not only bears the evidences of former thermophilic life (Farmer & Des Marais, 1999) but also colonized cyanobacteria (Parnell et al., 2004). Sulphide, sulphate and carbonate mineralization is identified in the crater, formed through impact-induced hydrothermal activity (Osinski et al., 2001). Crystals of clearly grown gypsum in the form of selenite occurs in the veins and cavity fillings within the crater's impact melt breccia deposits (Osinski and Spray, 2003). Selenite is considered as a part of the hydrothermal assemblage because it is generated as a result of cooling of circulating hot waters formed during the impact (Parnell et al., 2004). Impact related selenite

at Haughton is having colonization of cyanobacteria and visible even to the naked eye (Cockell et al., 2002, 2003; Parnell et al., 2004). The selenite crystals are compact with local frayed margins and of high purity and transparency; microscopically the selenite contains rock detritus, newly precipitated gypsum, other authigenic (new) mineral growths and microbial colonies (Parnell et al., 2004). Cyanobacteria which have penetrated 5 cm within the crystal from the margin, mainly belongs to the species *Gloeocapsa alpine* and *Nostoc commune* along with some filamentous components resembling *Scytonema* (Parnell et al., 2004). Although, monophase fluid inclusions present within the gypsum are the possible sites from where the microbial colonies might have evolved but they do not contain microbes (Parnell et al., 2004). Haughton gypsum has also got the advantage of being covered with snow for most of the months in the year making microbes dormant for the period (Parnell et al., 2004). Abundant fluid inclusions in the Haughton gypsum represent a preserved record of the water from which the gypsum precipitated (Parnell et al., 2004). In an analogous occurrence on Mars, this ancient water could be extracted and used to determine palaeo-water chemistry (Parnell et al., 2004). The authigenic gypsum shows a close relationship with cyanobacteria and evidences suggest that cavities have developed around the colonies (Parnell et al., 2004). The colonies had made access to more nutrients by modifying the mineral host to get more space in a protected environment and by accreting moisture (Parnell et al., 2004). Minor authigenic calcite is also found associated with cleavage planes within the gypsum crystal which denotes that the incorporation of other components by moisture, helping to flourish the microbes (Parnell et al., 2004). It is also discussed that gypsum cannot supply a whole range of nutrients; the melt breccia host could have been the good source of ions to be used as food as it is altered and fine grained (Parnell et al., 2004). For instance, the cyanobacterial colonization of the quartzose Beacon Sandstone in Antarctica (Friedmann, 1982) is supplied with the nutrients from blown particles of volcanic rocks elsewhere in the region (Weed and Ackert, 1986; Nienow and Friedmann, 1993). Transparency of Haughton selenite crystal makes it a good

habitat for photosynthesis as visible light could penetrate to a depth of at least 15 cm in them (Hughes and Lawley, 2003; Parnell et al., 2004).

Elsewhere in the solar system, Mars (Cooper and Mustard, 2002) and Europa (Kargel et al., 2000; Carlson et al., 2002) are identified with major sulphate salt deposits on the surface whereas Earth is known for major surficial carbonate in the form of calcite surface precipitates (Riding, 2000). Photosynthesis is the optimum mechanism for harvesting the energy from stars by primitive life (Wald, 1974), therefore crystalline sulphates which support photosynthetic activity and preserve the evidences of microbial activity make themselves significant habitats to look for astrobiology (Rothschild, 1990; Cid and Casanova, 2001; Wentworth et al., 2002). Inferences have been made regarding the ancient biological signatures on the planets within the well crystallized gypsum if found (Parnell et al., 2004) and the sulphate-cemented beds make a comparison with the sulphate-bearing sandy beds encountered by *Opportunity* on Mars Exploration Rover (Moore, 2004).

1.5.2 Palaeo-lacustrine jarosite deposit, Olduvai Gorge, Tanzania

The sedimentary succession of Olduvai Gorge, deposited in a shallow, saline-alkaline palaeo-lake has much of its sediments like volcanic ash supplied from adjacent Ngorongoro Volcanic Highlands (Hay, 1976; McHenry, 2005, 2011). Trachytic, trachyandesitic, and phonolitic tephra deposited or preserved in the lake has got altered into the secondary minerals such as zeolites, jarosite and Fe/Mg smectites (McHenry, 2010). The mineral assemblage at Olduvai includes mainly zeolites (phillipsite-closed basin environments only when the pH reaches 9–10), authigenic K-feldspar and Fe/Mg smectite indicating saline-alkaline diagenetic conditions (Langella et al., 2001; McHenry, 2010). Jarosite is one of the secondary mineral found in altered tephra at some sites in the

saline-alkaline Pliocene-Pleistocene paleolake deposits of Olduvai Gorge, Tanzania (Hay, 1973). Presence of jarosite in a sedimentary system is an indication of aqueous, acidic, and oxidizing environment at the time of its formation (Stoffregen et al., 2000; Elwood Madden et al., 2004; Papike et al., 2006). Jarosite in association with alkaline Fe/Mg smectites is unexpected and the site represents the same association, for which the formation mechanism has been proposed through the interaction of modern ground and or meteoric water with oxidized palaeo-lacustrine pyrite generating local and temporary acidic conditions (Baldridge et al., 2009; McHenry et al., 2011). A comparative and comprehensive account of the results of the samples collected from the site using chemical analyses techniques: X-ray Diffraction (XRD), Mossbauer spectroscopy, Fourier Transform Infrared (FTIR), Electron Probe Microanalysis (EPMA), X-ray Fluorescence (XRF), and Scanning Electron Microscopy (SEM) is presented by McHenry et al. (2011). Occurrence of jarosite in association with Mg/Fe smectites is reported in Martian paleolakes such as Columbus crater, a potential paleolake in Terra Sirenum (Wray et al., 2009) and Mawrth Vallis (Farrand et al., 2009). There has always been discussion about the occurrence and preservation of abundant jarosite in relation to the past geological activities on Mars, as conditions must remain acidic or water-limited over time for its preservation which doesn't seem possible in an environment dominated by basaltic weathering, as this leads to alkaline conditions by neutralizing acidity (McHenry et al., 2011). Therefore, jarosite on Mars has been suggested a more recent phenomenon probably Amazonian (would not had withstand the pre-Amazonian environmental changes if formed in Noachian/Hesperian time) as it is sensitive to changes in pH, temperature, oxidation conditions, and water-availability (Fairén et al., 2009). Jarosite along with Fe/Mg smectite deposit at Olduvai Gorge formed in alkaline to neutral conditions could be considered positively to propose complex diagenetic histories for the Martian deposits with mixed Mg/Fe phyllosilicate and jarosite or other Mg, Fe sulphates in the regions like paleolake deposit at Columbus crater/Terra Sirenum (Wray et al., 2009) or Terra Meridiani (Poulet et al., 2008).

1.5.3 Rio-Tinto Mars analogue site

The Rio Tinto basin in southwestern Spain is proposed as analog to the Meridiani rocks because both the sites possess similar mineralogy and the processes involved in the mineral genesis with different physicochemical conditions (Fernandez-Remolar et al., 2005). Rio Tinto has the deposits of modern, Holocene to Plio-Pleistocene time, which gives the opportunity to be compared with Meridiani rocks where depositional and diagenetic processes has to be inferred from ancient sedimentary rocks (Fernandez-Remolar et al., 2005). Rio Tinto has the mineral assemblage of hematite, jarosite and goethite with comparable mineralogy from Meridiani Planum jarosite, hematite, and an unidentified iron-bearing phase (Klingelhofer et al., 2004). Regionally distributed hematite in Meridiani Planum inferred to have formed under aqueous conditions on the early Martian surface (Christensen et al., 2000, 2001a and b) and the findings of *Opportunity* suggested its formation through chemical weathering of precursors basaltic rocks within sulphate rich sediments and deposited as dunes and playa-like beds in interdune depressions (Rieder et al., 2004; Squyres et al., 2004a; McLennan et al., 2005). Outcrops of Meridiani Planum contains hematite and ferric sulphates suggesting diagenesis under strong water limited conditions (Elwood Madden et al., 2004; Tosca et al., 2005) unlike Rio Tinto.

From the biological perspective, Rio Tinto waters support diverse biota of prokaryotic and eukaryotic microorganisms, despite having low pH and high metal concentration (Lopez-Archilla et al., 2001; Amaral Zettler et al., 2002; Sabater et al., 2003; Gonzalez-Toril et al., 2003). Bio-signatures preserved in the sedimentary rocks, mainly in iron-oxide precipitates of Rio-Tinto include macroscopic textures of coated microbial streamers, surface blisters formed by biogenic gas, and microfossils preserved as casts and moulds in iron oxides (Gerdes et al., 2000). In conclusion, it has been suggested that the outcrops on Mars with similar chemical composition carry a similar potential to preserve a record of life (if it existed) and environment (Fernandez-Remolar et al., 2005).

1.5.4 Kansas Mars analogue site

Nippewalla Group of Permian age is dominated by mud sand-flats and eolian deposits with ephemeral lake evaporites including bedded halite, occur throughout (Holdoway, 1978; Benison and Goldstein, 2001) in the Permian of the North American midcontinent (Zambito and Benison, 2013). Nippewalla halite in the Amoco Rebecca K. Bounds (RKB) core from Greeley County, Kansas (Zambito et al., 2012) located near the Permian equator (Ziegler, 1990) is studied in detail and homogenization temperatures of fluid inclusions has been collected (Zambito and Benison, 2013). Homogenization temperature patterns through the Nippewalla Group suggest palaeoclimate trends and records extreme palaeoweather conditions in regional to local scales. In southwestern Kansas, these rocks are composed of bedded halite, bedded gypsum/anhydrite, and red shales and sandstones (Benison and Goldstein, 2001). However, due to higher solubility of halite, the surface is left with the outcrops composed only of bedded gypsum/anhydrite, red shales, and red sandstones (Benison, 1997). Many gypsum/anhydrite beds contain rounded, fine- to medium-sized sand grains, which likely originated as lake-grown gypsum crystals and were later reworked locally during desiccation, wind, and flooding events (Benison, 2006). Benison et al. (1998) have shown that the halite is precipitated from acid lake waters of unaltered primary fluid inclusions in halite in Nippewalla Group, by analyzing through laser Raman microprobe. The fluid inclusions are sulphate rich and some are highly acidic with pH range from 0 to 1 (Benison, 1997; Benison et al., 1998). Nippewalla Group outcrops shows that shallow ephemeral saline acid lakes surrounded by mud flats, sand flats, and sand dunes, existed in Kansas ca. 270 Ma (Benison and Goldstein, 2001). The excellent field exposures of the Nippewalla Group allow it to be compared with greater ease to the lithified Martian outcrops.

The *Opportunity* rover provided the first documentation of chemistry of surface waters on Mars (Bell et al., 2004; Christensen et al., 2004; Herkenhoff et al., 2004; Klingelhofer et al., 2004; Rieder et al., 2004; Squyres et al., 2004a and

b). Mars Exploration Rovers (MER) has provided data related to the aqueous activity (groundwater and ephemeral shallow surface waters) on Mars in the form of images of sedimentary structures like bedding, cross-bedding, ripple marks, mud cracks etc., diagenetic features like displacive evaporate crystal molds, hematite concretions in the Burns Formation at Meridiani Planum (Grotzinger et al., 2005; Herkenhoff et al., 2004; Kargel, 2004; Squyres et al., 2004b). Mineralogy of Meridiani Planum includes fine-grained siliciclastics, sulphate minerals, hematite, and some jarosite (Clark et al., 2005; Squyres et al., 2004a and b). Similar mineralogical assemblage is the criteria for the recognition of acid deposition in terrestrial scenario (Benison and Goldstein, 2002).

The comparison suggested between Martian strata especially Meridiani Planum and Nippewalla Group (Benison, 2006) is (1) both are capped by relatively thick strata with overlying thinner slope-forming beds, (2) mineralogically, both contain fine-grained siliciclastic and/or sulphate mineral grains coated by pervasive hematite, (3) dominant sedimentary structure is bedding, (4) mud cracks overlying current ripple marks indicating shallow surface waters, and (5) diagenetic features are preserved in the form of pervasive hematite coatings and cement, hematite concretions, and evidence of displacive sulphate crystals. Presence of crystal shaped vugs and their random orientation in Martian outcrops as well as Nippewalla Group suggest that saline groundwater once existed on Mars (Squyres et al., 2004b). Other significant similarity between the Nippewalla and Martian outcrops by Benison (2006) is the presence of Cl^- (Clark et al., 2005), and the lack of carbonate minerals. The difference between Nippewalla and Martian outcrops as shown by Benison (2006), is the composition of siliciclastic sediments which contain primarily quartz in Nippewalla whereas in Martian outcrops the composition may have been basaltic grains (Reider et al., 2004).

1.5.5 Banded iron formation Coppin Gap Green-stone Belt, Pilbara Craton

Banded iron formations (BIFs) are fine grained layered sedimentary rocks having alternate layers of iron-rich and silica-rich bands of varying thickness 10-100 μm, mostly of Archean and Proterozoic age. BIFs from the Coppin Gap Green-stone Belt, Pilbara Craton which belongs to Panorama Formation of Warra-woona Group in Australia is a fine grained, red and white laminated chert with the laminae thickness in the range of 0.5 to 2 cm (Bost et al., 2013). The weathered surface is composed of fine-grained goethite, hematite and other undefined nanometric iron oxides and the white layers consist of microcrystalline quartz (Bost et al., 2013). The sedimentary structures are found in the form of soft sediment deformation structures, stylolites, ghost-structure, Fe-stained fractures and fractured layering (Bost et al., 2013). It is evident from the literature that BIFs are formed in aqueous basin setting through the oxidation of reduced Fe introduced into the seawater mostly by hydrothermal fluids. The exact origin of BIFs, the mechanism involved in the oxidation of Fe (microbial?) and layering (seasonal/microbial?) even in terrestrial conditions is highly debatable (Posth et al., 2010). Presence of BIFs on Mars is not yet established, but their eventual presence can be hypothesized based on high Fe-content in Martian rocks (15-18 wt%) (McSween et al., 2009) and the detection of hydrothermal silica- rich deposits on Mars (Squyres et al., 2008; Ruff et al., 2011).

1.5.6 Potential bio-signatures in iron-rich extreme environments

Iron has played a major role in the biosphere. Rio Tinto ecosystem along with other iron-rich acidic environments is suggested to be the relics of an an-

cient iron world (Archean) (Amils et al., 2004, 2007) with the hypothesis that similar processes might have operated on other planetary systems like Mars (Fernandez-Remolar et al., 2004). Biomass of Tinto ecosystem is mostly located on the river-bed, the surface of the rock forming dense biofilms, composed mainly of filamentous algae, fungi and minor heterotrophic protists (Amils et al., 2007). The mineralogy established by MER mission in Meridiani Planum includes sulphates and iron oxides, which is comparable with the geomicrobiology existing at Rio-Tinto (Fernandez-Remolar et al., 2005). The iron formations in the Rio-Tinto correspond to a natural environment, not an industrially contaminated environment (Van Geen et al., 1997; Davis et al., 2000; Elbaz-Poulichet et al., 2001). Although, the actual conditions in which the Tinto ecosystem operates are different from the ones prevailed in the Archean, but the properties of isolated microorganisms allow the extrapolation in the ancient systems. Table 1.1 represents a comparative account of the characteristic properties of Rio-Tinto sediments/subsurface and Meridiani Planum, Mars as suggested by Orgel et al. (2014).

Iron rich terrestrial Mars analogue sites like Rio Tinto and endolithic cyanobacterial colonization of Beacon sandstone in Mars Oasis, Antarctica will definitely provide insights into the iron-rich surface and subsurface of Mars. The major feature in endolithic cyanobacterial colonization in Oasis, Antarctica is the depletion of iron from the colonization zone (Varnali and Edwards, 2013). Varnali and Edwards (2013) has shown that the Raman spectroscopic differentiation between the parent scytonemin and a possible iron scytonemin complex, that could be formed by cyanobacterial colonization in iron-rich geological environments, must be focused upon the spectral wavenumber region 1400–1800 cm^{-1}, wherein several of the major differences appear for discriminatory purposes.

Table 1.1: Comparison between salient properties of Meridiani Planum, Mars, and Rio Tinto (Orgel et al., 2014).

Meridiani Planum, Mars	Properties studied	Charateristic of Rio Tinto Mining Area on Earth	References
Arid, acidic, oxidizing Low, Present(?), Low (0.09%)	Environmental conditions (Temperature, Methane, Oxygen)	Arid, acidic, oxidizing annual rainfall: 100 mm, 10-40^{o}C, Present, 21%	Chevrier et al., 2007; Amils et al., 2007
Iron-oxides and hydroxides, Mg and Ca sulphates (e.g. jarosite, copiapite, schwertmannite, rozenite, gypsum, hematite, goethite, szomolnokite)	Surface composition	Iron oxides and oxy-hydroxides, complex Mg and Ca sulphates (e.g. jarosite, pyrite, copiapite, scwertmannite, halotrichite, goethite, hematite)	Fernandez-Remolar et al., 2005; Squyres et al., 2006; Amils et al., 2007; Chevrier et al., 2007
Groundwater	Water interaction	Groundwater, Rainfall	Fernandez-Remolar et al., 2005; Chevrier et al., 2007
?	Biological interaction		Squyres et al., 2006; Amils et al., 2007
Dominant grain size is finer than 0.3-0.8 mm, coarsest particles are larger than 1 mm	Surface grain size	Few 100 μm-few mm (dominant)	Grotzinger et al., 2005
Hypotheses (A) Alteration of sulphide rich rocks or basaltic ashes in situ in the presence of SO_2 (acid fog or acidic groundwater). (B) Leaching, transport and subsequent deposition in a shallow lake or sea followed by evaporation processes	Origin of minerals	Alteration of sulphide rich rocks in the presence of water and with the correspondence of microbiological activity. Some jarosite may also be related to primary hydrothermal activity	Fernandez-Remolar et al., 2005; Chevrier et al., 2007; Fairén et al., 2009; Martinez-Frías et al., 2004

1.5.7 Hydrothermal chert veins

Stratified silicified sediments of the Buck reef Chert (3.24 Ga), Kromberg Formation of the Onverwacht Group, Barberton Greenstone Belt, South Africa have been infiltrated parallel to the sediment layering by a hydrothermal chert vein (Bost et al., 2013). The infiltration occurred possibly during diagenetic or post diagenetic lithification of the sediments by silicification (Hofmann and Bolhar, 2007). The original sedimentary layering and sedimentary textures are well preserved along with intrusive layers of bedding parallel hydrothermal chert. These hydrothermal chert veins consist of microcrystalline quartz and rare carbon-containing inclusions (Bost et al., 2013). The host rock consists of layers of volcanic clasts having a horizon of long slivers of silicified, finely laminated carbonaceous clasts and these may represent fragments of silicified microbial mats (Bost et al., 2013; Tice and Lowe, 2004; Tice, 2009). The whole sediment was lithified prior to intrusion of the hydrothermal vein (Bost et al., 2013). These hydrothermal chert veins are considered as an analogue of a hydrothermal silica veins on Mars (Bost et al., 2013).

1.6 Preservation of fluid inclusions in diverse surface precipitates and their potentiality for the search of life

Search for life on Mars has always been a topic of intensive research. It has been geared by the continuing debate about the putative evidence for life in meteorite ALH84001 (McKay et al., 1996; Gibson et al., 1999). The evidences are supposed to be preserved in the form of physical remains of microfossils (Westall, 1999) and organic molecules (Cabane et al., 2001), which could be detected by biogenic response to non-destructive techniques such as Ra-

man spectroscopy (Wynn-Williams & Edwards, 2000) or secondary ion mass spectrometry (Brinckerhoff and Cornish, 2000). With this background, the precipitates at or just near the surface must be seen for any such record where conditions would have been suitable for life in the past. Parnell and Baron. (2004) has shown that the deposits like duricrusts, biogenic lacustrine precipitates, hydrothermal and chemosynthetic precipitates, speleothems, travertines and evaporites contain water in the form of fluid inclusions in terrestrial environments and the water survives within samples in the geological record. Sulphates are identified on Mars by various means such as Martian albedo data (Cabrol and Grin, 2001), meteorites of Martian origin (Bridges and Grady, 2000), ponding of water and palaeo-lacustrine environments as suggested by morphological evidences (Forsythe and Zimbelman, 1995) and direct observations at the *Opportunity* Mars Exploration Rover landing site. Rothschild (1990) has suggested the evaporitic deposits like halite, gypsum and epsomite of subaqueous/desiccating environment as targets to be looked for the exploration for life on Mars. Similarly, stromatolites (Westall et al., 2000), travertine (Wynn-Williams et al., 2001), sinters (Farmer, 2000), chemosynthetic crusts (Barbieri et al., 2001), speleothem crusts (Boston et al., 2001) and evaporative/algal duricrusts (Knauth, 2001), mainly in carbonate/silica host and aqueous, subaqueous or subaerial environments, are explored for life activity on Earth and hence has the implication to Mars after locating the proxies. The fluid inclusions trapped within surface precipitates like gypcrete, calcrete and silcrete from diverse surface environments bear the characteristics like consistent presence of low temperature inclusions and good preservation thus containing record of the precipitating environment, microbes/biomolecules etc. (Parnell and Baron, 2004).

1.7 The search for evidence of life on Mars

1.7.1 Water

Water is the key ingredient to be looked for while searching for the life evidences in extra-terrestrial conditions with reference to Earth. It is also important to note that presence of water doesn't imply presence of life in extra-terrestrial scenario. Today, water is not a stable entity on Mars' surface, but its presence in Martian past has been speculated by many scientists. Martian surface is extensively explored through recent missions to locate the deposited hydrous mineralogy on the surface and its relation to water activity in surface to subsurface settings. All landing sites for various Mars rover missions are planned in the areas with the evidences of pronounced water activity like Meridiani Planum-sulphate deposit involving rock water interaction (Squyres et al., 2004a) and Gusev crater, supposed to be occupied by a lake (Grin and Cabrol, 1997). Identification of water vapour, ice clouds, ice within the subsurface at high latitudes and ice on the surface in the polar regions has been done with the help of spacecrafts and Earth-based telescopic measurements on Mars. Although the conditions on early Mars are not well understood but two views have been proposed: first being the cold and dry (Carr and Head, 2003; Christensen et al., 2008; Johnson et al., 2008; Ehlmann et al., 2011), and second being the warmer (Pollack et al., 1987; Chevrier et al., 2007). Recent studies have shown the possibilities of the Mars' surface temperature near freezing point of water (Johnson et al., 2008; Fairén, et al., 2010) and only short-lived, locally isolated flows of surface water which would have resulted into the deposition/formation of phyllosilicates, hydrous sulphates, and carbonates (Christensen et al., 2008; Ehlmann et al., 2011). Spectroscopic observations made using the datasets of different missions such as Mars Reconnaissance Orbiter and Mars Odyssey indicate rich hydrous mineralogy at the surface of the Mars, being hydrous sulphates, phyllosilicates and carbonates the main mineral groups which results from rock-water interactions (Squyres

et al, 2004b; Bibring et al., 2006). Young flow channels photographed by Mars Global Surveyor which are less than 1 Ma old (Malin and Edgett., 2000) are consistent with the flow of liquid water and they could only result out of catastrophic activity like the bursting of ice mass (Malin and Edgett, 2000). There are many mineralogical to geomorphological evidences such as large flood features, valley networks etc.. present on Martian surface which indicate the water activity on local to regional scale. In addition, extensive reservoirs of ground ice in circumpolar latitudes are hypothesized at a depth of 1 m (Boynton et al., 2002; Mitrofanov et al., 2003), and are confirmed by Phoenix lander mission (Smith et al., 2009) and ice excavating impact craters (Byrne et al., 2009). Subsurface water on the planet has always been a matter of discussion considering its instability in surficial conditions. The atmosphere composition suggest water at 10-15 m below the surface whereas surficial features such as flood related landforms suggest much larger figure of around 500 m calculated based on the water loss rate due to its instability on Mars' surface(Carr, 1983, 1987).

1.7.2 Methane

In spite of the formation of methane with hot water to rock interaction i.e. geological, major methane concentration is of biological origin that comes through living organisms' metabolism on Earth. 'Methane on Mars' has always been a hot topic of debate as it leads us to confirmation of the evidence of life on a planet. First mistaken report of methane on Mars was announced in 1969 by the Mariner 7 Infrared Spectrometer (IRS) team, by the detection of strong absorption band centered at 3.3 μm and weaker absorption at 3.0 μm from the Southern Polar cap on Mars (Sullivan, 1969). Later these mentioned absorption bands were attributed to CO_2 ice. With the progressive research on Mars, methane has been first detected in its atmosphere by the European Space Agency's Mars Express spacecraft in 2004 (Formisano

et al., 2004), and later NASA's Curiosity rover at its landing site in 2014. It's concentration varies from 10 ppbv in global abundance to >250 ppbv in local abundance as detected by the Fourier Transform Spectrometer (FTS) at Canada-French-Hawaii Telescope (CFHT) (Krasnopolsky et al., 2004) and Gemini Telescope/CSHELL (high resolution spectrograph at the Infrared Telescope Facility (IRTF)) (Mumma et al., 2004). On an average, 10-60 ppbv level of methane is reported on Mars (Geminale et al., 2008, 2011; Mumma et al., 2009; Fonti and Marzo, 2010). The possibilities for the formation of methane on Mars include either through biogenic processes or abiogenic processes i.e. volcanic hot spots/hydrothermal activity (Wong and Atreya, 2003) and or external sources such as cometary impacts (Kress and McKay, 2004). Mumma et al. (2009) has suggested methane origin from hotspot or plumes in the Martian atmosphere based on comprehensive observations made from the ground stations. Several discrete areas such as Arabia Terra are especially enriched in CH_4 concentration with associated higher enrichment of water vapours. Biogenic origin of methane could imply the subsurface methanogenic communities (Methanogens are a type of Archean microbe which are able to utilize inorganic compounds (H_2 and CO_2) as their only source of energy and generating methane as a product) (Boston et al., 1992; Niederberger et al., 2009; Etiope and Lollar, 2013). Presently, methanogens thrive in some of the harshest environments on Earth, including extremely acidic environments and inside Greenland glacial ice. Abiogenic methane could also be utilized as food by methanotrophic microorganisms. 'Methane on Mars' has been highly discussed by many scientists for its variable existence in the atmosphere (Zahnle et al., 2011; Yung and Chen, 2015) and the ESA-NASA 2016 ExoMars Trace Gas Orbiter mission is expected to produce the results of detecting limits of methane and other trace gases at levels below 10 pptv (Zurek et al., 2010) for further expansion of the knowledge regarding atmospheric composition and any biogenic activity on Mars.

CHAPTER 2

Chemical and Spectral Characterization of gypsum-phyllosilicate association in Tiruchirapalli, South India and its implications

Preclude

This chapter deals with detailed chemical and spectral characterization of gypsum-phyllosilicate association in Tiruchirapalli, South India using geochemical techniques (EPMA/XRF), X-ray diffraction and diverse spectroscopic techniques (VNIR/Raman/FTIR). Petrographic observations reveal the general optical characters of crystallized gypsum in fibrous form, peculiar crystal faces and cleavage planes. VNIR, Raman and FTIR spectroscopic techniques were used to obtain the excitation/vibration bands for the different mineral phases in the samples. The VNIR spectra has been recorded for the samples and compared with their counterparts in USGS spectral library. The combined results of various chemical and spectral studies suggest that these techniques have significant potential to be used to identify the pure/mixed minerals and or approximate chemical compositions. Fluid inclusions characterization has also been done using Raman and micro-thermometric analysis techniques. These findings have significant implications to the obtained spectral results for gypsum and phyllosilicates from Mars' surface using orbital data, and to the future missions, planned to study the Mars' surface through modern spectroscopic technique such as Raman.

2.1 Introduction

In terrestrial scenario, hydrous sulphates are found mainly in primary evaporite depositional environment, hydrothermal environment in the form of veins and in oxidizing zone of sulphide mineral deposit (Klein et al., 1993). In hydrous sulphates, gypsum is one of the most significant mineral from scientific perspective as it is found in diverse depositional environments and is a soft mineral with the composition $CaSO_4{\cdot}2H_2O$, a calcium sulphate dihydrate (Klein et al., 1993). Majority of the gypsum deposits explained to be formed by evaporation of SO_4^{2-} rich waters on the surface; but it's occurrence in other forms such as mineral veins has always been a matter of crucial research from genetic perspective. Literature suggests that gypsum veins are represented by palaeo-hydrofractures and are source of valuable information about formation of path-networks followed by the emplacement of the mineral through fluids movement in the fracture networks. The developed fractures can only be open if the fluid over-pressure exceeds the horizontal stress, and the effective stresses driving compaction must then be small in shallow sedimentary basins (2-3 km) where shales and sandstones are of brittle nature and poorly cemented (Bjorlykke, and Hoeg, 1997). It has significant implications to understand the flow of fluids through the fractures in the host rocks or reservoirs (Philipp, 2008). Other mechanisms has also been proposed to decipher the genesis of gypsum veins in the outcrop to regional level over surface to subsurface conditions; they include mineral precipitation in near surface fractures (Gustavson et al., 1994; El-Tabakh et al., 1998), due to pressure generated during crystallization (Taber, 1918; Halferdal, 1960) and hydraulic overpressure and fracturing (Shearman et al., 1972; Blair et al., 1989).

Sub horizontal gypsum veins and connecting gypsum nodules are observed in nodular gypsum horizons within red mudstones near Penarth, South Wales (White, 2008). Other sedimentary basins where similar fibrous gypsum veins are exposed include the Amadeus Basin of upper Proterozoic, Australia (Stewart, 1979), the Appalachian Basin of Silurian, USA (Taber, 1916), the Elk Point

Evaporites of Devonian, Alberta, Canada (Halferdal, 1960), the Newark Rift Basin, USA (El Tabakh et al., 1998; Herman, 2005), the Germanic or Central European Basin of Triassic (Ziegler, 1990) and the Mercia Mudstone Group of the Upper Triassic in the Bristol Channel Basin at Watchet on the Somerset Coast (SW England) (Bennison and Wright, 1969; Philipp, 2008). The subhorizontal nodule-connecting gypsum veins of Mercia Mudstone have been proposed to be formed as hydrofractures associated with the volume change resulting from the hydration of nodular anhydrite (Philipp, 2008). In similar geological settings, veined gypsum is observed in sedimentary sequence of Karai Shale Formation, near Karai village of Ariyalur, Tiruchirapalli, India. This veined gypsum and associated phyllosilicates has not been given much attention in literature for their genesis mechanisms yet. Due to badland topographic setting in the area, gypsum is broadly classified as an evaporite deposit (Sundaram et al., 2001) but its relation to the adjoining phyllosilicate mounds is not yet discussed in detail. In this work, we present a combination of the results availed from field and different geochemical to spectroscopic analytical techniques in order to realize the suitability of these laboratory techniques for characterization of the samples. This approach provides the classification of the phyllosilicates in the area. Based on field observations, herein we discuss the formation of gypsum veins through the pressure generated by crystal growth where crystallization forces push the vein walls apart, resulting in the precipitation of antitaxial veins in Karai Shale Formation, Tamil Nadu. Hydrofractures related to the fluid-overpressure may also have taken part in the genesis of gypsum veins in the area. Discussions and interpretations of geochemical and spectroscopic results obtained from the samples forms the major part of the paper. This study also has the scope to provide significant implications to the hydrous sulphate-phyllosilicate deposits on Mars. For instance, *Homestake* one of the most discussed hydrous sulphate vein in Endeavour Crater, Cape-York, Mars has been proposed to be formed by the movement of sulphate-rich fluids in the fractures of the host rock (Squyres et al., 2012).

The thick sedimentary record of Cauvery basin preserves a qualitative

record of sequential events responsible behind the formation of the sedimentary succession in the area. Palaeoclimate reconstruction often uses different criteria for environmental change such as stable isotope ratios, microbes, pollen, tree rings and sediment records. Fluid inclusion homogenization temperature studies have gained the importance as a direct method to be utilized to measure the past surface water temperature by using primary minerals like halite (Benison, 2006). This method have been extensively used for the deposits of various ages ranging from modern (Roberts and Spencer, 1995), Quaternary (Lowenstein et al., 1998, 1999), Permian (Benison, 1995; Benison and Goldstein, 1999; Satterfield et al., 2005a), Silurian (Losey and Benison, 2000; Satterfield et al., 2005b) and Precambrian (Meng et al., 2011) where from satisfactory results have been reported. Opeche Shale and modern lakes in Western Australia are other terrestrial acid saline lake deposits of Permian age which are sedimentologically and mineralogically counterparts of the Martian strata (Benison and LaClair, 2003). These lakes are shallow ephemeral, and acidic and precipitate abundant gypsum, halite, hematite, jarosite and alunite (Benison, 2006; Alpers et al., 1992; Benison et al., 2001; Gray, 1997; McArthur et al., 1991). Other evaporates used for similar kind of studies mainly includes gypsum (selenite) at Haughton impact structure, Devon Island, Canada, (Parnell et al., 2004).

In recent years, fluid inclusion studies of evaporites has become an active area of research, as they hold great information about the past climate of the arid regions. The procedure to study the fluid inclusions has long been proposed using petrography, Raman and microthermometry by Kerkhof and Hein (2001). Petrographic microscopy of the fluid inclusion bearing mineral or rock samples is the first and essential step to be done, which provide the detailed record of the distribution of fluid inclusions within the prepared sample. Without detailed petrography, it is difficult to propose a mechanism for the mineral/rock forming process on the basis of the data of analytical techniques like Raman spectroscopy and microthermometry. Petrographic analysis is also essential to distinguish different phases (liquid and gas) and types of fluids (primary, pseudo-secondary and secondary) (Roedder, 1984; Goldstein, 2003;

Bodnar, 2003). Petrography is an important step in determining the various aspects regarding fluid inclusion such as entrapment conditions, secondary processes: diffusion during crystal growth, re-crystallization, fluid migration, etc.. Primary fluid inclusions are significant as they provide information about the surface hydrochemistry in the past (Roberts and Spencer, 1995) and secondary fluid inclusions provide the significant information about the possible geologic disturbances in the past and its correlation. Apart from this, fluid inclusions also hold potentiality to get the record of surface temperatures of the depositional environment (Roberts and Spencer, 1995).

In the present study, fluid inclusions of gypsum from Karai Shale Formation, Tiruchirapalli have also been characterized using laser Raman and micro-thermometric analyses with the objective to obtain the chemistry of the fluid inclusions. Micro-thermometric analysis has been defined in quite detail in Pleistocene halite from Death Valley, California and claimed the technique as instrumental to study climate change with time by Roberts and Spencer (1995), to determine palaeo-temperatures preserved in fluid inclusion.

2.2 Geological Setting

Cauvery basin is a peri-cratonic rift basin which is formed all along the eastern continental margin of Peninsular India during the fragmentation of Gondwana supercontinent (Jafer, 1996; Biswas et al., 1992). A thick sedimentary sequence is deposited in the basin which is underlained by Archean granitic gneissic basement and the exposures of the sedimentary sequence are limited to 5 separate areas namely, Pondicherry, Vridhachalam, Ariyalur, Tanjore and Sivaganga (Banerji, 1972; Rangaraju et al., 1993). Our area of interest lies in Ariyalur region, where mainly sedimentary rocks of Cretaceous age are exposed (Fig 2.1a). Moreover, numerous studies are available in the area by a wide spectrum of geological research community ranging from stratig-

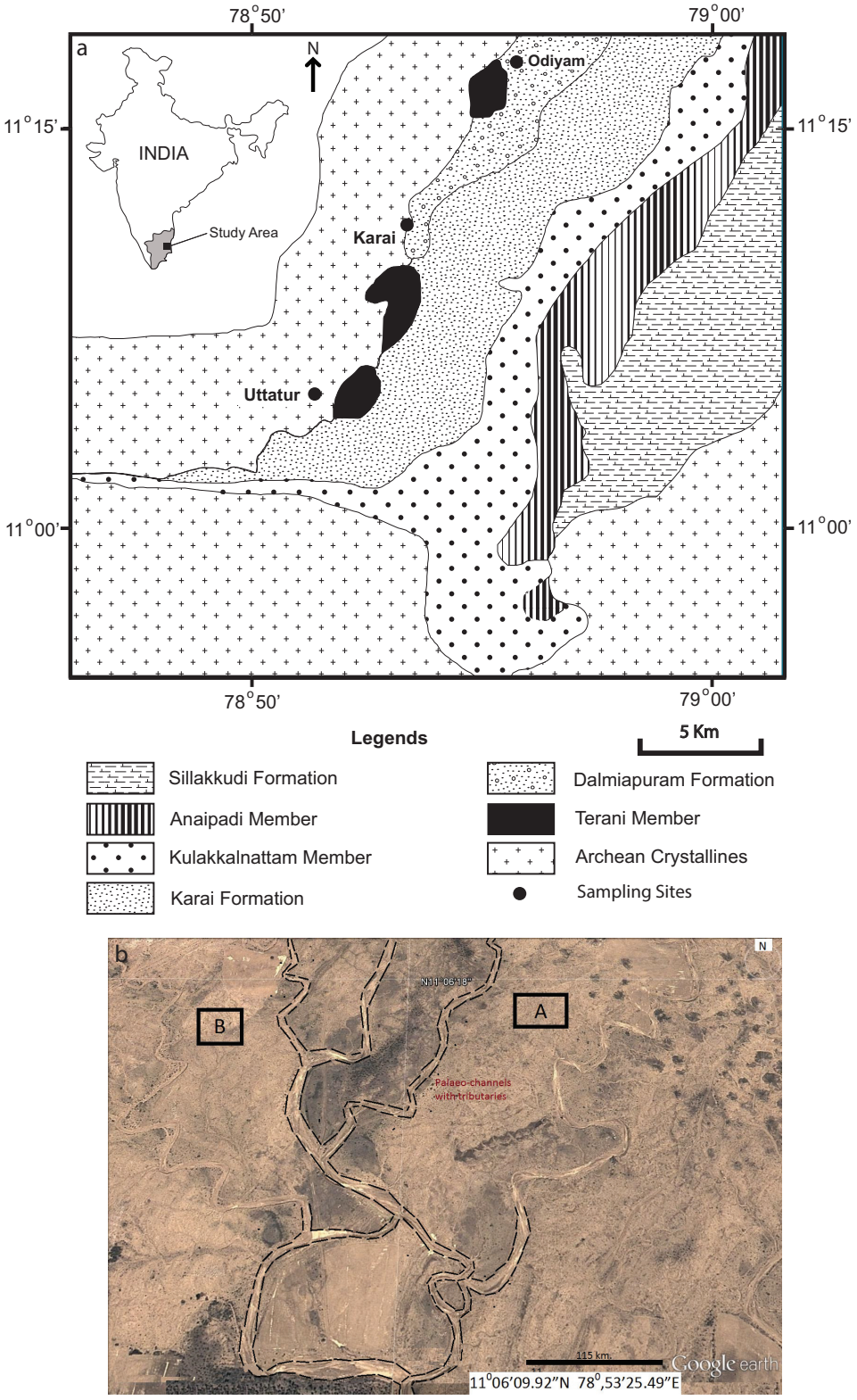

Figure 2.1: (a) Detailed geological map of the study areas, located in Cauvery basin, Tiruchirapalli, Tamil Nadu, India (modified after Tewari et al., 1996). (b) Google Earth image of the badland topographic setting of Karai Shale Formation.

raphy/biostratigraphy, sequence stratigraphy, palaeontology, geochemical to depositional history modeling (Ramanathan, 1968; Banerji, 1970, 1972; Sastry et al., 1972; Sastri et al., 1973; Jain, 1978; Sundaram and Rao, 1986; Ramasamy and Banerji, 1991; Govindan et al., 1996; Madhavaraju and Ramasamy, 2001; Sundaram et al., 2001; Nagendra et al., 2002; Madhavaraju et al., 2002, 2006, 2009; Nagendra et al., 2011). In literature, the sedimentary rocks of Ariyalur area are classified into three distinct groups namely, Uttatur, Trichinopoly (also denoted as Tiruchirapalli) and Ariyalur (Blanford, 1862). Here, for the present study Uttatur Group is taken into consideration, which comprises of four Formations, namely Terani, Arogyapuram, Dalmiapuram and Karai (Sundaram et al., 2001). Terani, Arogyapuram and Dalmiapuram Formations were deposited during early Cretaceous, and Karai Shale Formation was deposited in late Cretaceous (late Albian to early Turonian period) (Ramasamy and Banerji, 1991). Our focus is mainly on the Karai Shale Formation which is well exposed as badland (terrains where sedimentary rocks/phyllosilicate-rich exposures are heavily eroded by fluvial or eolian activity with high drainage density) in an easterly draining catchment to the east of Karai village in Tiruchirapalli (Ramkumar et al., 2004)(Fig 2.1b). Karai Shale Formation constitutes gypsiferous clay, silty sandy clays and sandstone suggesting a progressively shallowing basin, and unconformable/erosional contact with the overlying Kulakkalnattam Formation signifies a major regression which resulted into the termination of Uttatur Group (Sundaram et al., 2001). Sundaram and Rao (1986) have divided Karai Shale Formation into two Members based on type areas Odiyam and Kunnam. Odiyam Member constitutes gypsiferous mudstone with distinctive thin inter-beds of pink shale and siltstone, and sporadic lenticular beds of coquinite and sandstone in the lower part of the Formation (Sundaram et al., 2001). Kunnam member constitutes inter layered mudstone, gypsiferous siltstone and fine-grained sandstone with calcite and siderite cements in the upper part of the Formation. The contact between the Members of Karai Shale Formation is conformable (Sundaram et al., 2001). The Karai Shale Formation is conformably underlain by the

grey shales, mudstone, limestone, coquinite, calcareous sandstone and quartzose conglomerate of late Albian Dalmiapuram Formation and unconformably overlain by sandstone, mudstone, shale, coquinite and conglomerates of Turonian Kulakkalnattam Formation (Sundaram and Rao, 1986).

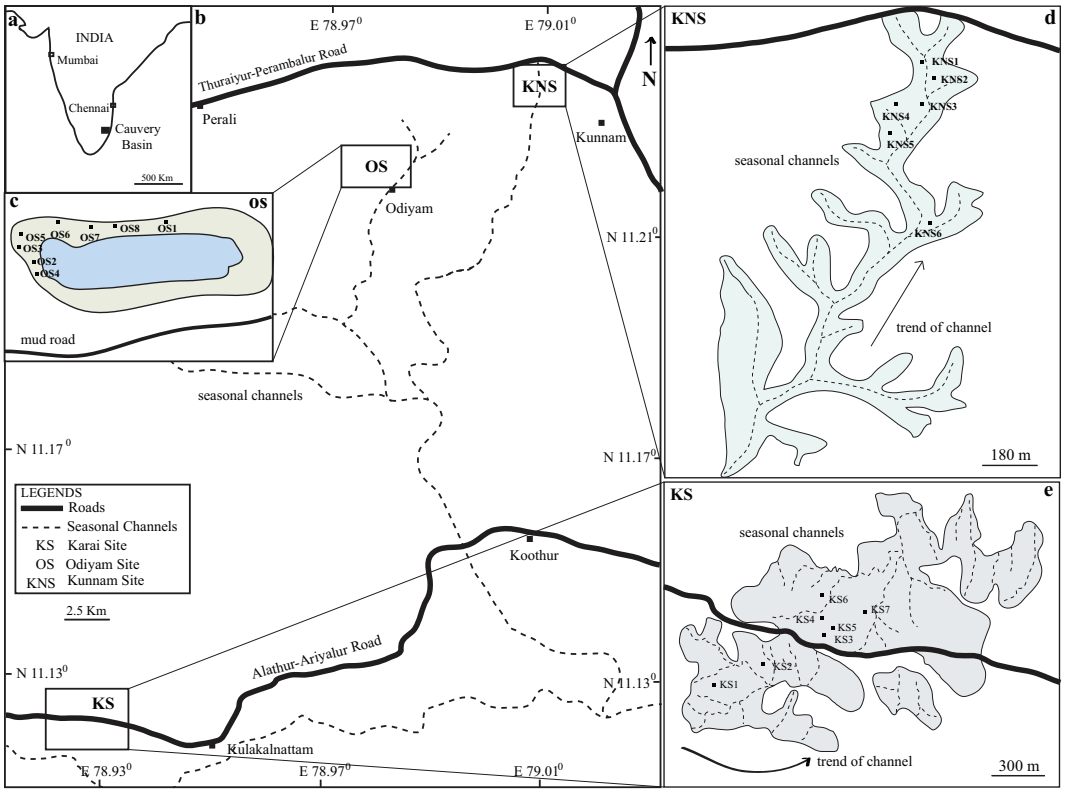

Figure 2.2: (a) Location of Cauvery basin, India. (b) Location of the study areas with respect to road networks and seasonal channels in the area. (c) Sampling locations in Odiyam area. (d) Sampling locations in Kunnam area along with the seasonal channel network. (e) Sampling locations in Karai area along with the seasonal channel network.

2.3 Materials and methods

2.3.1 Site Selection, Sampling and Sample Preparation

Samples have been collected in 2012, 2013, during the fieldwork in and around Ariyalur, Tamil Nadu, which was carried out for geological mapping of the

gypsum bearing areas (Singh et al., 2015). A sketch of the sites with the valley networks and sampling locations is provided in Fig 2.2. Occurrence of gypsum in different forms ranging from veined, surficial to layered type led to more detailed sampling and field mapping in the area. Systematic sampling was focused on gypsum (in different depositional settings) and types of phyllosilicates from kaolinitic to Fe/Mg rich ones. In this study, gypsum deposits from three regions namely, Karai, Kunnam and Odiyam were mapped and about 15 samples were collected from each site for further laboratory analyses. Samples were collected from several locations of phyllosilicate rich mounds in badland topographic setting of Karai (Fig. 2.3a). Occurrence of gypsum veins was consistent throughout the area. Kunnam site was marked with the presence of surficial gypsum with fibrous appearance on its top (Fig. 2.3b and b'). Several gypsum rich columns with comparatively lesser gypsum layers in the surrounding were prominent feature of the Odiyam site and hence, samples were collected from multiple locations within the area (Fig. 2.3c and c'). Gypsum was more weathered and not suitable to be used for -further laboratory analysis from Karai and Kunnam, therefore, unweathered selected samples from Odiyam site were used for - laboratory processing and analysis.

Collected samples were cleaned by removing the stuck clay portion from the hand-specimens and then, crushed into Fritsch Pulverisette with Ni-Ch grinding set (Fritsch GmbH; Germany) attached with air compressor and a Jaw Crusher (Insmart Systems) for preparing the samples for geochemical analyses like XRF and spectroscopic analyses like laser Raman and VNIR. XRD was also carried out with the same powder samples.

In addition, wafers were prepared for fluid inclusion studies by making doubly polished sections (diamond polishing) of 100-200 μm thickness. Honey-bee wax is used as a sticking media for the samples because it allows an easy removal of the prepared thin wafer from the slide. Utmost care has been taken during the wafer preparation, starting from well crystallized sample selection with minimum or no secondary infilling/weathering, minimum pressure during

polishing for minimum sample loss and effect to the fluid inclusions. Selection and grouping of the fluid inclusions has been made from wafers for further characterization using Raman and micro-thermometry as proposed by Kerkhof and Hein (2001).

2.3.2 Petrographic and Electron Probe Microanalysis

Representative 10 thin sections were prepared for petrographic analysis and photomicrographs were obtained using Eclipse LV100 Polarizing microscope. Thin sections were analyzed using CAMECA IMS 4f SIMS to determine the major oxide concentration of gypsum and phyllosilicates in Physical Research Laboratory, Ahmedabad. The instrument was kept at 15 kv and 6 nA using a focused beam. Larger gypsum grains were analyzed to make the accurate measurements at a point within the crystal and more phyllosilicate crystals were analyzed to explore the variations in composition.

2.3.3 XRF Analysis

Representative samples were analyzed for major elements using Bruker S4 Pioneer Wavelength Dispersive X-ray fluorescence (WD-XRF) spectrometer at Centre for Earth Science Studies (CESS), Thiruvananthapuram. Fused glass disks and pressed powder pellets were used for major element analysis. Calibration has been done in an in-house developed programme using international standards, representative of matrix and target element concentrations. - Loss on ignition was obtained by heating the sample at 120^o and 400^o for 20 and 30 minutes respectively in a muffle furnace.

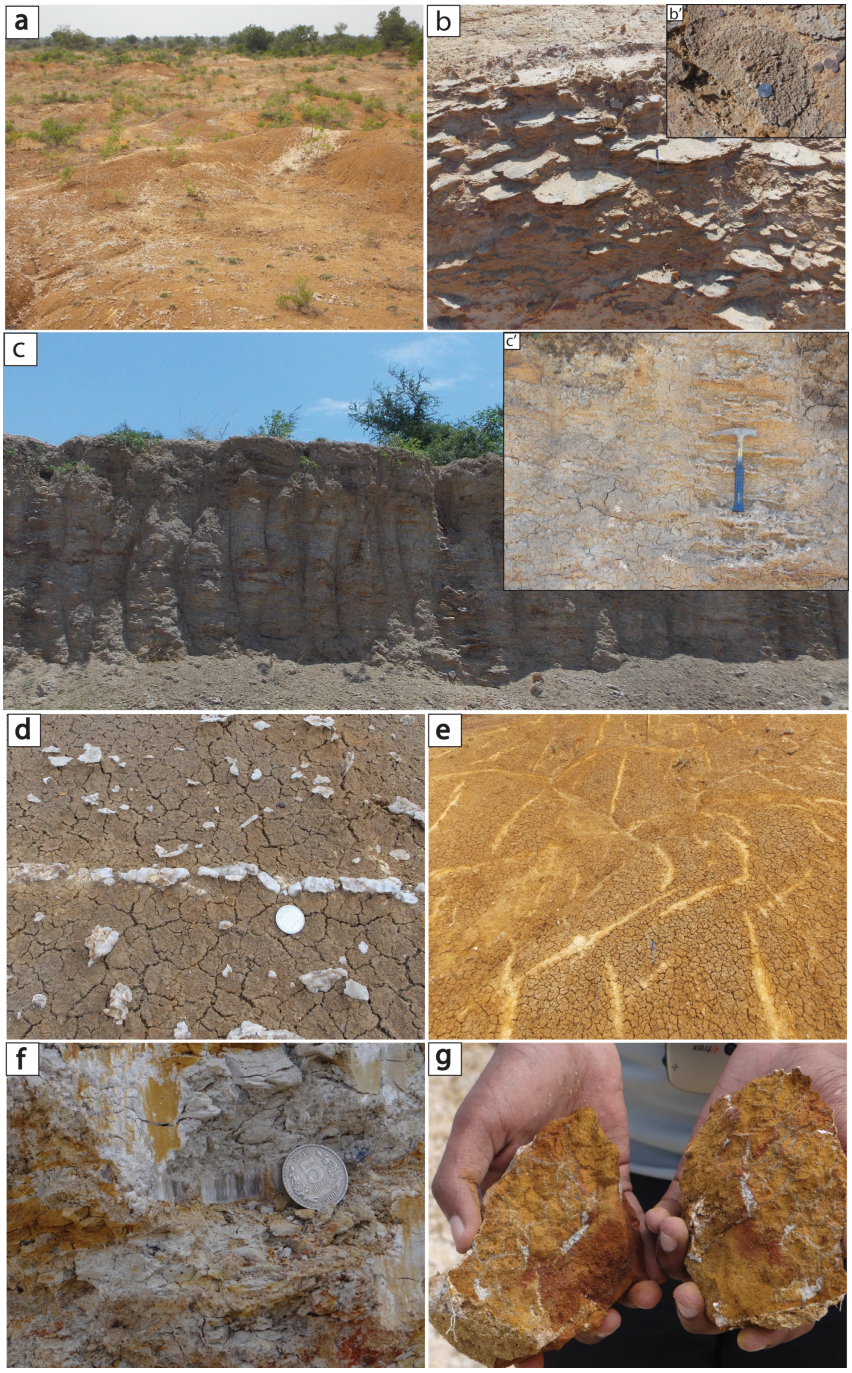

Figure 2.3: (a) Badland topographic setting in Karai with the mounds of phyllosilicates. (b) Side-view of gypsum deposits on seasonal river terraces, and (b') upper view of fibrous gypsum. (c) Cross sectional view in a mine in Odiyam where gypsum is found to be enriched in some columns with limited occurrences in between, and (c') closer view of observed columns. (d) A vertical broken gypsum vein in Karai. (e) Network of gypsum veins in Karai. (f) Gypsum layer sandwiched between upper and lower kaolinitic to Fe rich phyllosilicate layer. (g) Irregular gypsum veins running through Fe rich phyllosilicates.

2.3.4 Spectral Analysis

Spectral measurements were carried out in the laboratory for all samples including hand-specimens and powders with grain size of 500 μm in VIS-NIR-SWIR region of electromagnetic spectrum by ASD Field Spec-Pro HR from 350-2500 nm with spectral resolutions of 3 nm in VNIR and 10 nm in SWIR region. The measurements were taken by keeping the optical probe at 20 cms height with the incidence angle of 90^o and viewing angle of 1^o. The samples were kept over the black cloth and the spectra were obtained for hand specimens and powders in dark room environment for better collection of spectra. The spectra were obtained and displayed in terms of reflectance data relative to the reference plate data. The raw data for the sample and the reference plate are ratioed after the background removal. The stepped splice error, due to detector change usually at two spectral intervals at VNIR and SWIR2 vertices is removed by the parabolic correction of the data.

2.3.5 X-Ray Diffraction

Prepared powders were analyzed using PANalytical 3 kW X'pert PRO X-ray diffractometer at Centre for Earth Science Studies (CESS), Thiruvananthapuram. Every powder sample was analyzed in the conditions: 5-70^o 2Θ, step size 0.0840, Cu Kα radiation. Obtained diffractograms of the analyzed samples were compared using ICSD/JCPDS software. The phases were identified as major (peak intensity high to prominent) and minor (peak intensity moderate to low).

2.3.6 Laser Raman Spectroscopy and Fourier Transform Infrared

Micro Raman Spectroscopy was carried out using WiTech alpha 300 Raman System excited with 532 nm (fixed wavelength) laser with 300 mW output in Vikram Sarabhai Space Centre, Kerala. The spectral range of the equipment is 100 to 3600 cm^{-1} shift from the laser line, accomplished with an edge filter.The spectral resolution of the instrument is 1 cm^{-1}. The system is fully automated and self-validating with auto aligning and optimization of input laser power.

Raman spectroscopy of fluid inclusions has been performed using both sided diamond polished thin wafers of gypsum of about 100 μm thickness. For this purpose, Renishaw inVia Raman microscope was used in National Centre for Earth Science Studies (NCESS), Kerala. Its high sensitivity enables us to look at very weak Raman signals generated from the sample during the analysis. Renishaw uses a stigmatic on-axis optical design in inVia and provides high optical efficiency and excellent stray light rejection. The spectrometer uses a narrow entrance slit (between 10 μm and 65 μm) and the optimised Rayleigh filter mount is positioned away from the entrance slit in the instrument. Powerful WiRE^{TM} software for intuitive operation and easy data manipulation, attached with the Renishaw inVia Raman Microscope was used for spectral recordings of the gypsum samples. Gypsum wafers has been analysed by using 785 nm laser with 1200 l/mm grating and with laser exposure time of 30 S, laser power of 15 mW and spectrum range of 100-3600 nm.

FTIR spectroscopy was carried out with a PerkinElmer's Infrared (FTIR & IR) spectrometer in Department of Chemistry, Indian Institute of Space Science and Technology, Kerala, using the fine powder samples. The powders were pressed at 55 to 60 kb to obtain the transmittance spectra of the samples. The infrared (IR) spectra were recorded immediately after the separation of the powder sample from the bulk sample. Spectra were collected in the 700 to 4000 cm^{-1} range with an optical resolution of 0.5 cm^{-1} and wavelength

precision of 0.01 cm^{-1} at 220 V, 50 Hz power supply. A baseline correction was made before interpretation the data.

2.3.7 Micro-thermometry

Microthermometric studies conducted using a Motorised temperature controlled geology stage (MDSG600) working with Linksys 32 temperature control and video capture software. The system consists of a MDSG600 stage, aT95-Linkpad system controller, LNP95 liquid nitrogen cooling pump system. The stage is mounted on to a Linkam Imaging station that has been designed to easy access the heating/cooling stage. The temperature of first melting (T_{FM}), temperature of last melting (T_{LM}) and the homogenization temperature (T_h) of different inclusions were measured. The temperature limit used for the gypsum wafer analysis by heating and freezing stage is -80 to $+120^oC$. The upper limit (i.e. $+120^oC$) is defined as above this temperature gypsum starts burning/turning into a brownish black opaque material.

2.4 Results

2.4.1 Geomorphology, petrography and geochemistry

Badland topographic setting is characteristic geomorphological feature of the study areas with lithologies mudstone and siltstone in the type localities of the Members Odiyam and Kunnam of Karai Shale Formation (Fig. 2.3a). This geomorphologic setting provides excellent outcrops in the form of phyllosilicate rich mounds to study the orientation of the linear, subvertical-vertical vein features of the area. In Kunnam, the fibrous gypsum was mainly found on the abandoned river terraces (Fig. 2.3b and b'). In Odiyam, several gypsum rich columns were observed with minor occurrences of layered gypsum in the

phyllosilicate-rich mass between the columns. Gypsum layers were highly interconnected (Fig. 2.3c and c') within the kaolinite and Fe-rich phyllosilicate groundmass. In Karai, the surface was encountered with the anastomosing network of veins of gypsum in the phyllosilicate-rich groundmass (Fig. 2.3d and e). Network of veins is confined to the mounds of phyllosilicates in the regions (theses veins are missing on the floors of dried valley network). At places, veins are highly weathered and mixed into the groundmass, making it difficult to draw boundary between gypsum and phyllosilicates (Fig. 2.3e). Large part of the area is in the form of mounds and consists of relatively massive mudstones and siltstones with hardly any preserved bedding plane or sedimentary structures. In Odiyam, the layers of gypsum stacked within phyllosilicate-rich horizons (ferruginous and kaolinitic) were observed (Fig. 2.3f). Smaller scale gypsum veins of 2-5 millimeters in thickness were observed in Fe-rich phyllosilicate mass (Fig. 2.3g).

The microscopic study of the prepared thin sections suggests that the grains are coarse with very prominent cleavage planes (Fig. 2.4A). The contact between the euhedral gypsum grains is sharp. Some opaque mineral phases are also found between the grains which are mostly ilmenite grains as confirmed by EPMA data (52.32 wt.% TiO_2 and 47.22 wt.% FeO). Fluid inclusions have also been observed in the larger grains of gypsum which are mostly primary inclusions formed during the growth of the crystals and are mostly following the cleavage pattern (Figure 2.4B). A prominent microscopic level of alteration has been observed through the cleavage planes (Figs. 2.4C and D), which supports the hydration activity after the formation of gypsum crystals. Back scattered images, generated at the time of EPMA of gypsum show its crystalline nature along with embedded opaque mineral inclusions (Figs. 2.4E and F). Oxide totals obtained from EPMA are in the range of 71.42-79.88 wt.%, possibly due to excess water or void spaces within the grains. CaO and SO_3 contents are ranging from 43.23-45.52 wt.% and 31.57-34.16 wt.% respectively. Other oxides are found to be in negligible to very low concentration except P_2O_5 concentration, which is in the range of 0.472-0.597 wt.%. In phyllosilicates,

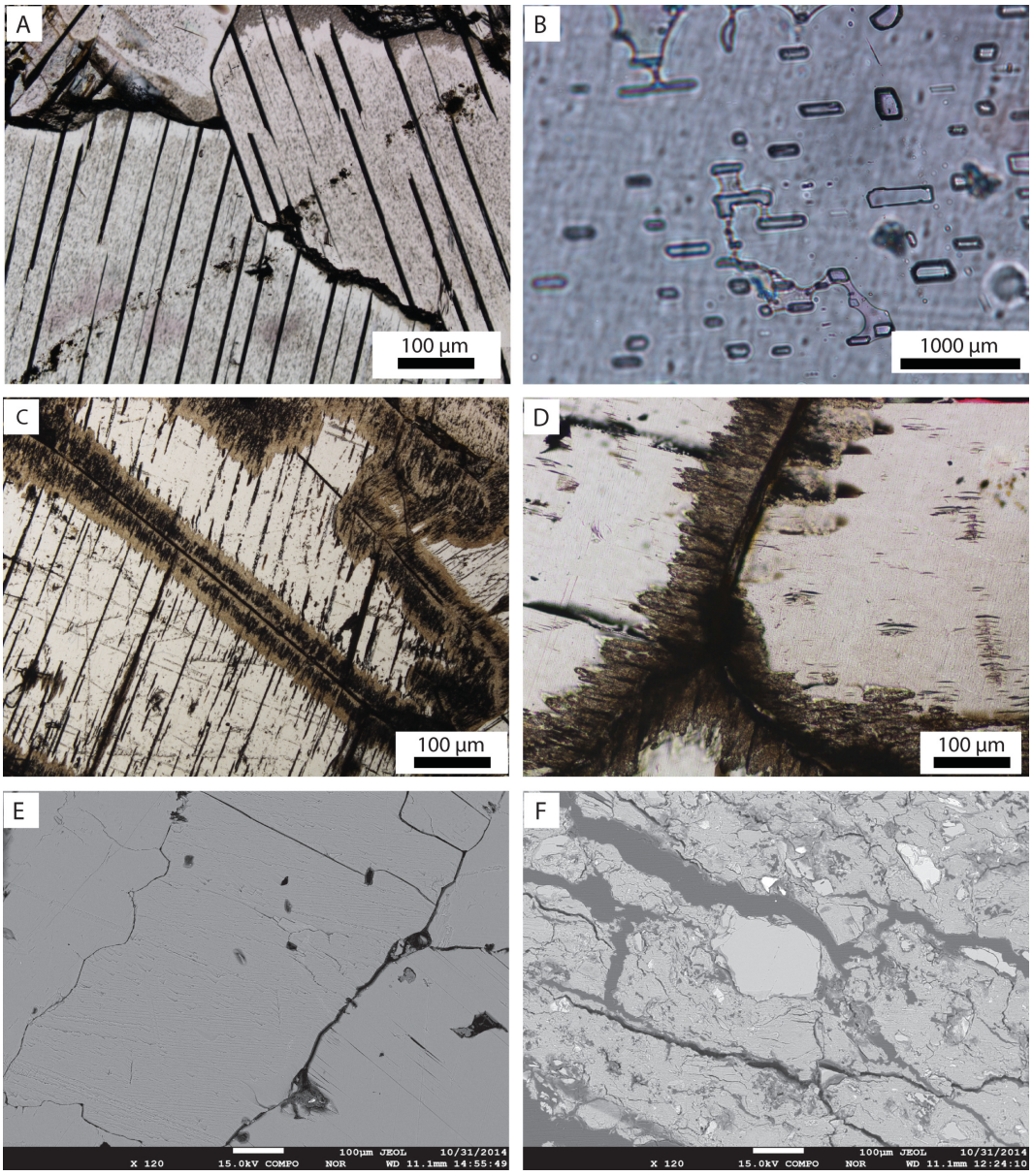

Figure 2.4: (A) Photomicrograph of gypsum with prominent grain boundaries and cleavage planes, (B) associated fluid-inclusions of varying dimensions present in the gypsum grains, (C) and (D) show alteration of gypsum through fracture planes and grain boundaries. (E) and (F) represent backscattered electron images of representative gypsum and gypsum-phyllosilicate association from Odiyam.

the content of CaO, FeO(t), MgO, TiO_2, SiO_2 and Al_2O_3 is in the range of 1.52, 15.23, 1.64, 1.42, 40.71 and 19.94 wt.% respectively. XRF analyses of gypsum samples show CaO and SO_3 contents in the range of 34.58 wt.% to 41.34 wt.% and 49.19 wt.% to 53.77 wt.% respectively. The percentages of other oxides are minor in amount or below detection limits. The XRF analysis of phyllosilicate samples shows the SiO_2 concentration in the range of 38.06 wt.% and Al_2O_3 concentration in the range of 18.63 wt.%. Concentration of $FeO_{(t)}$ is around 4.80 wt%. CaO and SO_3 concentrations are measured and found to be around 10.01 and 17.96 wt.%.

2.4.2 Spectral Observations

Laboratory reflectance spectra of minerals, measured over the VNIR/SWIR range of electromagnetic radiation represent the selective absorptions due to electrical and vibrational processes within the mineral structure (Gaffey et al., 1993). The reflectance spectra provide significant clues regarding the chemical composition, crystal structure and purity of the mineral. Here, only compositional measurements have been interpreted by resolving the reflectance spectra of the samples. Identification of hydrous sulphates and sheet silicates or Fe/Mg bearing silicates was done mainly by identification of set of absorption bands/features in the range of 1000-2400 nm. Secondary Fe mineral phases were identified using the peculiar absorption features in the electrical part of the spectrum (400-1300 nm). The areas selected for the sampling have extensive deposition of nearly pure minerals, which helped in better acquisition and identification of the optimum absorption bands. The obtained absorption features in the electrical and vibrational range of electromagnetic spectrum are at 560, 650, 900, 1000, 1200, 1445, 1750, 1900, 2200 and 2280 nm for pure gypsum sample, OS4 (Fig. 2.5a). The absorption bands in 350-1300 nm range are due to single and paired electron transitions in Fe between energy levels in unfilled 3d orbitals and metal-ligand electron transfers (Sherman and Waite, 1985).

The distinct absorption features in 1400-2500 nm range are characteristic of fundamental vibrations due to H_2O and OH combinations and overtones (Hunt et al., 1971; Clark et al., 1990; Clark, 1993). The reflectance spectra were acquired for the powder sample derived from the same hand specimen also used here to identify the peculiar absorption bands(Fig. 2.5b). The spectra have clear spectral responses as that of the hand specimen; the only difference found is the band-depth variation in electrical as well as vibrational range of electromagnetic radiation. An increase in band-depth of the absorption bands at 1000 and 1200 nm, and appreciable decrease in band-depth of absorption bands at 1445, 1750, 1900 and 2200 nm is observed. The spectra have shown albedo in the range of 35% for hand specimen and 40% for the powder sample. Hand specimen KS2 gypsum-phyllosilicate associate shows the absorption bands in the form of triplet at 1400-1500 nm and a doublet at 2200 nm (characteristic of gypsum) with an additional absorption band at 2370 nm (characteristic of phyllosilicate group of minerals) (Fig. 2.5c). The absorption feature at 2200 nm is the characteristic one of phyllosilicate group of minerals; the observed absorption features at 2200 and 2340 nm in the sample denote the composition of mixed kaolinite and illite (Hunt et al 1971; Clark, 1993). The spectral profile of the same sample in the powdered form shows the absorption bands as a triplet around 1400 nm and a doublet around 2200 nm which are assigned to gypsum (Fig. 2.5d). The spectra have shown albedo in the range of 34% for hand specimen and 12% for the powder sample.

Additionally, spectral profiles for phyllosilicate samples has also been derived and presented in Fig. 2.6. The spectral profile of the sample KS7 shows the absorption bands at 650, 900, 1400, 1900, and 2200 nm, which are basically due to ferric iron (650 and 900 nm), H_2O and OH (1400, 1900 and 2200 nm) (Fig. 2.6a). Apart from these major absorption bands, two minor absorption bands at 2310 and 2380 nm are also present, which are the characteristic features of kaolinite with major absorption features discussed earlier. The spectral profile of powder sample KS7 shows the absorption features same as that of the hand specimen (Fig. 2.6b). The spectra have shown albedo

in the range of 20-40% for hand specimen and 20% for the powder sample. The spectral profile of the sample OS6 shows the major absorption bands at 1400, 1900, and 2200 nm, which are basically due to H_2O, OH and Al-OH bond respectively and minor absorption bands at 2310 and 2380 nm due to Fe-OH/Mg-OH (Fig. 2.6c). The spectra have shown albedo in the range of 75% for hand specimen. The reference USGS spectral profiles of the identified major minerals in the study are presented in Fig. 2.6d.

2.4.3 X-Ray Diffraction

The gypsum and phyllosilicate samples were qualitatively identified using XRD. The XRD diffractograms for the selected gypsum and phyllosilicate samples are provided in Fig. 2.7. All the analyzed samples by XRD show mainly gypsum peaks above background in addition to one quartz peak in the sample KS2. Mostly the peaks fall into the vicinity of 20-55^o of 2Θ. The most prominent peak falls around 25^o along with the additional peaks at 31^o, 38^o, 41^o and 48^o for gypsum. All the peaks are narrow and prominent due to less compositional variability and good crystallinity.

The exact identification of phyllosilicate minerals in the samples KS7 and OS5 has also been carried out by XRD and the major phyllosilicate-phases identified using the diffraction peaks include kaolinite (also identified by VNIR-SWIR spectral results), montmorillonite, illite, hematite, gypsum and quartz. KS7 shows the prominent diffraction peak at around 25^o and OS5 shows minor diffraction peak at around 25^o, which is characteristic of gypsum. Other diffraction peaks of phyllosilicate samples show broader peaks, which could be attributed to the compositional variability. The findings confirm the identity of the mentioned minerals and having good correlation with the results of other applied chemical techniques. Quantification of the different mineral phases in the XRD diffractograms was not carried out as scientists have reported many difficulties in phase quantification of hydrous minerals due to constitutional

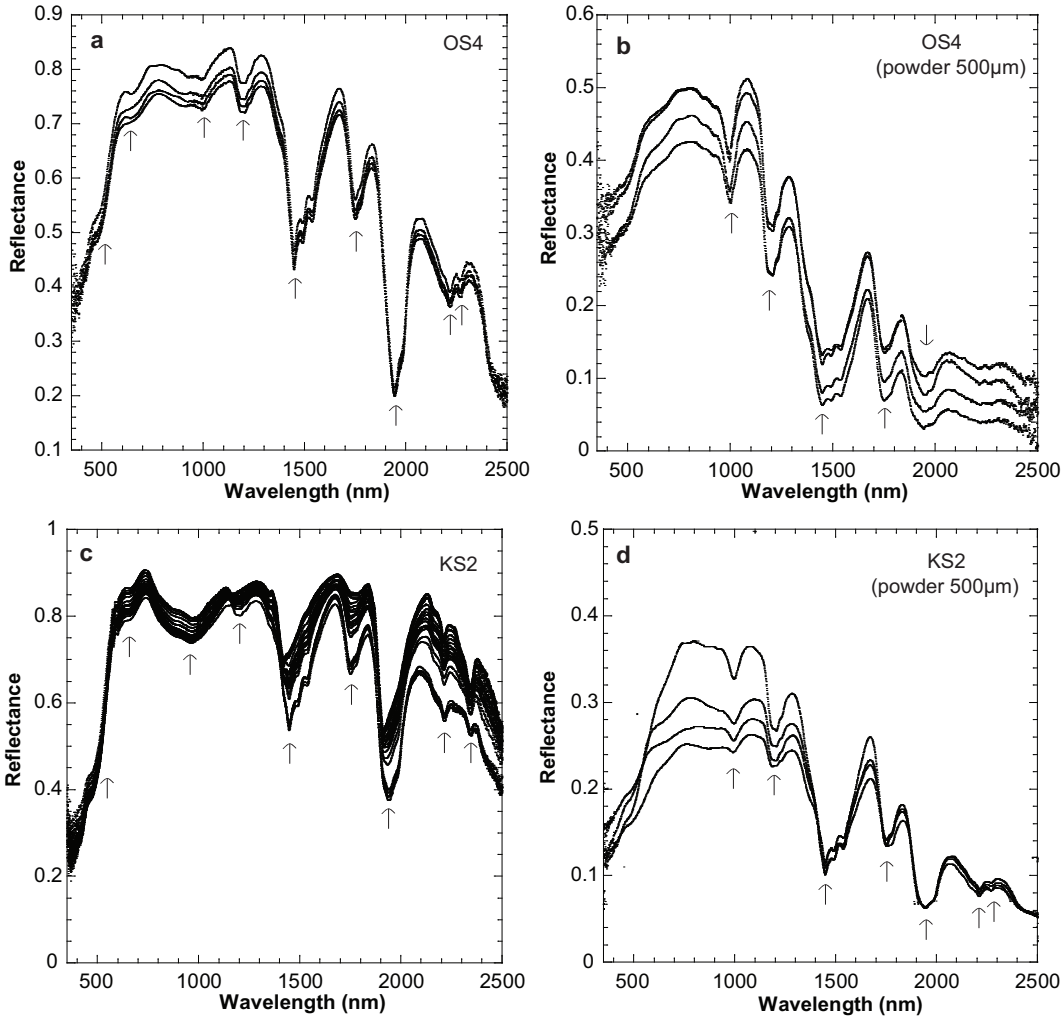

Figure 2.5: Visible-near infrared-shortwave infrared (VNIR) laboratory spectra of, (a) OS4 pure gypsum having characteristic spectral features as distinct triplet bands near 1400-1500 nm, a strong band near 1930-1940 nm, and multiple features near 2100-2300 nm (b) OS4 powder of 500 μm grain size having characteristic spectral features same as hand-specimen instead weaker absorption features at 2100-2200 nm, (c) KS2 with spectral features characteristics of the gypsum-phyllosilicate association: triplet absorption bands near 1400-1500 nm (characteristic of gypsum), and 1930-1940, 2200 and 2370 nm (characteristic of phyllosilicates) and (d) spectral features of powdered KS2 showing more compositional variation with triplet absorption bands near 1400-1500 nm for gypsum and absorption bands near 1400 nm and 1930-1940 nm for kaolinite.

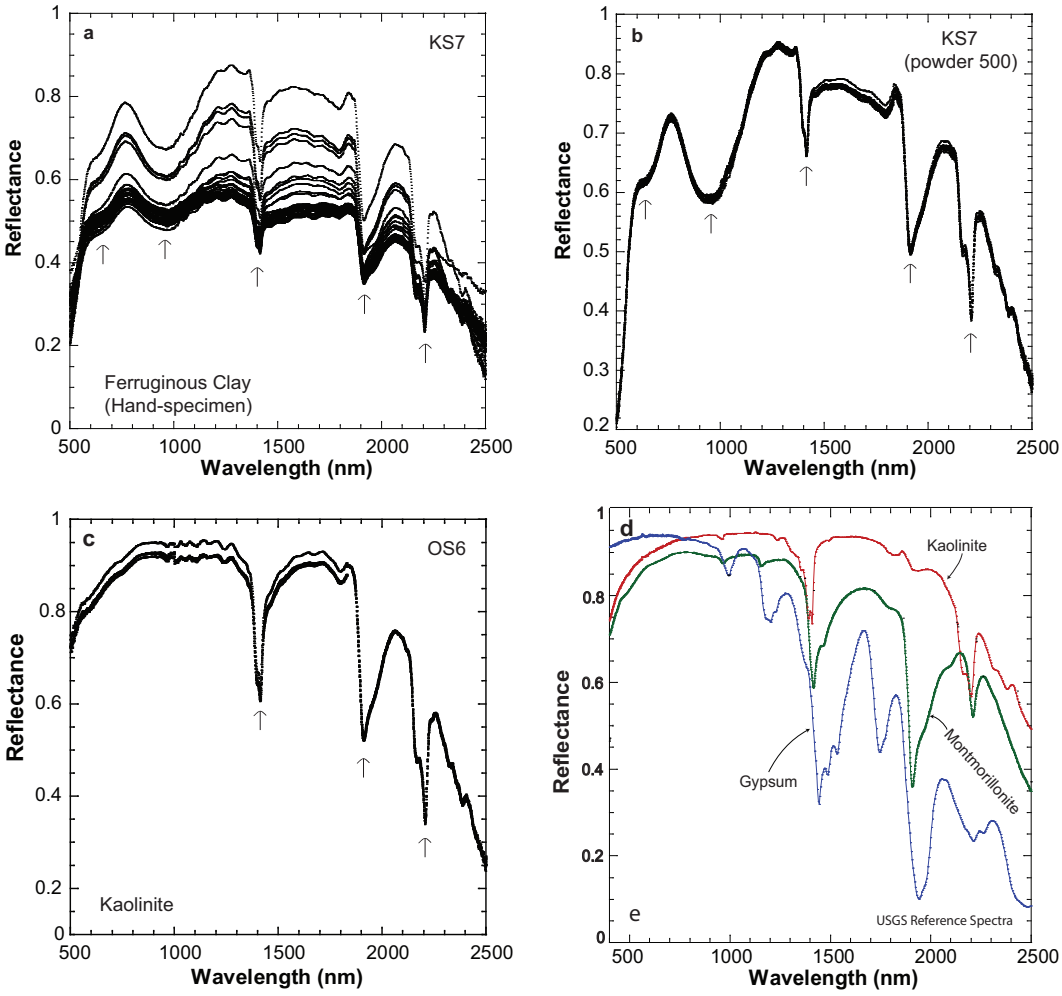

Figure 2.6: Laboratory reflectance spectra of hand-specimen (a) and powder (b) of phyllosilicate sample, mainly kaolinite with defined spectral features. (c) Spectral characteristic of hand specimen of Fe-rich phyllosilicate with defined absorption bands. (d) Reference spectra from USGS spectral library for the identified minerals in the study.

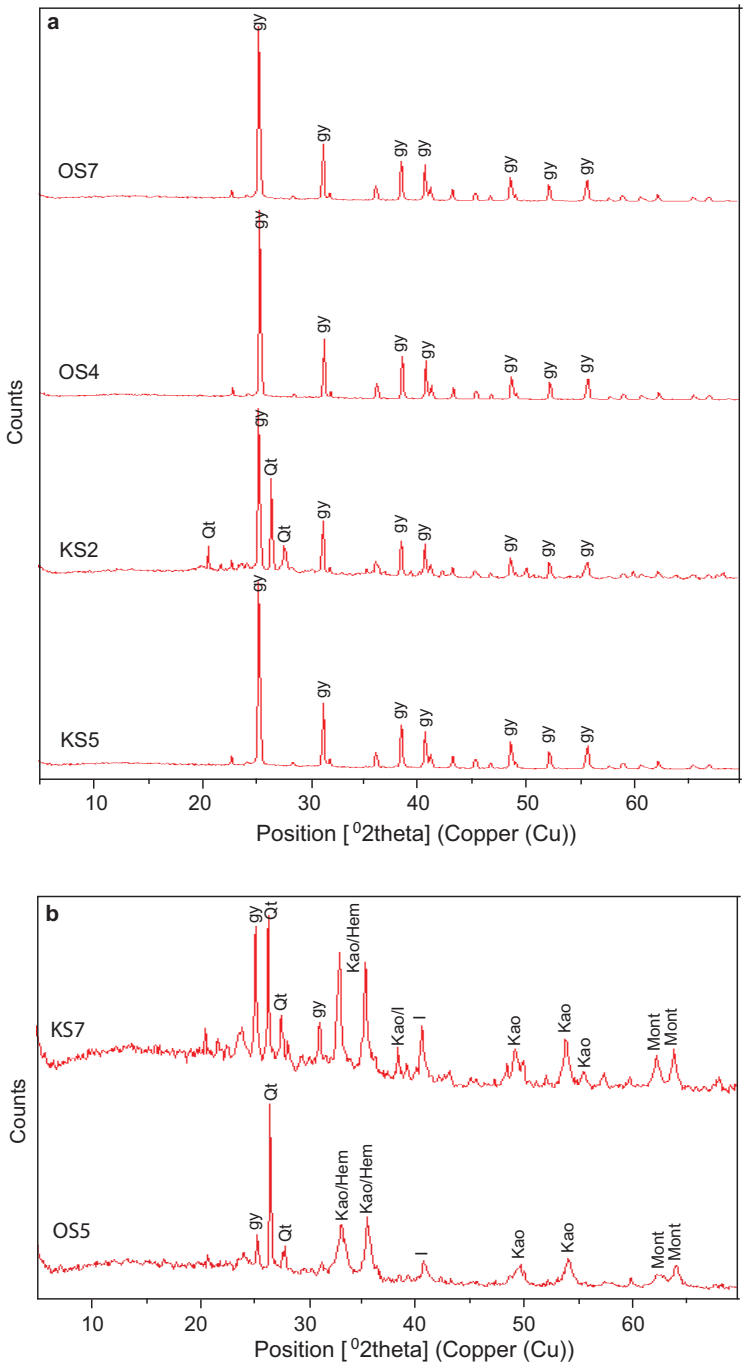

Figure 2.7: X-ray diffractograms for gypsum samples with characteristic peaks. (b) X-ray diffractograms for phyllosilicate samples with characteristic peaks. (Here gy represents gypsum, Qt represents quartz, Kao represents kaolinite, Hem represents hematite, I represents illite and Mont represents montmorillonite).

water loss during grinding (Eberl, 2003; Roy et al., 2003).

2.4.4 Laser Raman Spectroscopy and Fourier Transform Infrared

Multiple spectra were obtained for each mineral sample (KS2, KS4, OS4, and OS7) using 532 nm laser. It should be mentioned that the grain size of the powder was kept below 500 μm and orientation along with spot location were varying for the samples. Laser Raman spectroscopic results are presented with listed characteristic Raman peaks in the spectra in Fig. 2.8. For the samples, many grains were analyzed and the observed peaks were investigated to check for the consistency in the position of the mineral bands. Peak positions varied for few wavenumbers in most of the samples, but the Raman peak at 1009.75 cm^{-1} was constant. This shift in the band positions could be attributed to the non-uniqueness of results from the peak fitting routine or possibly due to slight compositional differences in the analyzed samples (White, 2008). Almost all the samples showed the same characteristic bands with appreciable intensity for each investigated spectrum. The Raman bands for the gypsum samples are mainly due to the vibrations within sulphate tetrahedral (SO_4^{2-}). The prominent Raman bands observed in the spectra are at 417.11, 496.06, 619.85, 673.46, 1006.75, 1009.75, ∼1137.44, ∼3403 and 3494.38 cm^{-1}. The most prominent Raman band at 1009.75 cm^{-1} is due to the symmetric stretching of SO_4^{2-} tetrahedra (ν_1 vibration). 417.11 and 496.06 cm^{-1} Raman bands are due to ν_2 vibration in-plane bending, 619.85 and 673.46 cm^{-1} Raman bands are due to ν_4 vibration, out of plane bending and Raman band at ∼1137.44 cm^{-1} is due to asymmetric stretching of SO_4^{2-} tetrahedra (ν_3 vibration) (White, 2008). The Raman bands observed in the form of a doublet at 3401.78-3405.68 cm^{-1} which are due to O-H stretching in the water incorporated into gypsum. Not many impurities were observed under the microscope and absence of fluorescence during the acquisition of Raman spectra also

showed the least/negligible existence of the impurities/trace elements/metals within gypsum.

Fig. 2.9 illustrates the FTIR spectra of the gypsum (OS4 and KS5) and phyllosilicate (KS7, OS5, KS1 and OS6) samples. The spectra of the samples OS4 and KS5 are practically identical denoting both the samples as gypsum. Comparison of acquired spectra with other published spectra helped in the confirmation and detection of optimum bands for gypsum (Farmer, 1974; Bensted, 1976; Stefov et al., 2000). The typical identified bands for gypsum are at 670, 1100, 1370, 1608, 1691, 2215, 3400 and 3506 cm^{-1}. The observed bands are due to stretching in water and SO_4^{2-} (asymmetric) molecules. The bands at 1608-1691 cm^{-1} and 3400-3506 cm^{-1} originate from H-O-H bending (due to correlation filed splitting) and the symmetric to asymmetric stretching in water molecule (Seidl et at., 1969; Cvetković et al., 1997; Stefov et al., 2000). Additional identified bands at 1100 and 2215 cm^{-1} are also well comparable with earlier published gypsum IR spectra (Stefov et al., 2000; Kiros et al., 2013). The band 670 cm^{-1} is attributed to asymmetric stretching vibration of SO_4^{2-} (Lane, 2007; Schiavon, 2007). The bands 800 and 1016 cm^{-1} are due mainly to the presence of kaolinite in the sample KS7, whereas other bands at 1608-1691 cm^{-1} and 3400-3506 cm^{-1} are due to vibrations in water molecule in gypsum. It also shows the bands at 3620 and 3694 cm^{-1}, which are due to inner hydroxyl stretch and OH stretching frequencies associated with the hydroxyl group in kaolinite. The band at $\sim$900 cm^{-1} is possibly due to presence of hematite in the sample KS7 (Gadsen, 1975). IR spectrum of OS5 shows the disappearance of bands at 900, 1691, 3400 and 3506 cm^{-1}, which are characteristic features of gypsum (apart from 900 cm^{-1} band, which is for hematite); the observed bands in the sample are at 800, 1016 cm^{-1} and a broad weak band at around 3400 cm^{-1} indicating kaolinite. Sample KS1 has the similar band pattern as that of OS6; only the 1100 cm^{-1} band is disappeared. Sample OS6 witnesses the presence of bands at 800, 1016, 1100, 1390, 1720 cm^{-1} and very shallow absorption band at 3694 cm^{-1}, which indicate more kaolinite content as the vibrations due to OH/HOH in 1600-1800 cm^{-1} and 3200-3600

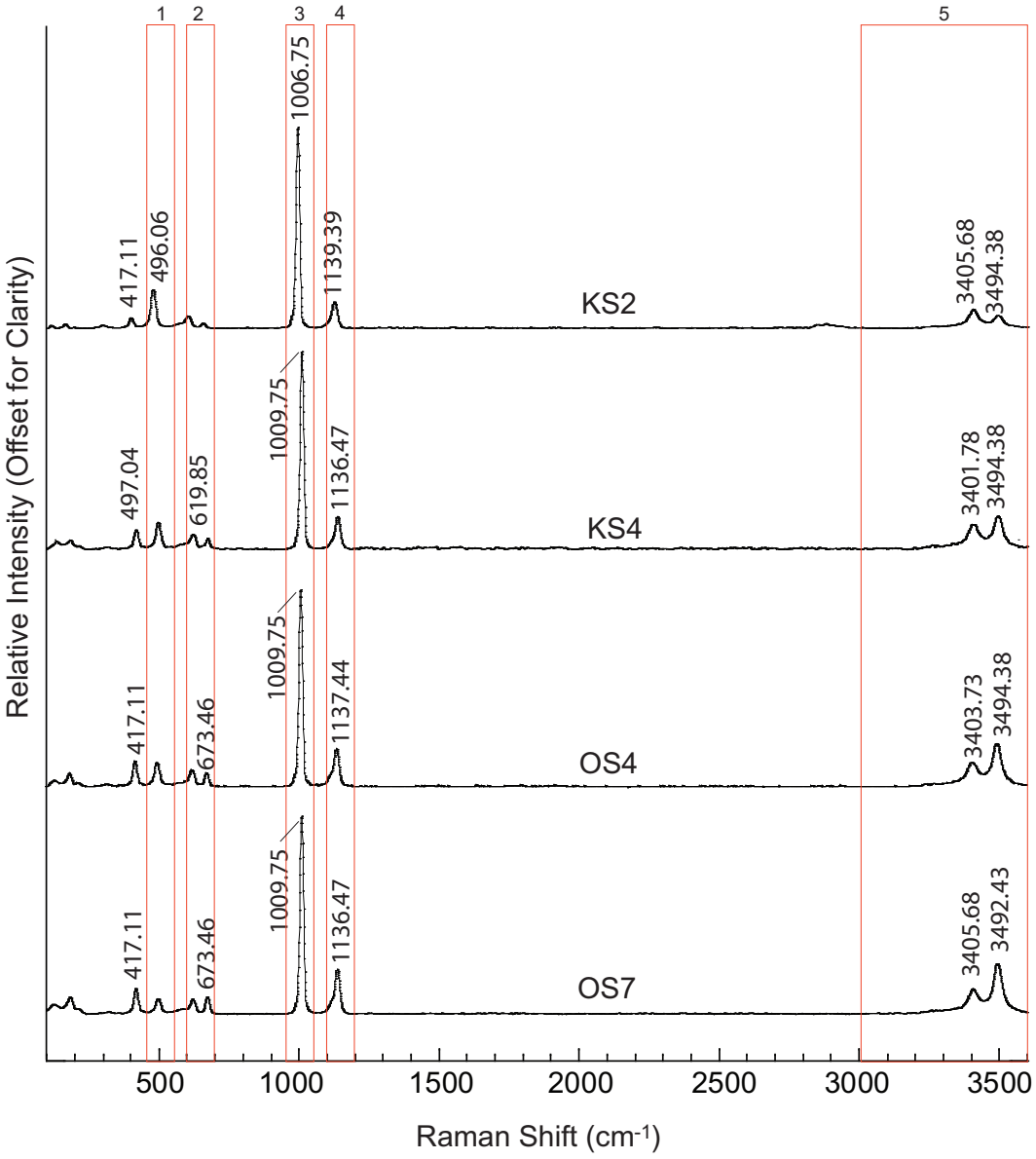

Figure 2.8: Raman analysis of gypsum samples namely KS2, KS4, OS4 and OS7 with mentioned characteristic peaks, where (1), (2), (3) and (4) represent SO_4^{2-} fundamental vibrations ν_2, ν_4, ν_1 and ν_3 respectively. (5) represents vibrations due to OH/H_2O in the range of 3000-3600 cm^{-1}.

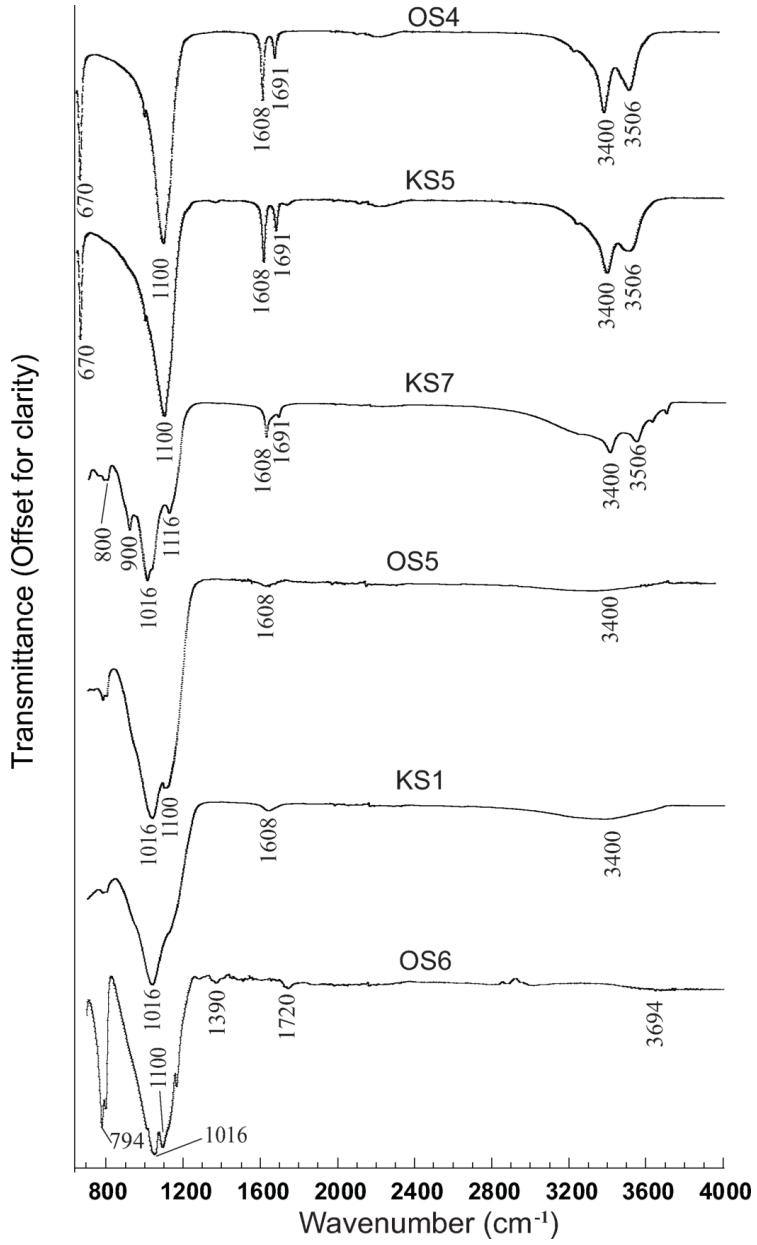

Figure 2.9: Fourier Transform Infra-red spectroscopic results of the samples OS4, KS5, KS7, OS5, KS1 and OS6, which show the characteristic features of gypsum, kaolinite, and hematite.

cm^{-1} region due to gypsum are shifted to 1720 and 3694 cm^{-1} respectively.

2.4.5 Fluid Inclusion characterization

Petrography

Fluid inclusions are present as clusters, trails and even in isolation (Fig. 2.10). Clusters of fluid inclusions are present within a single crystal bounded by a sharp grain boundary (Fig. 2.10a). Trails are following the trend of cleavage planes, fracture planes and grain boundaries (Fig. 2.10b). All the fluid inclusions are cylindrical in nature. In many gypsum grains, they are found in isolation, the possibility for their genesis is through trapping during the growth of the host (Fig. 2.10c and d). Clustered and trails of gypsum might have got incorporated into the system in later stage, after the crystallization of the host.

Laser Raman spectroscopic analysis

Gypsum is one of the common mineral found in sedimentary geologic setting as an evaporite/precipitate. It could easily be identified in the Raman spectroscopy by the characteristic Raman bands at 1135, 1008, 669, 613, 492 and 413 cm^{-1} (Fig. 2.11). Fluid inclusions are characterized by Raman analysis and the results have shown that all the inclusions are composed of water based on the Raman bands present after 3000 cm^{-1} (Fig. 2.12). Some fluid inclusions are composed of vapour as well as liquid water phase. Laser Raman has confirmed the vapour phase based on sharp peak at 3402 cm^{-1}. In some of the fluid inclusions, the peak after 3000 cm^{-1} is in the form of a triplet and designated for -OH in the composition. The Raman bands prominent for fluid inclusions composed primarily of water are at 3280, 3404, 3489 cm^{-1}.

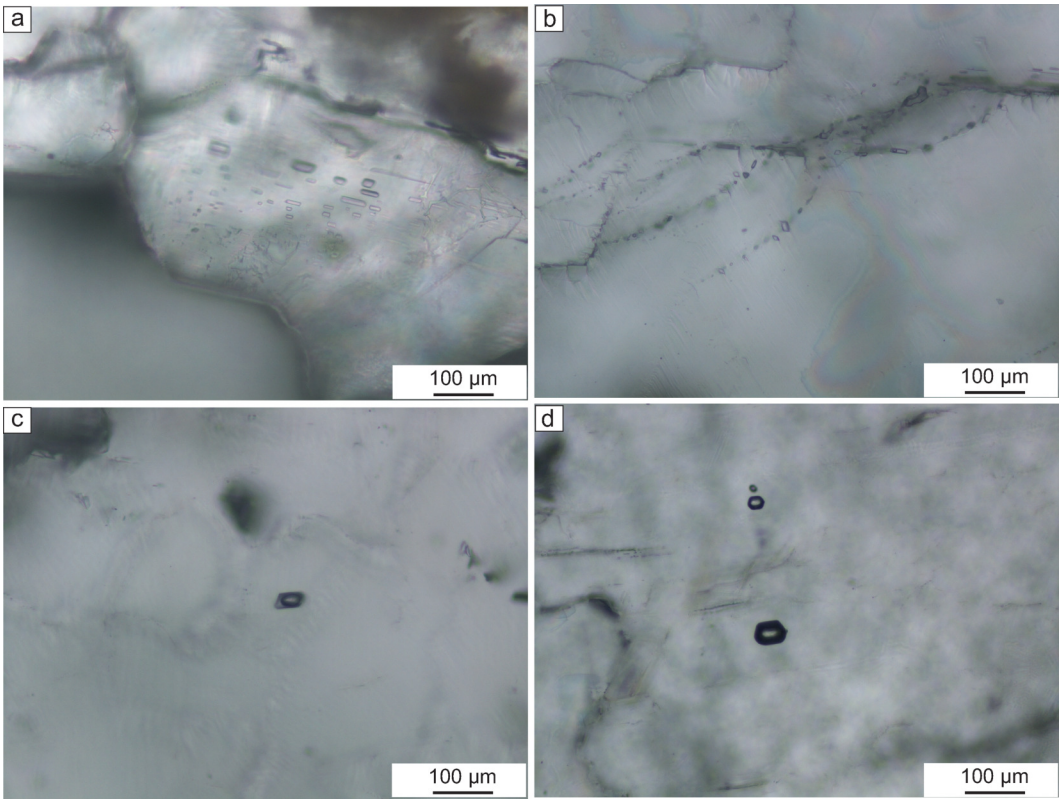

Figure 2.10: Petrographic analysis of fluid inclusions in gypsum. (a) Clusters of the fluid inclusions within a single grain of gypsum, (b) trails of fluid inclusions following fracture planes of the gypsum grain, and (c and d) isolated fluid inclusions within the grains.

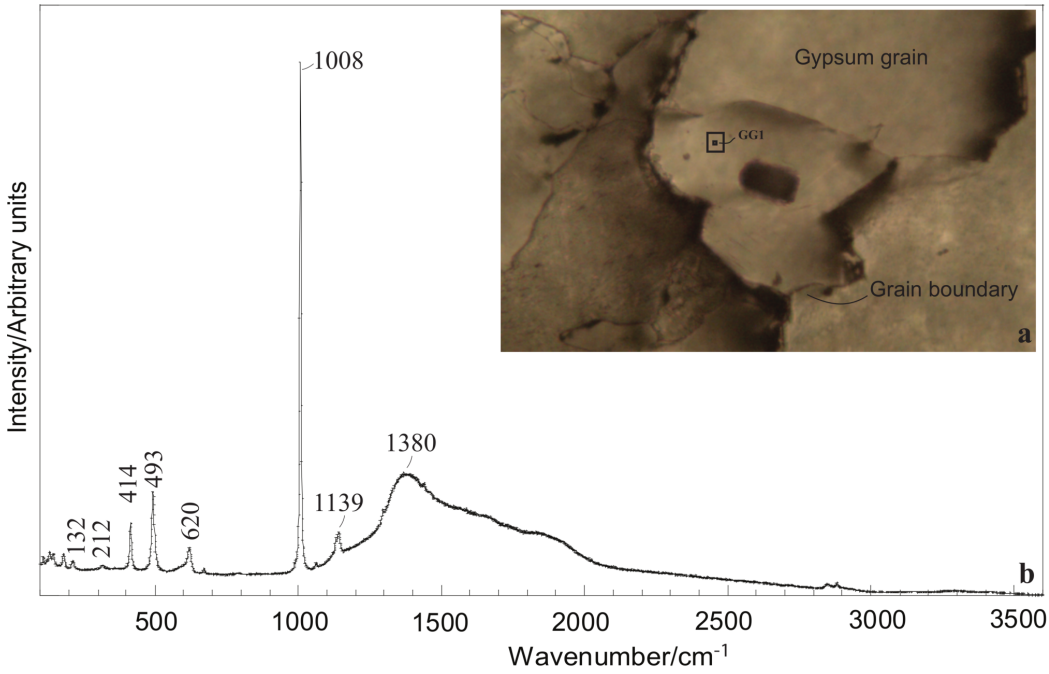

Figure 2.11: (a) Gypsum under microscope during Raman analysis, and (b) Raman spectra taken from the host mineral gypsum for background values.

Micro-thermometry

The change in gypsum-hosted fluid inclusions occurred during freezing run; include the changes in the wall-pattern and re-crystallization of new gypsum grains within the fluid inclusions. The first appearance of gypsum grain was noticed at -34.4^{o}C during the cooling stage which is consistent with the results reported by Vanko et al. (2005), where he has shown that most of the prismatic gypsum crystals appear between around -50 and 0 ^{o}C after several cycles of freezing and heating run. Newly formed gypsum crystal is again dissolved back into the inclusions at 116 ^{o}C which is consistent with the reported data in the literature (Tivey et al., 1998). Mostly the phase changes have been observed in trails where more number of inclusions could be seen together. Temperature of first ice melting (T_{FM}) and temperature of last melting (T_{LM}) was recorded in the range of -2.8 to -1.6 ^{o}C and -1.8 to -1.2 ^{o}C indicating low salinity of water fluid inclusions (below 0.5 wt.%). Very few inclusions have shown the temperature of last melting (T_{LM}) at -56.6^{o}C indicating the composition of

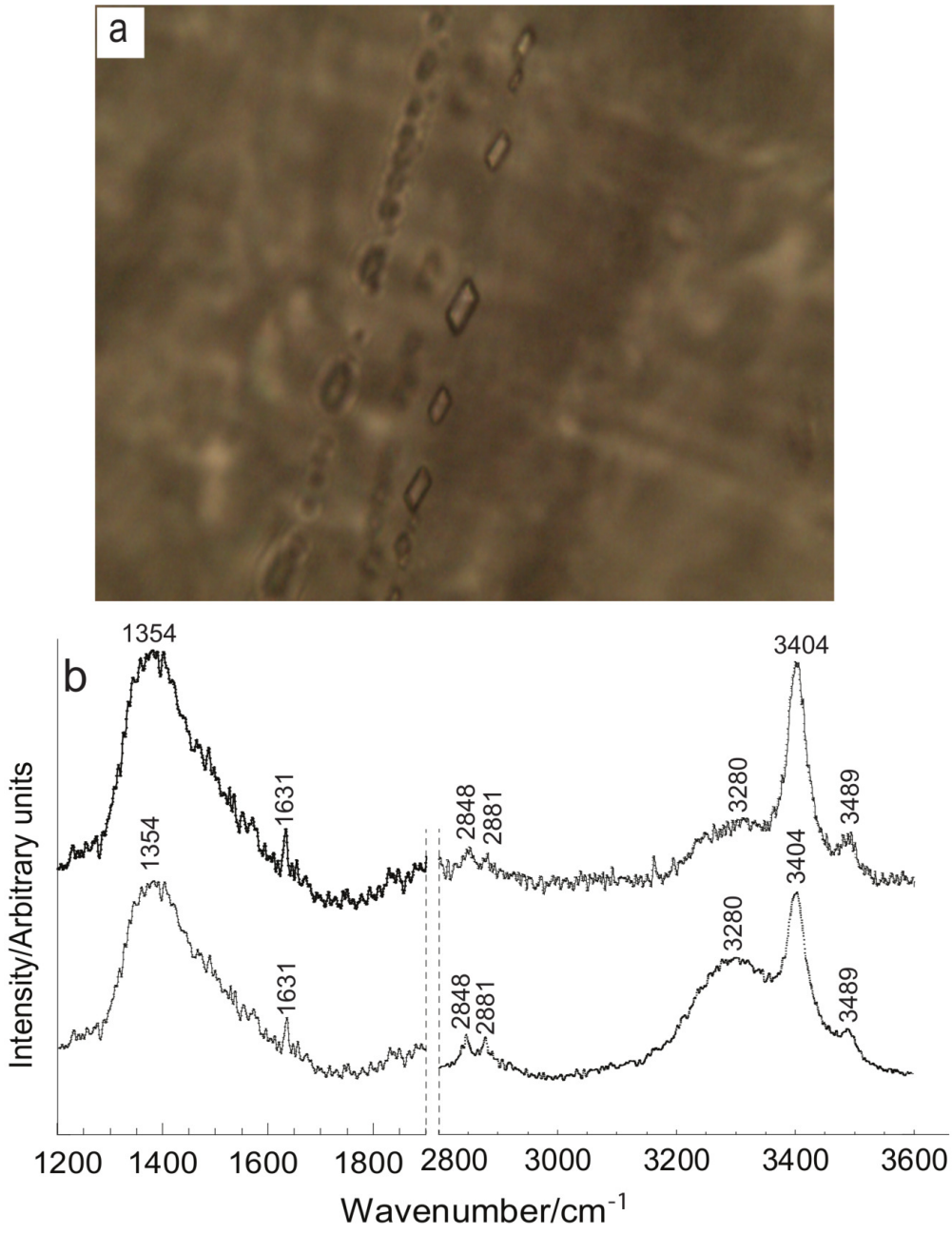

Figure 2.12: ((a) Monophase fluid inclusions within gypsum under microscope during Raman analysis, and (b) Raman spectra taken from the fluid inclusion in the range of 1200-3600 cm^{-1}.

the fluid as CO_2.

Micro-thermometric data can provide the significant information about the chemical properties of the fluids during the mineral precipitation and also about the palaeo-climate or subsequent events (Roedder, 1984). Garofalo et al. (2013) has determined the gypsum growth temperatures using monophase fluid inclusions. Though, many critical complications occur during the analysis such as the reaction between fluid inclusion and host, disturbing the trapped system from its original form etc.. For example, aqueous-carbonic inclusions in wollastonite back-react at lower temperature to produce calcite and quartz (Heinrich and Gottshalk, 1995).

2.5 Discussion

2.5.1 Interpretation of the acquired results

The data presented in the paper show the results from spectroscopic techniques namely VNIR, laser Raman and FTIR, which are proved to be powerful tools in identifying the mineral even when they are in minor quantity. The characteristic band positions obtained mentioned by spectroscopic techniques can be utilized for the identification of unknown similar composition minerals or mineral associates. All spectroscopic analyses have confirmed the composition of mineral veins/layers as gypsum and the associated groundmass as phyllosilicate. Absorption bands/peaks were used to identify the minerals in VNIR spectroscopy. Mostly hydrous sulphates and sheet silicates (here phyllosilicates) show the absorption bands between 1900 to 2500 nm. Secondary Fe-phases were identified using VNIR spectroscopic technique wherein the continuum removal and band-shape least squares algorithm were applied to obtain diagnostic Fe^{3+} absorption band in 400-1300 nm range in phyllosilicate samples. Identification of Fe^{3+} mineral phases using VNIR spectroscopy is

very obvious, as around 15.23 wt.% of $FeO_{(t)}$ content was measured in EPMA. These Fe-phases were confirmed by evaluating the XRD and FTIR analyses results either as hematite grains or coating/thin film of hematite over phyllosilicates. The distribution of Fe-pigmentation over phyllosilicates is irregular, and no correlation was observed in the field. Mixed gypsum and kaolinite sample have shown the peculiar absorption features mainly for gypsum with only absorption bands in 2100-2400 nm region due to kaolinite (Fig. 2.5c). The spectra have shown broader doublet absorption at 2200 nm and a narrow short absorption band at 2340 nm which is attributed to sheet silicates (mixed kaolinite and illite). Identification of sheet silicate kaolinite was confirmed by the VNIR spectra using 2160-2200 nm doublet absorption. Raman spectroscopy has also been proved to be a robust technique to identify the mineral phases in very extreme conditions such as hydrothermal vents along sea floor spreading ridges and cold seeps on ocean floor (Baker and German, 2004; White, 2008). Here, the technique is used in identifying the optimum wavenumbers where different vibrations excite for the minerals in consideration. There are several proposed mechanisms for the formation of fibrous gypsum veins in sedimentary rocks overlying evaporites and are summarized by Gustavson et al. (1994). These are (1) contraction of the host rock by dehydration (Richardson, 1920); (2) tectonism (Forbes, 1958); (3) force of crystallization (Taber, 1916; Halferdal, 1960); (4) hydraulic overpressure (Shearman et al., 1972); (5) hydration of anhydrite to gypsum (Stewart, 1979) and (6) subsidence due to dissolution of underlying evaporites (Goldstein and Collins, 1984). Usually, set of the mentioned mechanisms are responsible for the veined gypsum occurrences. At Karai, gypsum occurs as layers and veins in different geometrical settings. Subvertical-vertical fibrous gypsum veins occur in anastomosing network in phyllosilicate-rich groundmass. Fibrous gypsum layers and veins has cross-cutting relations, hence no general age relationship could be established indicating that both layers and subvertical-vertical veins were formed at the same time. Here, we propose that the fractures where gypsum precipitated, were formed due to the pressure or forces generated by crystal

growth/crystallization. Crystallization forces push the vein walls apart, resulting in antitaxial veins development (Taber, 1916, 1918). In this proposed mechanism, hydrofracturing/fluid overpressure (Wiltschko & Morse, 2001) is not an essential criterion, but would have taken part in vein propagation.

2.5.2 Implications to Mars

Based on the surface exploration and spectroscopic results from orbiters on Mars, gypsum in association with Fe/Mg phyllosilicates are deduced to be present on several locations, especially on the north polar regions (Langevin et al., 2005b; Massé et al., 2012). Additionally, gypsum has also been identified as one of the mineral constituent in the layered deposits of Juventae Chasma, Valles Marineris, Mars by OMEGA team (Gendrin et al., 2005). The gypsum deposits of Olympia Undae sand sea in north polar region of Mars are proposed to be formed as a result of evaporation, and or by direct alteration of high Ca sand dune grains, Fe-rich pyroxene and sulphide (Fishbaugh et al., 2007). The sulphate salts, underlained by the material of middle to late Noachian (Reider et al., 2004; Squyres et al., 2004a) in Meridiani Planum are detected to be ∼25 wt.% in concentration by MER *Opportunity* and are hypothesized to be formed by evaporation of fluids involved with weathering of basalts (Tosca and McLennan, 2006). The sulphate-rich sedimentary rocks of Endeavour Crater are widely explored by *Opportunity* and the results have shown the presence of phyllosilicates in crater rim (Squyres et al., 2006; Wray et al., 2009; Arvidson et al., 2011). The lithological sequence of Cape-York is suggested to be formed by the hydrothermal waters that altered basaltic crust to phyllosilicates and sulphates, and charged ground waters generated salt-rich sandstones are deposited widely over the areas in Meridiani Planum (Squyres et al., 2006). All of these major results and interpretations are made mainly based on analyzing the orbital data obtained from Mars through various inter-planetary missions.

With progressive missions to Mars, need of more sophisticated techniques

such as laser Raman spectroscopy for better detection and confirmation of surface mineralogy has been realized in recent past (Courréges-Lacostea et al., 2007). Spectroscopic techniques used in the present study have the potential to be utilized in detection of the group of the phyllosilicates and other associated minerals like hydrous sulphates. The obtained VNIR spectra have implications to the spectral data availed from OMEGA and CRISM datasets. In addition, Raman data for identified hydrous sulphate and phyllosilicate group of minerals could be utilized as database for the future extra-terrestrial missions. Petrography of crystalline gypsum revealed presence of biphase fluid inclusions in the weak planes/crystal defects, which are genetic waters got trapped during the precipitation of the host. Thus, the host could be utilized as the prime proxies to be looked into for the information regarding water chemistry for the hydrated planet, Mars. Despite proved Raman usefulness in characterizing fluid inclusions in terrestrial scenario, its utilization in such extraterrestrial conditions is far from imagination. Future research in this perspective should provide experimental set ups to meet with similar objectives.

Monophase fluid inclusions could be one of the pre-requisite to sustain flourish the life within the host as microbe-bearing cavities would have evolved from these inclusions (Parnell et al., 2004), which are identified in plenty here. Although, the sum of the conditions to start developing the microbial life within the mineral phases is yet not well known and is a topic of extensive research, but the microbial signatures are well identified within many hosts like halite, gypsum etc. (Parnell et al., 2004; Lowenstein et al., 2011). This research suggests that the sulphates (particularly gypsum) identified on Mars could be one of the potential target to be looked for any preserved signature of life.

2.6 Conclusions

The study focuses on the characterization of gypsum-phyllosilicate association of Tiruchirapalli, South India by petrography, XRD and other traditional spectroscopic techniques, namely VNIR, Raman and FTIR. Use of these sophisticated analytical techniques proved to be an efficient way to identify the minerals (here gypsum, kaolinite, quartz, hematite etc.) even if they are in smaller quantities. Obtained results offer detailed description of the peculiar bands for the identified minerals from VNIR, Raman and FTIR spectroscopic techniques. In particular, Raman bands for the identified minerals in the study will provide the database for the future studies in the similar domain. The spectra yield abundant information regarding the compositional variations. The VNIR spectroscopic results can be used to aid both interpretation and ground-truthing of remotely sensed data. Using combination of mentioned techniques will greatly enhance the accuracy of detection of various minerals on the planetary surfaces such as Mars. XRD is identified as a robust way of identification of minerals and their crystallinity and have been very useful in the confirmation of the mineralogy here. Here, the investigation of gypsum-phyllosilicate association by using mentioned spectroscopic techniques has the scope to be applied to identify the high to low concentration and other similar chemical composition minerals on Mars. The veined gypsum deposits of Karai Shale Formation are suggested to be formed by hydro-fracturing mechanism. Gypsum in the area possesses well preserved fluid inclusions and small cavities. Study area represents the temperature around 30^{o}C for most of the months in the year with minimum precipitation and heavy dry winds throughout the year. These conditions would have caused least damage to the host and fluid inclusions, hence preserving the pristine conditions of its formation. Petrography has revealed several microtextures preserved in the gypsum in the form of dislocations, microcracks and growth of secondary gypsum at deformed places and near fluid inclusion. This represents that geological processes has disturbed the deposit after its crystallization. This may have changed/modified the chemical

composition of fluid inclusions where these microtextures have been observed. Many of the fluid inclusions which are found in isolation within the crystal, probably would have preserved the primary chemical composition. Laser Raman analysis has shown that all fluid inclusions belong to -OH group/water either in liquid or vapour form. In addition, micro-thermometric analysis have shown the changes in shape and/or movement within the inclusion and indicated the gaseous component as CO_2 in few inclusions.

CHAPTER 3

Spectral characteristics of banded iron formations in Singhbhum craton, eastern India: Implications for hematite deposits on Mars

Preclude

This chapter defines the spectral characteristics of banded iron formations of Joda and Daitari located in Singhbhum craton in eastern India to check its potentiality as an analog to the aqueous/marine environment on Mars. Spectral investigations have been conducted in VIS/NIR region of electromagnetic spectrum in the laboratory conditions. Optimum absorption bands identified include 0.65, 0.86, 1.4 and 1.9 μm, in which 0.56 and 0.86 μm absorption bands are due to ferric iron and 1.4 and 1.9 μm bands are due to OH/H_2O. To validate the mineralogical results obtained from VIS/NIR spectral radiometry, laser Raman and Fourier transform infrared spectroscopic techniques were utilized and the results were found to be similar. The optimum bands identified for the minerals using various spectroscopic techniques can be used as reference for similar mineral deposits on any remote area on Earth or on other hydrated planetary surfaces like Mars.

3.1 Introduction

Banded iron formations (hereafter BIFs), reported over all continents in association with Precambrian greenstone belts, are defined as chemical sedimentary rocks with alternate layers (varying thickness) of iron oxides (magnetite and/or hematite) and silica (jasper, quartz and chert) (Cloud, 1973; Gross,

1980; Melnik, 1981; Klein, 2005; Polat and Frei, 2005 and references therein). They are formed mainly by sedimentation processes in which water plays a major role in deposition during the time span of Archean to Proterozoic epochs (Klein, 2005). The formation processes (seasonal/ microbial?) of various layers and the mechanisms for oxidizing Fe (possibly microbial) are still highly debated (Posth et al., 2010). Deposition of BIFs in ocean basins are the result of oxidation of reduced Fe, either generated through continents or by hydrothermal fluids. BIFs have also found their significance as a major rock unit to explain related sea water chemistry and the evolution of lithosphere-biosphere-atmosphere in terrestrial conditions (Klein and Beukes, 1989; Derry and Jacobsen, 1990; Kaufman and Knoll, 1995; Rao and Naqvi, 1995; Johnson et al., 2003, 2008; Trendall and Blockley, 2004). Systematic chemical studies of representative iron phases from BIFs provide significant information about thermal regime of host basin, the redox conditions of deep ocean water and the source of Fe and other elements (Holland, 1973; Klein and Ladeira, 2004; Bhattacharya et al., 2007; Frei and Polat, 2007; Pecoits et al., 2009). Higher concentrations of Ti, V, Cr, Mn and Ni provides the clues regarding the influx of high-temperature metalliferous hydrothermal brines produced from rock water interaction in the spreading related mafic-ultramafic oceanic crust and or mixing of mafic-ultramafic debris derived from weathering of oceanic crust. These parameters make BIFs a good proxy to be considered for planetary studies. Presence of BIFs has been speculated on Mars based on the identification of extensive layered hematite and hydrothermal silica rich deposits (Christensen et al., 2000, 2001a; Squyres et al., 2008; Ruff et al., 2011; Bost et al., 2013). Crowley et al. (2008) studied the diversity of spectral signatures of terrestrial BIFs in detail and proposed the implications for the identification of similar type of deposits on Mars. The well preserved sedimentary structures with least deformation, unmetamorphosed deposit (except few local thermal metamorphic effects) and extensively mined areas to get samples devoid of any atmospheric effects are some of the features of BIFs which make them suitable candidates for terrestrial analogs for the interpretation of the regional evolu-

tion of hematite deposits and palaeo-environments on Mars (Christensen et al., 2000, 2001a and b; Hynek et al., 2002; Ormo et al., 2004; Glotch and Christensen, 2005). Several studies have been carried out with the BIF samples of Lake Superior (Canada) and Carajas (Brazil) to interpret the formation conditions of regional hematite deposits on Mars (Christensen et al., 2000, 2001a; Fallacaro and Calvin, 2006; Bridges et al., 2008). Spectral signatures along with preliminary geochemical results of these BIFs have been utilized to interpret the sites as potential Martian analog sites. The BIFs of these two areas along with BIFs from Coppin Gap Greenstone Belt, Pilbara craton, Australia, were listed in the International Space Analog Rockstore (Bost et al., 2013).

Mars surface has been marked with the widespread layered hematite deposits and other FeO-OH polymorphs (Fe-oxides and Fe-(oxy-)-hydroxides), mainly in Meridiani Planum, Aram Chaos, and Valles Marineris regions (Christensen et al., 2000, 2001a, 2004). Layered hematite deposits of Meridiani Planum on Mars are proposed to be of sedimentary origin due to absence of any volcanogenic geomorphic features such as lava flows and fissures. Many authors have discussed the formation mechanism of the layered hematite deposits, but climatic conditions during their formation are yet to be studied in detail. Bridges et al. (2008) proposed that Carajas BIFs, formed as a supracrustal sequence at lower temperature (Dalstra and Guedes, 2004) are suitable to interpret the ancient marine environments on Mars and the spectral data in VIS-NIR-SWIR-TIR region would aid in identifying similar deposits on Mars. Therefore, detailed characterization of different BIFs in terrestrial environments will sequentially improve the superiority of our understanding for identifying mineralogical composition of the planet and its evolutionary history. Though, there are several occurrences of banded iron formations in India (Radhakrishna and Naqvi, 1986), studies considering them as analog sites are not yet initiated (Singh et al., 2015). Banded iron formation of Singhbhum craton in eastern India has long been discussed as geochemically similar to Lake Superior type BIFs. These BIFs are comparable to those BIFs in Carajas (Brazil), Finland and Australia (Majumder et al., 1982). This study

provides the results from VIS/NIR radiometry, back scattered image interpretation, laser Raman and ATR-FTIR (Attenuated total reflectance- Fourier transform infrared) spectroscopy which helped constrain spectral aspects of BIF of Singhbuhm craton and it will add the information to our understanding about the regions with similar mineralogy in extraterrestrial conditions. Laboratory VIS/NIR radiometry and laser Raman measurements of these rocks will contribute in better detection of similar rock types on Mars. On this context, the study of Precambrian BIFs in relation to Martian hematite deposits could be significant to have a better understanding on the palaeo-environmental conditions. The optimum bands identified for hematite and goethite can be used as a reference for unidentified similar mineral deposits for future extraterrestrial missions.

3.2 Regional geology, sample description and analytical methods

The Singhbhum-Odisha craton forms a triangular crustal block, bounded by Chotanagpur gneissic complex to the North, eastern Ghat Granulite belt to the South and the Bastar craton to the West and by recent alluvium to the East (Saha and Ray, 1984; Misra, 2006). This craton consists mainly of granitoid rocks, metasedimentary (Iron Ore Group), meta-volcanic schists and granites (Mahalik, 1987; Saha, 1994; Mazumder, 2005; Misra, 2006; Mukhopadhyay et al., 2006). The BIFs of North Odisha are extensively developed supracrustals encircling the Singhbhum granite complex and various views have been proposed on the evolution of these supracrustals and their relation to the granite intrusives (Fig. 3.1). Jones (1934); Dunn (1940) and Saha (1994) believed that all the BIFs were formed as a single assemblage during the Archean underlain and/or intruded by the different phases of Singhbhum granites. According to Saha (1994), the age of formation could be between 3.3 and 3.1 Ga. Iyen-

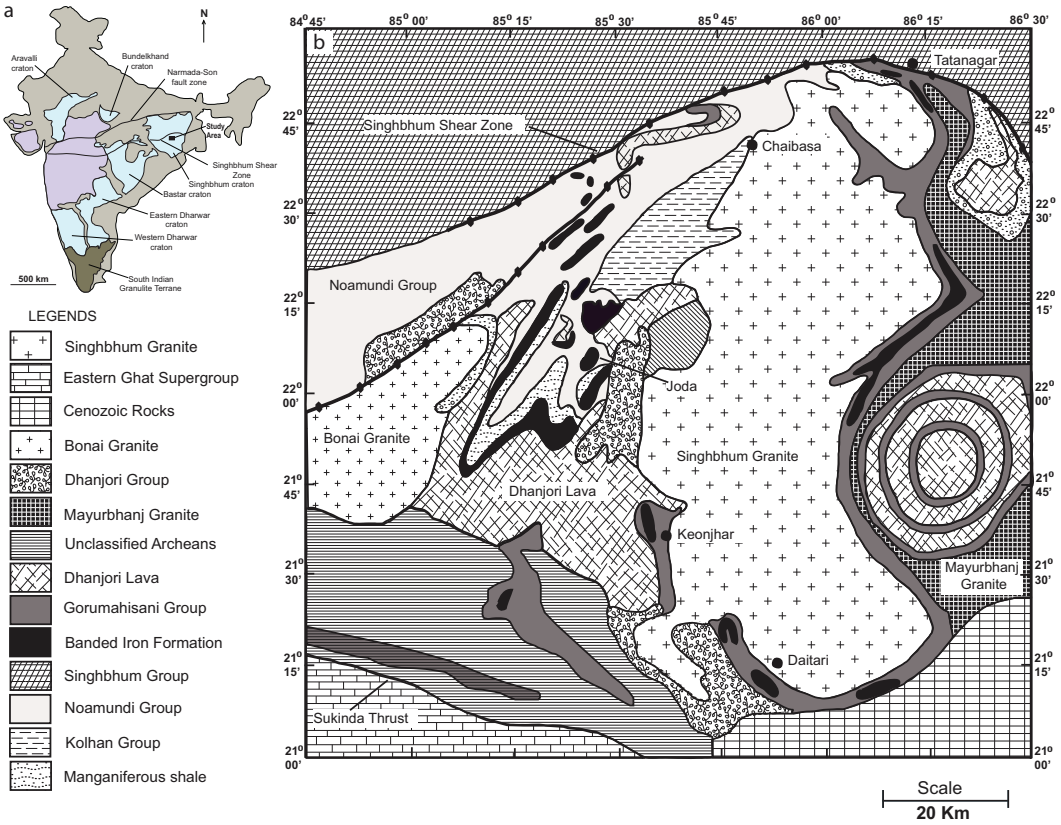

Figure 3.1: (a) Generalized tectonic map of India (modified after French et al., 2008). (b) Generalized geological map of iron ore deposits, Singhbhum craton, Odisha, India (modified after Roy and Venkatesh, 2009).

gar and Banerjee (1971); Banerji (1974, 1975, 1980) and Iyengar and Murthy (1982) classified BIFs into two distinct age groups; older (Gorumahisani group) and younger (Noamundi group). Prasad Rao et al. (1964) and Acharya (1976, 1984) has categorized the BIFs into three distinct stratigraphic formations, the oldest around Pallahara and Gorumahisani, the intermediate at Daitari and the youngest at the Joda-Koida region. The youngest one contains rich deposits of iron and manganese ores and forms a horse-shoe shaped synclinal structure (Jones, 1934). Relatively younger metasedimentary deposits of banded iron formations of Joda and Daitari region have two types of mineral assemblages: first, banded hematite jasper and second, banded hematite quartzite. These BIFs are conspicuous by the presence of alternate bands composed predominantly of iron oxide and silica. Secondary hematite formed after metamorphism, is generally found in the form of bladed crystals, specular variety called specularite whereas silica is of cryptocrystalline type, admixed with iron oxide dust and granules in jasper to mega quartz. The extensive volcano-sedimentary sequences in the Simlipal and Keonjhar plateaus are considered equivalent to the Dhanjoris and younger to BIFs by Saha and his associates, while others (Prasad Rao et al., 1964; Iyengar and Banerjee, 1971; Banerji, 1974) found them sandwiched between BIFs. The extensive lava flows designated as Malangtoli Lava, occur between Malangtoli and Pallahara, and underlie the undeformed Kolhan sequence of the area (Saha, 1994). The age of volcanics and the volcanosedimentary sequences in the North Odisha craton is early Proterozoic (Saha, 1994). The U-Pb SHRIMP Zircon age of the Dacite Lava of the Southern Iron Ore Group (volcanice-BIF-ultramafic) in Singhbhum craton is estimated to be 3.51 Ga (Mukhopadhyay et al., 2008).

The spatial view of the study areas, Joda from Noamundi-Jamda belt and Daitari from Tumka-Daitari belt is clear from Fig. 3.2. The field observations confirm the presence of BIF (Fig. 3.3a), conglomerate (Fig. 3.3b) and massive chert (Fig. 3.3c) occurrences in the areas.

Systematic sampling was done during the field work for further laboratory

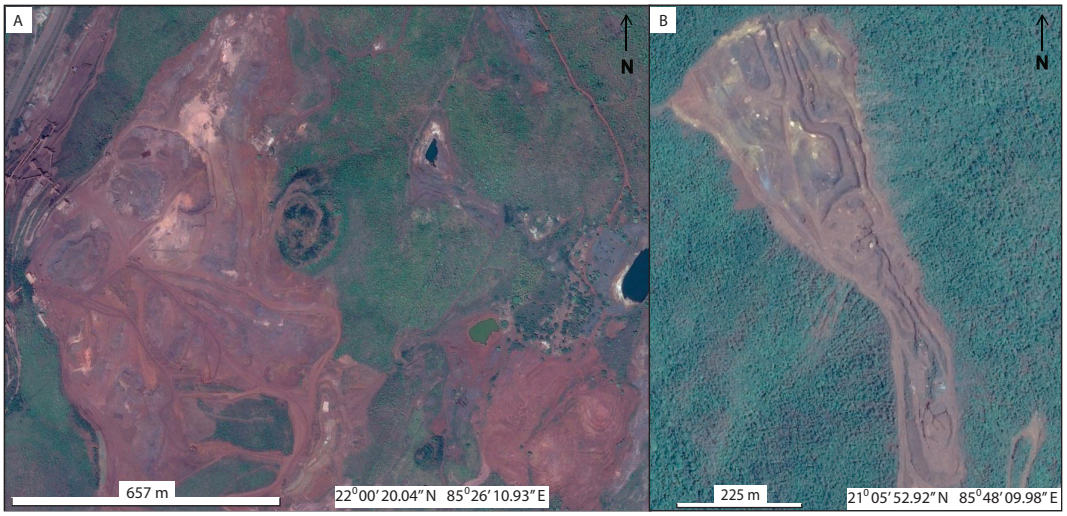

Figure 3.2: Stepped landscape feature exposed on the surface, and developed due to mining in Joda and Daitari respectively as obtained from Google Earth.

analyses. The samples collected from the study areas, Joda and Daitari, in Odisha have been characterized by VIS/NIR, Raman and FTIR techniques. Freshly cut surfaces were used for VIS/NIR spectra acquisition. Hyperspectral signatures (VIS/NIR) of the BIF samples (hand-specimen and powders of 500 μm) were collected using ASD FieldSpec3 spectroradiometer in the wavelength range of 0.35 to 2.5 μm. The fiber optic cable along with the gun holding it was mounted on the tripod at nadir position. Spectral signatures were collected in a controlled laboratory dark room environment. In another tripod, a tungsten filament halogen lamp with the wavelength range of 0.4 to 2.5 μm was used as artificial light source for spectral data collection. Spectralon, the standard white reference panel was used for measurement of irradiance for each set of measurement. The collected spectra were processed and then matched with the reference spectra available in USGS (United States Geological Survey) spectral library to confirm the minerals present in the samples. Spectral Feature Fitting (SFF) and Spectral Angle Mapper (SAM) techniques have been used to match the unknown spectra from the Joda and Daitari region of Odisha to the standard reference from USGS spectral library.

The polished thin sections were studied for petrography and further ana-

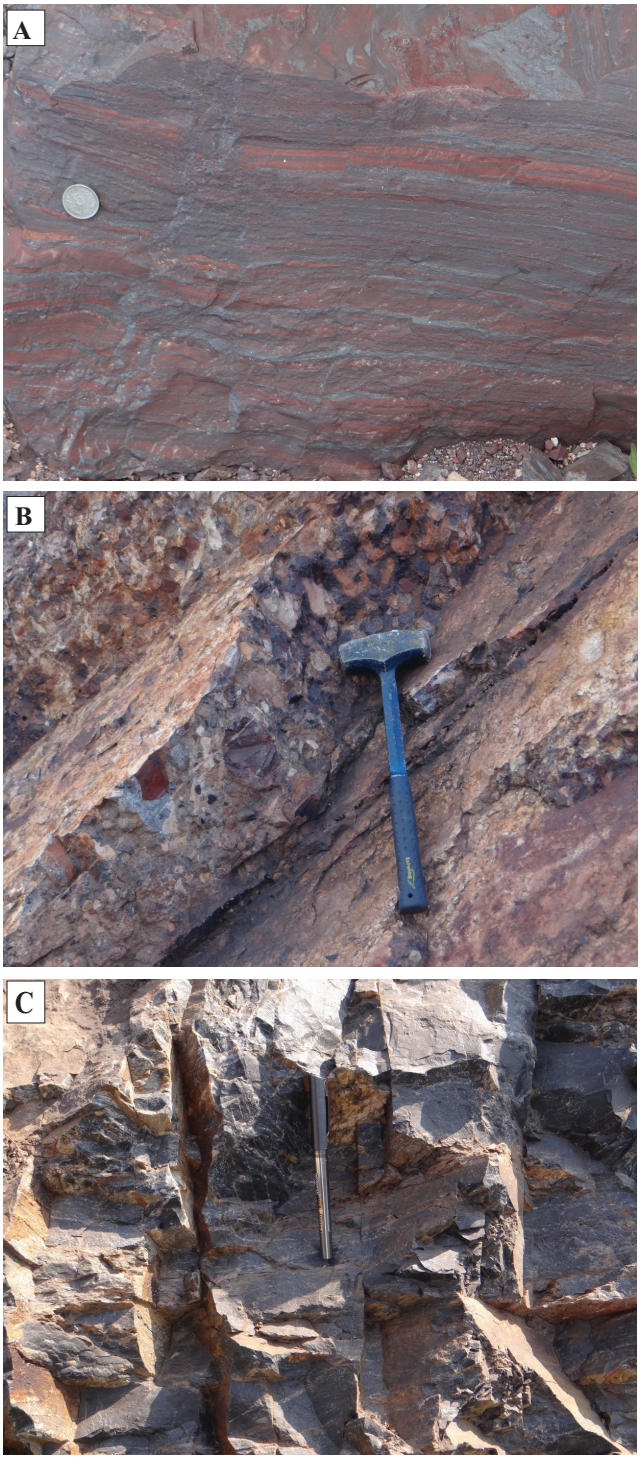

Figure 3.3: Field photographs illustrating (a) gray hematite and reddish jaspilitic chert, typical in banded iron formation, (b) conglomerate having iron rich matrix and boulders of chert/jasper, (c) black massive chert.

lyzed using SX-100 Electron Microprobe Analysis housed in Physical Research Laboratory, Ahmedabad, India. The analytical conditions were: current of 30 nA and voltage of 15 kV for hematite, magnetite, specularite and jaspilitic chert, and a current of 10 nA and voltage of 12 kV for chamosite. Silicate and oxide standards were used for calibration of the samples.

Laser Raman Spectroscopic analysis of BIF samples was conducted on a laser Raman spectrometer at Indian Institute of Science (IISc), Bangalore, India. Laser Raman spectrometer at IISc equipped with a SPEX double monochromator, an intensified CCD and 2 ns pulsed ND-YAG lasers with frequency doubled output was used for analysis.

The infrared spectroscopic data was obtained by means of a Fourier Transform Infrared spectrometer with an attenuated total reflectance accessory (FTIR-ATR) housed at Indian Institute of Space Science and Technology (IIST), Thiruvananthapuram, India. The spectra were collected with the PerkinElmer's Infrared (FTIR & IR) spectrometer using fine powders of samples. The powders were pressed at 55 to 60 kb. The infrared (IR) spectra were recorded immediately after the separation of the sample powder from the bulk sample. Spectra were collected in 700 to 4000 cm^{-1} range with an optical resolution of 0.5 cm^{-1} and wavelength precision of 0.01 cm^{-1} at 220 V, 50 Hz power supply. A baseline correction was made before interpretation of the data.

3.3 Results

3.3.1 VIS/NIR Spectra

The spectral characteristics of the samples were studied to specify the characteristic absorption bands for different minerals in BIFs. It has been observed that the spectra of the samples (Hem_J011 and Goe_J017) from Joda and

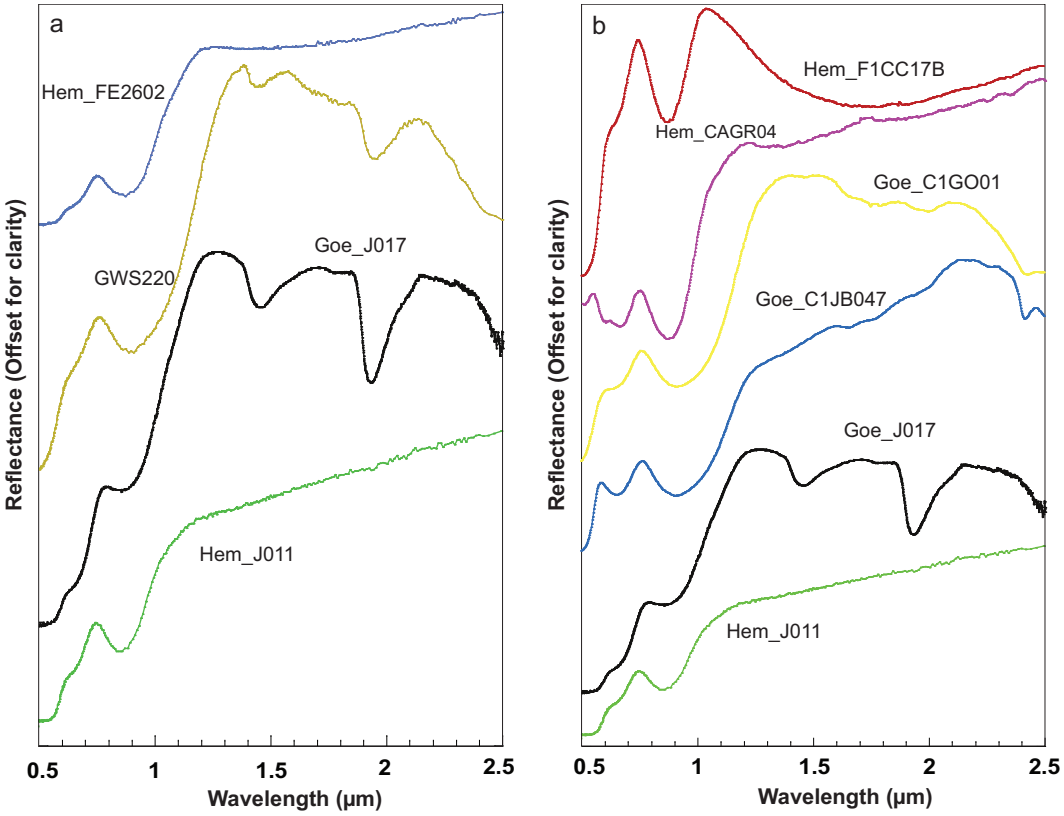

Figure 3.4: (a) VIS/NIR laboratory spectra of the samples Hem_J011 and Goe_J017 of Odisha BIFs along with the USGS spectral library spectra with the sample names Hem_FE2602 and GWS220 (Source: http://speclab.cr.usgs.gov/spectral). (b) VIS/NIR laboratory spectra of BIF samples Hem_J011 and Goe_J017 along with the CRISM spectral library spectra (with the sample names Hem_F1CC17B, Hem_CAGR04, Goe_C1GO01 and Goe_C1JB047).

Daitari, Odisha are found to match with the spectra of hematite and goethite minerals of USGS spectral library (mineral ID Hem_FE2602 and GWS220) (Fig. 3.4a). The spectra of the sample Hem_J011 shows the characteristic absorption features at 0.65 (weak) and 0.86 μm (strong) which are basically due to strong iron-oxygen charge transfer absorption and electronic band related to crystal field transitions in ferric iron respectively (Thangavelu et al., 2011). The representative spectrum of hematite is devoid of any absorption after 1 to 2.5 μm, but has a moderate increase in the reflectance in the region. Sample Goe_J017 has shown the spectral signature with typical absorption bands at 0.65 (weak), 0.86 (strong), 1.4 (strong) and 1.9 μm (strong), in which 0.65 and

0.86 μm are due to strong iron-oxygen charge transfer absorption and electronic band related to crystal field transitions in ferric iron and 1.4 and 1.9 μm are due H_2O and OH/H_2O respectively. Presence of hydrous absorption bands in VIS-NIR spectra confirms the existence of goethite in these samples. The spectra of samples Hem_J011 and Goe_J017 have been compared with the CRISM (Compact Reconnaissance Imaging Spectrometer for Mars) spectral library spectra of 4 samples (Hem_F1CC17B, Hem_CAGR04, Goe_C1GO01 and Goe_C1JB047) for the assessment of the differences/similarities in the spectral signatures (Fig. 3.4b). A careful investigation on the spectral signatures of hematite from present study (Hem_J011) and spectral library spectrum (Hem_F1CC17B and Hem_CAGR04) revealed that the spectral signatures of Hem_J011 and Hem_CAGR04 are similar with a minor variation in the absorption pattern in 0.5-0.8 μm wavelength regions. This difference in the absorption pattern can be attributed to the compositional variations of iron oxides in the samples. Apart from this variation in the spectrum in this region, there are no other visible differences in both the spectra. CRISM spectral library spectrum of the sample Hem_F1CC17B shows similar absorption pattern to the sample Hem_J011 spectrum in the 0.5 to 1 μm wavelength region whereas a prominent difference is being observed in 1 to 2.5 μm region. The difference is a huge sag centered at around 1.6 μm in the spectral library spectrum Hem_F1CC17B, whereas no such feature is observed in the spectrum of hematite present in the sample Hem-J011 from the study area. Spectral signature of Goe_C1GO01 and Goe_C1JB047 from CRISM spectral library are found to be matching well with the spectrum of Goe_J017 from the study area. The representative spectra show absorption bands at 0.65 (weak), 0.86 (strong), 1.4 (weak for CRISM spectral library spectra and strong for samples from present study) and 1.9 μm (weak for CRISM spectral library spectra and strong for samples from present study), and these absorption bands assignment is same as in the earlier described text. Additionally, CRISM spectral library spectra of Goe_C1GO01 and Goe_C1JB047 show weak and narrow absorption at 2.4 μm, which is typical to the OH bond in water. Summary

Table 3.1: Summary of the absorption bands identified in the samples from BIFs in Singhbhum craton, USGS mineral spectral library and CRISM spectral library. X indicates that these absorption bands were observed in the spectral signature.

Identity	Study area		USGS Spectral library		CRISM Spectral Library				
Sample Name	Hem _J011	Goe_ J017	Hem _FE2 602	GWS 220	Hem_ F1CC1 7B	Hem_ CAG R04	Goe_ C1G O01	Goe_ C1J B047	Assignments
0.65 μm	X	X	X	X	X	X	X	X	Ferric ion
0.85 μm	X	X	X	X	X	X	X	X	Ferrous ion
1.4 μm		X		X				X	OH/H_2O
1.9 μm		X		X			X	X	OH/H_2O
2.4 μm							X	X	OH/H_2O

of the absorption bands detected in the samples from present study, USGS mineral spectral library and CRISM spectral library are given in Table 3.1.

3.3.2 Petrographic studies

Mineralogical studies of Joda and Daitari BIFs revealed that they consist of hematite, magnetite, specularite and jaspilitic chert. Alternate bands of hematite and jaspilitic chert have been observed (Fig. 3.5). Contacts between the microbands of hematite and jaspilitic chert are usually sharp, with more transition towards low hematite (Fig. 3.5a, b).

Hematite microbands are comparatively thick, mainly consist of hematite grains (in high proportion), and large grains of magnetite and specularite. Jaspilitic chert band comprises mainly quartz grains with some large distorted grains of hematite. Quartz veins of varying thickness are present intruding alternate bands of hematite and jaspilitic quartz (Fig. 3.5b). Chamosite, a hydrous aluminum silicate of iron, is also present in very small amounts. The iron-rich layer is mainly composed of hematite grains with different textures.

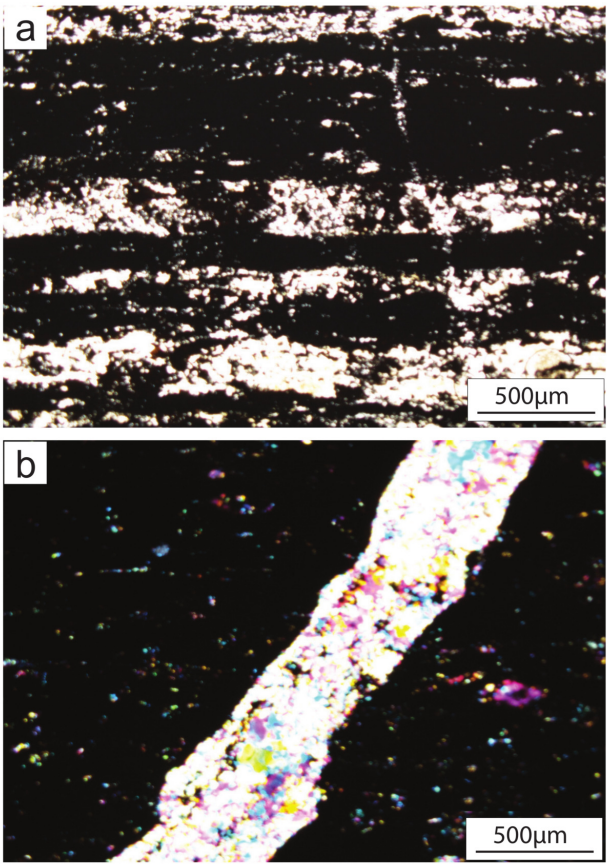

Figure 3.5: (a) Photomicrographs of finely laminated BIFs where iron-'rich' microbands are defined by hematite and/magnetite, interbedded with occasional pure chert micro-layers and (b) prominent microbands of hematite and interbedded light colored chert along with the micro-intrusion of quartz vein.

Massive anhedral aggregates of hematite and xenomorphic hematite crystals are common (Fig. 3.6a, b). Sporadic distribution of relatively larger hematite grains is conspicuous. Quartz veins are also marked with the presence of hematite crystals (Fig. 3.6c). Mostly, platy specularite aggregates are found associated with the jaspilitic chert microbands rather than hematite rich layer (Fig. 3.6d). Chamosite is found associated with platy specularites. Specularite, also called gray hematite, is mainly found in the form of platy crystals in the groundmass of fine grained hematite. A very small amount of magnetite is present in the hematite rich layers. Jaspilitic chert occurs inter-bedded with Fe-rich microbands.

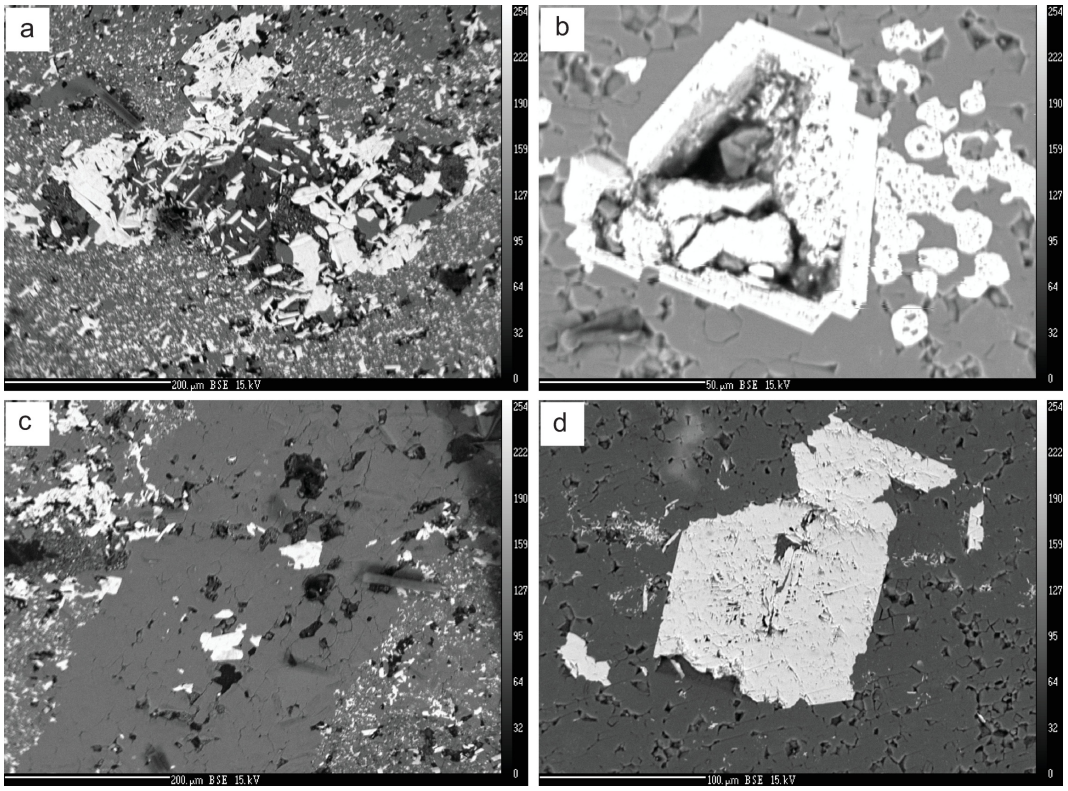

Figure 3.6: Back scattered electron images illustrating various textures of studied BIFs: (a) finely crystallized laths of hematite, (b) cryptocrystalline specularite, (c) quartz vein with hematitic inclusions and (d) a single large grain of specularite.

3.3.3 Laser Raman spectra

Laser Raman spectra of characteristic minerals are presented in Fig. 3.7. The main phases identified using laser Raman spectroscopic technique include quartz and hematite; observed Raman peaks at 142, 209, 353, 469 and 1160 cm^{-1} correspond to quartz (Fig. 3.7a, b, and c) and 224, 291 and 1315 cm^{-1} correspond to hematite (Fig. 3.7d and e) in accordance with the literature (Shebanova and Lazor, 2003).

Raman spectral quality depends mainly on grain size; therefore it is necessary to take into consideration the crystallinity/grain size of the samples. Hematite, the main crystalline mineral in oxide group is considered as a strong Raman scatterer, gives strong peaks in 210-294 cm^{-1} region, mainly due to translational movements of Fe. Apart from these Raman peaks of hematite, one moderate peak has also been observed at 1315 cm^{-1} (Fig. 3.7f). Presence of goethite is clear in the samples with the VIS-NIR analysis, but no prominent peaks are observed in the Raman spectra, a broad peak is observed in the form of a doublet at 386-412 cm^{-1} in which 386 cm^{-1} peak corresponds to goethite (Fig. 3.7c and d). Magnetite is recognized as a minor phase and identified by the typical Raman peak at 670 cm^{-1} (Fig. 3.7f).

3.3.4 ATR-FTIR spectra

The average of 6 collected spectra using ATR-FTIR analyses is presented in (Fig. 3.8) where most intense vibrations fall in the wavelength region 700 to 1800 cm^{-1}. The most intense vibrations in the wavelength range 900-1130 cm^{-1} are attributed to hematite and quartz (Brinatti et al., 2010). Relatively mild vibrations in the region of 1200 of 1800 cm^{-1} are due to hydroxyl bending in the sample (Ruan et al., 2002). Apart from these intense vibrations, the wavelength region 2800 to 3000 cm^{-1} is marked by mild vibrations which are attributed to hydroxyl stretching. The problem observed here is that

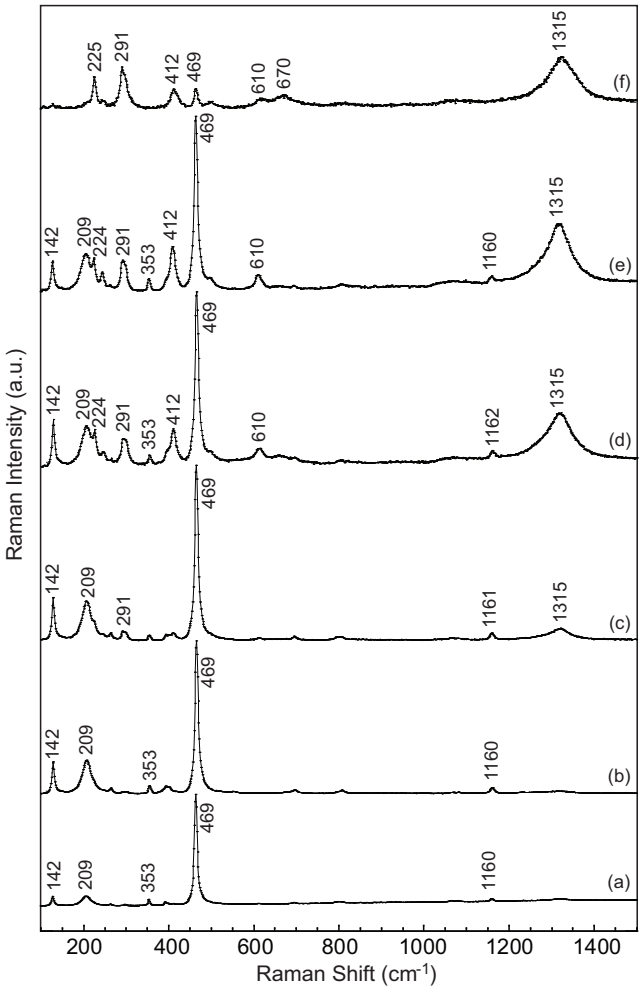

Figure 3.7: Raman spectra of the major mineral phases in BIFs: (a) and (b) the characteristic peaks of quartz, (c) a minor peak of hematite, (d) and (e) characteristic peaks for hematite and quartz, and (f) the characteristic peak for hematite as a major component and magnetite and quartz as minor components.

Table 3.2: Summary of the minerals detected in the samples using different techniques. X indicates that these species were uniquely identified with the technique, while O indicates that there is a weak and inconclusive, though compatible, feature. I indicates that no feature was observed.

Detected Mineral Species	Odisha BIF			
	VIS-NIR	BSE	Raman	ATR-FTIR
Hematite	X	X	X	X
Goethite	X	O	X	X
Specularite	I	X	O	O
Magnetite	I	X	X	O
Quartz	I	X	X	X
Chamosite	I	X	I	I

minor mineral phases (goethite, quartz) are masked by the major mineral phase (hematite) when the sample is crushed and mixed, and hence these phases cannot be detected in the spectra due to a relatively high detection threshold inherent to this kind of technique. However, ATR-FTIR analysis is a very sensitive technique to the hydrogen bonding and water vibrations (Rull et al., 2007; Nakamoto, 2009), thus being used for the determination of hydrous phases in natural mineral/rock samples. The water vibration has been confirmed by the observed 3600 cm^{-1} vibration in the spectra. The results point to the hydration of outcrops by percolating water in the aerial to sub-aerial environment.

A summary of various mineral phases detected by different techniques is listed in Table 3.2.

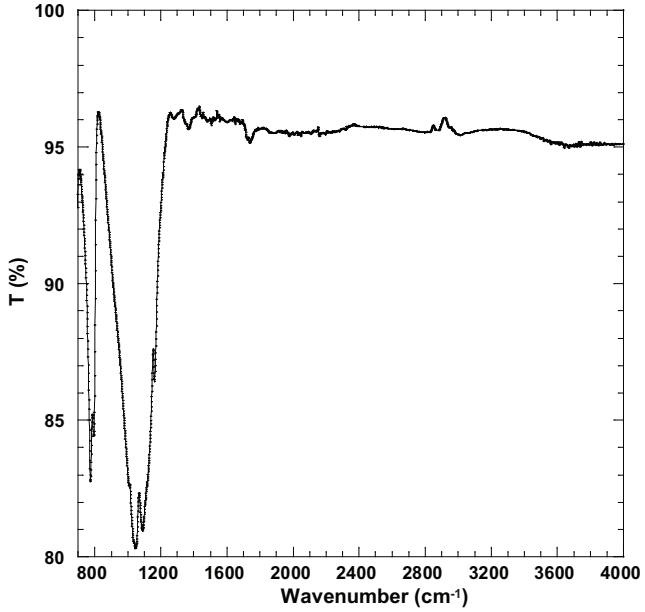

Figure 3.8: ATR-FTIR spectra from studied BIF samples (average spectra of 6 analyses performed with BIF samples powders).

3.4 Discussion

Most significant aspect of iron phases is that, they occur in a variety of geological settings, beginning from modern iron rich environments such as Rio Tinto to older ones such as BIFs and their comparison may help in generating the feasible models for the early formation of primary iron phases and the initiation of hematite formation on Mars. Joda and Daitari iron ore mines consist of stratigraphic layering or bands of hematite and quartz (mainly jasper and/or chert) of sedimentary nature. VIS/NIR results show characteristic spectral signatures of BIFs with absorption bands at 0.65, 0.86, 1.4 and 1.9 μm by which the presence of hematite and goethite can be easily confirmed (Fig. 3.4a, b). Apart from these Fe-oxide spectral signatures in terrestrial BIFs, silicate minerals (mainly quartz polymorphs) could also be identified in thermal infrared region (8-14 μm) of electromagnetic spectrum (Bridges et al., 2008). The reflectance maxima caused by silicon oxygen stretching vibrations in quartz is a distinctive sharply pointed shape related to the polycrystalline grain fabrics and thin iron oxide coating (Crowley et al., 2008).

Specularite in Singhbhum craton BIFs is the secondary mineral phase similar to goethite, and has been generated from magnetite (Beura and Satpathy, 2012). Initiatives to use laser Raman spectroscopy for planetary studies has already been taken up as it has several advantages over other types of spectroscopic techniques (Hirschfeld, 1974; Wang et al., 1995; Sharma et al., 2002). Raman analysis provides sharp spectral features for minerals and/mixtures. Hence, it is most likely to be employed in interplanetary missions to detect spectral features of various minerals in a particular region. The laser Raman and ATR-FTIR spectra obtained for the BIF samples of Singhbhum craton demonstrates the presence of oxide and silicate minerals such as hematite and quartz (Fig. 3.7 and 3.8). Based on the ATR-FTIR spectral results (moderate peak at 3600 cm^{-1}), it is clear that hydrated phases of iron oxide are present. VIS/NIR spectra also confirm the hydrous phase of iron oxide, i.e. goethite, based on the identified absorption bands at 1.4 and 1.9 μm. Mossbauer spectroscopic results are also reported for the native iron samples from the Precambrian Chaibasa shales, Singhbhum craton, eastern India (Chandra et al., 2010). Iron being sensitive to environmental conditions due to variable oxidation states could form different minerals in response to the existing environmental conditions such as Eh, pH and concentrations of certain active species like CO_2, SiO_2, S etc.. In terrestrial conditions, hematite occupies a wider field of stability with high Eh (>0.6) and high pH (>4) in Precambrian BIFs (including Odisha BIFs) and its formation is subjected to the activity of CO_2, S and SiO_2 and therefore, always associated with silicates, carbonates and sulphides (Garrels and Christ, 1965; Stanton, 1972). The common belief on the formation of BIFs in terrestrial conditions is through direct precipitation from low temperature aqueous solutions in response to changes in environmental conditions (Eh/pH) or different diagenetic alterations of precipitated ferric-hydroxides, but it has also been reported that the BIF mineralogy is the outcome of metamorphic processes (Mucke and Annor, 1993). On Mars, lepidocrocite in addition to goethite is possibly precipitated from low temperature aqueous solutions in basaltic regolith (Posey-Dowty et al., 1986; King and

McSween, 2005). After the formation of iron phases in conditions of a warmer and H_2O-CO_2 rich atmospheres, hematite was formed from these previously formed Fe-oxide phases (Gooding, 1978). Therefore, the mechanisms for the formation of hematite from other iron phases on both planetary surfaces are proposed to be similar (King and McSween, 2005). The geomorphological and mineralogical evidences revealed early Mars has hosted diverse environments dominated by water masses (Carr, 1981, 1996; Banin et al., 1992; Longhi et al., 1992; Morris et al., 2006) and these circumstances has raised the possibility of occurrence of BIFs on Mars, which is not yet confirmed. Analysis of thermal emissivity spectrometer (TES) data has proved the occurrences of coarse-grained crystalline hematite (Christensen et al., 2000, 2001a), with no evidences of cherty silica in Meridiani region on Mars. Considering the absence of any cherty silica deposit in association with hematite deposits, the Rio Tinto system deposits have been studied in detail as an analog to ancient environment on Mars in a regional scale. The Tinto River basin, an extreme acidic environment, has water enriched in ferric iron and sulphates and these acidic waters produce sediments rich in ferric iron dominated by sulphate and oxyhydroxide associations, in which silicates are absent (Fernández-Remolar et al., 2004). Further, the mineralogical assemblage identified includes hematite deposits along with other silicate minerals and sulphate salts (Squyres et al., 2004a, 2008; Clark et al., 2005). Identification of silicate phases in hematite rich regions increases the possibility for the detection of deposits comparable to terrestrial BIFs. Midinfrared analysis of crystallographically oriented (c-axis) chemically precipitated terrestrial platy gray hematite support aqueous origin for hematite in Sinus Meridiani as emission is predominantly from the crystallographic c-face of hematite in the region (Lane et al., 2002). Genesis of layered hematite in Sinus Meridiani has been proposed to be formed though the precipitation of insoluble hydrous ferric oxide during the oxygenation of the upper layers of the sea, and further through burial metamorphism (Christensen et al., 2000; Lane et al., 2000, 2002; Fernández Remolar et al., 2002, 2004). Considering the extent of hematite outcrops in Mars, the environment

that hosted BIFs have been proposed to be analog to the environments in which Martian hematite could have been formed (Catling and Moore, 2000, 2003). From the analog point of view, the mineralogy detected in Odisha BIFs show similarities to those obtained from Mars, especially hematite rich Sinus Meridiani on Mars. Mineralogy of Singhbhum craton BIFs detected by several techniques includes Fe oxide phases (hematite, goethite, magnetite and specularite) and silicate phases (chert/jasper/quartz). The optimum absorption bands identified by VIS-NIR radiometry for hematite and goethite could be used as a reference for future interplanetary mineralogical orbital explorations along with the USGS and CRISM spectral libraries. In the Martian scenario, the reflectance spectra could be used to locate BIFs/a similar deposit, as it is very much likely that they would be present at regional scale (Bridges et al., 2008). Specularite, a secondary iron oxide in the study area was formed from the earlier iron phases (possibly from magnetite). We envisage a similar mechanism for the formation of extensive specularite/platy hematite deposits on Mars. Therefore, Singhbhum craton BIFs provide planetary geoscientists with an excellent analog for water driven processes that resulted in the generation of specularite/hematite on Earth and Mars.

A comparative account of the results from Singhbhum craton BIFs to other proposed analog BIFs sites namely Lake Superior BIFs and Brazilian Carajas BIFs is given in Table 3.3.

BIFs are chemical sediments, typically thinly bedded or laminated, whose principal chemistry comprises anonymously high content of Fe, commonly but not inevitably containing silica rich layers, mainly chert (Klein and Beukes, 1992, 1989). The very first evidence of ancient life on Earth has been found associated with the Gunflint Iron Formation, which contains a variety of filamentous to coccoidal forms of microorganisms (Barghoorn and Tyler, 1965; Awramik and Barghoorn, 1977; Strother and Tobin, 1987). Filamentous and coccoidal microorganisms of Gunflint Iron Formation has been investigated by many scientists and has been found that some of the filamentous microfossils

Table 3.3: Comparative account of the different features of BIFs in Singhbhum craton to that of earlier studied Martian analog sites like Lake Superior and Carajas (Brazil) and Mars.

Features	Odisha BIF	Lake Superior BIF	Carajas BIF (Brazil)
Hyperspectral characterization	Absorption band at 0.65-0.86 μm corresponding to Fe content in hematite	Absorption band at 0.65-0.86 μm corresponding to Fe content in hematite	Deep absorption band at 0.88 μm
Metamorphism/ deformation	Unmetamorphosed except for localised thermal metamorphism effect (Majumder et al., 1982)	more metamorphosed state as a whole deposit	Supracrustals sequence with little deformation (Bridges et al., 2008)
Research as analogue to Mars	Early environments of different regions and implications to formation of specularite on Mars (present study)	Spectral observations to locate the BIFs on Mars (Fallacaro and Calvin, 2003)	Ancient water processes (Bridges et al., 2008)

were mineralized by hematite (Allen et al., 2001; Schelble et al., 2004; De Gregorio and Sharp, 2006). Several microfossils have been detected in chert, including Gunflint Chert (Barghoorn and Tyler, 1965), Dressler Formation (Van Kranendonk, 2006) and Apex Chert (Schopf, 1993). The precipitation of silica forms an ideal environment for the preservation of microfossils in geologically significant periods (Preston and Genge, 2010), because it provides a harder substrate which is less prone to reworking and removal of biomolecules. Rhyne chert has been studied for its silicified microorganisms by Preston and Genge (2010) and proposed that if life had ever existed on Mars, microorganisms would have likely been silicified by Martian hot spring deposit with regards to the similar early evolution of Earth and Mars. Black chert deposits of iron ore group of Singhbhum craton can also add valuable information and help in identifying similar characters. Black chert that is associated with BIFs in Singhbhum craton has been proved as a potential host revealing several

clues on the palaeobiogical evolution of our early Earth (Barghoorn and Tyler, 1965; Schopf, 1993; Van Kranendonk, 2006). Bridges et al. (2008) proposed that where spectra indicate bands of hematite and jaspilitic quartz, without discernable clays, and where this pattern extends from the millimeter to meter scale and is laterally continuous, it is highly likely BIFs are present. On Mars, these signatures should be observable at the regional scale from orbiters and at outcrop scale from rovers (Bridges et al., 2008). Other important aspect to be analyzed is that BIFs have a strong magnetic signature. NASA's Mars Global Surveyor (MGS) mission found strong magnetic lineation in the planet's ancient crust that exceed terrestrial values by an order of magnitude, indicating the presence of an intense ancient Martian magnetic field (Connerney et al., 2001). The magnetized material might be ancient lava flows or magmatic intrusions, although a contribution from Martian BIFs cannot be discounted (Bridges et al., 2008). The search for the banded iron formation on Mars would be an outstanding breakthrough to get the insights into the geological past of the planet. The hematite deposits therefore, could be treated as potential target rocks for probing ancient microbial and hydration processes. The terrestrial BIFs have recorded primitive aqueous habitable environments where early forms of life such as stromatolites have been reported (Cloud, 1965, 1972; Hartmann, 1984; Konhauser et al., 2002, 2003). The planetary geosciences community consider BIFs as potential Martian analogs for hematite deposition (Fallacaro and Calvin, 2003; Bridges et al., 2008).

3.5 Conclusions

This study on geological and spectral characteristics of BIFs in Singhbhum craton will help to have a better understanding on the palaeo-environmental conditions of formation of iron deposits on Mars. Spectroscopic studies could aid in differentiating the iron ore deposits on Mars and also help in the relative enrichment of Fe content in different deposits. Laser Raman and ATR-FTIR

spectroscopic techniques are proved to be very significant in analyzing different mineral mixtures, whereas it is difficult to identify each mineral species in a mixture through VIS/NIR radiometry. Chert/quartz, an integral part of BIFs could not be identified in VIS/NIR analysis, but it is easily distinguishable by laser Raman and ATR-FTIR spectroscopic techniques. We hope that this geologic and spectral study of BIFs will help during the testing and calibration phase of the on-going and future missions to Mars.

CHAPTER 4

Spectral and chemical characterization of jarosite in a palaeolacustrine depositional environment in Warkalli Formation in Kerala, South India and its implications

Preclude

This chapter deals with jarosite, a hydrous sulphate associated with other hydrous mineral phases of phyllosilicate family in a palaeo-lacustrine depositional environment near Varkala in Warkalli Formation of the Tertiary sequence of Kerala, South India. The Formation marks the abundance of phyllosilicates in the mineral assemblage, and jarosite occurs as a prominent secondary phase formed during acid-sulphate alteration of iron sulphide in this area. Here, we discussed about the potentiality of spectroscopic techniques to identify the possible mineral phases in the collected samples. The samples from the coastal cliffs have been characterized by hyperspectral analysis (VIS-NIR-SWIR), X-ray Diffraction (XRD), Fourier Transform Infra-red (FTIR), Electron Probe Microanalysis (EPMA) and Laser Raman spectroscopy. This study of jarosite formation in terrestrial environment will influence our understanding on the mineral precipitation, diagenesis and hydration processes on Mars. Additionally, it also shows the importance of spectroscopic techniques like Raman spectrometry to be used in future missions to Mars to further validate the results of orbital spectroscopy.

4.1 Introduction

Jarosite group of minerals with the general chemical formula [$AB_3(SO_4)_2(OH)_6$, where A represents K^+ and B represents Fe^{3+} for typical jarosite], are the key minerals indicating aqueous, acidic and oxidizing conditions of its formation on earth (Bigham and Nordstrom, 2000 and references therein). The stability and reactivity of these minerals depend on the degree of substitution of the ions K^+, Fe^{3+} and tetrahedral sites with other ions such as Na^+ (natrojarosite), Ag^+ (argentojarosite), NH_4^+ (ammoniojarosite) and H_3O^+ (hydronium jarosite) into the A site, Cr^{3+} V^{3+} Ga^{3+} into the B site and CrO_4^{2-} for SO_4^{2-} in the tetrahedral site (Welch et al., 2007). For instance, Na^+ or H_3O^+ substitution into the position A highly increases jarosite solubility and reactivity (Stoffregen, 1993; Drouet and Navrotsky, 2003; Gaboreau and Viellard, 2004; Gasharova et al., 2005; Welch et al., 2007). Other important factors on which the stability of jarosite relies on include chemical and biological properties such as pH, Eh, relative humidity, oxygen and microbial activity (Greenwood et al., 2005; Singh et al., 1999; Brady et al., 1986).

Pyrite or iron sulphide is one of the most common sulphide mineral, which plays a major role in the formation of several meta-stable secondary mineral species such as ferrihydrite ($5Fe_2O_3{\cdot}9H_2O$), schwertmannite [$Fe_8O_8(OH)_6(SO_4){\cdot}nH_2O$ or $Fe_{16}^{3+}O_{16}(OH,SO_4)_{12-13}{\cdot}10\text{-}12H_2O$], and goethite ($FeO(OH)$), along with some comparatively more stable secondary minerals like jarosite [$KFe_3(SO_4)_2(OH)_6$], and hematite (Fe_2O_3) (Nordstrom, 1982; Dutrizac and Jambor, 2000; Cornell and Schwertmann, 2003; Bigham et al., 1996; Jerz and Rimstidt, 2004). Among these minerals, formation of jarosite involves three major steps: first oxidation of sulphur, second oxidation of ferrous iron and third hydrolysis and precipitation of ferric complexes and minerals (Dold, 2014). Generally, jarosite is found associated with acid mine drainage or acidic sulphate rich soils and have their application in hydrometallurgy as a potential scavenger of heavy metals because of its very less solubility in water (Baron and Palmer, 1996; Dutrizac and Jambor, 2000; Gieré et al., 2003). In general,

dominance of jarosite in mineralogical assemblage indicates the acidic aqueous conditions with pH close to 2 (Dold and Fontboté, 2001). Apart from the traditional jarosite formation mechanism in terrestrial conditions, i.e. in acidic conditions with pH <4, it could also be generated from oxidizing pyrite in neutral fresh water spring environment similar to Loboi Swamp, Kenya (Ashley et al., 2004). With the increasing knowledge of mineralogically complex jarosite and its non-acidic occurrences, it is apparent that jarosite does not strictly follow a single diagenetic environment on Earth (McHenry et al., 2011). Jarosite can also be used as an indicator of geochemical conditions that prevailed at the time of its formation in extra-terrestrial environment (Murad and Rojik, 2005).

Present study focuses on the occurrences of jarosite in association with phyllosilicates located on the coastal cliffs, fringing the Arabian Sea near Varkala in Warkalli Formation of the Tertiary sequence of Kerala, South India. Jarosite is an important mineral associated with the carbonaceous clay in Warkalli Formation. The geological setting of the area suits well to study jarosite formation conditions in terrestrial palaeolacustrine depositional environment since carbonaceous clay with minor lignite seams which hosts jarosite could have been generated into a peat swamp in the geological past. Jarosite is formed as an alteration product of marcasite/pyrite. The coastal affinity provided surplus supply of sodium through the moisture laden wind, converting jarosite into natrojarosite. The objectives of the present research are; (i) to understand the field relationship of mineral assemblages and defining their coexistence with respect to present-day environmental conditions; (ii) chemical and spectral characterization of mineralogical assemblage of the study area, and (iii) possible implications to Mars.

4.2 Geological setting

The Cenozoic sedimentary succession of Kerala unconformably overlies the Precambrian crystalline rocks. The crystallines are mainly represented by the gneiss-granulite suit of rocks with the younger igneous complexes (Soman, 1980), and are affected by polyphase deformation and metamorphism, resulting into the development of complex tectonites such as fractures, faults and shear zones (Rao, 1976). These tectonites have played a major role in graben subsidence and hence, in the development of sedimentary basins in the West coast (Eremenko and Gagelganz, 1966). Two major basins are identified, which are (i) between Trivandrum and Ponnani in the South and the central Kerala, and (ii)Cannanore and Kasargod in North Kerala (Paulose and Narayanaswamy, 1968). Major portion of the Cenozoic sediments is deposited in a deep basin bordering the sea and currently occur under the cover of Recent sediments. The sedimentation in the basins attained its maximum in Late Oligocene to Early Miocene in the transgression phase which was followed by a regression phase with active erosion of the deposited sediments in Late Miocene. Study area belongs to the coastal cliff edging the Arabian Sea near Varkala, which is situated about 55 km north-west of Thiruvananthapuram - the capital of Kerala state, India (Fig. 4.1). The cliffs run for a length of 5.5 km between Vettur ($8^o43'59.34''N$ & $76^o42'19.91''E$) and Edava ($8^o44'35.75''N$ & $76^o41'54.21''E$). These coastal cliffs are the type area for the Warkalli Formation of Mio-Pliocene resting unconformably over the Precambrian crystallines of Kerala Khondalite Belt (KKB). Coastal cliffs of Varkala are mainly comprised of arkosic sand, kaolinitic sandy clay, carbonaceous clay and peat with plant remains (Desikachar, 1976). The whole Cenozoic sediments of Kerala is divided into four units from the oldest to youngest: Unit I comprises pebbly sands and sandy clays with black clay and lignite; Unit II comprises limestone with sand and clay; Unit III comprises arkosic sand claywith lignite and IIIA comprises laterite, ferruginous sandstone and clay; and Unit IV comprises beach sand and alluvial clay (Nair and Rao, 1980). Jarosite shows the grainy

occurrence onto the clayey base with basic replacement texture (Fig. 4.2a and b). Jarosite also occurs in carbonaceous clay layer as encrustations due to diagenetic replacement process (Fig. 4.2c) and depicts a typical efflorescence texture (Fig. 4.2d). Efflorescent iron sulphate minerals form when solutions rich in iron sulphate and in sulphuric acid evaporate in surficial conditions (Jerz and Rimstidt, 2004). The evolution from ferrous sulphate minerals to iron oxy-hydroxides minerals occurs by a series of oxidation, dehydration, and neutralization reactions. The mineralogy that develops at any particular site is controlled by the relative rates of each of these types of reactions. Jarosite in this part was first reported and identified as a natrojarosite (Tassel, 1965). This mineral will be periodically washed away by waves during high tide and hence cannot be seen throughout the year. Carbonaceous clay which hosts jarosite is black organic-rich clay bed consisting of variable amounts of silt and poorly-sorted sands and is partly iron oxide-coated.

4.3 Methodology

The present work includes field investigations, systematic sampling, characterization of the collected samples with the aid of electron microprobe analysis (EPMA), hyperspectral analysis (VIS-NIR-SWIR), X-ray diffraction analysis, laser Raman analysis and Fourier transform infrared spectroscopy. The samples were purified by removing any associated crack fillings. The samples were then were crushed and finely powdered using Fritsch Pulverisette with Ni-Ch grinding set (Fritsch GmbH; Germany) attached with air compressor and a Jaw Crusher (Insmart Systems) after VIS-NIR-SWIR spectra generation of the solid samples. The same powders were used for other analyses.

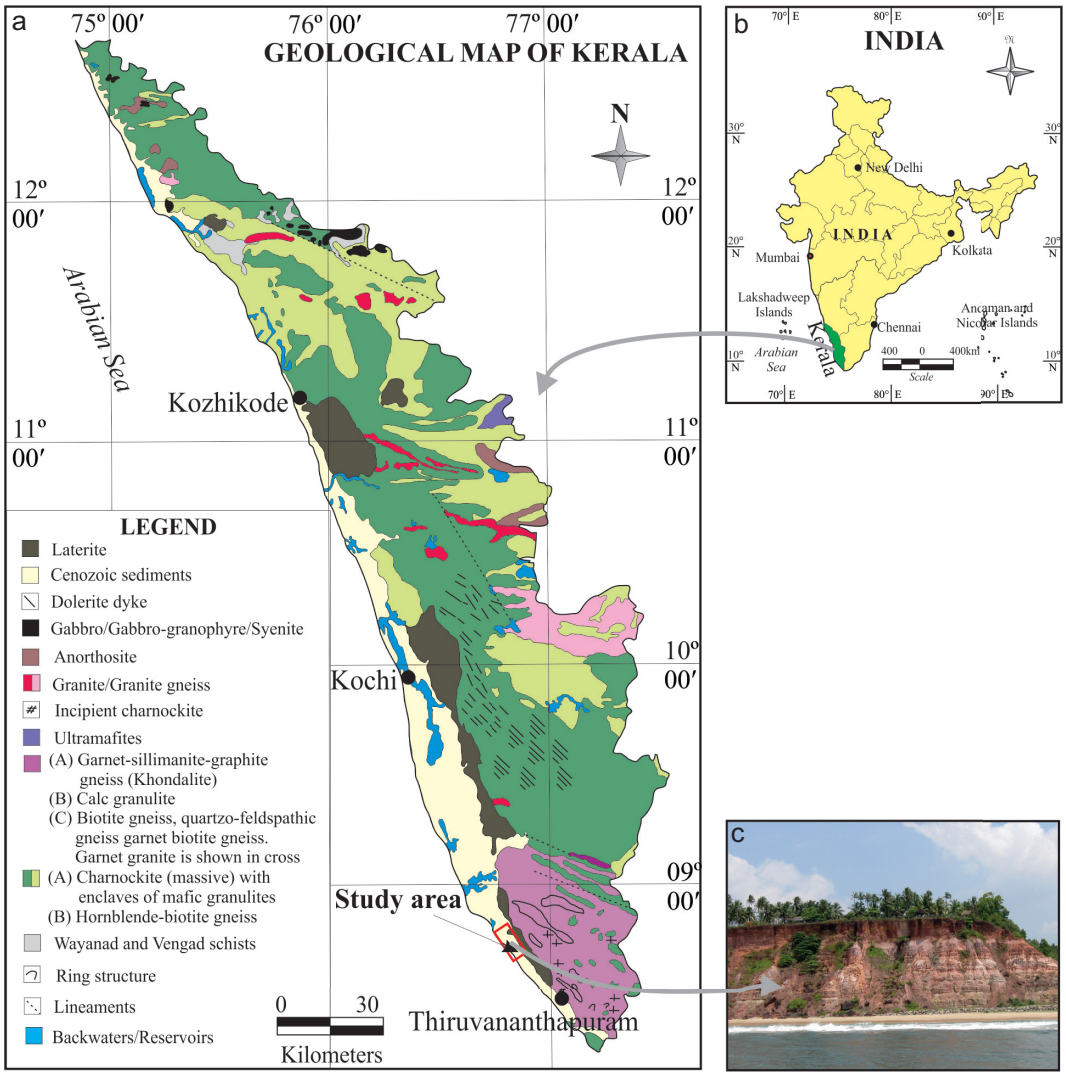

Figure 4.1: (a) Location map of the study area with respect to India. (b) Geological map of Kerala (Source: Geological Survey of India: Geological and mineral map of Kerala state published in 1995) (c) Terrestrial view of Varkala Cliffs- A view off the coast of Varkala.

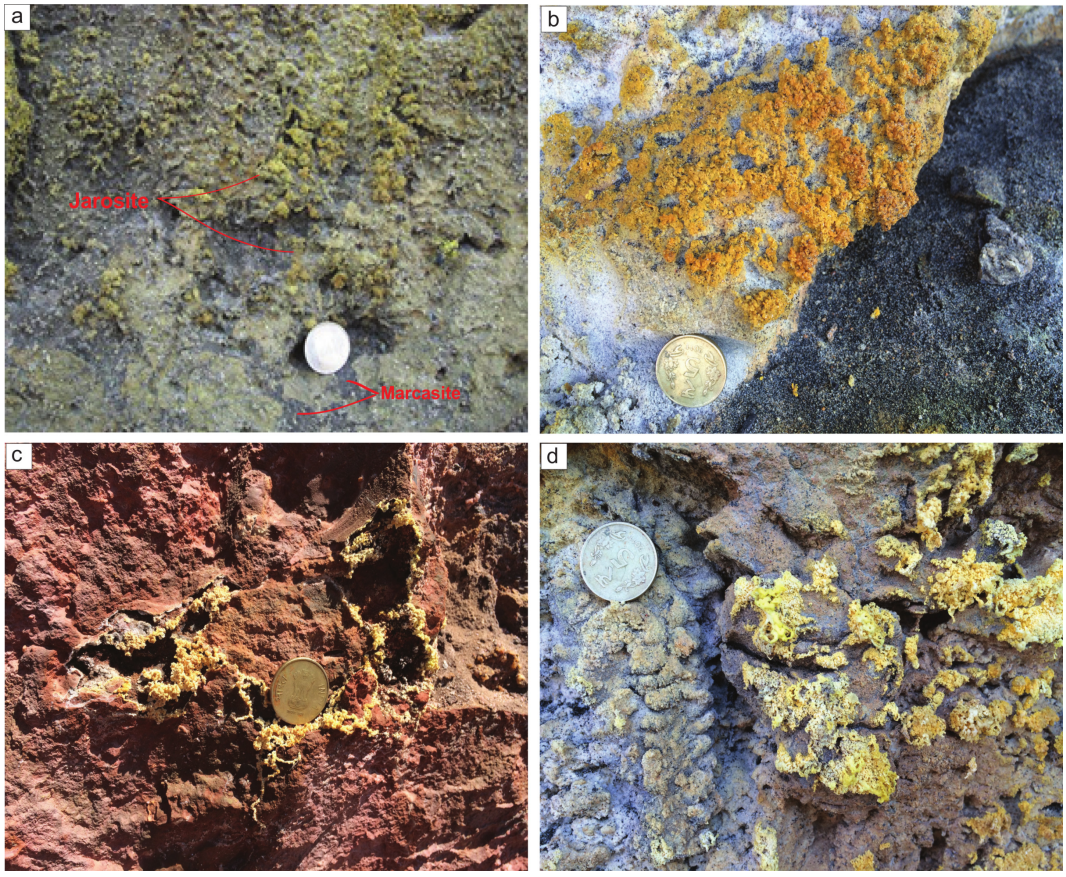

Figure 4.2: Photograph of the sampling locations with surficial jarosite deposits in different geological setting. (a) Replacement type jarosite deposit on clayey groundmass. (b) Replacement type jarosite associated within sandy groundmass. (c) Jarosite in carbonaceous clay: as encrustations due to diagenetic replacement process. (d) A typical efflorescence texture in jarosite deposit.

4.3.1 Field investigation and sample collection

Field investigation included studying the entire 5.5 km stretch of cliffs and identifying the different mineral assemblages. Warkalli Formation is an embodiment of different minerals like authigenic quartz, feldspar, biotite and rare earths; secondary minerals like clay, oxides and hydroxides of iron and aluminium; replacement minerals like marcasite and jarosite besides the minor lignite seams. The vertical and horizontal disposition of the cliffs was studied well and the mineralogical assemblages were characterized in detail. The different physico-chemical conditions were able to be deciphered from the mode of occurrence and association with other minerals. Except a few specimens, most of the collected samples were loose sediments.

4.3.2 Electron probe micro-analysis

The elemental mapping of selected jarosite grains was performed with well-polished thin sections using Electron Probe Micro-Analyser (EPMA) positioned at Indian Institute of Science, Bangalore. EPMA of jarosite grains has been done at operating conditions of 10 kV, 20 nA, and 5 μm beam diameter to avoid the change in Na and K count rates for the entire analysis time with no specimen damage. Elemental mapping for Na, S, Si, K and Fe has been done. The instrument was calibrated using sulphate and silicate standards. Back-scattered images have also been generated through EPMA to check for the grain size and their distribution along with other mineral species.

4.3.3 Spectral analysis

Laboratory hyperspectral signatures of the samples (hand-specimen and powders of 500 μm in diameter) were collected using ASD FieldSpec® 3 spectro-radiometer in the wavelength range of 500 nm to 2500 nm. The fibre optic

cable along with the gun holding it, were mounted on the tripod at nadir position. Spectral signatures were collected in a controlled laboratory dark room environment. In another tripod, a tungsten filament halogen lamp with the wavelength range of 400 nm to 2500 nm was used as artificial light source for spectral data collection. Spectralon®, the standard white reference panel was used for measurement of irradiance for each set of measurement. The splice and parabolic corrections were made for the collected spectra and then matched with the reference spectra available in USGS spectral library to confirm the composition of minerals. Spectral Feature Fitting (SFF) and Spectral Angle Mapper (SAM) techniques have been used to match the unknown spectra from the study area to the standard reference from USGS spectral library.

4.3.4 X-ray diffraction

X-ray diffraction analysis was made using a Bruker D8 ADVANCE Xray diffractometer in University of Kerala, Thiruvananthapuram, India. The XRD analytical conditions are as follows: copper-alpha radiation, $10^o - 78^o$ 2θ, step size 0.020305 at a scan step time of 96 s.

4.3.5 Laser-Raman analysis

Micro Raman Spectrometry is done using WITec alpha 300 Raman System excited with 532 nm laser with 300 mW output at Vikram Sarabhai Space Centre, Thiruvananthapuram, India. The spectral range of the equipment is from 100 to 3600 cm^{-1} shift from the laser line, accomplished with an edge filter. The Raman system is fitted with XYZ mapping stage as well as confocal arrangement enabling imaging studies with spatial and depth resolutions of 1 and 2 μm respectively. The system is fully automated and self-validating with auto aligning and optimization of input laser power.

4.3.6 Fourier transform infrared spectroscopy

Spectra were collected in fine powdered samples with a Perkin Elmer Infrared (FTIR) spectrometer positioned at Department of Chemistry, Indian Institute of Space Science and Technology, Thiruvananthapuram. The powders were pressed at 55 to 60 kb. The spectra were recorded immediately after the separation of the powder sample from the bulk sample. Spectra were collected in the 700 to 4000 cm^{-1} range with an optical resolution of 0.5 cm^{-1} and wavelength precision of 0.01 cm^{-1} at 220 V, 50 Hz power supply. A baseline correction was made before interpretation the data.

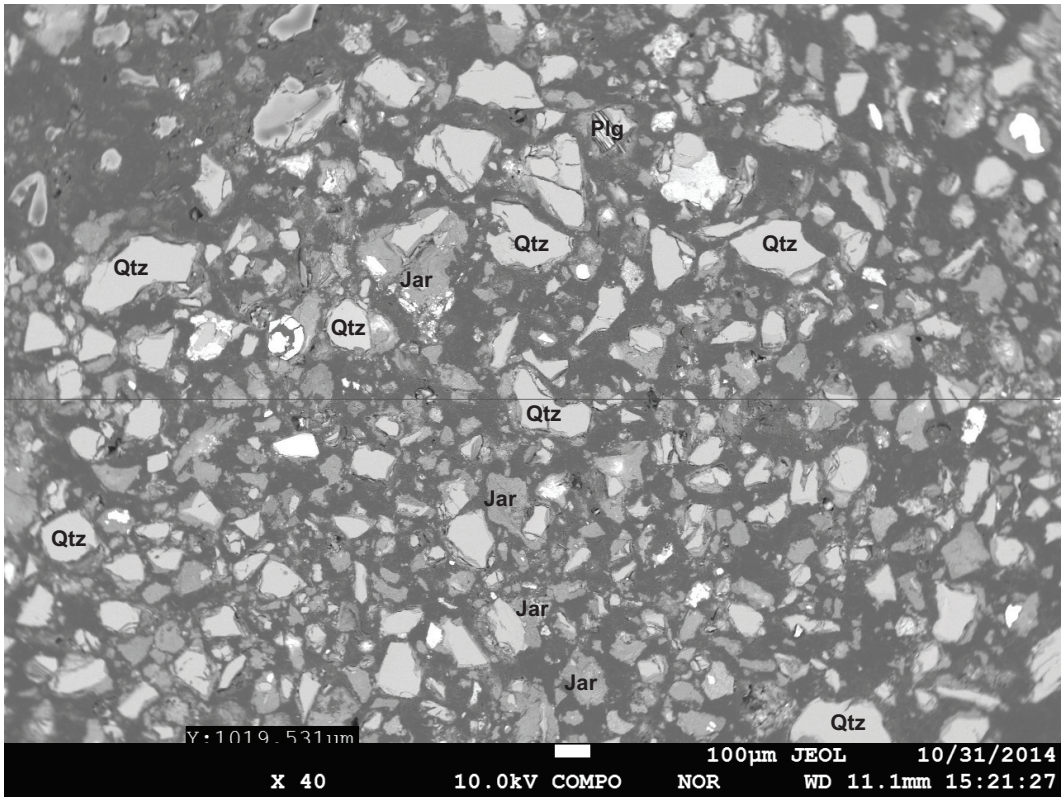

Figure 4.3: Back Scattered Electron image of jarosite (Jar) and associated minerals of quartz (Qtz) and plagioclase (Plag) in a polished thin section of sample.

4.4 Results

4.4.1 Electron probe micro-analysis and back-scattered images

The crystalline nature of jarosite is observed from the back scattered images (Fig. 4.3). Apart from jarosite, other identified minerals identified in BSE images are goethite, plagioclase, quartz and few ilmenite grains. Quartz and plagioclase are in the form of angular grains whereas jarosite and goethite grains are subangular to subrounded.

Elemental mapping for the jarosite grains on well-polished thin sections has been done for Na, S, Si, K and Fe and results are displayed in the Fig. 4.4. These results show varying degree of elemental concentrations throughout the grains and they are strongly correlated. The Fe map shows the enrichment throughout the grain, leaving some specific structural pattern of Fe-deficiency (Fig. 4.4a). The Si map shows Si depletion in the areas where Fe and S are enriched. The enrichment pattern of Fe and S are same in the elemental maps. Si is highly correlated with the Fe and S enriched locations; the lower the concentration of Fe and S in a location, the higher the Si concentration. The K map shows the elemental enrichment throughout the grain, whereas an appreciable concentration of Na within the grain suggests the jarosite as natrojarosite. Less structurally deformed jarosite grain shows similar patterns for Fe and S enrichment. A weathered jarosite grain shows relatively higher Fe enrichment than S with similar Si enrichment patterns throughout the grain. Highly weathered and deformed grain shows Fe enriched locations with lower concentration of S. K and Na maps are also highly correlated. The less weathered grain show similar enrichment patterns for Fe and S with relatively high Na enrichment patterns, which is highly correlated with the K concentration (Fig. 4.4b). Apart from elemental mapping, determination of chemical composition by EPMA was also carried out. Total concentrations (water excluded)

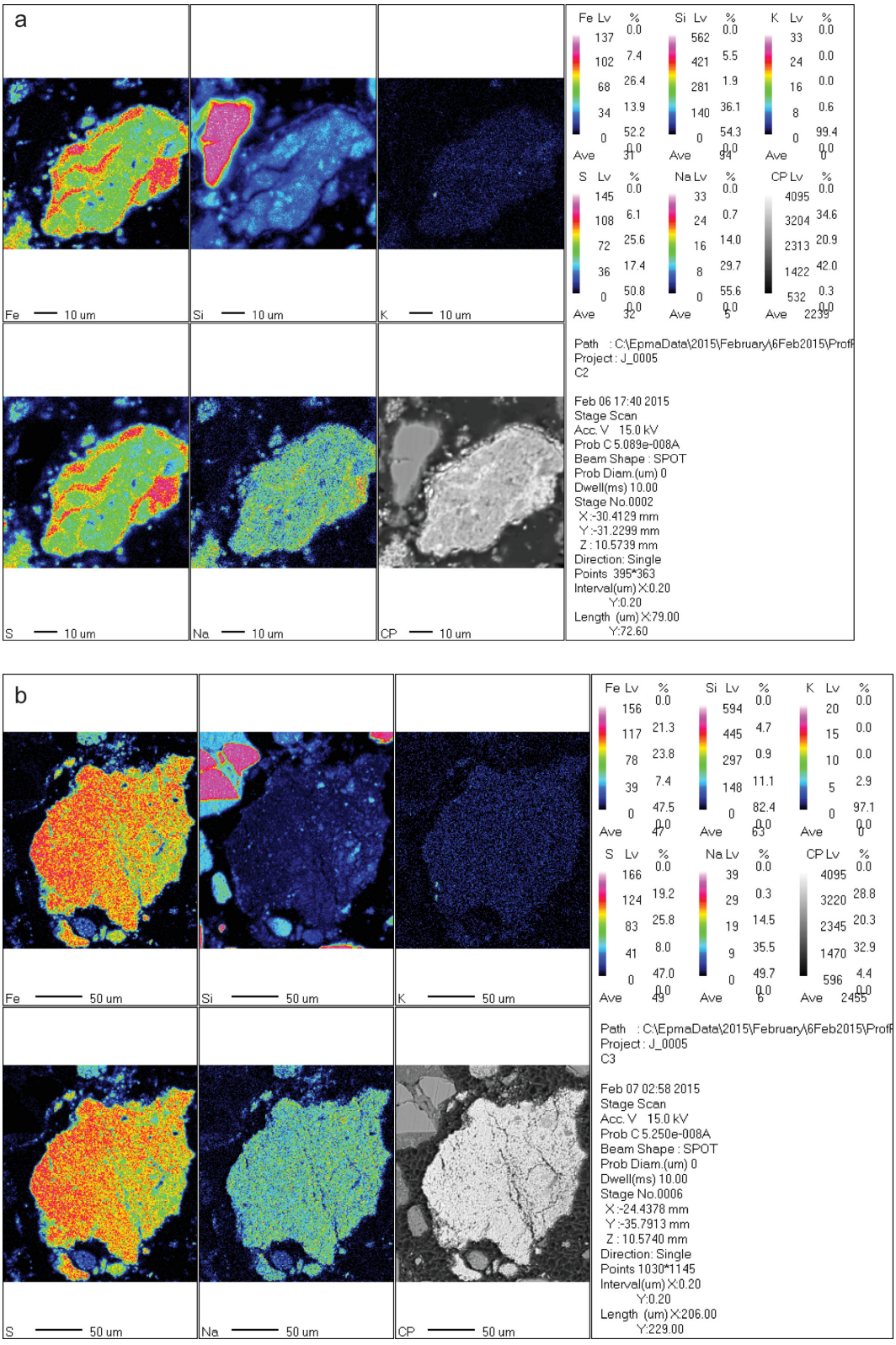

Figure 4.4: (a and b) Representative figures showing elemental mapping for Na, S, Si, K and Fe of selected least weathered jarosite grains. Red = high; black= low.

were in the range of 65 to 78 wt% with considerable variation in the concentration of FeO and SO_3. Low totals could be the result of void space of excess water (McHenry et al., 2011). Due to low totals, only preliminary compositional measurements are possible. Na_2O concentrations range from 1.27 to 2.89 wt% compared to ∼0.01 wt% of K_2O.

4.4.2 Spectral analysis

The spectral characteristics of the samples collected from sea cliffs, Varkala, Kerala are listed in Table 4.1. Spectral characteristics and albedo of the solid and powder samples of the study area in ultraviolet-visible-near-infrared region of electromagnetic spectrum have been measured to understand characteristic absorption features of identified minerals (Fig. 4.5a-d). Results confirm that the samples collected from the Warkalli Formation are dominated by jarosite and kaolinite minerals. Due to the clear deep absorption band of Fe^{3+}, other minerals (such as goethite, pyrite) absorption features are suppressed. Spectral profile of the jarosite sample JAR011 has the absorption bands centered at 910 nm, 1470 nm, 1849-1864 nm (in the form of a doublet), 1940 nm and 2270 nm, which are due to Fe^{3+}, OH, Na-OH, OH and Mg-OH vibrations respectively (Fig. 4.5a). All the hydrous phase vibrational absorptions are weak to moderate and narrow. The reflectivity spectrum of solid hand specimen is smooth with very shallow absorption at around 600 nm whereas USGS spectral library spectrum is smooth with well-defined shallow absorption band at 580 nm (Fig. 4.5b).

Powder sample of JAR011 also shows the same characteristic absorption bands as those of hand-specimen, having the absorption bands centered at 910 nm, 1470 nm, 1849-1864 nm (in the form of a doublet), 1940 nm and 2270 nm with the relatively lower reflectance (Fig. 4.5c). Powder reflectivity spectrum shows no peculiar absorption band in the wavelength region of 500-700 nm (Fig. 4.5d).Lower reflectance intensity is mainly attributed to grain size differ-

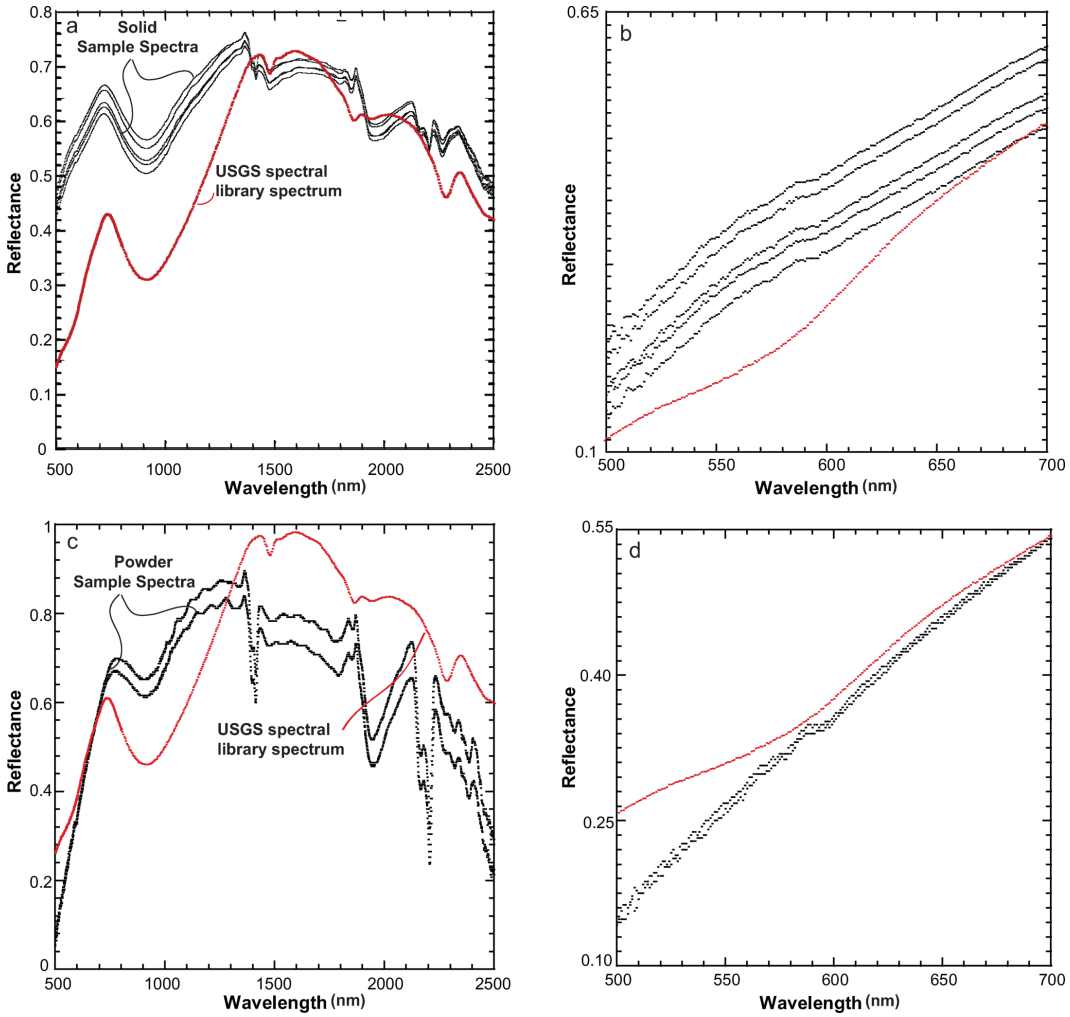

Figure 4.5: Laboratory reflectance spectra of hand-specimen and powdered sample of JAR011. (a) Spectral profile of the jarosite hand specimen (black) having the absorption bands at 900 nm, 1400 nm, 1900 nm and 2200 nm, corresponding to Fe^{3+}, OH and SO^{4-} overtones and the comparable jarosite spectra from USGS spectral library (red). (b) The variability in the reflectance of jarosite solid sample (black) and its comparison to USGS spectral library spectrum (red) in the wavelength range of 500-700 nm and powder. (c) Spectral profile of jarosite powdered sample having same absorption bands as that of hand specimen with relatively lower reflectance value. (d) Powdered sample spectrum with no absorption in the wavelength range of 500-700 nm (Source: http://speclab.cr.usgs.gov/spectral). Box A represents the absorption bands into visible region and box B represents the absorption bands in near-infrared and short-wave-infrared region of electromagnetic spectrum. Dotted lines are drawn to locate the absorption band centers at wavelength axis.

Table 4.1: Characteristics absorption bands of laboratory reflectance spectra and their assignments to the particular compositions, of the collected samples from Varkala cliff, Kerala.

Sample Identity	Absorption band (nm)	Absorption band characteristics	Assignments
JAR011 (hand-specimen)	600	Weak, broad	Iron(III) ion
	910	Very strong, broad, symmetrical	Iron(III) oxide (Fe_2O_3)
	1400 (doublet)	Weak, narrow	OH absorption
	1470	Moderate, narrow	OH stretching band
	1864	Weak, narrow	Na-OH vibration
	1945	Strong, broad	Ferric iron/H_2O absorption
	2200 (doublet)	Moderate, broad	Al-OH absorption
	2280	Moderate, narrow, symmetrical	Mg-OH vibration
JAR011 (powder >250 μm)	600	Weak, broad	Iron(III) ion
	910	Strong, broad	Iron(III) oxide (Fe_2O_3)
	1400 (doublet)	Strong, narrow	OH absorption
	1470	Weak, narrow	OH stretching band
	1800	Moderate, broad	OH bend vibration
	1864	Weak, narrow	Na-OH vibration
	1945	Very strong, broad	Ferric iron/H2O absorption
	2200 (doublet)	Very strong, narrow	Al-OH absorption
	2280	Weak, narrow	Na-OH vibration
	2300	Weak, narrow	Na-OH vibration/CO_3-absorption
	2400	Weak, narrow	Mg-OH vibration
JAR015 (hand-specimen)	900	Very strong, broad, symmetrical	Iron(III) oxide (Fe_2O_3)
	1400 (doublet)	Strong, narrow	OH absorption
	1470	Weak, narrow	OH stretching band
	1864	Weak, narrow	Na-OH vibration
	1945	Strong, broad	Ferric iron/H_2O absorption
	2200 (doublet)	Moderate, narrow	Al-OH absorption
	2260	Moderate, narrow, symmetrical	Na-OH vibration
KAO015 (hand-specimen)	1400 (doublet)	Strong, narrow	OH absorption
	1944	Strong, broad	Ferric iron/H_2O absorption
	2200 (doublet)	Moderate, narrow	Al-OH absorption

ence here. The characteristic absorption feature of jarosite between 400 and 1300 nm is due to Fe^{3+} spin-forbidden ligand field transitions in iron atoms that are linked through edge or corner-shared $Fe^{3+}(O/OH)_6$ octahedra. Other mineral associated with the jarosite sample is kaolinite as indicated by the spectral observations of the sample which are centered at 1400 nm, 1900 nm and 2200 nm. This characteristic spectra match well with the kaolinite spectra of USGS/JPL spectral library. Reflectivity spectra of samples JAR015 and KAO021 show the characteristic -OH absorption bands at 1400 nm, 1950 nm and 2200 nm of phyllosilicate group of minerals (Fig. 4.6a,b). Reflectivity spectrum of sample JAR015 shows a deep trough at 900 nm due to overtones of Fe^{3+}. Measurement of albedo of the spectra is one of the important and peculiar features during the spectral measurements of different minerals. Jarosite show albedo in the range from 15 to 70%. Powder samples of jarosite have comparatively low albedo, in the range of 25-60%. The phyllosilicate phase kaolinite has albedo in the range of 30-90%.

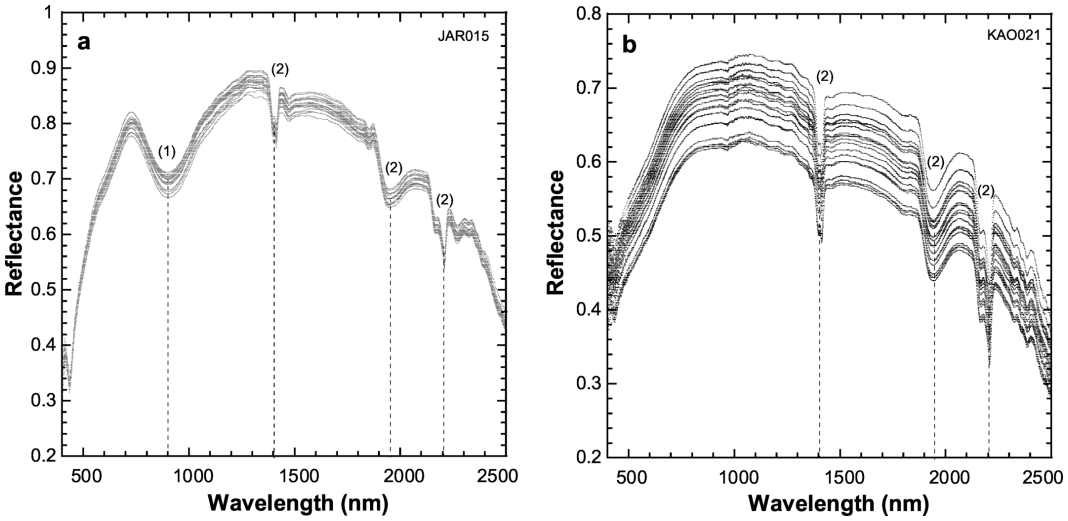

Figure 4.6: Laboratory reflectance spectra of the hand-specimen of (a) JAR015 and (b) KAO021, in which the notations (1) and (2) defines the absorptions due to Fe^{3+} and OH/H_2O overtones.

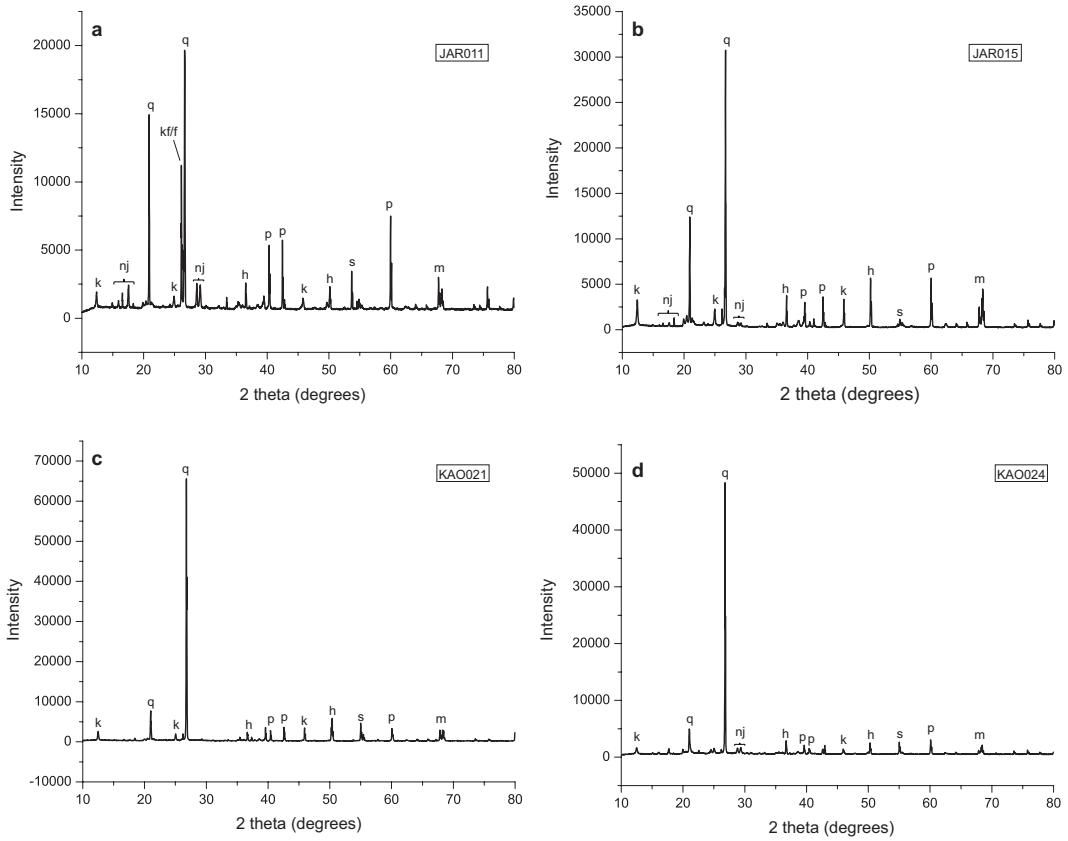

Figure 4.7: (a-d). X-ray diffractograms of the samples JAR011, JAR015, KAO021 and KAO024 with mentioned characteristic peaks for different minerals, in which nj stands for natrojarosite, q stands for quartz, k stands for kaolinite, kf/f stands for feldspars, p stands for pyrite, s stands for smectite, h stands for hematite and m stands for marcasite.

4.4.3 X-ray diffraction

Fig. 4.7 shows four diffractograms of the fine powdered samples JAR011, JAR015, KAO021 and KAO024 collected from the Warkalli Beds (Tertiary) exposed in the Varkala sea cliffs. The characteristic XRD peaks for sample JAR011 (Fig. 4.7a) are at $\sim 17.5^o$, 16^o and 15^o, which basically correspond to natrojarosite (Tassel et al., 1965; McCollom et al., 2014). Apart from these XRD peaks for the sample, a doublet at $\sim 28^o$ is also attributed to natrojarosite. Other prominent XRD peaks are at $\sim 12^o$ (Kaolinite), 20^o (Quartz), 25^o (Kaolinite), 26.1^o (K-Feldspar/plagioclase), 26.6^o (Quartz), 36^o (Hematite)

40^o (Pyrite), 43^o (Pyrite), 50^o (Hematite), 46^o (Kaolinite) 54^o (Smectite), 60^o (Pyrite) and 68^o (Marcasite). Diffractogram of sample JAR015 shows similar peak pattern with the variation in the intensity of peaks; the peak at $\sim 54^o$ is omitted completely suggesting the removal of smectite clays (Fig. 4.7b). Omission of natrojarosite peaks from the diffractogram of KAO021 sample suggests its composition more towards clay and sand rich (Fig. 4.7c) whereas the minor peaks are again noticed in the carbonaceous clay rich KAO024 sample (Fig. 4.7d).

4.4.4 Laser Raman analysis

The Raman spectrum of the sample JAR011 (Fig. 4.8) shows six bands assigned to the vibrational modes of Fe-O and S-O bonding. In the range below 700 cm^{-1} where the peaks from ν_2, ν_4, and lattice modes occur, main peaks are at 228, 261.15, 387.86, 469.74, 536.03 and 625.7 cm^{-1}. The band at 387.86 cm^{-1} is assigned to the vibrational modes of Fe-S bonding in pyrite and the band at 469.74 cm^{-1} assigned to the stretching modes of S-S in elemental sulphur (Li et al., 1993, Sasaki et al., 1998). In the range between 1200 and 900 cm^{-1} where the ν_1 and ν_3 peaks of SO_4 tetrahedra occur, the most prominent peak is at 1012.68 which is assigned to symmetric stretching vibration mode ν_1 of SO_4 tetrahedra with highest peak intensity. The two prominent peaks at 1114.05 and1150.12 cm^{-1} were assigned to asymmetric stretching vibration mode ν_3 of SO_4 tetrahedra. In the spectral range of 3600-3400 cm^{-1}, a triplet of Raman peaks is observed, which is due to OH in the crystal lattice.

4.4.5 Fourier transform infrared spectroscopy

Fig. 4.9a shows Fourier transform infra red transmittance spectra in the wavelength range of 700-4000 cm^{-1} for the powdered sample JAR011. These results show the transmittance minima in the wavenumber range of 700-1200 cm^{-1}

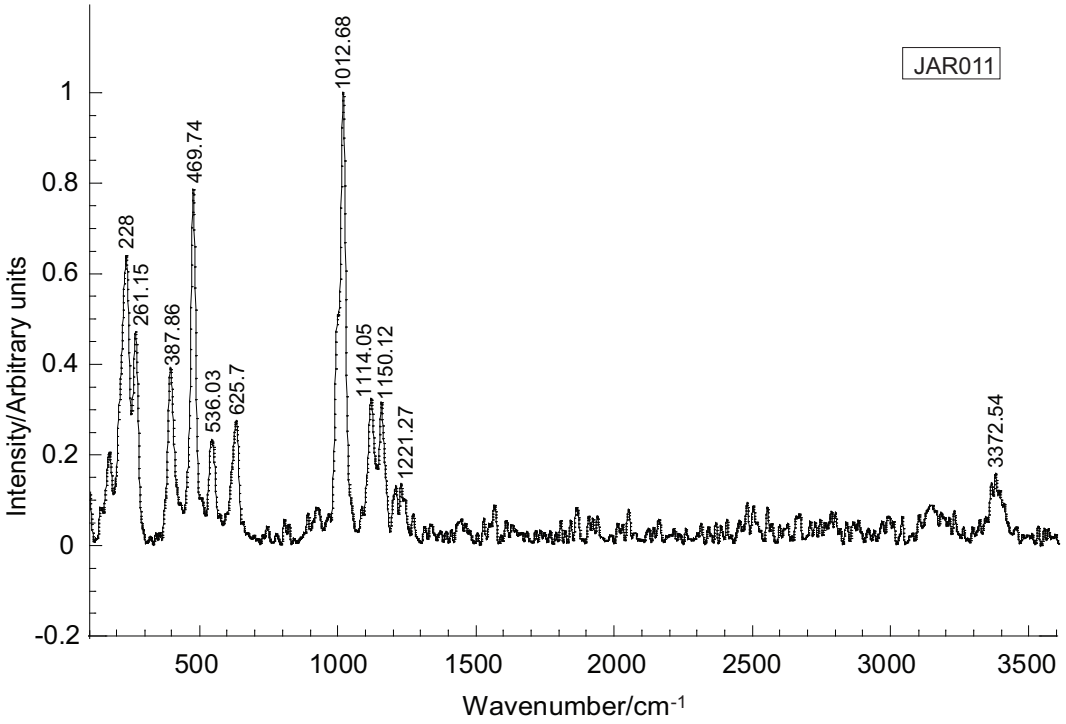

Figure 4.8: Laser Raman spectrumof the sample JAR011 with characteristic peak positions. For the interpretation of the peak values, refer to the text.

and 3550-3750 cm^{-1}. In 700-1200 cm^{-1} range three transmittance minima have been identified and all these three minima show two doublets with little variations in the transmittance percentages (Fig. 4.9b). These paired transmittance minima are present at 755-790 cm^{-1}, 910-945 cm^{-1} and 1003-1028 cm^{-1} and are assigned to the vibration modes of ν_1 (SO_4^{2-}) and ν_1 (SO_4^{2-}) for lower and higher wavenumbers respectively. Apart from these three transmittance minima, one single transmittance minimum is present at about 1125 cm^{-1}. In the wave-number range of 3550-3750 cm^{-1}, two major (3617 and 3688 cm^{-1}) and two minor (3649-3669 cm^{-1}) transmittance minima are present (Fig. 4.9c), assigned to the stretching vibration modes of OH (ν_{OH} band).

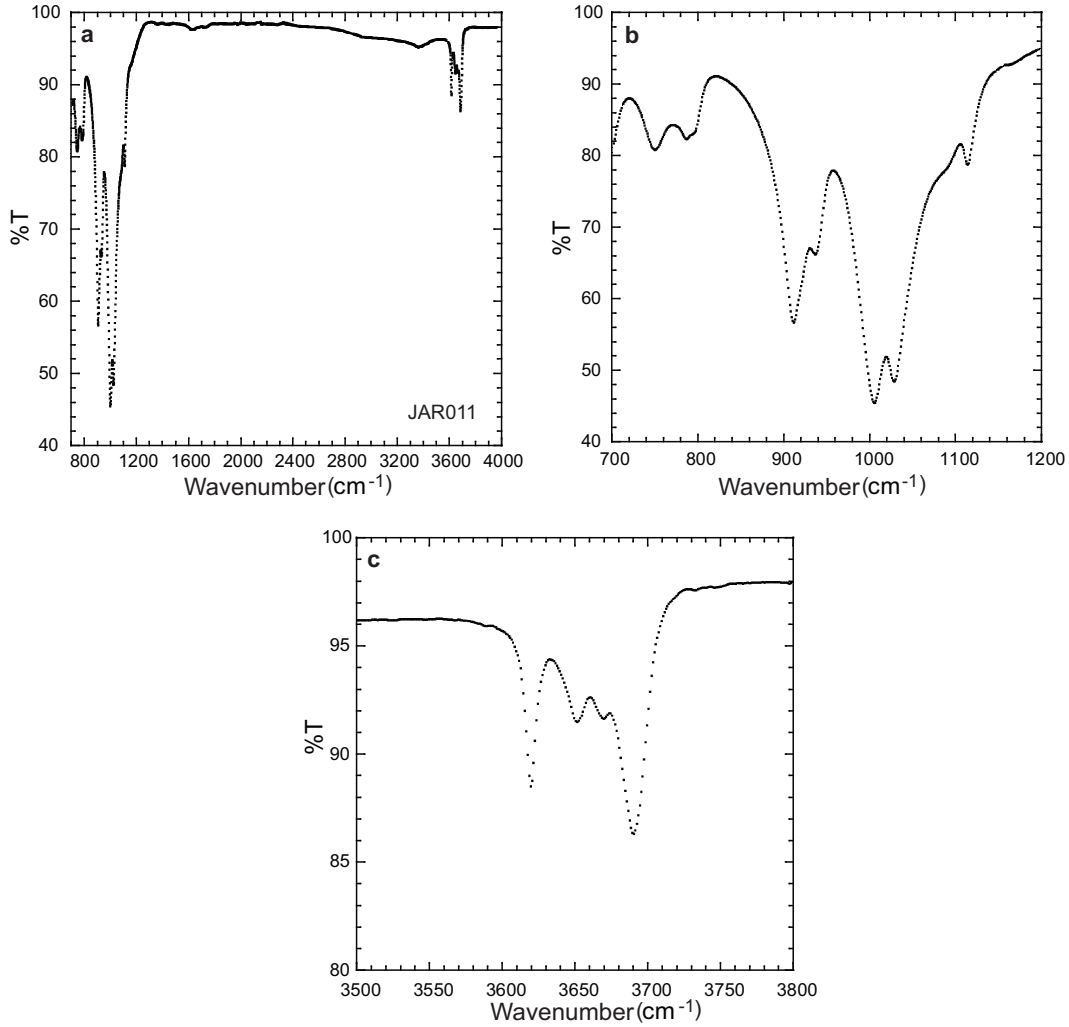

Figure 4.9: (a) FTIR spectra show the characteristic transmittance bands for hydrous phases in the sample JAR011 in the 800-1200 wavenumber region and 3550-3750 wavenumber region. All the peculiar absorptions are either due to O-H bend or free hydroxyl molecule. (b) Focused view of the transmittance bands in the 800-1200 wavenumber region (c) Focused view of the transmittance bands in the 3550-3750 wavenumber region.

4.5 Discussions

The mineralogy detected by petrographic observations, VIS-NIR-SWIR spectroradiometry, XRD, laser Raman spectroscopy and FTIR is represented in Table 4.2.

Visible-near infrared reflectance spectroscopic analysis, XRD, laser Raman analysis and petrographic analysis all confirmed the presence of jarosite in the studied samples. VNIR spectroscopy results are more consistent with petrographic observations (EPMA and BSE images). VNIR reflectance spectroscopy is proved to be very significant in identifying the various minerals and rocks, and is emerging as a powerful tool in examining the mineralogy of other planets through orbiters equipped with the spectroradiometer with essential specification. The spectra are collected in the wavelength range of 450-2500 nm. The major spectral features displayed by jarosite include absorption bands at around 910 nm, 1470 nm, 1940 nm and 2270 nm as presented in the Fig. 4.5. The VNIR spectrum in 600-1000 nm range of wavelength is mainly attributed to Fe oxides, iron bearing sulphates, or iron rich mineral families such as pyroxenes and olivine (King and Ridley, 1987; Clark et al., 2005). The absorption bands at 1400 nm, 1900 nm and 2200 nm are due to the overtones of hydroxyl group (Hunt, 1970; Hunt et al., 1971) (Fig. 4.5b and d). Results from XRD and laser Raman are compliment with each other, as all are representing similar mineralogical composition. Characterization of jarosite group of minerals was performed many scientists for mineralogy and crystal chemistry (Sasaki et al., 1998; Drouet and Navrotsky, 2003; Drouet et al., 2004, Basciano and Peterson, 2007, 2008; Desborough et al., 2010; McCollom et al., 2014). The Raman spectrum in the region 100-3600 cm^{-1}, as represented in Fig. 4.7 shows the most prominent bands at 1012.68 cm^{-1}, which defines symmetric stretching vibration mode ν_1 of SO_4 tetrahedra.

XRD analysis of the sample reveals the varying composition of the sample with different prominent diffraction peaks. Most of the peaks in XRD diffrac-

Table 4.2: Summary of the minerals detected in the samples from different techniques. X indicates that these minerals were uniquely identified with this technique, while O indicates that there is a weak and inconclusive, though compatible, feature. I indicates no feature observed.

Detected Mineral Species	Varkala Cliff Jarosite and Clay samples				
	EPMA/BSE	VIS-NIR-SWIR	XRD	Raman	ATR-FTIR
Natrojarosite	X	X	X	X	X
quartz	X	I	X	O	X
Plagioclase	X	I	X	O	I
Kaolinite	X	X	X	O	O
Pyrite	O	O	X	I	I
Marcasite	I	O	X	I	I
Smectite	I	O	X	O	O
Hematite	I	X	X	I	I

togram define the composition towards iron sulphides (Pyrite and Marcasite), natrojarosite, clay (kaolinite and smectite) quartz and hematite. The diffraction peaks for natrojarosite are moderate in intensity. Thus all analytical techniques prove natrojarosite in the area.

4.5.1 Jarosite distribution and its genesis in Warkalli Formation

The genetic environment for the formation of particular minerals depends mainly on climatic, hydrologic and lithologic factors present in the area. Concretions of pyrite/marcasite have been observed in the Warkalli Formation, which usually converts into hydrated ferric oxides/jarosite after oxidation. Varkala Cliffs exposes all the lithounits of Warkalli Formation formed under a fluvio-lacustrine environment. The base of Warkalli Formation is marked by carbonaceous clay rich in lignite or the peat swamps. Abundance of organic matter deposited in a fluvio-lacustrine environment normally develops an anaerobic environment by removing available oxygen through decomposi-

tion of organic matter containing sulphur compounds as well as by creating a ferricrete layer preventing the underlying layers to have any contact with atmospheric oxygen. The sulphur thus liberated combines with hydrogen from the water to form H_2S. Marcasite (FeS_2) occurs as radiating/ ramifying clusters indicating replacement of organic matter from tree twigs. Marcasite reacts more readily than pyrite under conditions of high humidity (oxidation) and disintegrate to form jarosite (disintegration of marcasite is referred as 'pyrite decay'). In marcasite and lignite seams, sulphide mineral oxidation precipitates efflorescent jarosite during the coincidence of a dry climatic spell and low tide level. The formed jarosite undergo dissolution to form ferric oxyhydroxides during the monsoonal climatic conditions and this dissolution results in lowering the pH of the spring water spouting from this cliff. The typical efflorescent nature of jarosite suggests a longer dry spell prevailing seasonally in this area. At place, the replacement texture produced by jarosite indicates a complete replacement of marcasite to jarosite. Usually the upwelling of groundwater is a major prerequisite for the formation of jarosite in Martian scenario (Hanna et al., 2007). In this area, the sandstone overlying the carbonaceous clay layer acts as a perched as well as a confined aquifer and hence contributes water for the formation of jarosite. The coastal nearness of this geologic formation facilitated the supply of sodium which made it a natrojarosite. Natrojarosite also shows the typical replacement texture. Generally non-stoichiometric (non-ideal chemical formula) jarosites are formed in lacustrine environment, but the presence of natrojarosite makes this area different from other areas (Swayze et al., 2000).

Usually, inorganic oxidation of pyrite/marcasite leads to the production of sulphuric acid, which reacts with the calcite of the country rock to form gypsum (Sass et al., 1965). VIS-NIR-SWIR data indicate the presence of some carbonate species in the area, but they have not been identified in XRD or Raman analyses. The seasonal absence of jarosite could be attributed to its solubility in the waters either in the rains or occasional floods in the area. On the other hand, formation of jarosite/natrojarosite could be explained by

the mechanism which involves the attack of sulphuric acid on clay group of mineral to leach out alkalis (K, Mg) and alumina, resulting into the formation of jarosite/natrojarosite in the area. The restricted occurrence of natrojarosite to the far shore part of coastal cliffs in association with clay is due to long-established acidic conditions (pH 2-3) compare to the near shore part of the coastal cliffs. Slight increase in the pH values most likely on near shore coastal cliff zones leads to the formation of hydrated iron oxides (Merwin and Posnjak, 1937). The most important reason which makes the Warkalli Formation as a unique is that the association of jarosite in a peat swamp helps as a proxy in orbital data to locate such organic rich layer in other terrestrial and extra-terrestrial world where such deposits are expected.

4.5.2 Implications to Mars

Jarosite is reported at a few sites on Mars, for instance, Eagle Crater (Klingelhofer et al., 2004) and Meridiani Planum (Squyres and Knoll, 2005) by using the Mossbauer spectrometer data aboard Mars Exploration Rover (MER) Opportunity and Mawrth Vallis by using MRO-CRISM data (Farrand et al., 2009). Although many of the places on Mars, distribution of phyllosilicate and sulphate is stratigraphically and temporally different, jarosite and Fe/Mg phyllosilicate are observed in close vicinity in the regions such as Terra Meridiani (Poulet et al., 2008). Other places on Mars, those have been detected with both jarosite and Fe/Mg phyllosilicates are Columbus Crater, a potential palaeo-lake in Terra Sirenum (Wray et al., 2009) and Mawrth Vallis, where a jarosite-rich layer directly overlying a Fe/Mg smectite layer (Farrand et al., 2009). Formation of jarosite in Mawrth Vallis has been postulated that it could have formed by later acid-sulphate alteration of the Fe/Mg smectite layers below (Altheide et al., 2010). Jarosite requires a specific environment for crystallization like highly acidic (preferably <4) S-rich brines under highly oxidizing conditions (Papike et al., 2006). The possibilities of formation of such

an ideal hotspots are either volcano/hot springs or oxidation of iron sulphide where there is an abundance of SO_2 (Rao and Gluskoter, 1973). The other terrestrial analogue sites are generally temperate [e.g. Rio Tinto, formed by biomineralization (Oggerin et al., 2014)]; permafrost [e.g. Golden Deposit, Canadian Arctic; (Battler et al., 2013)] and volcanic province [e.g. Deccan Volcanic Province, India; (Mitra et al., 2014; Bhattacharya et al., 2016)]. The coexistence of jarosite and Fe/Mg phyllosilicates, which is consistent with the jarosite-phyllosilicate deposit of Olduvai Gorge, Tanzania, presents a significant site in determining the aqueous geochemical conditions at the time of deposition/diagenesis (McHenry et al., 2011). Although, Varkala jarosite deposit has been formed as a precipitate under a warm humid tropical condition with surplus supply of sodium from the adjacent sea, it has the consistency with the diverse diagenetic environments occurred in the palaeolake deposits of Columbus crater, Terra Sirenum (Wray et al., 2009) or Terra Meridiani (Poulet et al., 2008) where the association of jarosite and Fe/Mg phyllosilicates prevails. Varkala jarosite deposit is short-lived and local due to warm and wet conditions, unlike to the stable jarosite deposits on Mars consistent with cold and dry conditions (Elwood Madden et al., 2009). In addition, Varkala jarosite deposit witnesses different diagenetic textures and therefore, Martian jarosite deposits, which are thermodynamically stable in most of the present-day temperature and pressure conditions, could also have preserved the chemical and textural characteristics of early Mars (Navrotsky et al., 2005; Cloutis et al., 2008). The identified optimum bands/peaks by different spectroscopic techniques for various hydrous and anhydrous minerals will further help in locating the similar mineralogical deposits that could be different paragenesis on Mars. Relevancy to carry out in-situ spectroscopic studies (through laser Raman and ATR-FTIR) on planetary surfaces is also validated and that will improve the quality of scientific information, one has today.

4.6 Conclusions

Jarosite occurs in various local sedimentary conditions ranging from replacement to diagenetic types in palaeo-lacustrine settings in Varkala, India. In spite of having a close relation to saline-alkaline environment as major mineralogical entity belongs to phyllosilicate group, presence of jarosite proves the local and unstable acidic environment in time. Though Varkala jarosite is formed by major sedimentary processes without any involvement of direct volcanic evidence in terrestrial conditions, its jarosite-phyllosilicate association gives direct indication of diverse environmental conditions at the time of its formation. Similarly, jarosite-phyllosilicate association on Mars such as palaeolake deposits of Columbus crater, Terra Sirenum (Wray et al., 2009) or Terra Meridiani (Poulet et al., 2008) proves local diverse environmental conditions at the time of their deposition. In addition, Varkala jarosite deposit is also helpful in validating the proposed depositional mechanisms for much localized jarosite formations on Mars (Farrand et al., 2009) and also to give the insights into the regions with complex diagenetic history of different hydrous sulphate and phyllosilicate mineral species.

CHAPTER 5

Mineralogical Investigations in East Candor Chasma, Valles Marineris, Mars and Possible Implications

Preclude

This chapter deals with spectral reflectance data of East Candor Chasma, studied using MRO-CRISM (Mars Reconnaissance Orbiter-Compact Reconnaissance Imaging Spectrometer for Mars) datasets. Important hydrous group of minerals namely carbonates and sulphates have been detected on three different spatial locations, these are plateau, wall (layered deposits) and floor regions, which provide significant inputs in depicting the hydrous processes on the planet. Identified carbonate group of minerals mainly on plateau surface include calcite and hydro-magnesite with peculiar absorption bands in 1.2-2.6 μm and 3.2-3.9 μm. They could be the alteration products of high calcium or magnesium minerals of igneous origin in the presence of water. Wall region or interior layers deposits are found to be rich in sulphate and phyllosilicate group of minerals such as kieserite which could be one of the important clues in understanding the weathering pattern on or within the surface. Floor region of East Candor Chasma is found to be rich in pyroxenes and iron bearing minerals, which might be preserving unaltered/prestine or partially weathered host rock primarily rich in mafic minerals. Detected mineralogy such as carbonates and phyllosilicates has strong support to the alkaline nature for their formation and surely adds the information to the evolutionary history of the region.

5.1 Introduction

Orbital mapping of aqueous minerals by various inter-planetary missions such as Thermal Emission Spectrometer (TES) on Mars Global Surveyor (Christensen et al., 2001), Observatoire pour la Mineralogie, L'Eau, les Glaces et l'Activité (OMEGA) on Mars Express (Bibring et al., 2005, 2006; Poulet et al., 2005; Gendrin et al., 2005), and Compact Reconnaissance Imaging Spectrometer for Mars (CRISM) on Mars Reconnaissance Orbiter (Murchie et al., 2007; Mustard et al., 2008) has given confirmation to the existence of liquid water on/near surface environments in the geological history. Interpretation of the data obtained from these missions suggests that the altered minerals formed on Mars' surface in early to middle Noachian period are phyllosilicate-dominated with minor carbonates (Poulet et al., 2005; Mustard et al., 2008; Ehlmann et al., 2008) whereas Hesperian period is dominated by sulphate-rich assemblages with limited regional occurrences of hydrated silica (Mangold et al., 2008; Milliken et al., 2008). The depositional environments for phyllosilicate and carbonates suggest neutral to alkaline pH (Bibring et al., 2005, 2006) in Noachian period and sulphate-rich assemblage suggest acidic conditions prevailed during Hesperian period (Gendrin et al., 2005; Bibring et al., 2006). This variation in the depositional conditions is hypothesized by an early wet period when phyllosilicates were formed and ended with the weakening of the magnetic field around Mars (Murchie et al., 2009) and by the rise of Tharsis volcanoes SO_2 emissions acidified the available liquid water resulting into the formation of sulphate-rich assemblages (Solomon et al., 2005). Adding to the existing information, CRISM has detected more diverse and widespread distribution of alteration products, for instance phyllosilicate and carbonate mineral assemblages, which are reported in Capri Chasma using CRISM datasets (Jain and Chauhan, 2015). On Earth, carbonates are either formed by living organisms' activity in liquid water or alteration of igneous minerals by sulphur (Tosca et al., 2004; Hausrath et al., 2008). Martian carbonate occurrences are interpreted by various ways and they are: 1) reaction between hot CO_2 rich fluids

generated due to impacts and ultramafic rocks (Harvey and McSween, 1996), (2) as a precipitate from shallow ephemeral lakes (Melezhik et al., 2001), and (3) percolation of groundwater through fractures in olivine-rich igneous rocks at higher temperatures (Ehlmann et al., 2008). The major occurrences of sulphates are identified mainly in layered deposits, Meridiani Planum (Arvidson et al., 2005), Aram Chaos (Glotch and Christensen, 2005), and the interior layered deposits (ILDs), Valles Marineris chasma system on Mars (Gendrin et al., 2005; Mangold et al., 2008). ILDs of Candor Chasma are studied in quite detail (Murchie et al., 2009) and are found to be enriched in hydrated sulphate minerals, finely crystalline ferric oxides as detected by OMEGA (Gendrin et al., 2005; Mangold et al., 2008) and coarser-grained gray-colored hematite patches as identified by TES (Christensen et al., 2001a and b). The genetic mechanism and the relationship between the sulphates and hematite bearing deposits of the ILDs of Valles Marineris is a well studied aspect, particularly in Meridiani Planum by TES, OMEGA and landed measurements by the Mars Exploration Rover (MER) *Opportunity* (Arvidson et al., 2006; Squyres et al., 2006) and Candor chasma (Murchie et al., 2009).

Here we report new mineralogical results based on reflectance spectroscopy in East Candor chasma of Valles Marineris using CRISM datasets. This study focuses on reflectance spectroscopy based aqueous minerals detection in East Candor chasma. We show that the interior layered deposits and plateau regions are dominated with dust and basaltic sand with hydrated sulphates, ferric oxides and carbonates. We discuss the acquired spectral results of East Candor chasma to decipher the probable mechanism for the formation of sulphate-carbonate mineral assemblage in the study area.

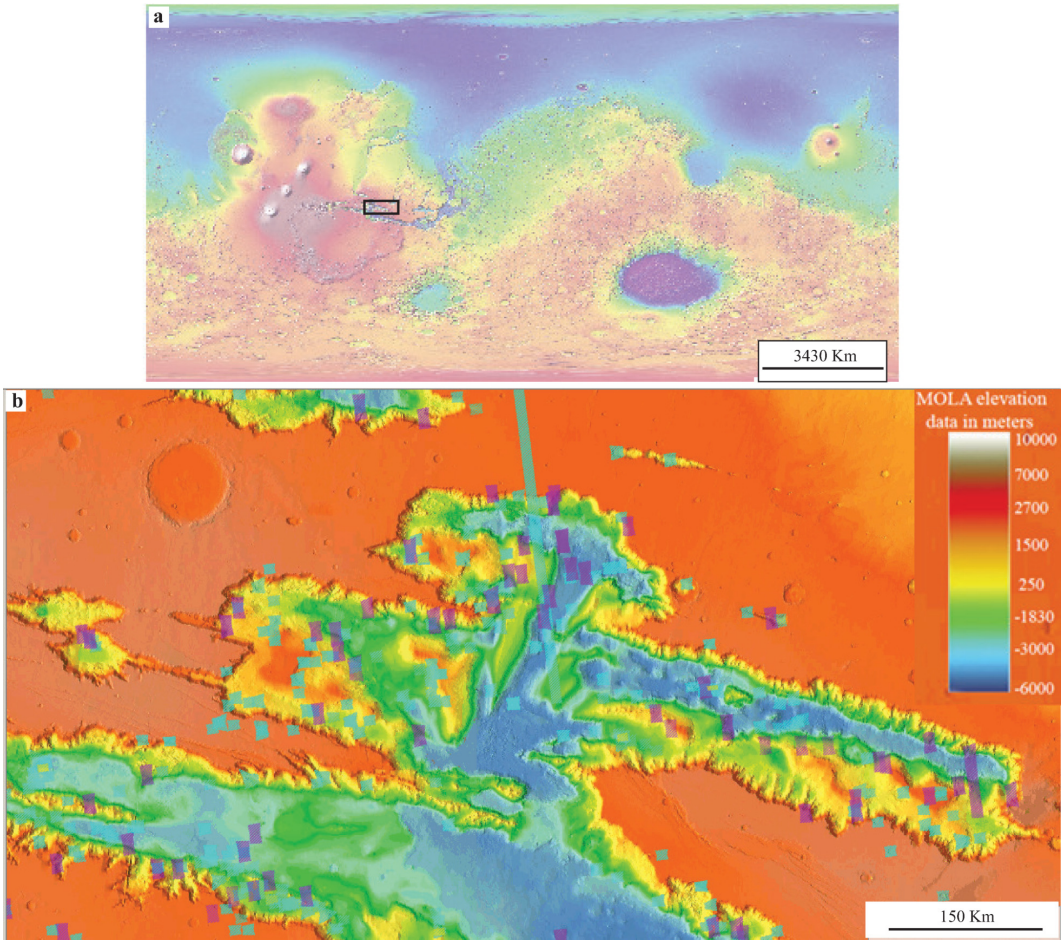

Figure 5.1: (a) The Mars Global Surveyor-Mars Orbiter Laser Altimeter (MGS-MOLA) Shaded Relief Map showing the location of Candor Chasma within Valles Marineris, (b) focused area of Candor Chasma studied here.

5.2 Geological Setting

Candor chasma is one of the largest canyons in Valles Marineris and has been considered into two divisions based on its linear stretch in E-W direction: East Candor chasma and West Candor chasma (Fig. 5.1 and 5.2). Nedell et al. (1987) and Komatsu et al. (1993) has reviewed the geology and geologic setting of the ILDs, which form eroded plateaus of several kilometers in relief mainly on the floors of many chamsas namely, Hebes, Melas, Ophir, Candor and Ganges. Scientists have not discussed the mineralogical and hydrological aspects, and genetic mechanism of layered deposits in the area (Murchie et al.,

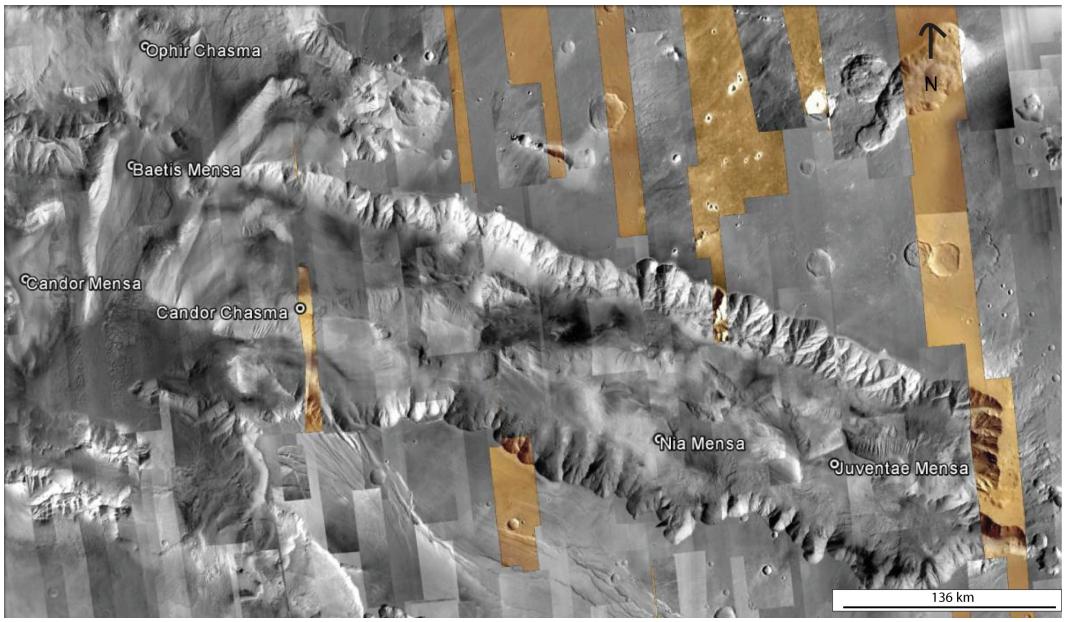

Figure 5.2: MRO-CTX image showing East Candor chasma with Nia Mensa and Juventae Mensa.

2009). Okubo et al. (2008) has shown that the parts of the deposits of West Candor chasma are highly deformed. The compositional study done by Mangold et al. (2008) in ILDs of Western Candor chasma using OMEGA data has shown the scarce presence of pyroxenes with dominant hydrated sulphates, mainly monohydrated Mg-rich kieserite. Steeper slopes of Western Candor chasma are mainly composed of monohydrated sulphates whereas comparatively gentler slopes are composed of polyhydrated sulphates. In Western Candor chasma the lower and middle parts of the walls are dominated with kieserite which is overlain by polyhydrated sulphates (Murchie et al., 2009). Formation mechanism of polyhydrated sulphates is possibly due to the hydration of monohydrated sulphates under modern ambient conditions as predicted by Vaniman et al. (2004) in sulphate stability model or at the time of kieserite formation, polyhydrated sulphates would have resulted as evaporites. Eastern Candor chasma witnesses multiple intercalated layers of polyhydrated and monohydrated phases (Roach et al., 2008, 2009). Roach et al. (2009) suggested that monohydrated sulphates are not actively being altered to polyhydrated sulphates based on three main regions: 1) co-occurrence of both phases in ad-

jacent layers of the ILDs, 2) interbedding, and 3) persistence of monohydrated sulphates in OMEGA and CRISM results without alteration to polyhydrated phases. Ferric minerals are also found associated with sulphates in Valles Marineris (Christensen et al., 2001a).

The genetic mechanism of ILDs has been proposed by many scientists and it shows broad spectrum of processes ranging from accumulation of eolian dust or sand (Peterson, 1982) to subaqueous volcanism (Nedell et al., 1987). Other proposed mechanisms include subaerial fluvial deposition or volcanism (Lucchitta et al., 1988) and evaporite precipitation (McKay and Nedell, 1988). Edgett and Malin (2003) has proposed that the ILDs are eroded remnants of pre-existing layered chasma wall materials which has been supported by Lucchitta et al. (1994) where volumetric calculations show that the wall materials was only one among the sources for ILDs compositions. Therefore, there are many uncertainties associated with the ILDs of Valles Marineris regarding their evolution, concentrations of sulphates, depositional and diagenetic environments.

5.3 Results and discussions

5.3.1 Mineralogy of the study area

West Candor chasma has been studied from the quite ancient times for its specific deposits either for the mineralogical variations or their genesis (Geissler et al., 1993; Mangold et al., 2008). Geissler et al. (1993) has analyzed the layered deposits using Viking Orbiter multispectral images and Phobos ISM 2 instrument data with the indication of local compositional difference, produced by secondary alteration of the sediments in geological past. Using OMEGA (Observatoire pour la Minéralogie, l'Eau, les Glaces et l'Activité) datasets, kieserite and polyhydrated sulphates has been identified in the chasma by the definite

combination of spectral absorption bands; for kieserite the absorption bands fall at 1.6 μm, 2.1 μm and 2.4 μm, and for polyhydrated sulphates the absorption bands fall at 1.4 μm, 1.9 μm and 2.4 μm (Hunt et al., 1971; Bishop and Murad et al., 2005; Gendrin et al., 2005). Mangold et al. (2007) has studied the mineralogy of the sulphate rich regions in West Candor chasma using OMEGA spectral data and HRSC (High Resolution Stereo Camera) datasets, and major mineralogy identified include sulphates, iron oxides and mafic minerals. In the present study, we have used one of the most recent spectral data MRO-CRISM available in the 0.4-3.9 μm region of electro-magnetic radiation (EMR) for the identification of mainly hydrous minerals in East Candor chasma. Using the standard processing technique after removing the atmospheric gas absorptions for each pixel, it has been found that spectral signatures of mafic minerals (pyroxene and olivine) and hydrated minerals (sulphates, phyllosilicates) can be identified in the 1-2.5 μm wavelength range. The studied area is found enriched in sulphate and carbonate group of minerals and the confirmation of the mineral species is being done by the comparison of absorption bands of the target area to the CRISM spectral library. The obtained results have confirmed the presence of hydrous minerals such as sulphates i.e. kieserite and other polyhydrated sulphates, palagonite (an alteration product of volcanic glass) and carbonates i.e. calcite and hydromagnesite (Fig. 5.3).

The main mineral groups identified are as follows:

Sulphates

Kieserite

Kieserite, a magnesium monohydrate sulphate ($MgSO_4 \cdot H_2O$) is commonly found in marine evaporites with rare occurrences in volcanic environments as sublimates in terrestrial scenario. The spectra of kieserite shows the absorption bands at 1.6, 2.1 and 2.4 μm (Fig. 5.3), in which 1.6 and 2.1 μm

absorption features are due to overtones and combinations of the symmetric H-O-H stretch (ν_1), the asymmetric H-O-H stretch (ν_3), and the H-O-H bend (ν_2), and 2.4 μm absorption feature is due to SO_4^{2-} stretch (Clark et al., 1990; Gendrin et al., 2005). Here, 1.6 and 2.1 μm absorption bands correspond to 1.4 and 1.9 μm absorption features due to shift towards longer wavelength; the shift is due to strong coupling between the single water molecule and the sulphate ion (Crowley et al., 2003). Alternatively, monohydrated Fe-sulphate szomolnokite ($FeSO_4 \cdot H_2O$) which has similar features as kieserite in the 1.5-2.5 μm range could also be considered to be fit for the observed spectra. These two minerals differ only in terms of major cation Fe^{2+} and Mg^{2+}, but szomolnokite has a broad ferrous band from 1.2 to 1.6 μm which is not observed in the spectrum. Kieserite is very unstable when exposed to water and gets converted into hexahydrite ($MgSO_4 \cdot 6H_2O$) and epsomite ($MgSO_4 \cdot 7H_2O$) unless provided with specific thermo-dynamic conditions as expressed in Vaniman et al. (2004). The bulk of the sulphates detected in Valles Marineris are located within the light toned, several kilometers wide to thousands of meters thick layered deposits (Gendrin et al., 2005; Bishop et al., 2009; Murchie et al., 2009). Further, polyhydrated and monohydrated sulphates are identified in Juventae Chasma and Aram Chaos. In Juventae Chasma, polyhydrated sulphates overlie monohydrated sulphates and are distinguished with a distinct geologic contact. Upper beds in Juventae Chasma are dominated by polyhydrated sulphates.

The ILDs in Aram chaos resemble well with the layered material of Juventae and Western Candor chasma with polyhydrated sulphates overlying monohydrated sulphates. There are several hypotheses given to define the formation of distinct monohydrated and polyhydrated sulphates on Mars, including 1) sequential deposition in an evaporating basin, 2) dehydration of a polyhydrated Mg sulphate to kieserite by heating after burial and or 3) dehydration of an existing polyhydrated sulphate deposit by upwelling hydrophillic chloride-rich brines within a tectonically active fault basin (Hardie, 1991; Roach et al., 2010). East Candor chasma that falls in the vicinity of Valles Marineris, a

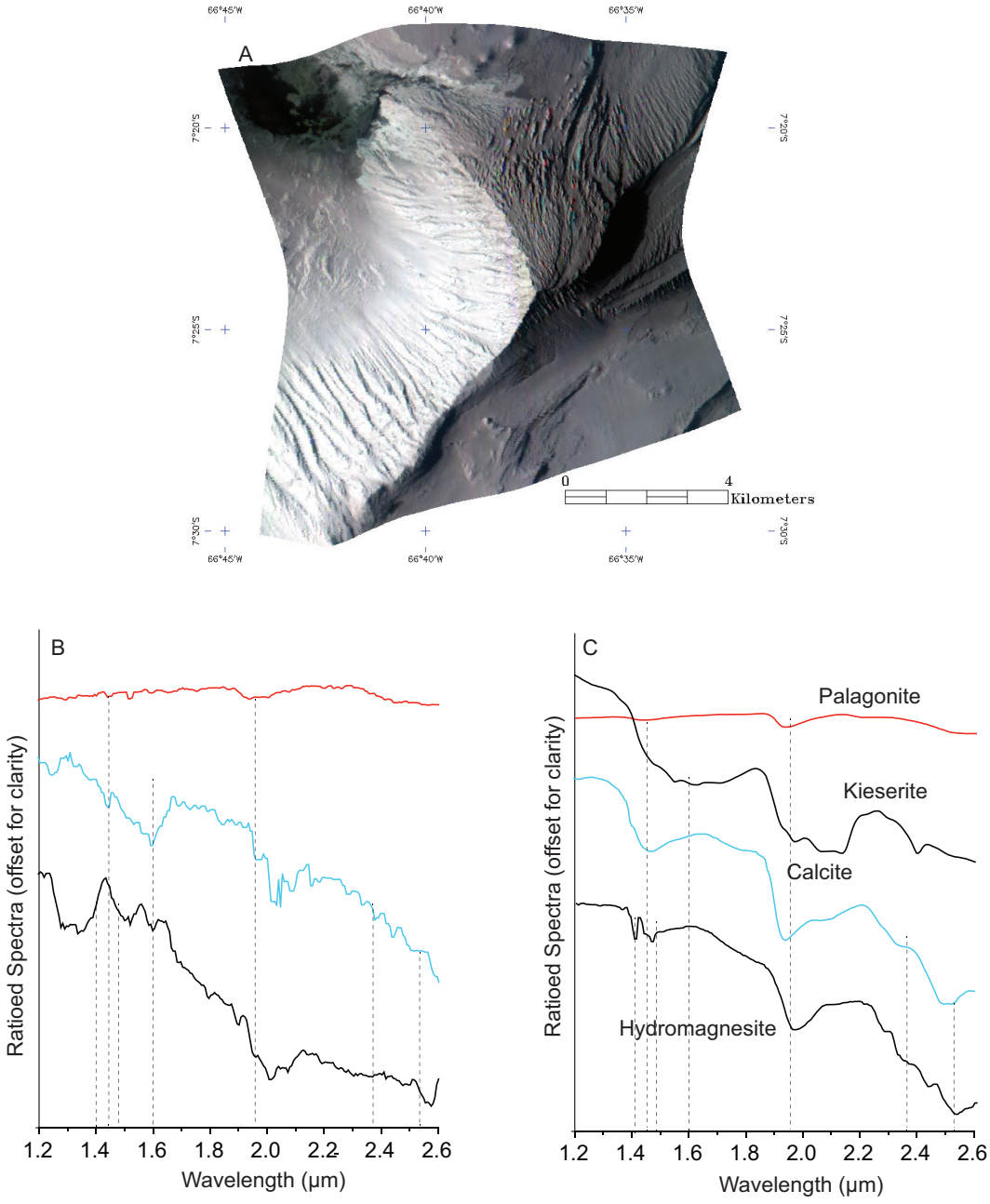

Figure 5.3: (A) CRISM scene frt00010e3e_07_if165l_trr3 (B) Reflectance spectra of different mineral phases from interior layered deposits of East Candor chasma, namely palagonite, kieserite, calcite and hydromagnesite. (C) Reference spectra from CRISM spectral Library for the identified minerals.

major canyon system of Mars could have witnessed dehydration of an existing polyhydrated sulphate into monohydrated sulphate deposit by upwelling hydrophillic chloride-rich brines.

Carbonates

Calcite and hydromagnesite

Calcite is the most stable polymorph of calcium carbonate. Carbonates are identified on the basis of the absorption bands at 1.9, 2.30 and 2.51 μm in orbital reflectance spectroscopy as reported by Ehlmann et al. (2008). The absorption band at 1.9 μm correspond to -OH group. In the present study, the carbonates are identified based on the absorption bands at 1.9, 2.35 and 2.55 μm along with the characteristic absorption bands at 3.4 and 3.9 μm (Fig. 5.3). These orbital spectra are compared with the carbonate reference spectra recorded in CRISM spectral library. Although, the absorption bands are not very clear in 1.2-2.6 μm region, but the absorption bands in 3.2-.3.9 μm region are very clear and prominent (Fig. 5.4). Hydromagnesite ($Mg_5(CO_3)_4(OH)_2{\cdot}4H_2O$) is a hydrated magnesium carbonate mineral and is generally found associated with the pristine magnesium containing minerals such as serpentines. This is also one of the carbonate which shows the similarity in the absorption bands positions with the observed spectra from Candor chasma (Fig. 5.3).

Discussion based on absorption bands of carbonates has been given by Ehlmann et al. (2008) where she has reported extensive carbonate exposures identification in Nili Fossae. Carbonates suggest a warmer and wetter climate in the geological past on any planet and on Mars this could be explained by the identified carbonate exposures on the surface of Columbia Hills of Gusev crater (Morris et al., 2010) Nili fossae, (Ehlmann et al., 2008) and Capri Chasma (Jain et al., 2015).

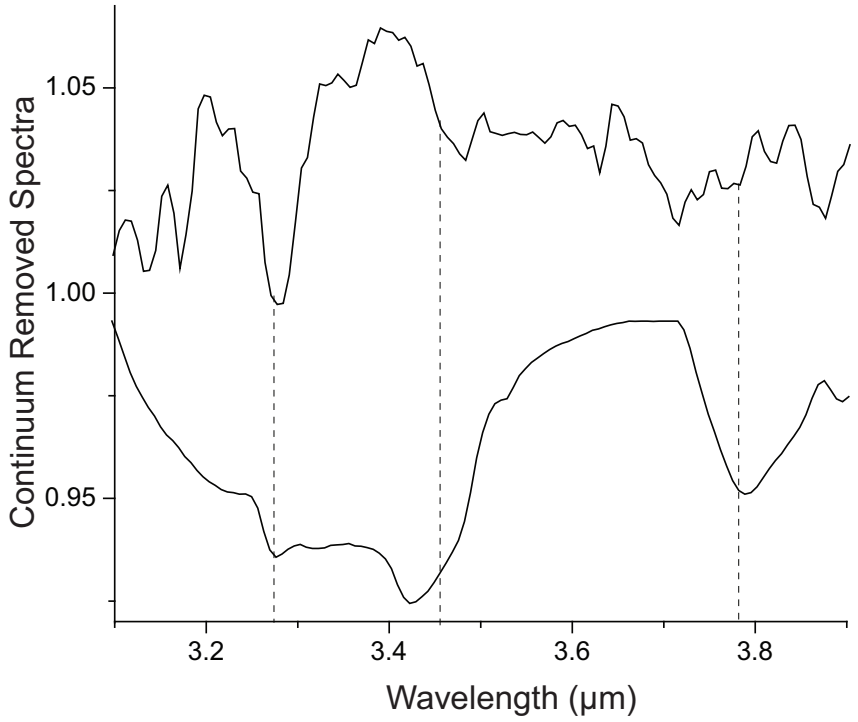

Figure 5.4: Reflectance spectra of calcite in 3.1-3.9 μm wavelength range.

Silicates

Palagonite

Palagonite is an alteration product formed through the interaction of water with volcanic glass of basaltic composition. Palagonite can also be formed by slower weathering of lava. Palagonite has also been detected onto Martian surface and the best match, to the spectral properties for it, is found in Mauna-Kea palagonite deposit on Earth and the palagonitic tephra from a cinder cone in Hawaii, which has been used to create Martian regolith simulant (Allen et al., 1981; Singer, 1982; Guinness et al., 1987). Palagonite is identified on the basis of the absorption bands at 1.45, 1.93 and 2.52 μm. Terrestrial palagonitic soil is considered as a good analogue to the Martian dust (Allen et al., 1998).

5.4 Conclusions

Interior layered deposits and plateau regions in the East Candor Chasma are found to be rich in carbonates and polyhydrated sulphates. These mineral species would have been formed either through deposition by surface alteration or during the weathering of the plateau material. Presence of carbonates in the area suggests the activity of water/hydrothermal activity. Additionally, sulphates and carbonates require liquid water to form at least at 2-3 km depth. Therefore, presence of these minerals helps in defining the hydrologic conditions in the area. Sulphates detected in the study area require presence of liquid water to form by precipitation, either in an intermittent lacustrine environment or by hydrothermal fluid circulation environment.

CHAPTER 6

Comparison of reflectance spectroscopic data from the study areas to their counterparts on Mars

Preclude

This chapter presents a comparative account based on reflectance spectroscopic data from the sites gypsum deposit, Tiruchirapalli, Tamil Nadu, banded iron formation, Odisha and jarosite deposit, Kerala to their counterparts on Mars. Spectral, geomorphological and mineralogical comparisons are made. Further, implication of the findings to Mars are given.

6.1 Introduction

Mars has always been a topic of intensive research for astrobiological evidences due to its established hydrated nature, which is anticipated by means of hydrous mineralogy detected (e.g. hydrous sulphates, phyllosilicates and carbonates) (Tosca et al., 2008; Bibring et al., 2006; Gendrin et al., 2005). On Earth, all the organisms' life is supported by water; therefore existence/presence of water in liquid form on any planet raises the possibility for the existence of life activity in surface to subsurface environments. Considering the habitability, research suggests that all types of water are not habitable for life activity in terrestrial conditions and the limiting factors comprises: water activity, temperature, pH, and thermodynamic measure of salinity (Knoll et al., 2005; Tosca et al., 2008). The habitability of Mars is discussed mainly after the detection of water ice in the areas such as polar caps and ice/water within the

top meter of the high latitude regolith (Carr, 1996; Malin and Edgett, 2000; Mellon and Phillips, 2001). Although, the conditions when minerals precipitate on Martian surface could be little different than in terrestrial scenario, like evaporation of dilute Martian waters results in distinct saline mineral assemblages, causing some minerals that are common in terrestrial settings to precipitate at lower water activity than they do on Earth (Tosca et al., 2008). Despite the difference in the habitability and atmospheric conditions of Earth and Mars, extensive research has been done to define the habitability of different mineral assemblage in different hydration conditions (Jakosky et al., 2003; Atreya et al., 2007; Fairén et al., 2010; Westall et al., 2013; Léveillé et al., 2014). In the field any breakthrough is yet to come about life signatures from Mars and the potential habitats are being proposed with more details from terrestrial sites in different geological settings (Fairén et al., 2010; Mahaffy, 2008; Fernández-Remolar et al., 2008).

Gypsum deposits explained to be formed by evaporation of SO_4 rich waters on the surface; but it's occurrence in other forms such as mineral veins in hydrothermal systems. Haughton impact structure, where gypsum possesses fluid inclusions of monophase nature and preserved microbial colonization within the gypsum grains is proposed to be checked for life-signatures and palaeo water chemistry (Parnell et al., 2004). Jarosite occur in acidic and oxidising environment on Earth, which is also reported from Meridiani Planum, Mars suggesting intermittent acidic, oxidizing, and saline groundwater conditions (McLennan et al., 2005; Grotzinger et al., 2005). Banded iron formations (BIFs) which are chemical sedimentary rocks with alternate iron-rich and silica-rich layers, formed with or without direct involvement of volcanic activity are always considered as a potential analogue to the layered hematite deposit in Meridiani Planum on Mars because of their larger extent (Catling and Moore, 2000). Although, defining the occurrence of BIFs on Martian surface could be a tricky task as no hydrothermal hot fluid or aqueous environment is detected, but the correlation of layered hematite deposit in Meridiani Planum to less proportion siliciclastic BIFs such as Proterzoic iron formations in terrestrial scenario

and underground iron-rich sources whose hydrochemistry and thermodynamics favoured precipitation of Fe-bearing minerals but not silicate deposition is proposed (Fernández-Remolar et al., 2003).

Gypsum, BIFs, jarosite and have direct or indirect potential towards preservation or support to life activity (Christensen et al., 1999; Amaral et al., 2005; Martinez-Frias et al., 2006; Amaral et al., 2007; Schopf et al., 2012). Considering these aspects, gypsum-phyllosilicate association of Karai Shale Formation, jarsite deposit of Varkala and banded iron formations (BIFs) of Singhbhum craton, Odisha have been characterized by using a wide range of spectroscopic techniques, which could be used as database for later research in the field. In this chapter, spectral comparison of the dominant minerals identified in the study is provided with their Martian counterparts.

6.2 Geological background of the study areas

Near Karai village, marine gypsiferous phyllosilicates are exposed in mine cuttings. The colour of the gypsiferous clay is white to yellow and this change in colour is attributed to change in the provenance. Karai Shale Formation is comprising of two Members: Odiyam sandy clay and gypsiferous clay, and are well exposed as badland (terrains where sedimentary rocks/clay rich exposures are heavily eroded by fluvial or eolian activity with high drainage density) in an easterly draining catchment to the East of Karai village in Tiruchirappalli (Ramkumar et al., 2004). Sundaram and Rao (1986) have divided Karai Shale Formation into two members based on a type areas: Odiyam and Kunnam. Odiyam Member constitutes gypsiferous mudstone with distinctive thin inter beds of pink shale and siltstone, and sporadic lenticular beds of coquinite and sandstone comprising the lower part of the Formation (Sundaram et al., 2001). In the upper part of the Formation, gypsum is present in the form of regular to irregular veins in Fe-rich phyllosilicates along with the sporadic

and inter-layered occurrences. Kunnam Member constitutes inter layered mudstone, gypsiferous siltstone and fine-grained sandstone with calcite and siderite cements.

The BIFs of North Odisha are extensively developed supracrustals encircling the Singhbhum granite complex and various views have been proposed on the evolution of these supracrustals and their relation to the granite intrusives. Jones (1934), Dunn (1940) and Saha (1994) believed that all the BIFs were formed as a single assemblage during the Archean underlain and/or intruded by the different phases of Singhbhum granites. Relatively younger metasedimentary deposits of banded iron formations of Joda and Daitari region have two types of mineral assemblages: first, banded hematite jasper and second, banded hematite quartzite. These BIFs are conspicuous by the presence of alternate bands composed predominantly of iron oxide and silica. Secondary hematite formed after metamorphism, is generally found in the form of bladed crystals, specular variety called specularite whereas silica is of cryptocrystalline type, admixed with iron oxide dust and granules in jasper to mega quartz. The extensive volcano-sedimentary sequences in the Simlipal and Keonjhar plateaus are considered equivalent to the Dhanjoris and younger to BIFs.

Jarosite deposit, Warkalli Formation, Kerala belongs to the coastal cliff edging the Arabian Sea near Varkala, Thiruvananthapuram-the capital of Kerala state, India. These coastal cliffs are the type area for the Warkalli Formation of Mio-Pliocene resting unconformably over the Precambrian crystallines of Kerala Khondalite Belt (KKB). Jarosite shows the grainy occurrence onto the clayey base with basic replacement texture. Jarosite also occurs in carbonaceous clay layer as encrustations due to diagenetic replacement process and depicts a typical efflorescence texture. This mineral will be periodically washed away by waves during high tide and hence cannot be seen throughout the year. Carbonaceous clay which hosts jarosite is black organic-rich clay bed consisting of variable amounts of silt and poorly-sorted sands and is partly

iron oxide-coated.

6.3 Results and discussion

Geomorphological results collected during the field work in the areas and spectral results obtained during VIS-NIR-SWIR spectroscopy are compared with their counterparts available on Mars.

6.3.1 Gypsum-phyllosilicate association of Karai Formation, Tiruchirapalli

Karai Formation possesses a thick sedimentary sequence dominated by hydrous sulphate-phyllosilicate association (Sundaram et al., 2001). Hydrous sulphate is found as vein-type deposit within phyllosilicate (shale) mass with regular to irregular trends (Fig.6.1A). Although, the formation mechanism for this gypsum is proposed to be evaporitic (Sundaram et al., 2001; Ramkumar et al., 2004); precipitation by circulating brines in the fractures developed due to fluid over-pressure during compaction could be more relevant, particularly veined gypsum of Karai area. *Homestake*, one of the most discussed hydrous sulphate vein (calcium sulphate) in Endeavour crater, Cape-York, Mars has been proposed to be formed by the movement of sulphate rich fluids in the fractures of the host rock (Squyres et al., 2012) (Fig.6.1B). Direct correlation between *Homestake* and gypsum at Karai is not plausible because of two different country rocks.

Reflectance spectra acquired for gypsum, show the absorption features in the electrical and vibrational range of electromagnetic spectrum at 0.56, 0.65, 0.90, 1.0, 1.2, 1.44, 1.75, 1.9, 2.2 and 2.28 μm (Fig. 6.2). The absorption bands in 350-1300 nm range are due to single and paired electron transitions

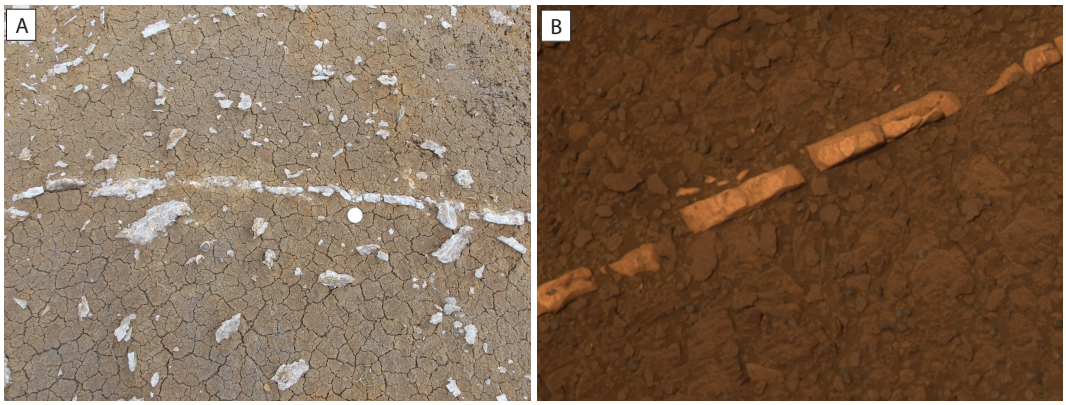

Figure 6.1: Gypsum vein in Karai (A), and the colour view of a mineral vein *Homestake* from *Opportunity's* panoramic camera at Cape-York, Endeavour crater, Mars (B). (Source: NASA/Jet Propulsion Laboratory/ Cornell).

in Fe between energy levels in unfilled 3d orbitals and metal-ligand electron transfers (Sherman and Waite, 1985). The distinct absorption features in 1.4-2.5 μm range are characteristic of fundamental vibrations due to H_2O and OH combinations and overtones (Hunt et al., 1971; Clark et al., 1990; Clark, 1993). OMEGA spectra for gypsum show the absorption bands at 1.44, 1.9 and 2.28 μm and it is to note that the absorption bands are clearer in ratioed spectra than observed spectra. The average spectrum from Karai is having all the characteristic absorption bands derived for the gypsum Northern polar deposits, Mars (Pelkey et al., 2007).

OMEGA imaging spectrometer observed absorption bands at wavelengths of 1.45, 1.75, 1.94, 2.22, 2.26, and 2.48 μm in the Northern circumpolar regions of Mars, which are attributed to calcium-rich sulphates, most likely gypsum (Massé et al., 2012). Gypsum were also detected in Olympia Planum and other parts of the Circumpolar Dune Field (Fishbaugh et al., 2007), and on the North polar cap (Massé et al., 2010) by the OMEGA imaging spectrometer (Langevin et al., 2005a) and the CRISM imaging spectrometer. Gypsum has also been identified as one of the mineral constituent in the layered deposits of Juventae Chasma, Valles Marineris, Mars by OMEGA team (Gendrin et al., 2005). The mineralogical observations suggest that water alteration played a major role in

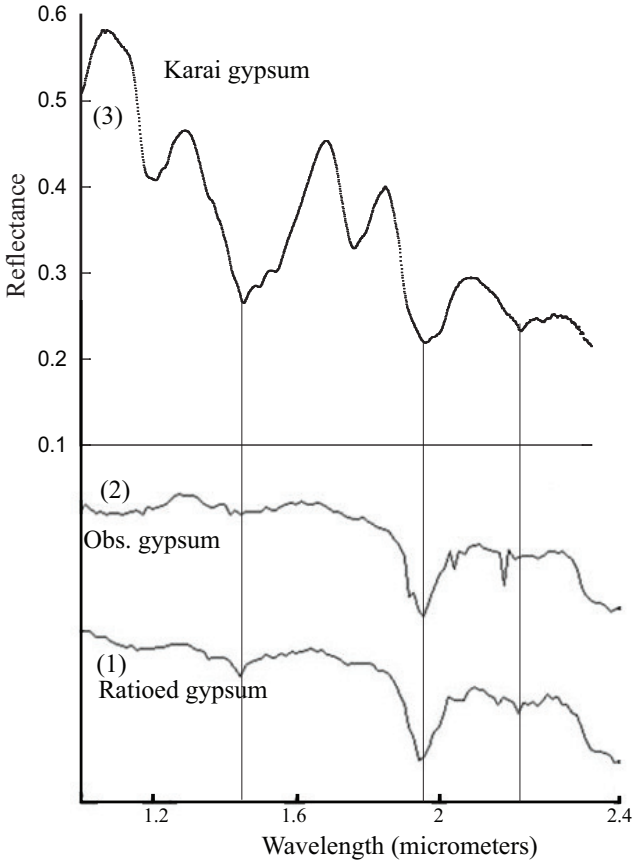

Figure 6.2: OMEGA spectra for gypsum obtained from Northern polar deposits, Mars [(1) Ratioed spectra (2) Observed spectra (modified after Pelkey et al., 2007) and laboratory spectra of gypsum (3) obtained from Karai Formation, Tiruchirapalli.

the formation of the constituting minerals of Northern circumpolar terrains. Fishbaugh et al. (2007) proposed that gypsum could form from a combination of direct, in situ alteration of sulphide and high-calcium-pyroxene-bearing dunes. Gypsum deposits of Meridiani Planum are detected to be 25 wt.% in concentration by MER *Opportunity* and are hypothesized to be formed by evaporation of fluids involved with weathering of basalts (Tosca and McLennan., 2006). Mini-TES observations of the outcrop reveal evidence for Mg and Ca sulphates in Merdiani Planum (Christensen et al., 2004; Glotch et al., 2006b) and cation abundances measured by APXS (Rieder et al., 2004) show dominant Mg-sulphates content with subordinate amounts of Ca-sulphate minerals and jarosite (Clark et al., 2005). The gypsum veins in Cape-York show

the evidences of relatively dilute water at a moderate temperature (Tosca et al., 2008; Squyres et al., 2012).

Reflectance spectra acquired for the gypsum vein of Karai Shale Formation matches well with the spectral data from Mars surface as discussed earlier, hence the results could be used for ground-truthing of any Ca-sulphate rich region in extraterrestrial scenario. Fluid inclusions, preserved within the gypsum grains are one of the significant component which could be analyzed for water chemistry determination. Microbial activity is also pronounced in nearness to the fluid inclusions in gypsum (Parnell et al., 2004), hence gypsum could be one of the prime targets to be explored for life-signatures on Mars. This study proposes that *Homestake* with remnants of fibrous texture in the form of transverse lineations, must be considered for water-chemistry and astrobiological analysis as it has huge potential to preserve fluid inclusions and microbial remnants.

6.3.2 Banded Iron Formation, Singhbhum craton, Odisha

Banded iron formations are chemical sediments, typically thinly bedded or laminated, whose principal chemistry comprises anonymously high content of Fe, commonly but not, inevitably containing silica rich layers, mainly chert (Klein and Beukes, 1992, 1989). The very first evidence of ancient life on Earth has been found associated with the Gunflint Iron Formation, which contains a variety of filamentous to coccoidal forms of microorganisms (Barghoorn and Tyler, 1965; Awramik and Barghoorn, 1977; Strother and Tobin, 1987). BIFs from Carajas (Brazil) and Lake Superior has already been discussed as analogue to layered hematite deposits on Mars (Fig. 6.3A), which are geochemically similar to Odisha BIFs (Fig. 6.3B) (Majumder et al., 1982).

The average spectra of BIFs sample shows the characteristic absorption features at 0.65 (weak) and 0.86 μm (strong) which are basically due to strong iron-oxygen charge transfer absorption and electronic band related to crystal

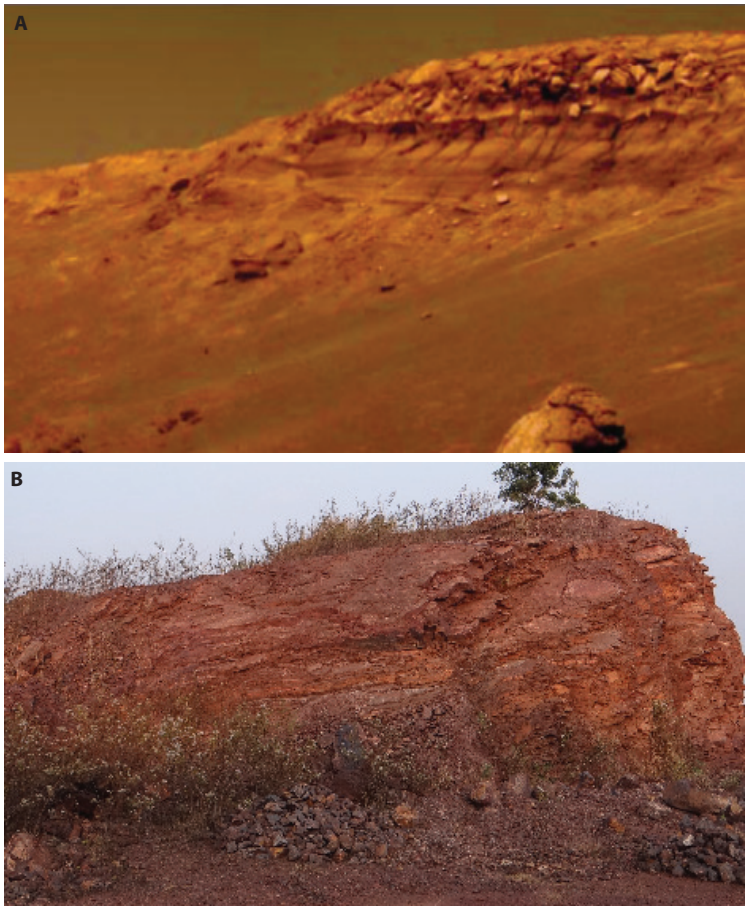

Figure 6.3: (A) Photograph of outcrop of Burns Cliff within Endurance crater (Source: NASA/Jet Propulsion Laboratory/ Cornell), and (B) photograph of outcrop of banded iron formation, Singhbhum craton, Odisha.

field transitions in ferric iron respectively. The representative spectrum of hematite is devoid of any absorption after 1.0 μm, but has a moderate increase in the reflectance.

Due to fundamental Si-O stretching vibration, all silicates show absorption bands in 650-1500 cm^{-1} (Farmer, 1974; Rendon and Sema, 1981; Sema et al., 1982). Oxides and hydroxides show the absorption bands below 800 cm^{-1}, which is shown by the dominant mineral present in Sinus Meridiani. To differentiate between different oxide phases, the shape and position of the absorption bands in the spectra could be one of identifying criteria (Hunt and Ashley, 1979; Christensen et al., 2000). Christensen et al. (2000) have

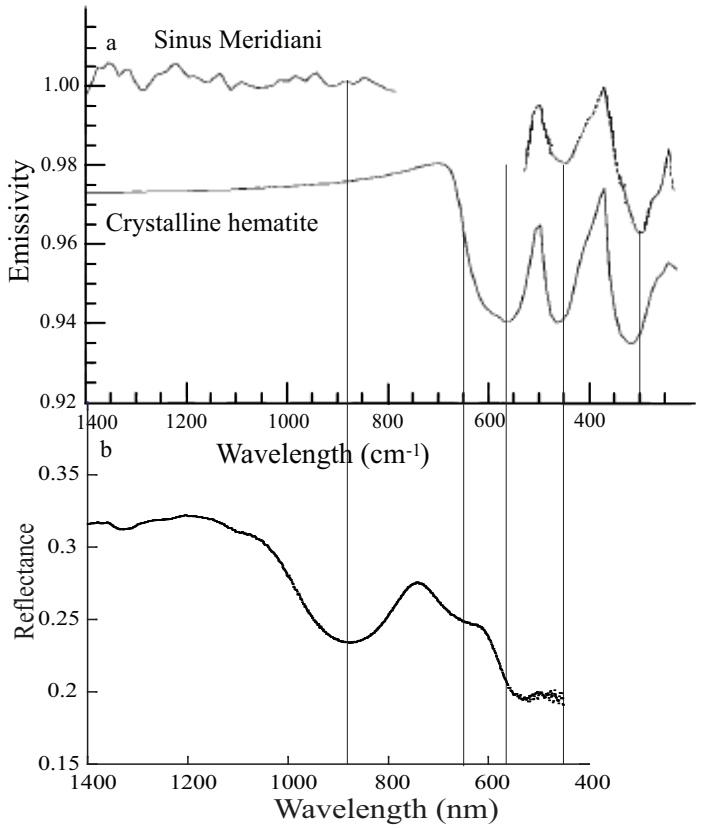

Figure 6.4: (a) Average Sinus Meridiani spectrum and laboratory spectra of hematite acquired using emission spectroscopy (modified after Christensen et al., 2000) and (b) Average laboratory spectra from the banded iron formation, Singhbhum craton, Odisha.

collected emission spectra for a suite of oxide and oxyhydroxides minerals collected in 1600-200 cm^{-1}, and compared the average Sinus Meridiani spectrum to the crystalline hematite. The results from spectral comparison suggest crystalline hematite from spectral library generated using emission spectroscopy, a good match for the surface mineralogy in Sinus Meridiani, with prominent absorption bands at 300 and 450 cm^{-1} and emission maxima at 375 and 500 cm^{-1} (Christensen et al., 2000) (Fig. 6.4a). A careful investigation on the spectral signatures of hematite from present study (Fig. 6.4b) and spectral library spectrum revealed that the spectral signatures are similar with a minor variation in the absorption pattern in 0.5-0.8 μm wavelength regions.

BIFs are proved to be very significant in defining the aqueous processes in

geological time period and preservation of life signatures in hematite as well as silica (Schopf, 1993; Allen et al., 2001; Schelble et al., 2004; Van Kranendonk, 2006; Preston and Genge, 2010). Iron is very prevalent on Mars. Meridiani Planum outcrops are well established in iron-bearing minerals in the form of layered hematite deposits (Christensen et al., 2001b; Hynek et al., 2002; Glotch and Rogers, 2007) (Fig. 6.3A). Apart from hematite, Meridiani Planum outcrops contain fine-grained siliciclastics, sulphate minerals, and some jarosite (Clark et al., 2005; Squyres et al., 2004a and b). Geomorphology of Meridiani Planum show sedimentary structures and diagenetic features, which include ripple marks, cross-bedding, mud cracks and hematite concretions (Squyres et al., 2004a; Grotzinger et al., 2005). The extent of the layered hematite deposit in Meridiani Planum makes it relevant to be compared with terrestrial BIFs. Amorphous silica is also detected with Mini-TES spectra (Squyres et al., 2006; Glotch and Bandfield, 2006). In other areas like Ius chasma, Melas chasma, West of Juventae chasma and Noctis Labyrinthus, silica is identified based on orbital spectroscopy. Considering mineralogical aspect, Meridiani Planum mainly constitutes layered hematite deposit (Christensen et al., 2001b) along with the signatures of silica (Squyres et al., 2006), which are essential components of terrestrial BIFs. Hence, it is of immense possibility that with higher resolution mineralogical data, banded iron formations in a similar or modified version could be detected on Mars, as Earth since Mars possesses similar geological past during Archean and Proterozoic eons. In addition, this study provides BIFs (Fig. 6.3B) spectral data with absorption bands comparable to the spectra of hematite reported from Mars (Christensen et al., 2000). In the preliminary studies BIFs are considered as geochemical analogues to hematite deposition on Mars (Fallacaro and Calvin, 2003; Bridges et al., 2008).

Figure 6.5: Mode of occurrence of jarosite in Varkala, Kerala.

6.3.3 Jarosite deposit, Varkala, Kerala

Jarosite shows the grainy occurrence onto the clayey base with basic replacement texture. Jarosite also occurs in carbonaceous clay layer as encrustations due to diagenetic replacement process (Fig. 6.5) and depicts a typical efflorescence texture. Natrojarosite was first reported and identified by Tassel (1965) in the area.

Average spectral profile of jarosite sample shows the absorption bands centered at 0.91, 1.47, 1.84-1.86 (in the form of a doublet), 1.94 and 2.27 μm, assigned to Fe^{3+}, OH, Na-OH, OH and Mg-OH vibrations respectively (Fig. 6.6). The spectral analysis of jarosite shows the clear deep absorption band of Fe^{3+} at 0.91 μm, masking the absorption features of minerals goethite and pyrite. The intensity of vibrational absorptions is high to moderate for all the hydrous phases.

CRISM ratioed spectrum from Mawrth Vallis region of Mars, smoothed using the Savitsky-Golay filter, acquired in the region from 2.1 to 2.65 μm,

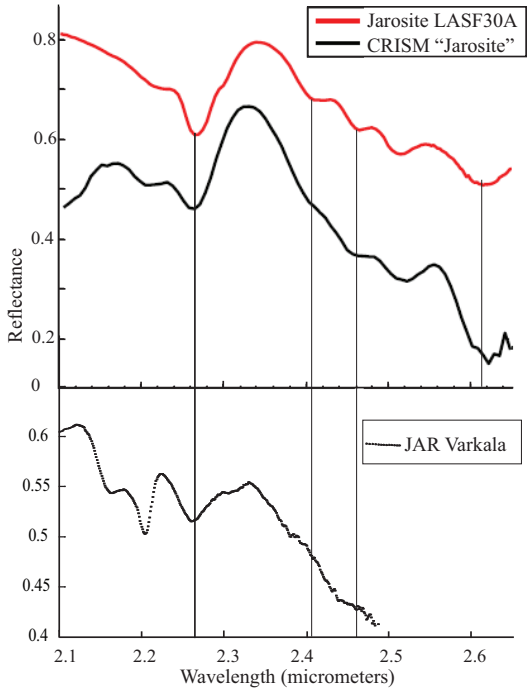

Figure 6.6: Smoothed CRISM spectrum compared with a CRISM-library jarosite spectrum (ID: LASF30A) (modified after Farrand et al., 2009) and jarosite spectra from Varkala, Kerala, India.

compared with the jarosite spectrum from the CRISM spectral library and the matching absorption feature are at the 2.26, 2.46, 2.51, and 2.62 μm (Farrand et al., 2009) (Fig. 6.6). Fig. 6.6 depicts the good match of the spectral response of jarosite from Varkala to the CRISM spectra from Mawrth Vallis and CRISM library spectrum.

Jarosite has been analyzed directly at Meridiani Planum by *Opportunity* where its presence is consistent with other indicators of acidic environment including Mg-sulphates (Tosca et al., 2005). Jarosite and Fe/Mg phyllosilicates are identified in small exposures in Columbus crater, a potential paleolake in Terra Sirenum (Wray et al., 2009). Farrand et al. (2009) has identified jarosite rich layer directly overlying a Mg/Fe smectite-rich deposit in a potential paleolake environment in the Mawrth Vallis, and suggested its formation by later acid-sulphate alteration of the Mg/Fe smectite layers beneath (Altheide et al., 2010).

Varkala jarosite deposit is short-lived and local due to warm and wet conditions prevailing in the area, unlike stable jarosite deposits on Mars consistent with cold and dry conditions (Elwood Madden et al., 2009). Varkala jarosite deposit witnesses different diagenetic textures and therefore, Martian jarosite deposits, which are thermodynamically stable in most of the present-day temperature and pressure conditions, should also have preserved the chemical and textural characteristics of early Mars (Navrotsky et al., 2005; Cloutis et al., 2008). The similar textures, if identified on Martian surface will provide significant information about the aqueous geochemical conditions prevailed in planet's history. The identified optimum absorption bands/peaks by reflectance spectroscopy will further help in ground-truthing or locating the similar mineralogical deposits on Mars.

6.4 Summary and conclusions

The chapter discussed the overall spectral, geo-morphological and sedimentological similarities between the study areas and their counterparts on Mars. The comparison of laboratory spectral data from the study areas and orbital spectral data from Mars is compared effectively. Karai gypsum is formed by the hydrofracturing model which is comparable with the model proposed by Squyres et al. (2012) for *Homestake* on Mars. The difference between *Homestake*, Cape York and Karai gypsum is the compositional variation in the country rocks and the source of the fluids. Additionally, gypsum contains fluid inclusions and thus have implications for *Homestake* as due to its crystalline nature it may posses them. Banded iron formations are extensive iron deposits on Earth with large extent and with this consideration, layered hematite in Meridiani Planum are proposed to be formed in the similar environmental settings (Bridges et al., 2008). Today, comparison of BIFs and layered hematite deposits is valid as silica has also been identified on Mars which is an essential component of BIFs. Jarosite is mostly associated with acidic, oxidizing deposi-

tional environment (Bigham and Nordstrom, 2000) and its presence elsewhere definitely suggests acidic environmental conditions. It is found associated with kaolinite in the study area which suggests that diverse environmental conditions and complex diagenetic processes could be responsible for its formation.

CHAPTER 7

Summary and Conclusions

Preclude

This chapter summarizes the overall investigations, observations, interpretations and conclusions made during the research presented in the thesis. Further, limitations and future directions of the thesis are provided.

This thesis has investigated three different potential terrestrial analogue sites in India with the selected proxies which are known for preservation of the past climate clues in Martian environment. First site has the sedimentary succession rich in aqueous mineralogy and include gypsum-phyllosilicate association, presently in arid climate at Karai, Tiruchirapalli, Tamil Nadu. Gysum-phyllosilicate association of Karai Shale Formation is studied in detail by sophisticated spectroscopic techniques such as reflectance spectroscopy, Raman, XRD, Fourier transform infrared. The site features gypsum in the form of veins with cross-cutting relationship with the phyllosilicate groundmass. Fluid inclusions trapped within the gypsum has been characterized by Raman and microthermometry; the results show that mostly fluids are water rich (monophase and biphase) with minor carbon di-oxide. Second site is the banded iron formation deposit, Singhbhum craton, Odisha which is mainly composed of alternate layers of iron rich and silica rich bands. The samples have been characterized by the same methodology and spectral interpretations have been given. Third site is selected at Varkala, Kerala which has the unique mineralogical association of jarosite and kaolinite with minor iron sulphides and oxides as shown by the results obtained during the research.

Characterization of gypsum and phyllosilicates association of Tiruchirapalli, South India with petrography, XRD and other traditional spectroscopic

techniques, namely VNIR, Raman and FTIR has been carried out. The use of these sophisticated analytical techniques proved to be an efficient way to identify the minerals (here gypsum, kaolinite, quartz, hematite etc.) even if present in very small amount. The VNIR spectroscopic results derived here can be used to aid both interpretation and ground-truth verification of remotely sensed data. The spectra have yielded abundant information regarding the purity and variations in the composition of the samples. Characteristic bands from both Raman and FTIR spectroscopic techniques were identified and correlated with the available data in literature. In particular, Raman bands identified for different minerals in the study will provide the database for the similar future studies in the extra-terrestrial scenario. Using these techniques in combination will greatly enhance the accuracy of detection of various minerals on the planetary surfaces such as Mars. XRD, identified as a robust way of identification of minerals and their crystallinity has also been very useful for mineral identification for the study. The veined gypsum deposits of Karai is suggested to be formed by hydro-fracturing in the host rock. Here, the investigation of gypsum and phyllosilicates using spectroscopic techniques has the scope to be applied for identification of high to low concentration minerals on Mars. This study has shown that although reflectance spectroscopy is a good tool for surface mineralogy detection, but the minerals like gypsum which could easily be detected from orbital spectroscopy, may mask other minerals. Therefore, it is highly recommended that modern more sophisticated potable spectroscopic instruments like Raman must be placed in the rover.

Although, gypsum of Karai formation does not possesses well developed microbial colonies in them, but fluid inclusions, small cavities, optimum moisture content in the host arid climate makes it one of the promising target for microbial activity. Study area presents the temperature above $+40^{o}$C for most of the months in the year with minimum precipitation and heavy dry winds throughout the year. These conditions would not allow any environmental damage to the host and fluid inclusions, hence preserving the conditions which prevailed at the time of gypsum formation. Many of the fluid inclusions which

are found in isolation within the crystal probably would have preserved the primary chemical composition of the waters. Laser Raman analysis have shown all the fluid inclusions belong to -OH group/water either in liquid or vapour form. Micro-thermometric analysis has shown that mostly the fluid inclusions are water-rich with traces of CO_2 (Homogenization temp: -56^{o}C and 104^{o}C). This study recommends that in future landing missions of Mars, gypsum should be one of the prime targets to be sampled as it may contain ancient waters in the form of fluid inclusions and biological-activity signatures.

The study on geological and spectral characteristics of BIFs in Singhbhum craton will help to have a better understanding on the palaeo-environmental conditions responsible for iron-deposits on Mars. Spectroscopic studies could aid in differentiating the iron ores on Mars and also help in identifying the relative enrichment of Fe content in different deposits. Laser Raman and ATR-FTIR spectroscopic techniques are proved to be very significant in analyzing different mineral mixtures, whereas it is difficult to identify the mineral species separately in a mixture through VIS/NIR radiometry. Chert/ quartz, an integral part of BIFs could not be identified in VIS/NIR analysis, but it is easily distinguishable by laser Raman and ATR-FTIR spectroscopic techniques. This geologic and spectral study of BIFs will help during the testing and calibration phase of the on-going and future missions to Mars.

Jarosite occurs in various local sedimentary conditions ranging from replacement to diagenetic types in palaeo-lacustrine settings in Varkala, India. In spite of having a close relation to saline-alkaline environment as major mineralogical entity belongs to phyllosilicate group, presence of jarosite proves the local and unstable acidic environment in time. Though Varkala jarosite is formed by major sedimentary processes without any involvement of direct volcanic evidence in terrestrial conditions, its jarosite-phyllosilicate association gives direct indication of diverse environmental conditions at the time of its formation. Similarly, jarosite-phyllosilicate association on Mars such as palaeolake deposits of Columbus crater, Terra Sirenum (Wray et al., 2009) or Terra

Meridiani (Poulet et al., 2008) proves local diverse environmental conditions at the time of their deposition. In addition, Varkala jarosite deposit is also helpful in validating the proposed depositional mechanisms for very localized jarosite formations on Mars and also to give the insights into the regions with different hydrous-sulphate and phyllosilicate mineral phases occurring in co-existence, suggesting complex diagenetic history.

Interior layered deposits and plateau regions in East Candor chasma are found to be rich in carbonates and polyhydrated sulphates. These mineral phases would have been formed either through deposition by surface alteration or during the weathering of the plateau material. Presence of carbonates in the area suggests water/hydrothermal activity. Sulphates detected in the area require presence of liquid water to form by precipitation, either in an intermittent lacustrine environment or by hydrothermal fluid circulation. Additionally, sulphates and carbonates require liquid water to form at least at 2-3 km below the surface. Therefore, presence of these minerals helps in identifying the hydrologic conditions in the area. Strong signatures of iron oxides are present on sulphate-rich scarps and at the base of layered deposits. Pyroxenes have mainly been encountered on the low lying terrains, mainly wall slopes and floor of the chasma. Plateau/ Mensa region is devoid of pyroxenes. This study provides the direct indication of intense subsurface water activity in the area.

The comparison of laboratory spectral data from the study areas and orbital spectral data from Mars is done. Gypsum-phyllosilicate association has been proved to be very significant for interpreting the geochemical behaviour of different hydrous mineral groups. Additionally, gypsum contains fluid inclusions which could be analyzed for palaeo-water chemistry measurements. Banded iron formations are significant in defining the geochemical environment in which layered hematite of Meridiani Planum could have deposited. Jarosite, which is mainly confined to acidic and oxidizing depositional environment could be a part of modified environment as suggested by mineral

association and may possess a complex diagenetic history.

Recommendation and future research:

Based on the research presented in the thesis, following recommendations are made to further enhance and add significant knowledge to the studied areas:

1. Fluid inclusions in gypsum of Karai Shale Formation, Tiruchirapalli have been studied and presented as part of the thesis, but the supporting data is quite limited. We believe that detailed characterization of fluid inclusions from the area will definitely give interesting results regarding the water chemistry, microbial colonization (as dark pigmentation has been observed during analysis), palaeo-climate etc..

2. Wide variety of marine and nonmarine evaporites are being confirmed on their potential to record information about palaeoclimates, ancient tectonic settings and the history of seawater chemistry by using ^{34}S, ^{18}O and Sr isotope compositions. Although literature suggests the evaporitic origin of gypsum in the area, but isotopic characterization using ^{34}S, ^{18}O sulphate and Sr isotope compositions will highly improve the understanding about it's genesis.

3. Jarosite ($KFe_3(SO_4)_2(OH)_6$) are often precipitated during the oxidation of sulphide-bearing rocks by meteoric solutions in acidic conditions. Dating of jarosite by the $^{40}Ar/^{39}Ar$ method allows to time the progression of the oxidation front and alteration during chemical weathering. In the Varkala area, jarosite is present in coastal cliff setting where its dating using $^{40}Ar/^{39}Ar$ will provide oxidation front, alteration behaviour with time and relation with the co-existing kaolinite.

REFERENCES

1. Acharya, S., 1976. Iron formations and iron ores of Orissa-their stratigraphy and correlation. In Proc Symp Geol etc. Fer and Fe-alloy Mine, Bangalore (pp. 86-100).

2. Acharya, S., 1984. Stratigraphy and structural evolution of the rocks of iron ore basin in Singhbhum-Orissa Iron Ore Province. In Crustal Evolution of the Indian Shield and its bearing on Metallogeny. Indian Jour. Earth Sci., Seminar Vol (pp. 19-28).

3. Allen, C.C., Gooding, J.L., Jercinovic, M., Keil, K., 1981. Altered basaltic glass: A terrestrial analog to the soil of Mars. Icarus, 45(2), pp.347-369.

4. Allen, C.C., Jager, K.M., Morris, R.V., Lindstrom, D.J., Lindtsrom, M.M., Lockwood, J.P., 1998. Martian soil simulant available for scientific, educational study. Eos, Transactions American Geophysical Union, 79(34), pp.405-409.

5. Allen, C.C., Westall, F., Schelble, R.T., 2001. Importance of a martian hematite site for astrobiology. Astrobiology, 1(1), pp.111-123.

6. Alpers, C.N., Rye, R.O., Nordstrom, D.K., White, L.D., King, B.S., 1992. Chemical, crystallographic and stable isotopic properties of alunite and jarosite from acid–Hypersaline Australian lakes. Chemical Geology, 96(1-2), pp.203-226.

7. Altheide, T.S., Chevrier, V.F., Dobrea, E.N., 2010. Mineralogical characterization of acid weathered phyllosilicates with implications for secondary Martian deposits. Geochimica et Cosmochimica Acta, 74(21), pp.6232-6248.

8. Amaral, G., Martinez-Frias, J., Vázquez, L., 2005. Astrobiological significance of minerals on Mars surface environment: UV-shielding properties of Fe (jarosite) vs. Ca (gypsum) sulphates. arXiv preprint physics/0512140.

9. Amaral, G., Martínez-Frías, J., Vázquez, L., 2007. UV shielding properties of jarosite vs. gypsum: astrobiological implications for Mars.

10. Amaral-Zettler, L.A., Gómez, F., Zettler, E., Keenan, B.G., Amils, R., Sogin, M.L., 2002. Eukaryotic diversity in Spain's river of fire. Nature, 417, 137.

11. Amils, R., González-Toril, E., Gómez, F., Fernández-Remolar, D., Rodríguez, N., Malki, M., Zuluaga, J., Aguilera, A., Amaral-Zettler, L.A., 2004. Importance of chemolithotrophy for early life on earth: the Tinto River (Iberian Pyritic Belt) case. In Origins (pp. 463-480). Springer Netherlands.

12. Amils, R., González-Toril, E., Fernández-Remolar, D., Gómez, F., Aguilera, á., Rodríguez, N., Malki, M., García-Moyano, A., Fairén, A.G., de la Fuente, V., Sanz, J.L., 2007. Extreme environments as Mars terrestrial analogs: the Rio Tinto case. Planetary and Space Science, 55(3), pp.370-381.

13. Anthony, J.W., Bideaux, R.A., Bladh, K.W., Nichols, M.C., 2011. Handbook of mineralogy, mineralogical society of America, Chantilly, VA 20151-1110, USA.

14. Arvidson, R.E., Poulet, F., Bibring, J.P., Wolff, M., Gendrin, A., Morris, R.V., Freeman, J.J., Langevin, Y., Mangold, N., Bellucci, G., 2005. Spectral reflectance and morphologic correlations in eastern Terra Meridiani, Mars. Science, 307(5715), pp.1591-1594.

15. Arvidson, R.E., Squyres, S.W., Anderson, R.C., Bell, J.F., Blaney, D., Brueckner, J., Cabrol, N.A., Calvin, W.M., Carr, M.H., Christensen, P.R., Clark, B.C., 2006. Overview of the spirit Mars exploration rover mission to Gusev Crater: Landing site to Backstay Rock in the Columbia Hills. Journal of Geophysical Research: Planets, 111(E2).

16. Arvidson, R.E., Ashley, J.W., Bell, J.F., Chojnacki, M., Cohen, J., Economou, T.E., Farrand, W.H., Fergason, R., Fleischer, I., Geissler, P., Gellert, R., 2011. Opportunity Mars Rover mission: Overview and selected results from Purgatory ripple to traverses to Endeavour crater. Journal of Geophysical Research: Planets, 116(E7).

17. Ashley, G.M., Maitima Mworia, J., Muasya, A.M., Owen, R.B., Driese, S.G., Hover, V.C., Renaut, R.W., Goman, M.F., Mathai, S., Blatt, S.H., 2004. Sedimentation and recent history of a freshwater wetland in a semi-arid environment: Loboi Swamp, Kenya, East Africa. Sedimentology, 51(6), pp.1301-1321.

18. Atreya, S.K., Mahaffy, P.R., Wong, A.S., 2007. Methane and related trace species on Mars: Origin, loss, implications for life, and habitability. Planetary and Space Science, 55(3), pp.358-369. Averner, M.M. and Macelroy, R.D., 1976. On the habitability of Mars: an approach to planetary ecosynthesis.

19. Awramik, S.M., Barghoorn, E.S., 1977. The Gunflint microbiota. Precambrian Research, 5(2), pp.121-142. Ayyasami, K., 2006. Role of oysters in biostratigraphy: A case study from the Cretaceous of the Ariyalur area, southern India. Geosciences Journal, 10(3), pp.237-247.

20. Baker, E.T., German, C.R., 2004. On the global distribution of hydrothermal vent fields. Mid-ocean ridges, pp.245-266.

21. Baldridge, A.M., Hook, S.J., Crowley, J.K., Marion, G.M., Kargel, J.S., Michalski, J.L., Thomson, B.J., de Souza Filho, C.R., Bridges, N.T., Brown, A.J., 2009. Contemporaneous deposition of phyllosilicates and sulphates: Using Australian acidic saline lake deposits to describe geochemical variability on Mars. Geophysical Research Letters, 36(19).

22. Banerji, R.K., Mohan, R., 1970. Foraminiferal Biostratigraphy of Meso-Cenozoic Sequence of the Cauvery Basin, South India. Geological Society of India, 11(4), pp.348-357.

23. Banerji, R.K., 1972. Stratigraphy and micropalaeontology of the Cauvery Basin. Part-I. Exposed area. Journal of the Palaeontological Society of India, 17, pp.1-24.

24. Banerji, A.K., 1974. On the stratigraphy and tectonic history of the iron ore bearing and associated rocks of Singhbhum and adjoining areas of Bihar and Orissa. Geological Society of India, 15(2), pp.150-157.

25. Banerji, A.K., 1975. On the evolution of the Singhbhum nucleus, eastern India. QJ Geol. Min. Met. Soc. India, 47(1), pp.51-60.

26. Banerji, A.K., 1980. Role of volcanism and tectonism in ore genesis, a case history from the northeastern part of the Indian Precambrian shield. In Proc. 5th Quad. IAGOD. Symp., Stuttgart (pp. 261-273).

27. Banin, A., Clark, B.C., Wanke, H., 1992. Surface chemistry and mineralogy. Mars, 1, pp.594-625.

28. Barbieri et al. 2001 Barbieri, R., Ori, G.G. & Taviani, M. 2001. Phanerozoic submarine cold vent biota and its exobiological potential. In Proc. First European Workshop on Exo/Astrobiology, ESA Spec. Publ., vol. 496, pp. 295-298. European Space Agency, Noordwijk.

29. Barghoorn, E.S., Tyler, S.A., 1965. Microorganisms from the Gunflint chert. Science, 147(3658), pp.563-575.

30. Baron, D., Palmer, C.D., 1996. Solubility of jarosite at 4-35 ^{o}C. Geochimica et Cosmochimica Acta, 60(2), pp.185-195.

31. Basciano, L.C., Peterson, R.C., 2007. Jarosite-hydronium jarosite solid-solution series with full iron site occupancy: Mineralogy and crystal chemistry. American Mineralogist, 92(8-9), pp.1464-1473.

32. Basciano, L.C., Peterson, R.C., 2008. Crystal chemistry of the natrojarosite-jarosite and natrojarosite-hydronium jarosite solid-solution series: A synthetic study with full Fe site occupancy. American Mineralogist, 93(5-6), pp.853-862.

33. Battler, M.M., Osinski, G.R., Lim, D.S., Davila, A.F., Michel, F.A., Craig, M.A., Izawa, M.R., Leoni, L., Slater, G.F., Fairen, A.G., Preston, L.J., 2013. Characterization of the acidic cold seep emplaced jarositic Golden Deposit, NWT, Canada, as an analogue for jarosite deposition on Mars. Icarus, 224(2), pp.382-398.

34. Bell, J.F., Squyres, S.W., Arvidson, R.E., Arneson, H.M., Bass, D., Blaney, D., Cabrol, N., Calvin, W., Farmer, J., Farrand, W.H., Goetz, W., 2004. Pancam multispectral imaging results from the Spirit rover at Gusev Crater. Science, 305(5685), pp.800-806.

35. Benison, K.C., 1995. Permian surface water temperatures from Nippewalla Group halite, Kansas. Carbonates and Evaporites, 10(2), pp.245-251.

36. Benison, K.C., 1997. Acid water deposition and diagenesis in Permian red bed-hosted evaporites, midcontinent, USA [Ph. D. dissertation]. The University of Kansas, Lawrence.

37. Benison, K.C., Goldstein, R.H., Wopenka, B., Burruss, R.C., Pasteris, J.D., 1998. Extremely acid Permian lakes and ground waters in North America. Nature, 392(6679), pp.911-914.

38. Benison, K.C., Goldstein, R.H., 1999. Permian paleoclimate data from fluid inclusions in halite. Chemical Geology, 154(1), pp.113-132.

39. Benison, K.C., Goldstein, R.H., 2001. Evaporites and siliciclastics of the Permian Nippewalla Group of Kansas, USA: a case for non-marine deposition in saline lakes and saline pans. Sedimentology, 48(1), pp.165-188.

40. Benison, K.C., Goldstein, R.H., 2002. Recognizing acid lakes and groundwaters in the rock record. Sedimentary Geology, 151(3), pp.177-185.

41. Benison, K.C., LaClair, D.A., 2003. Modern and ancient extremely acid

saline deposits: terrestrial analogs for martian environments?. Astrobiology, 3(3), pp.609-618.

42. Benison, K.C., 2006. A martian analog in Kansas: comparing martian strata with Permian acid saline lake deposits. Geology, 34(5), pp.385-388.

43. Bennison, G.M., Wright, A.E., 1969. Geological history of the British Isles.

44. Bensted, J., 1976. Characterization of sulphate bands in the IR-spectra of minerals. Naturwissenschaften, 63(4), pp.193-193.

45. Beura, D., Satpathy, B., 2012. Petrographic characterisation of Banded Iron Formation of Bonai-Keonjhar Belt with special reference to Banspani-Jilling-Jajang Sector, Odisha. Int. J. of Earth Sc. and Eng., 05, pp.767-774

46. Bhattacharya, H.N., Chakraborty, I., Ghosh, K.K., 2007. Geochemistry of some banded iron-formations of the Archean supracrustals, Jharkhand-Orissa region, India. Journal of Earth System Science, 116(3), pp.245-259.

47. Bhattacharya, S., Mitra, S., Gupta, S., Jain, N., Chauhan, P., Parthasarathy, G., 2016. Jarosite occurrence in the Deccan Volcanic Province of Kachchh, western India: Spectroscopic studies on a Martian analog locality. Journal of Geophysical Research: Planets, 121(3), pp.402-431.

48. Bibring, J.P., Langevin, Y., Gendrin, A., Gondet, B., Poulet, F., Berthé, M., Soufflot, A., Arvidson, R., Mangold, N., Mustard, J., Drossart, P., 2005. Mars surface diversity as revealed by the OMEGA/Mars Express observations. Science, 307(5715), pp.1576-1581.

49. Bibring, J.P., Langevin, Y., Mustard, J.F., Poulet, F., Arvidson, R., Gendrin, A., Gondet, B., Mangold, N., Pinet, P., Forget, F., Berthé,

M., 2006. Global mineralogical and aqueous Mars history derived from OMEGA/Mars Express data. Science, 312(5772), pp.400-404.

50. Bigham, J.M., Nordstrom, D.K., 2000. Iron and aluminum hydroxysulphates from acid sulphate waters. Reviews in mineralogy and geochemistry, 40(1), pp.351-403.

51. Bigham, J.M., Schwertmann, U., Traina, S.J., Winland, R.L., Wolf, M., 1996. Schwertmannite and the chemical modeling of iron in acid sulphate waters. Geochimica et Cosmochimica Acta, 60(12), pp.2111-2121.

52. Bishop, J.L., Murad, E., 2005. The visible and infrared spectral properties of jarosite and alunite. American Mineralogist, 90(7), pp.1100-1107.

53. Bishop, J.L., Dobrea, E.Z.N., McKeown, N.K., Parente, M., Ehlmann, B.L., Michalski, J.R., Milliken, R.E., Poulet, F., Swayze, G.A., Mustard, J.F., Murchie, S.L., 2008. Phyllosilicate diversity and past aqueous activity revealed at Mawrth Vallis, Mars. Science, 321(5890), pp.830-833.

54. Bishop, J.L., Parente, M., Weitz, C.M., Noe Dobrea, E.Z., Roach, L.H., Murchie, S.L., McGuire, P.C., McKeown, N.K., Rossi, C.M., Brown, A.J., Calvin, W.M., 2009. Mineralogy of Juventae Chasma: Sulphates in the light-toned mounds, mafic minerals in the bedrock, and hydrated silica and hydroxylated ferric sulphate on the plateau. Journal of Geophysical Research: Planets, 114(E2).

55. Biswas, S.K., 1992. Tectonic framework and evolution of graben basins of India. Indian Journal of Petroleum Geology, 1(2), pp.276-292.

56. Bjorlykke, K., Hoeg, K., 1997. Effects of burial diagenesis on stresses, compaction and fluid flow in sedimentary basins. Marine and Petroleum Geology, 14(3), pp.267-276.

57. Blair, S.C., Thorpe, R.K., Heuze, F.E., Shaffer, R.J., 1989. Laboratory observations of the effect of geologic discontinuities on hydrofracture

propagation. In The 30th US Symposium on Rock Mechanics (USRMS). American Rock Mechanics Association.

58. Blanford, H.F., 1862. On the Cretaceous and other rocks of the South Arcot, and Trichinopoly districts, Madras. Government of India.

Bock, E., 1961. On the solubility of anhydrous calcium sulphate and of gypsum in concentrated solutions of sodium chloride at 25 ^{o}C, 30 ^{o}C, 40 ^{o}C, and 50 ^{o}C. Canadian Journal of Chemistry, 39(9), pp.1746-1751.

59. Bodnar, R.J., 2003. Introduction to aqueous-electrolyte fluid inclusions. Fluid Inclusions: Analysis and Interpretation, 32, pp.81-100.

60. Bost, N., Westall, F., Ramboz, C., Foucher, F., Pullan, D., Meunier, A., Petit, S., Fleischer, I., Klingelhofer, G., Vago, J.L., 2013. Missions to Mars: characterisation of Mars analogue rocks for the International Space Analogue Rockstore (ISAR). Planetary and Space Science, 82, pp.113-127.

61. Boston, P.J., Ivanov, M.V., McKay, C.P., 1992. On the possibility of chemosynthetic ecosystems in subsurface habitats on Mars. Icarus, 95(2), pp.300-308.

62. Boston, P.J. et al., 2001. Cave biosignature suites : microbes, minerals, and Mars. Astrobiology 1, 25-55.

63. Boynton, W.V., Feldman, W.C., Squyres, S.W., Prettyman, T.H., Brückner, J., Evans, L.G., Reedy, R.C., Starr, R., Arnold, J.R., Drake, D.M., Englert, P.A.J., 2002. Distribution of hydrogen in the near surface of Mars: Evidence for subsurface ice deposits. science, 297(5578), pp.81-85.

64. Brady, K.S., Bigham, J.M., Jaynes, W.F., Logan, T.J., 1986. Influence of sulphate on Fe-oxide formation: Comparisons with a stream receiving acid mine drainage. Clays and Clay Minerals, 34(3), pp.266-274.

65. Bridges, J.C., Grady, M.M., 2000. Evaporite mineral assemblages in the nakhlite (martian) meteorites. Earth Planet. Sci. Lett. 176, 267-279.

66. Bridges, N.T., Hook, S.J., Thomson, B.J., Crowley, J.K., Souza Filho, C.R., Macambira, J.B. and Lima Pereira Silva, G., 2008. Brazilian analog for ancient marine environments on Mars. Eos, Transactions American Geophysical Union, 89(36), pp.329-330.

67. Brinatti, A.M., Mascarenhas, Y.P., Pereira, V.P., Partiti, C.S.D.M., Macedo, Á., 2010. Mineralogical characterization of a highly-weathered soil by the Rietveld Method. Scientia Agricola, 67(4), pp.454-464.

68. Brinckerhoff, W.B. & Cornish, T.J., 2000. Elemental, isotopic and organic analysis on Mars with laser TOF-MS. Concepts and Approaches for Mars Exploration, abstract 6027. Lunar and Planetary Institute, Houston.

69. Brophy, G.P., Sherdian, M.F., 1965. Sulphate studies. 4. Jarosite-natrojarosite-hydronium jarosite solid solution series. American Mineralogist, 50(10), pp.1595.

70. Byrne, S., Dundas, C.M., Kennedy, M.R., Mellon, M.T., McEwen, A.S., Cull, S.C., Daubar, I.J., Shean, D.E., Seelos, K.D., Murchie, S.L., Cantor, B.A., 2009. Distribution of mid-latitude ground ice on Mars from new impact craters. Science, 325(5948), pp.1674-1676.

71. Cabane, M. et al., 2001. In situ inorganic and organic analysis (Pyr/CDGC/MS) of the Martian soil, on the Mars 2005 mission. Planet. Space Sci. 49, pp.523-531.

72. Cabrol, N.A. & Grin, E.A., 2001. The evolution of lacustrine environments on Mars: is Mars only hydrologically dormant? Icarus 149, pp.291-328.

73. Carlson, L., Bigham, J.M., Schwertmann, U., Kyek, A., Wagner, F., 2002. Scavenging of As from acid mine drainage by schwertmannite

and ferrihydrite: a comparison with synthetic analogues. Environmental Science & Technology, 36(8), pp.1712-1719.

74. Carr, M.H., 1981. The Surface of MarsYale Univ. Press, New Haven.

75. Carr, M.H., 1983. Stability of streams and lakes on Mars. Icarus, 56(3), pp.476-495.

76. Carr, M., 1987. Water on Mars. Physics Bulletin, 38(10), pp.374.

77. Carr, M.H., 1996. Water on Mars: Oxford University Press. New York.

78. Carr, M.H., Head, J.W., 2003. Oceans on Mars: An assessment of the observational evidence and possible fate. Journal of Geophysical Research: Planets, 108(E5).

79. Catling, D., Moore, J., 2000. Iron oxide deposition from aqueous solution and iron formations on Mars.

80. Catling, D.C., Moore, J.M., 2003. The nature of coarse-grained crystalline hematite and its implications for the early environment of Mars. Icarus, 165(2), pp.277-300.

81. Chandra, U., Sharma, P., Parthasarathy, G., Sreedhar, B., 2010. 57Fe Mossbauer spectroscopy and electrical resistivity studies on naturally occurring native iron under high pressures up to 9.1 GPa. American Mineralogist, 95 (5-6), 870-875

82. Chevrier, V., Poulet, F., Bibring, J.P., 2007. Early geochemical environment of Mars as determined from thermodynamics of phyllosilicates. Nature, 448(7149), pp.60-63.

83. Christensen, P.R., Bandfield, J., Clark, R., Edgett, K.S., Hamilton, V., Lane, M., Kieffer, H.H., Malin, M., Morris, D., Ruff, S., Roush, T., 1999. The composition of Martian surface materials: Mars Global Surveyor thermal emission spectrometer observations. In Lunar and Planetary Science Conference (Vol. 30, pp. 1461).

84. Christensen, P.R., Bandfield, J.L., Clark, R.N., Edgett, K.S., Hamilton, V.E., Hoefen, T., Kieffer, H.H., Kuzmin, R.O., Lane, M.D., Malin, M.C., Morris, R.V., 2000. Detection of crystalline hematite mineralization on Mars by the Thermal Emission Spectrometer: Evidence for near surface water. Journal of Geophysical Research: Planets, 105(E4), pp.9623-9642.

85. Christensen, P.R., Bandfield, J.L., Hamilton, V.E., Ruff, S.W., Kieffer, H.H., Titus, T.N., Malin, M.C., Morris, R.V., Lane, M.D., Clark, R.L., Jakosky, B.M., 2001(a). Mars Global Surveyor Thermal Emission Spectrometer experiment: investigation description and surface science results. Journal of Geophysical Research: Planets, 106(E10), pp.23823-23871.

86. Christensen, P.R., Morris, R.V., Lane, M.D., Bandfield, J.L., Malin, M.C., 2001(b). Global mapping of Martian hematite mineral deposits: Remnants of water-driven processes on early Mars. J. Geophys. Res, 106(E10), pp.23873-23885.

87. Christensen, P.R., Wyatt, M.B., Glotch, T.D., Rogers, A.D., Anwar, S., Arvidson, R.E., Bandfield, J.L., Blaney, D.L., Budney, C., Calvin, W.M., Fallacaro, A., 2004. Mineralogy at Meridiani Planum from the Mini-TES experiment on the Opportunity Rover. Science, 306(5702), pp.1733-1739.

88. Christensen, P.R., Bandfield, J.L., Fergason, R.L., Hamilton, V.E., Rogers, A.D., 2008. The compositional diversity and physical properties mapped from the Mars Odyssey Thermal Emission Imaging System. The Martian Surface-Composition, Mineralogy, and Physical Properties, 1, pp.221.

89. Cid, A., Casanova, I., 2001. Sulphates in Martian soils : a clear exobiological target. In Proc. First European Workshop on Exo-/Astro-Biology, ESA SP-496, pp. 201-202. European Space Agency, Noordwijk.

90. Clark, R.N., Swayze, G.A., Singer, R.B., Pollack, J.B., 1990. High resolution reflectance spectra of Mars in the 2.3 μm region: Evidence for

the mineral scapolite. Journal of Geophysical Research: Solid Earth, 95(B9), pp.14463-14480.

91. Clark, B.C., 1993. Geochemical components in Martian soil. Geochimica et Cosmochimica acta, 57(19), pp.4575-4581.

92. Clark, B.C., Morris, R.V., McLennan, S.M., Gellert, R., Jolliff, B., Knoll, A.H.,..... Rieder, R., 2005. Chemistry and mineralogy of outcrops at Meridiani Planum. Earth and Planetary Science Letters 240 (1), 73-94.

93. Cloud, P.E., 1965. Significance of the Gunflint (Precambrian) microflora. Science, 148(3666), pp.27-35.

94. Cloud, P., 1972. A working model of the primitive Earth. American Journal of Science, 272(6), pp.537-548.

95. Cloud, P., 1973. Paleoecological significance of the banded iron-formation. Economic Geology, 68(7), pp.1135-1143.

96. Cloutis, E.A., Hawthorne, F.C., Mertzman, S.A., Krenn, K., Craig, M.A., Marcino, D., Methot, M., Strong, J., Mustard, J.F., Blaney, D.L., Bell, J.F., 2006. Detection and discrimination of sulphate minerals using reflectance spectroscopy. Icarus, 184(1), pp.121-157.

97. Cloutis, E.A., Craig, M.A., Kruzelecky, R.V., Jamroz, W.R., Scott, A., Hawthorne, F.C., Mertzman, S.A., 2008. Spectral reflectance properties of minerals exposed to simulated Mars surface conditions. Icarus, 195(1), pp.140-168.

98. Cockell, C.S., McKay, C.P., Omelon, C., 2002. Polar endoliths- an anti-correlation of climatic extremes and microbial biodiversity. International Journal of Astrobiology, 1(04), pp.305-310.

99. Cockell, C., Rettberg, P., Horneck, G., Scherer, K., Stokes, D.M., 2003. Measurements of microbial protection from ultraviolet radiation in polar terrestrial microhabitats. Polar Biology, 26(1), pp.62-69.

100. Connerney, J.E.P., Acuna, M.H., Wasilewski, P.J., Kletetschka, G., Ness, N.F., Reme, H., Lin, R.P., Mitchell, D.L., 2001. The global magnetic field of Mars and implications for crustal evolution. Geophysical Research Letters, 28(21), pp.4015-4018.

101. Cooper, C.D., Mustard, J.F., 2002. Spectroscopy of loose and cemented sulphate-bearing soils: Implications for duricrust on Mars. Icarus, 158(1), pp.42-55.

102. Cornell, R.M., Schwertmann, U., 2003. The iron oxides: structure, properties, reactions, occurrences and uses. John Wiley & Sons.

103. Courreges-Lacoste, G.B., Ahlers, B., Pérez, F.R., 2007. Combined Raman spectrometer/laser-induced breakdown spectrometer for the next ESA mission to Mars. Spectrochimica Acta Part A: Molecular and Biomolecular Spectroscopy, 68(4), pp.1023-1028.

104. Crowley, J.K., Williams, D.E., Hammarstrom, J.M., Piatak, N., Chou, I.M., Mars, J.C., 2003. Spectral reflectance properties (0.4-2.5 μm) of secondary Fe-oxide, Fe-hydroxide, and Fe-sulphate-hydrate minerals associated with sulphide-bearing mine wastes. Geochemistry: Exploration, Environment, Analysis, 3(3), pp.219-228.

105. Crowley, J.K., Hook, S.J., de Souza Filho, C.R., de Pereira Silva, G., Bridges, N.T., Thomson, B.J., Kargel, J.S., Brown, A.J., Ribeiro da Luz, B., Baldwin, A., Marion, G.M., 2008. Spectral diversity of terrestrial banded iron formations and associated rocks: Implications for Mars remote sensing. In Lunar and Planetary Science Conference (Vol. 39, pp. 1263).

106. Cvetković, J., Petrusevski, V.M., soptrajanov, B., 1997. Reinvestigation of the water bending region in the spectra of gypsum-like compounds–an FTIR study. Journal of molecular structure, 408, pp.463-466.

107. Dalstra, H., Guedes, S., 2004. Giant hydrothermal hematite deposits with Mg-Fe metasomatism: a comparison of the Carajás, Hamersley, and other iron ores. Economic Geology, 99(8), pp.1793-1800.

108. Dang, M.Z., Rancourt, D.G., Dutrizac, J.E., Lamarche, G., Provencher, R., 1998. Interplay of surface conditions, particle size, stoichiometry, cell parameters, and magnetism in synthetic hematite-like materials. Hyperfine Interactions, 117(1-4), pp.271-319.

109. Davis Jr, R.A., Welty, A.T., Borrego, J., Morales, J.A., Pendon, J.G., Ryan, J.G., 2000. Rio Tinto estuary (Spain): 5000 years of pollution. Environmental Geology, 39(10), pp.1107-1116.

110. De Gregorio, B.T., Sharp, T.G., 2006. The structure and distribution of carbon in 3.5 Ga Apex chert: Implications for the biogenicity of Earths oldest putative microfossils. American Mineralogist, 91(5-6), pp.784-789.

111. Derry, L.A., Jacobsen, S.B., 1990. The chemical evolution of Precambrian seawater: evidence from REEs in banded iron formations. Geochimica et Cosmochimica Acta, 54(11), pp.2965-2977.

112. Desborough, G.A., Smith, K.S., Lowers, H.A., Swayze, G.A., Hammarstrom, J.M., Diehl, S.F., Leinz, R.W., Driscoll, R.L., 2010. Mineralogical and chemical characteristics of some natural jarosites. Geochimica et Cosmochimica Acta, 74(3), pp.1041-1056.

113. Desikachar, S.V. 1976. Coastal Sedimentaries of India, 18.

114. Dold, B., Fontboté, L., 2001. Element cycling and secondary mineralogy in porphyry copper tailings as a function of climate, primary mineralogy, and mineral processing. Journal of Geochemical Exploration, 74(1), pp.3-55.

115. Dold, B., 2014. Mineralogical and geochemical controls in biomining and bioremediation. In Geomicrobiology and Biogeochemistry (pp. 119-135). Springer Berlin Heidelberg.

116. Dove, P.M., 1994. The dissolution kinetics of quartz in sodium chloride solutions at 25 degrees to 300 degrees C. American Journal of Science, 294(6), pp.665-712.

117. Drouet, C., Navrotsky, A., 2003. Synthesis, characterization, and thermochemistry of K-Na-H_3O jarosites. Geochimica et Cosmochimica Acta, 67(11), pp.2063-2076.

118. Drouet, C., Pass, K.L., Baron, D., Draucker, S., Navrotsky, A., 2004. Thermochemistry of jarosite-alunite and natrojarosite-natroalunite solid solutions. Geochimica et Cosmochimica Acta, 68(10), pp.2197-2205.

119. Dunlop, D.J., Ozdemir, O., 2001. Rock magnetism: fundamentals and frontiers (Vol. 3). Cambridge university press.

120. Dunn, J.A., 1940. The stratigraphy of south Singhbhum. Office of the Geological Survey of India.

121. Dutrizac, J.E., Jambor, J.L., 2000. Jarosites and their application in hydrometallurgy. Reviews in Mineralogy and Geochemistry, 40(1), pp.405-452.

122. Eberl, D.D., 2003. User guide to RockJock-A program for determining quantitative mineralogy from X-ray diffraction data (No. 2003-78). US Geological Survey.

123. Edgett, K., Malin, M., 2003. The layered upper crust of Mars: An update on MGS MOC observations after two Mars years in the mapping orbit. Lunar Planet. Sci., Abstract 1124.

124. Ehlmann, B.L., Mustard, J.F., Murchie, S.L., Poulet, F., Bishop, J.L., Brown, A.J., Calvin, W.M., Clark, R.N., Des Marais, D.J., Milliken, R.E., Roach, L.H., 2008. Orbital identification of carbonate-bearing rocks on Mars. Science, 322(5909), pp.1828-1832.

125. Ehlmann, B.L., Mustard, J.F., Swayze, G.A., Clark, R.N., Bishop, J.L., Poulet, F., Des Marais, D.J., Roach, L.H., Milliken, R.E., Wray, J.J., Barnouin-Jha, O., 2009. Identification of hydrated silicate minerals on Mars using MRO-CRISM: Geologic context near Nili Fossae and implications for aqueous alteration. Journal of Geophysical Research: Planets, 114(E2).

126. Ehlmann, B.L., Mustard, J.F., Murchie, S.L., Bibring, J.P., Meunier, A., Fraeman, A.A., Langevin, Y., 2011. Subsurface water and clay mineral formation during the early history of Mars. Nature, 479(7371), pp.53-60.

127. El Tabakh, B., Warren, J.K. 1998. Origin of fibrous gypsum in the Newark Rift Basin, eastern North America. Journal of Sedimentary Research 68(1).

128. Elbaz-Poulichet, F., Morley, N.H., Beckers, J.M., Nomerange, P., 2001. Metal fluxes through the Strait of Gibraltar: the influence of the Tinto and Odiel rivers (SW Spain). Marine Chemistry, 73(3), pp.193-213.

129. Elwood Madden, M.E., Bodnar, R.J., Rimstidt, J.D., 2004. Jarosite as an indicator of water-limited chemical weathering on Mars. Nature, 431, pp.821-823.

130. Elwood Madden, M.E., Madden, A.S., Rimstidt, J.D., 2009. How long was Meridiani Planum wet?: Applying a jarosite stopwatch to determine the duration of aqueous diagenesis. Geology, 37, pp.635-638.

131. Eremenko, N.A., Gagelganz, A.A., 1966. New data on the tectonic frame work of the Indian Peninsula. Bull. ONGC 3 pp.1-8.

132. Etiope, G., Sherwood Lollar, B., 2013. Abiotic methane on Earth. Reviews of Geophysics, 51(2), pp.276-299. Fairén, A.G., 2010. A cold and wet Mars. Icarus, 208(1), pp.165-175.

133. Fairén, A.G., Davila, A.F., Gago-Duport, L., Amils, R., McKay, C.P.,

2009. Stability against freezing of aqueous solutions on early Mars. Nature, 459(7245), pp.401-404.

134. Fairén, A.G., Davila, A.F., Lim, D., Bramall, N., Bonaccorsi, R., Zavaleta, J., Uceda, E.R., Stoker, C., Wierzchos, J., Dohm, J.M., Amils, R., 2010. Astrobiology through the ages of Mars: the study of terrestrial analogues to understand the habitability of Mars. Astrobiology, 10(8), pp.821-843.

135. Fallacaro, A., Calvin, W., 2003. Spectral and chemical characteristics of Lake Superior banded iron formation: Analog for Martian hematite outcrops. In Sixth International Conference on Mars (Vol. 1, p. 3067).

136. Fallacaro, A., Calvin, W.M., 2006. Spectral properties of Lake Superior banded iron formation: Application to Martian hematite deposits. Astrobiology, 6(4), 563-580.

137. Farmer, V.C., 1974. Infrared spectra of minerals. Mineralogical society.

138. Farmer, J.D., Des Marais, D.J., 1999. Exploring for a record of ancient Martian life. Journal of Geophysical Research: Planets, 104(E11), pp.26977-26995.

139. Farmer, J.D., 2000. Hydrothermal systems: doorways to early biosphere evolution. GSA Today, 10(7), pp.1-9.

140. Farrand, W.H., Glotch, T.D., Rice, J.W., Hurowitz, J.A., Swayze, G.A., 2009. Discovery of jarosite within the Mawrth Vallis region of Mars: Implications for the geologic history of the region. Icarus, 204(2), pp.478-488.

141. Faure, G. Mensing, T.M., 2007. Introduction to Planetary Science: The Geological Perspective. Berlin: Springer.

142. Fernández Remolar, D., Amils, R., Morris, R.V., Knoll, A.H., 2002. The Tinto river Basin: An analog for Meridiani hematite formation on Mars?. In Lunar and Planetary Science Conference (Vol. 33, p. 1226).

143. Fernández-Remolar, D.C., Rodriguez, N., Gómez, F., Amils, R., 2003. Geological record of an acidic environment driven by iron hydrochemistry: The Tinto River system. Journal of Geophysical Research: Planets, 108(E7).

144. Fernández-Remolar, D., Gómez-Elvira, J., Gómez, F., Sebastian, E., MartÄ±in, J., Manfredi, J.A., Torres, J., Kesler, C.G., Amils, R., 2004. The Tinto River, an extreme acidic environment under control of iron, as an analog of the Terra Meridiani hematite site of Mars. Planetary and Space Science, 52(1), pp.239-248.

145. Fernández-Remolar, D.C., Morris, R.V., Gruener, J.E., Amils, R., Knoll, A.H., 2005. The Río Tinto Basin, Spain: mineralogy, sedimentary geobiology, and implications for interpretation of outcrop rocks at Meridiani Planum, Mars. Earth and Planetary Science Letters, 240(1), pp.149-167.

146. Fernández-Remolar, D.C., Gómez, F., Prieto-Ballesteros, O., Schelble, R.T., Rodríguez, N., Amils, R., 2008. Some ecological mechanisms to generate habitability in planetary subsurface areas by chemolithotrophic communities: The Río Tinto subsurface ecosystem as a model system. Astrobiology, 8(1), pp.157-173.

147. Fishbaugh, K.E., Poulet, F., Chevrier, V., Langevin, Y., Bibring, J.P., 2007. On the origin of gypsum in the Mars north polar region. Journal of Geophysical Research: Planets, 112(E7).

148. Fonti, S., Marzo, G.A., 2010. Mapping the methane on Mars. Astronomy and Astrophysics, 512, pp.A51.

149. Forbes, B.G., 1958. Folded Permian gypsum of Ripon Parks, Yorkshire. Yorkshire Geological Society Proceedings, 31, pp.351-358.

150. Formisano, V., Atreya, S., Encrenaz, T., Ignatiev, N., Giuranna, M., 2004. Detection of methane in the atmosphere of Mars. Science, 306(5702), pp.1758-1761.

151. Forsythe, R.D., Zimbelman, J.R., 1995. A case for ancient evaporates on Mars. J. Geophys. Res. 100, 5553-5563.

152. Frei, R., Polat, A., 2007. Source heterogeneity for the major components of ∼3.7 Ga Banded Iron Formations (Isua Greenstone Belt, Western Greenland): tracing the nature of interacting water masses in BIF formation. Earth and Planetary Science Letters, 253(1), pp.266-281.

153. French, J.E., Heaman, L.M., Chacko, T., Srivastava, R.K., 2008. 1891-1883 Ma Southern Bastar-Cuddapah mafic igneous events, India: a newly recognised large igneous province. Precambrian Research, 160, pp.308-322.

154. Friedmann, E.I., 1982. Endolithic microorganisms in the Antarctic cold desert. Science, 215(4536), pp.1045-1053.

155. Gaboreau, S., Vieillard, P., 2004. Prediction of Gibbs free energies of formation of minerals of the alunite supergroup. Geochimica et Cosmochimica Acta, 68(16), pp.3307-3316.

156. Gadsen J.A., 1975. Infrared spectra of minerals and related inorganic compounds (London: Butterworths).

157. Gaffey, S.J., McFadden, L.A., Nash, D., Pieters, C.M., 1993. Ultraviolet, visible, and near-infrared reflectance spectroscopy: Laboratory spectra of geologic materials. Remote geochemical analysis: Elemental and mineralogical composition, pp.43-77.

158. García-Ruiz, J.M., Villasuso, R., Ayora, C., Canals, A., Otálora, F., 2007. Formation of natural gypsum megacrystals in Naica, Mexico. Geology, 35(4), pp.327-330.

159. Garofalo, P.S., Forti, P., Gunther, D. 2013. Determining gypsum growth temperatures using monophase fluid inclusions- Application to the giant gypsum crystals of Naica, Mexico. Geology, 41(12), pp.305.

160. Garrels, R.M., Christ, C.L., 1965. Solutions, Minerals, and Equilibria. first ed. Harper and Row, London.

161. Gasharova, B., Gottlicher, J., Becker, U., 2005. Dissolution at the surface of jarosite: an in situ AFM study. Chemical Geology, 215(1), pp.499-516.

162. Geissler, P.E., Singer, R.B., Komatsu, G., Murchie, S., Mustard, J., 1993. An unusual spectral unit in West Candor Chasma: Evidence for aqueous or hydrothermal alteration in the Martian canyons. Icarus, 106(2), pp.380-391.

163. Geminale, A., Formisano, V., Giuranna, M., 2008. Methane in Martian atmosphere: average spatial, diurnal, and seasonal behaviour. Planetary and Space Science, 56(9), pp.1194-1203.

164. Geminale, A., Formisano, V., Sindoni, G., 2011. Mapping methane in Martian atmosphere with PFS-MEX data. Planetary and Space Science, 59(2), pp.137-148.

165. Gendrin, A., Mangold, N., Bibring, J.P., Langevin, Y., Gondet, B., Poulet, F., Bonello, G., Quantin, C., Mustard, J., Arvidson, R., LeMouélic, S., 2005. Sulphates in Martian layered terrains: the OMEGA/Mars Express view. Science, 307(5715), pp.1587-1591.

166. Gerdes, G., Krumbein, W.E., Noffke, N., 2000. Evaporite microbial sediments. In Microbial sediments (pp. 196-208). Springer Berlin Heidelberg.

167. Gibson, E.K., McKay, D.S., Thomas-Keprta, K., Westall, F. & Romanek, C.A., 1999. It's dead Jim. But was it ever alive ? Ad Astra 11(1), pp.1-5.

168. Gieré, R., Carleton, L.E., Lumpkin, G.R., 2003. Micro-and nanochemistry of fly ash from a coal-fired power plant. American Mineralogist, 88(11-12), pp.1853-1865.

169. Glotch, T.D., Christensen, P.R., 2005. Geologic and mineralogic mapping of Aram Chaos: Evidence for a water rich history. Journal of Geophysical Research: Planets, 110(E9).

170. Glotch, T.D., Bandfield, J.L., 2006. Determination and interpretation of surface and atmospheric Miniature Thermal Emission Spectrometer spectral end-members at the Meridiani Planum landing site. Journal of Geophysical Research: Planets, 111(E12).

171. Glotch, T.D., Bandfield, J.L., Christensen, P.R., Calvin, W.M., McLennan, S.M., Clark, B.C., Rogers, A.D., Squyres, S.W., 2006a. Mineralogy of the light-toned outcrop at Meridiani Planum as seen by the Miniature Thermal Emission Spectrometer and implications for its formation. Journal of Geophysical Research: Planets, 111(E12).

172. Glotch, T.D., Christensen, P.R. Sharp, T.G., 2006b. Fresnel modeling of hematite crystal surfaces and application to Martian hematite spherules. Icarus, 181(2), pp.408-418.

173. Glotch, T.D., Rogers, A.D., 2007. Evidence for aqueous deposition of hematite-and sulphate-rich light-toned layered deposits in Aureum and Iani Chaos, Mars. Journal of Geophysical Research: Planets, 112(E6).

174. Goldstein, A.G., Collins, E.W., 1984. Deformation of Permian strata overlying a zone of salt dissolution and collapse in the Texas Panhandle. Geology, 12, 314-17.

175. Goldstein, R.H., 2003. Petrographic analysis of fluid inclusions. Fluid Inclusions: Analysis and Interpretation, 32, pp.9-53.

176. González-Toril, E., Llobet-Brossa, E., Casamayor, E.O., Amann, R., Amils, R., 2003. Microbial ecology of an extreme acidic environment, the Tinto River. Applied and Environmental Microbiology, 69(8), pp.4853-4865.

177. Govindan, A., 1993. Cretaceous anoxic events, sea level changes and microfauna in Cauvery Basin, India. In: Proceedings of Second Seminar on Petroliferous Basins of India, vol. 1. Indian Petroleum Publishers, pp.161-176.

178. Govindan, A., Ravindran, C.N., Rangaraju, M.K., 1996. Cretaceous Stratigraphy and Planktonic Foraminiferal Zonation of the Cauvery Basin, South India. Memoirs-geological society of India, pp.155-188.

179. Gray, N.F., 1997. Environmental impact and remediation of acid mine drainage: a management problem. Environmental Geology, 30(1-2), pp.62-71

180. Greenwood, J.P., Gilmore, M.S., Merrill, M.D., Blake, R.E., Martini, A.M., Varekamp, J., 2005, March. Jarosite Mineralization in St. Lucia, WI: Preliminary Geochemical, Spectral, and Biological Investigations of a Martian Analogue. In 36th Annual Lunar and Planetary Science Conference (Vol. 36).

181. Grin, E.A., Cabrol, N.A., 1997. Limnologic analysis of Gusev crater paleolake, Mars. Icarus, 130(2), pp.461-474.

182. Gross, G.A., 1980. A classification of iron formations based on depositional environments. The Canadian Mineralogist, 18(2), pp.215-222.

183. Grotzinger, J.P., Arvidson, R.E., Bell, J.F., Calvin, W., Clark, B.C., Fike, D.A., Golombek, M., Greeley, R., Haldemann, A., Herkenhoff, K.E., Jolliff, B.L., 2005. Stratigraphy and sedimentology of a dry to wet eolian depositional system, Burns formation, Meridiani Planum, Mars. Earth and Planetary Science Letters, 240(1), pp.11-72.

184. Guinness, E.A., Arvidson, R.E., DaleBannister, M.A., Singer, R.B., Bruckenthal, E.A., 1987. On the spectral reflectance properties of materials exposed at the Viking landing sites. Journal of Geophysical Research: Solid Earth, 92(B4).

185. Gustavson, T.C., Hovorka, S.D., Dutton, A.R., 1994. Origin of satin spar veins in evaporite basins. Journal of Sedimentary Research, 64(1).

186. Halferdal, L.B., 1960. Gypsum deposit at Peace Point, northern Alberta. Alberta Research Council Internal Report, 12.

187. Hanna, A., Phillips, R.J., Zuber, M.T., 2007. Meridiani Planum and the global hydrology of Mars. Nature, 446 pp.163-166.

188. Haq, B.U., Hardenbol, J., Vail, P.R., 1987. Chronology of fluctuating sea levels since the Triassic. Science, 235(4793), pp.1156-1167.

189. Hardie, L.A., 1991. On the significance of evaporites. Annual Review of Earth and Planetary Sciences, 19, p.131.

190. Hartmann, W.K., 1984. Does crater "saturation equilibrium" occur in the solar system?. Icarus, 60(1), pp.56-74.

191. Harvey, R.P., McSween, H.Y., 1996. A possible high-temperature origin for the carbonates in the Martian meteorite ALH84001.

192. Hausrath, E.M., Navarre-Sitchler, A.K., Sak, P.B., Steefel, C.I., Brantley, S.L., 2008. Basalt weathering rates on Earth and the duration of liquid water on the plains of Gusev Crater, Mars. Geology, 36(1), pp.67-70.

193. Hay, 1973; Hay, R. L., 1973. Lithofacies and environments of Bed I, Olduvai Gorge, Tanzania, Quat. Res., 3, 541-560, doi:10.1016/0033-5894(73)90030-6.

194. Hay, R.L., 1976. Geology of the Olduvai Gorge: a study of sedimentation in a semiarid basin. Univ of California Press.

195. Heinrich, W., Gottschalk, M., 1995. Metamorphic reactions between fluid inclusions and mineral hosts. I. Progress of the reaction calcite + quartz = wollastonite + CO_2 in natural wollastonite-hosted fluid inclusions. Contributions to Mineralogy and Petrology, 122(1-2), pp.51-61.

196. Herkenhoff, K.E., Squyres, S.W., Arvidson, R., Bass, D.S., Bell, J.F., Bertelsen, P., Ehlmann, B.L., Farrand, W., Gaddis, L., Greeley, R., Grotzinger, J., 2004. Evidence from Opportunity's microscopic imager for water on Meridiani Planum. Science, 306(5702), pp.1727-1730.

197. Herman, G.C., 2005. Joints and veins in the Newark basin, New Jersey, in regional tectonic perspective. In Newark Basin-View from the 21st Century, 22nd Annual Meeting of the Geological Association of New Jersey, College of New Jersey, Ewing, New Jersey (pp. 75-116).

198. Hirschfeld, T., 1974. Range independence of signal in variable focus remote Raman spectrometry. Applied optics, 13(6), pp.1435-1437.

199. Hofmann, A., Bolhar, R., 2007. Carbonaceous cherts in the Barberton greenstone belt and their significance for the study of early life in the Archean record. Astrobiology, 7(2), pp.355-388.

200. Holdoway, K.A., 1978. Deposition of evaporites and red beds of the Nippewalla Group, Permian, western Kansas (p. 43). Kansas Geological Survey, University of Kansas.

201. Holland, H.D., 1973. The oceans; a possible source of iron in iron-formations. Economic Geology, 68(7), pp.1169-1172.

202. Horneck G., Baumstark-Khan, 2002. The Quest for the Conditions of Life. Astrobiology.

203. Hughes, K.A., Lawley, B., 2003. A novel Antarctic microbial endolithic community within gypsum crusts. Environmental Microbiology, 5(7), pp.555-565.

204. Hunt, G.R., 1970. Visible and near-infrared spectra of minerals and rocks: I silicate minerals. Modern Geology, 1, pp.283-300.

205. Hunt, G.R., Salisbury, J.W., Lenhoff, C.J., 1971. Visible and near-infrared spectra of minerals and rocks. VI. Sulphides and sulphates. Modern Geology, 3, pp. 1-14.

206. Hunt, G.R., Ashley, R.P., 1979. Spectra of altered rocks in the visible and near infrared. Economic Geology, 74(7), pp.1613-1629.

207. Hynek, B.M., Arvidson, R.E., Phillips, R.J., 2002. Geological setting and origin of Terra Meridiani hematite deposit on Mars: Journal Geophysical Research, v. 107. E10, 5088.

208. Iyengar, S.V.P., Banerjee, P.K., 1971. The Iron ore, Bengpal Dharwar Group. Rec. Geol. Surv. India, 101(pt 2), pp.43-59.

209. Iyengar, S.V.P., Murthy, Y.G.K., 1982. The evolution of the Archaean-Proterozoic crust in parts of Bihar and Orissa, eastern India. Records of the Geological Survey of India, 112(3), pp.1-5.

210. Jafar, S.A., 1996. The Evolution of marine Cretaceous Basins of India: Calibration with nonnofossil zones. Memoirs-geological society of India, pp.121-134.

211. Jain, K.P., 1978. An Upper Cretaceous dinoflagellate assemblage from Vriddhachalam area, Cauvery Basin, South India. Palaeobotanist, 25, pp.146-160.

212. Jain, N., Chauhan, P., 2015. Study of phyllosilicates and carbonates from the Capri Chasma region of Valles Marineris on Mars based on Mars Reconnaissance Orbiter-Compact Reconnaissance Imaging Spectrometer for Mars (MRO-CRISM) observations. Icarus, 250, pp.7-17.

213. Jakosky, B.M., Shock, E.L., 1998. The biological potential of Mars, the early Earth, and Europa. Journal of Geophysical Research: Planets, 103(E8), pp.19359-19364.

214. Jakosky, B.M., Nealson, K.H., Bakermans, C., Ley, R.E., Mellon, M.T., 2003. Subfreezing activity of microorganisms and the potential habitability of Mars' polar regions. Astrobiology, 3(2), pp.343-350.

215. Jerz, J.K., Rimstidt, J.D., 2004. Pyrite oxidation in moist air. Geochimica et Cosmochimica Acta, 68(4), pp.701-714.

216. Johnson, C.M., Beard, B.L., Beukes, N.J., Klein, C., O'Leary, J.M., 2003. Ancient geochemical cycling in the Earth as inferred from Fe isotope studies of banded iron formations from the Transvaal Craton. Contributions to Mineralogy and Petrology, 144(5), pp.523-547.

217. Johnson, S.S., Mischna, M.A., Grove, T.L., Zuber, M.T., 2008. Sulphur-induced greenhouse warming on early Mars. Journal of Geophysical Research: Planets, 113, 1-15.

218. Jones, H.C., 1934. The iron-ore deposits of Bihar and Orissa. Office of the Geological Survy of India.

219. Kargel, J.S., Kaye, J.Z., Head, J.W., Marion, G.M., Sassen, R., Crowley, J.K., Ballesteros, O.P., Grant, S.A., Hogenboom, D.L., 2000. Europa's crust and ocean: Origin, composition, and the prospects for life. Icarus, 148(1), pp.226-265.

220. Kargel, J.S., 2004. Mars-A warmer, wetter planet. Springer Science & Business Media.

221. Kaufman, A.J., Knoll, A.H., 1995. Neoproterozoic variations in the C-isotopic composition of seawater: stratigraphic and biogeochemical implications. Precambrian Research, 73(1), pp.27-49.

222. Kerkhof, A.M., Hein, U.F., 2001. Fluid inclusion petrography. Lithos, 55(1), pp.27-47.

223. King, P.L., McSween, H.Y., 2005. Effects of H_2O, pH, and oxidation state on the stability of Fe minerals on Mars. Journal of Geophysical Research: Planets, 110, (E12).

224. King, T.V., Ridley, W.I., 1987. Relation of Spectroscopic Reflectance of Olivine to Mineral Chemistry. Meteoritics, 22, p.428.

225. Kiros, A., Gholap, A.V., Gigante, G.E., 2013. Fourier transform infrared spectroscopic characterization of clay minerals from rocks of Lali-

bela churches, Ethiopia. International Journal of Physical Sciences, 8(3), pp.109-119.

226. Klein, C., Beukes, N.J., 1989. Geochemistry and sedimentology of a facies transition from limestone to iron-formation deposition in the early Proterozoic Transvaal Supergroup, South Africa. Economic Geology, 84(7), pp.1733-1774.

227. Klein, C., Beukes, N.J., 1992. Time distribution, stratigraphy, and sedimentologic setting, and geochemistry of Precambrian iron-formations. The Proterozoic Biosphere: A Multidisciplinary Study, pp.139-146.

228. Klein, C., Hurlbut, C.S. and Dana, J.D., 1993. Manual of mineralogy. Wiley.

229. Klein, C., Ladeira, E.A., 2004. Geochemistry and mineralogy of Neoproterozoic banded iron-formations and some selected, siliceous manganese formations from the Urucum District, Mato Grosso do Sul, Brazil. Economic Geology, 99(6), pp.1233-1244.

230. Klein, C., 2005. Some Precambrian banded iron-formations (BIFs) from around the world: Their age, geologic setting, mineralogy, metamorphism, geochemistry, and origins. American Mineralogist, 90(10), pp.1473-1499.

231. Klingelhofer, G.R.D.S., Morris, R.V., Bernhardt, B., Schroder, C., Rodionov, D.S., De Souza, P.A., Yen, A., Gellert, R., Evlanov, E.N., Zubkov, B., Foh, J., 2004. Jarosite and hematite at Meridiani Planum from Opportunity's Mossbauer spectrometer. Science, 306(5702), pp.1740-1745.

232. Knauth, L.P., 2001. Isotopic biosignature in calcite formed during weathering of basalt : implications for past life on Mars, early life on Land, and ALH 84001. Astrobiology 1, 363-364.

233. Knoll, A.H., Carr, M., Clark, B., Des Marais, D.J., Farmer, J.D., Fischer, W.W., Grotzinger, J.P., McLennan, S.M., Malin, M., Schroder, C.,

Squyres, S., 2005. An astrobiological perspective on Meridiani Planum. Earth and Planetary Science Letters, 240(1), pp.179-189.

234. Komatsu, G., Geissler, P.E., Strom, R.G., Singer, R.B., 1993. Stratigraphy and erosional landforms of layered deposits in Valles Marineris, Mars. Journal of Geophysical Research: Planets, 98(E6), pp.11105-11121.

235. Konhauser, K.O., Hamade, T., Raiswell, R., Morris, R.C., Ferris, F.G., Southam, G., Canfield, D.E., 2002. Could bacteria have formed the Precambrian banded iron formations?. Geology, 30(12), pp.1079-1082.

236. Konhauser, K.O., Jones, B., Reysenbach, A.L., Renaut, R.W., 2003. Hot spring sinters: keys to understanding Earth's earliest life forms. Canadian Journal of Earth Sciences, 40(11), pp.1713-1724.

237. Kraft, M.D., Michalski, J.R., Sharp, T.G., 2003. Effects of pure silica coatings on thermal emission spectra of basaltic rocks: Considerations for Martian surface mineralogy. Geophysical Research Letters, 30(24).

238. Krasnopolsky, V.A., Maillard, J.P., Owen, T.C., 2004. Detection of methane in the martian atmosphere: evidence for life?. Icarus, 172(2), pp.537-547.

239. Kress, M.E., McKay, C.P., 2004. Formation of methane in comet impacts: implications for Earth, Mars, and Titan. Icarus, 168(2), pp.475-483.

240. Lane, M.D., 2007. Mid-infrared emission spectroscopy of sulphate and sulphate-bearing minerals. American Mineralogist, 92(1), pp.1-18.

241. Lane, M.D., Morris, R.V., Christensen, P.R., 2000. Sinus Meridiani shows spectral evidence for oriented hematite grains. In Lunar and Planetary Science Conference (Vol. 31, p. 1140).

242. Lane, M.D., Morris, R.V., Mertzman, S.A., Christensen, P.R., 2002. Evidence for platy hematite grains in Sinus Meridiani, Mars. Journal of Geophysical Research: Planets, 107(E12).

243. Langella, A., Cappelletti, P., de'Gennaro, R., 2001. Zeolites in closed hydrologic systems. Reviews in mineralogy and geochemistry, 45(1), pp.235-260.

244. Langevin, Y., Poulet, F., Bibring, J.P., Schmitt, B., Douté, S., Gondet, B., 2005a. Summer evolution of the north polar cap of Mars as observed by OMEGA/Mars express. Science, 307(5715), pp.1581-1584.

245. Langevin, Y., Poulet, F., Bibring, J.P., Gondet, B., 2005b. Sulphates in the north polar region of Mars detected by OMEGA/Mars Express. Science, 307(5715), pp.1584-1586.

246. Léveillé, R.J., Bridges, J., Wiens, R.C., Mangold, N., Cousin, A., Lanza, N., Forni, O., Ollila, A., Grotzinger, J., Clegg, S., Siebach, K., 2014. Chemistry of fracture-filling raised ridges in Yellowknife Bay, Gale Crater: Window into past aqueous activity and habitability on Mars. Journal of Geophysical Research: Planets, 119(11), pp.2398-2415.

247. Li, J., Zhu, X., Wadsworth, M.E., 1993. Raman spectroscopy of natural and oxidized metal sulphides. In EPD Congress 1993 (pp. 229-244).

248. Longhi, J., Knittle, E., Holloway, J.R., Waenke, H., 1992. The bulk composition, mineralogy and internal structure of Mars. Mars, 1, pp.184-208.

249. López-Archilla, A.I., Marín, I., Amils, R., 2001. Microbial community composition and ecology of an acidic aquatic environment: the Tinto River, Spain. Microbial ecology, 41(1), pp.20-35.

250. Losey, A.B., Benison, K.C., 2000. Silurian paleoclimate data from fluid inclusions in the Salina Group halite Michigan Basin. Carbonates and Evaporites, 15(1), pp.28-36.

251. Lowenstein, T.K., Li, J., Brown, C.B., 1998. Palaeo-temperatures from fluid inclusions in halite: method verification and a 100,000 year pa-

leotemperature record, Death Valley, CA. Chemical Geology, 150(3), pp.223-245.

252. Lowenstein, T.K., Li, J., Brown, C., Roberts, S.M., Ku, T.L., Luo, S. Yang, W., 1999. 200 ky paleoclimate record from Death Valley salt core. Geology, 27(1), pp.3-6.

253. Lowenstein, T.K., Schubert, B.A., Timofeeff, M.N., 2011. Microbial communities in fluid inclusions and long-term survival in halite. GSA Today, 21(1), pp.4-9.

254. Lucchitta, B.K., Ferguson, H.M., 1988. Ganymede:" Moat" craters compared with palimpsests and basins. In Lunar and Planetary Science Conference (Vol. 19).

255. Lucchitta, B.K., Isbell, N.K., Howington-Kraus, A., 1994. Topography of Valles Marineris: Implications for erosional and structural history. Journal of Geophysical Research: Planets, 99(E2), pp.3783-3798.

256. Madhavaraju, J., Ramasamy, S., 2001. Clay mineral assemblages and rare earth element distribution in the sediments of Ariyalur Group, Tiruchirapalli District, Tamil Nadu-Implication for paleoclimate. Geological Society of India, 58(1), pp.69-77.

257. Madhavaraju, J., Ramasamy, S., Ruffell, A., Mohan, S.P., 2002. Clay mineralogy of the late Cretaceous and early Tertiary successions of the Cauvery Basin (southeastern India): implications for sediment source and palaeoclimates at the K/T boundary. Cretaceous Research, 23(2), pp.153-163.

258. Madhavaraju, J., Lee, Y.I., 2009. Geochemistry of the Dalmiapuram Formation of the Uttatur Group (Early Cretaceous), Cauvery basin, southeastern India: Implications on provenance and paleo-redox conditions. Revista Mexicana de Ciencias Geológicas, 26(2), pp.380-394.

259. Mahaffy, P., 2008. Exploration of the habitability of Mars: Development of analytical protocols for measurement of organic carbon on the 2009 Mars Science Laboratory. Space Science Reviews, 135(1-4), pp.255-268.

260. Mahalik, N.K., 1987. Geology of rocks lying between Gangpur Group and Iron Ore Group of the horse-shoe syncline in north Orissa. Indian J. Earth Sci, 14, pp.73-83.

261. Majumder, T., Chakraborty, K.L. Bhattacharyya, A., 1982. Geochemistry of banded iron formation of Orissa, India. Mineralium Deposita, 17(1), pp.107-118.

262. Malin, M.C., Edgett, K.S., 2000. Evidence for recent groundwater seepage and surface runoff on Mars. Science, 288(5475), pp.2330-2335.

263. Mangold, N., Poulet, F., Mustard, J.F., Bibring, J.P., Gondet, B., Langevin, Y., Ansan, V., Masson, P., Fassett, C., Head, J.W., Hoffmann, H., 2007. Mineralogy of the Nili Fossae region with OMEGA/Mars Express data: 2. Aqueous alteration of the crust. Journal of Geophysical Research: Planets, 112(E8).

264. Mangold, N., Gendrin, A., Gondet, B., LeMouelic, S., Quantin, C., Ansan, V., Bibring, J.P., Langevin, Y., Masson, P., Neukum, G., 2008. Spectral and geological study of the sulphate-rich region of West Candor Chasma, Mars. Icarus, 194(2), pp.519-543.

265. Martínez-Frías, J., Lunar, R., Rodríguez-Losada, J.A., Delgado, A., Rull, F., 2004. The volcanism-related multistage hydrothermal system of El Jaroso (SE Spain): implications for the exploration of Mars. Earth, planets and space, 56(7), pp.v-viii.

266. Martinez-Frias, J., Amaral, G., Vázquez, L., 2006. Astrobiological significance of minerals on Mars surface environment. Reviews in Environmental Science and Bio/technology, 5(2-3), pp.219-231.

267. Massé, M., Bourgeois, O., Le Mouélic, S., Verpoorter, C., Le Deit, L., Bibring, J.-P., 2010. Martian polar and circum-polar sulphate-bearing deposits: sublimation tills derived from the North Polar Cap. Icarus209 (2), 434-451. http://dx.doi.org/10.1016/j.icarus.2010.04.017.

268. Massé, M., Bourgeois, O., Le Mouélic, S., Verpoorter, C., Spiga, A., Le Deit, L., 2012. Wide distribution and glacial origin of polar gypsum on Mars. Earth and Planetary Science Letters, 317, pp.44-55.

269. Mazumder, R., 2005. Proterozoic sedimentation and volcanism in the Singhbhum crustal province, India and their implications. Sedimentary Geology, 176(1), pp.167-193.

270. Mazur, P., Barghoorn, E.S., Halvorson, H.O., Jukes, T.H., Kaplan, I.R., Margulis, L., 1978. Biological implications of the Viking mission to Mars. Space Science Reviews, 22(1), pp.3-34.

271. McArthur, J.M., Turner, J.V., Lyons, W.B., Osborn, A.O., Thirlwall, M.F., 1991. Hydrochemistry on the Yilgarn Block, Western Australia: Ferrolysis and mineralisation in acidic brines. Geochimica et Cosmochimica Acta, 55(5), pp.1273-1288.

272. McCollom, T.M., Ehlmann, B.L., Wang, A., Hynek, B.M., Berquó, T.S., 2014. Detection of iron substitution in natroalunite-natrojarosite solid solutions and potential implications for Mars. American Mineralogist, 99(5-6), pp.948-964.

273. McHenry, L.J., 2010. Element distribution between coexisting authigenic mineral phases in argillic and zeolitic altered tephra, Olduvai Gorge, Tanzania. Clays and Clay Minerals, 58(5), pp.627-643.

274. McHenry, L.J., Chevrier, V., Schroder, C., 2011. Jarosite in a Pleistocene East African saline-alkaline paleolacustrine deposit: Implications for Mars aqueous geochemistry. Journal of Geophysical Research: Planets, 116(E4).

275. McKay, C.P., Nedell, S.S., 1988. Are there carbonate deposits in the Valles Marineris, Mars?. Icarus, 73(1), pp.142-148.

276. McKay, C.P., Stoker, C.R., 1989. The early environment and its evolution on Mars: Implication for life. Reviews of Geophysics, 27(2), pp.189-214.

277. McKay, D.S. et al., 1996. Search for past life on Mars: possible relic biogenic activity in Martian meteorite ALH84001. Science 273, 924-930.

278. McKay, C.P., Grunthaner, F.J., Lane, A.L., Herring, M., Bartman, R.K., Ksendzov, A., Manning, C.M., Lamb, J.L., Williams, R.M., Ricco, A.J., Butler, M.A., 1998. The Mars Oxidant experiment (MOx) for Mars' 96. Planetary and space science, 46(6), pp.769-777.

279. McLennan, S.M., Bell, J.F., Calvin, W.M., Christensen, P.R., Clark, B.D., De Souza, P.A., Farmer, J., Farrand, W.H., Fike, D.A., Gellert, R., Ghosh, A., 2005. Provenance and diagenesis of the evaporite-bearing Burns formation, Meridiani Planum, Mars. Earth and Planetary Science Letters, 240(1), pp.95-121.

280. McSween, H.Y., Taylor, G.J., Wyatt, M.B., 2009. Elemental composition of the Martian crust. Science, 324(5928), pp.736-739.

281. Melezhik, V.A., Gorokhov, I.M., Kuznetsov, A.B., Fallick, A.E., 2001. Chemostratigraphy of Neoproterozoic carbonates: implications for 'blind dating'. Terra Nova, 13(1), pp.1-11.

282. Mellon, M.T., Phillips, R.J., 2001. Recent gullies on Mars and the source of liquid water. Journal of Geophysical Research: Planets, 106(E10), pp.23165-23179.

283. Melnik, I.P., 1981. Precambrian Banded Iron-formations: Physicochemical Conditions of Formation. Elsevier Scientific Publishing Company.

284. Meng, F., Ni, P., Schiffbauer, J.D., Yuan, X., Zhou, C., Wang, Y., Xia, M., 2011. Ediacaran seawater temperature: Evidence from inclusions of Sinian halite. Precambrian Research, 184(1), pp.63-69

285. Merwin, H.E., Posnjak, E., 1937. Sulphate incrustations in the copper Queen mine, Bisbee, Arizona. American Mineralogist, 22(5), pp.567-571.

286. Michalski, J.R., Kraft, M.D., Sharp, T.G., Williams, L.B., Christensen, P.R., 2005. Mineralogical constraints on the high-silica Martian surface component observed by TES. Icarus, 174(1), pp.161-177.

287. Miller, K.G., Kominz, M.A., Browning, J.V., Wright, J.D., Mountain, G.S., Katz, M.E., Sugarman, P.J., Cramer, B.S., Christie-Blick, N., Pekar, S.F., 2005. The Phanerozoic record of global sea-level change. science, 310(5752), pp.1293-1298.

288. Milliken, R.E., Swayze, G.A., Arvidson, R.E., Bishop, J.L., Clark, R.N., Ehlmann, B.L., Green, R.O., Grotzinger, J.P., Morris, R.V., Murchie, S.L., Mustard, J.F., 2008. Opaline silica in young deposits on Mars. Geology, 36(11), pp.847-850.

289. Ming, D.W., Mittlefehldt, D.W., Morris, R.V., Golden, D.C., Gellert, R., Yen, A., Clark, B.C., Squyres, S.W., Farrand, W.H., Ruff, S.W., Arvidson, R.E., 2006. Geochemical and mineralogical indicators for aqueous processes in the Columbia Hills of Gusev crater, Mars. Journal of Geophysical Research: Planets, 111(E2).

290. Misra, S., 2006. Precambrian chronostratigraphic growth of Singhbhum-Orissa craton, Eastern Indian shield: an alternative model. Geological Society of India, 67(3), pp.356.

291. Mitra, S., Gupta, S., Bhattacharya, S., Banerjee, S., Chauhan, P., Parthasarathy, G., 2014. Jarosite Precipitation from Acidic Saline Waters in Kachchh, Gujarat, India: an Appropriate Martian Analogue?. In AGU Fall Meeting Abstracts (Vol. 1, p. 3891).

292. Mitrofanov, I.G., Zuber, M.T., Litvak, M.L., Boynton, W.V., Smith, D.E., Drake, D., Hamara, D., Kozyrev, A.S., Sanin, A.B., Shinohara, C., Saunders, R.S., 2003. CO_2 snow depth and subsurface water-ice abundance in the northern hemisphere of Mars. Science, 300(5628), pp.2081-2084.

293. Moore, J.C., Berlow, E.L., Coleman, D.C., Ruiter, P.C., Dong, Q., Hastings, A., Johnson, N.C., McCann, K.S., Melville, K., Morin, P.J., Nadelhoffer, K., 2004. Detritus, trophic dynamics and biodiversity. Ecology letters, 7(7), pp.584-600.

294. Moore, J.M., 2004. Mars: Blueberry fields for ever. Nature, 428(6984), pp.711-712.

295. Morris, R.V., Ruff, S.W., Gellert, R., Ming, D.W., Arvidson, R.E., Clark, B.C., Golden, D.C., Siebach, K., Klingelhofer, G., Schroder, C., Fleischer, I., 2010. Identification of carbonate-rich outcrops on Mars by the Spirit rover. Science, 329(5990), pp.421-424.

296. Mucke, A., Annor, A., 1993. Examples and genetic significance of the formation of iron oxides in the Nigerian banded iron-formations. Mineralium Deposita, 28, (2), 136-145.

297. Mukhopadhyay, J., Ghosh, G., Nandi, A.K., Chaudhuri, A.K., 2006. Depositional setting of the Kolhan Group: its implications for the development of a Meso to Neoproterozoic deep-water basin on the South Indian craton. South African Journal of Geology, 109(1-2), pp.183-192.

298. Mukhopadhyay, J., Beukes, N.J., Armstrong, R.A., Zimmermann, U., Ghosh, G., Medda, R.A., 2008. Dating the oldest greenstone in India: a 3.51-Ga precise U-Pb SHRIMP zircon age for dacitic lava of the southern Iron Ore Group, Singhbhum craton. The Journal of Geology, 116(5), pp.449-461.

299. Mumma, M.J., Novak, R.E., DiSanti, M.A., Bonev, B.P., Dello Russo, N., 2004. Detection and mapping of methane and water on Mars. In Bulletin of the American Astronomical Society (Vol. 36, p. 1127).

300. Mumma, M.J., Villanueva, G.L., Novak, R.E., Hewagama, T., Bonev, B.P., DiSanti, M.A., Mandell, A.M., Smith, M.D., 2009. Strong release of methane on Mars in northern summer 2003. Science, 323(5917), pp.1041-1045.

301. Murad, E., Rojik, P., 2005. Iron mineralogy of mine-drainage precipitates as environmental indicators: review of current concepts and a case study from the Sokolov Basin, Czech Republic. Clay Minerals, 40(4), pp.427-440.

302. Murchie, S., Arvidson, R., Bedini, P., Beisser, K., Bibring, J.P., Bishop, J., Boldt, J., Cavender, P., Choo, T., Clancy, R.T., Darlington, E.H., 2007. Compact reconnaissance imaging spectrometer for Mars (CRISM) on Mars reconnaissance orbiter (MRO). Journal of Geophysical Research: Planets, 112(E5).

303. Murchie, S.L., Mustard, J.F., Ehlmann, B.L., Milliken, R.E., Bishop, J.L., McKeown, N.K., Noe Dobrea, E.Z., Seelos, F.P., Buczkowski, D.L., Wiseman, S.M., Arvidson, R.E., 2009. A synthesis of Martian aqueous mineralogy after 1 Mars year of observations from the Mars Reconnaissance Orbiter. Journal of Geophysical Research: Planets, 114(E2).

304. Mustard, J.F., Poulet, F., Gendrin, A., Bibring, J.P., Langevin, Y., Gondet, B., Mangold, N., Bellucci, G., Altieri, F., 2005. Olivine and pyroxene diversity in the crust of Mars. Science, 307(5715), pp.1594-1597.

305. Mustard, J.F., Murchie, S.L., Pelkey, S.M., Ehlmann, B.L., Milliken, R.E., Grant, J.A., Bibring, J.P., Poulet, F., Bishop, J., Dobrea, E.N., Roach, L., 2008. Hydrated silicate minerals on Mars observed by the

Mars Reconnaissance Orbiter CRISM instrument. Nature, 454(7202), pp.305-309.

306. Nagendra, R., Raja, R., Reddy, A.N., Jaiprakash, B.C., Bhavani, R., 2002. Outcrop sequence stratigraphy of the Maastrichtian Kallankurchchi Formation, Ariyalur Group, Tamil Nadu. JOURNAL-Geological Society of India, 59(3), pp.243-248.

307. Nagendra, R., Kannan, B.K., Sen, G., Gilbert, H., Bakkiaraj, D., Reddy, A.N., Jaiprakash, B.C., 2011. Sequence surfaces and paleobathymetric trends in Albian to Maastrichtian sediments of Ariyalur area, Cauvery Basin, India. Marine and Petroleum Geology, 28(4), pp.895-905.

308. Nair, K.M., Rao, M.R., 1980. Stratigraphic analysis of Kerala basin. In Proc. Symp. on Geology and Geomorphology of Kerala. Geol. Surv. India. Spl. Publ (No. 5, p. 18).

309. Nakamoto, K., 1986. Infrared and Raman spectra of inorganic and coordination compounds. John Wiley & Sons, Ltd.

310. Navrotsky, A., Forray, F.L., Drouet, C., 2005. Jarosite stability on Mars. Icarus, 176(1), pp.250-253.

311. Nedell, S.S., Squyres, S.W., Andersen, D.W., 1987. Origin and evolution of the layered deposits in the Valles Marineris, Mars. Icarus, 70(3), pp.409-441.

312. Newsom, H.E., Hagerty, J.J., Thorsos, I.E., 2001. Location and sampling of aqueous and hydrothermal deposits in Martian impact craters. Astrobiology, 1(1), pp.71-88.

313. Newsom, H.E., Barber, C.A., Hare, T.M., Schelble, R.T., Sutherland, V.A., Feldman, W.C., 2003. Paleolakes and impact basins in southern Arabia Terra, including Meridiani Planum: Implications for the formation of hematite deposits on Mars. Journal of Geophysical Research: Planets, 108(E12).

314. Niederberger, T.D., Perreault, N.N., Lawrence, J.R., Nadeau, J.L., Mielke, R.E., Greer, C.W., Andersen, D.T., Whyte, L.G., 2009. Novel sulphur-oxidizing streamers thriving in perennial cold saline springs of the Canadian high Arctic. Environmental microbiology, 11(3), pp.616-629.

315. Nienow, J.A., Friedmann, E.I., 1993. Terrestrial lithophytic (rock) communities. Antarctic microbiology, pp.343-412.

316. Nordstrom, D.K., 1982. Aqueous pyrite oxidation and the consequent formation of secondary iron minerals. Acid sulphate weathering, (acidsulphateweat), pp.37-56.

317. Oggerin, M., Rodríguez, N., del Moral, C., Amils, R., 2014. Fungal jarosite biomineralization in Rio Tinto. Research in microbiology, 165(9), pp.719-725.

318. Okubo, C.H., Lewis, K.W., McEwen, A.S., Kirk, R.L., 2008. Relative age of interior layered deposits in southwest Candor Chasma based on high-resolution structural mapping. Journal of Geophysical Research: Planets, 113(E12).

319. Orgel, C., Kereszturi, á., Váczi, T., Groemer, G., Sattler, B., 2014. Scientific results and lessons learned from an integrated crewed Mars exploration simulation at the Rio Tinto Mars analogue site. Acta Astronautica, 94(2), pp.736-748.

320. Ormo, J., Komatsu, G., Chan, M.A., Beitler, B., Parry, W.T., 2004. Geological features indicative of processes related to the hematite formation in Meridiani Planum and Aram Chaos, Mars: a comparison with diagenetic hematite deposits in southern Utah, USA. Icarus, 171(2), pp.295-316.

321. Osinski, G.R., Spray, J.G., LEE, P., 2001. Impact-induced hydrothermal activity within the Haughton impact structure, arctic Canada: Genera-

tion of a transient, warm, wet oasis. Meteoritics & Planetary Science, 36(5), pp.731-745.

322. Osinski, G.R., Spray, J.G., 2003. Evidence for the shock melting of sulphates from the Haughton impact structure, Arctic Canada. Earth and Planetary Science Letters, 215(3), pp.357-370.

323. Papike, J.J., Karner, J.M., Shearer, C.K., 2006. Comparative planetary mineralogy: Implications of martian and terrestrial jarosite. A crystal chemical perspective. Geochimica et Cosmochimica Acta, 70(5), pp.1309-1321.

324. Parente, M., 2008. A new approach to denoising CRISM images. In Lunar and Planetary Science Conference (Vol. 39, pp. 2528).

325. Parnell, J., Baron, M., 2004. The preservation of fluid inclusions in diverse surface precipitates: the potential for sampling palaeo-water from surface deposits on Mars. International Journal of Astrobiology, 3(01), pp.21-30.

326. Parnell, J., Lee, P., Cockell, C.S., Osinski, G.R., 2004. Microbial colonization in impact-generated hydrothermal sulphate deposits, Haughton impact structure, and implications for sulphates on Mars. International Journal of Astrobiology, 3(03), pp.247-256.

327. Paulose, K.V., Narayanaswamy, S., 1968. The Tertiaries of Kerala. Mem. Geol. Soc. Ind. 2, pp. 300-308.

328. Pecoits, E., Gingras, M.K., Barley, M.E., Kappler, A., Posth, N.R., Konhauser, K.O., 2009. Petrography and geochemistry of the Dales Gorge banded iron formation: Paragenetic sequence, source and implications for palaeo-ocean chemistry. Precambrian Research, 172(1), pp.163-187.

329. Pelkey, S.M., Mustard, J.F., Murchie, S., Clancy, R.T., Wolff, M., Smith, M., Milliken, R., Bibring, J.P., Gendrin, A., Poulet, F., Langevin, Y., 2007. CRISM multispectral summary products: Parameterizing mineral

diversity on Mars from reflectance. Journal of Geophysical Research: Planets, 112(E8).

330. Peterson, C., 1982. A secondary origin for the central plateau of Hebes Chasma. In Lunar and Planetary Science Conference Proceedings (Vol. 12, pp. 1459-1471).

331. Philipp, S.L., 2008. Geometry and formation of gypsum veins in mudstones at Watchet, Somerset, SW England. Geological Magazine, 145(06), pp.831-844.

332. Polat, A., Frei, R., 2005. The origin of early Archean banded iron formations and of continental crust, Isua, southern West Greenland. Precambrian Research, 138(1), pp.151-175.

333. Pollack, J.B., Kasting, J.F., Richardson, S.M., Poliakoff, K., 1987. The case for a wet, warm climate on early Mars. Icarus, 71(2), pp.203-224.

334. Posey-Dowty, J., Moskowitz, B., Crerar, D., Hargraves, R., Tanenbaum, L., Dowty, E., 1986. Iron oxide and hydroxide precipitation from ferrous solutions and its relevance to Martian surface mineralogy. Icarus 66 (1), 105-116.

335. Posth, N.R., Huelin, S., Konhauser, K.O., Kappler, A., 2010. Size, density and composition of cell-mineral aggregates formed during anoxygenic phototrophic Fe (II) oxidation: Impact on modern and ancient environments. Geochimica et Cosmochimica Acta, 74(12), pp.3476-3493.

336. Poulet, F., Bibring, J.P., Mustard, J.F., Gendrin, A., Mangold, N., Langevin, Y., Arvidson, R.E., Gondet, B., Gomez, C., Berthé, M., Erard, S., 2005. Phyllosilicates on Mars and implications for early Martian climate. Nature, 438(7068), pp.623-627.

337. Poulet, F., Mangold, N., Loizeau, D., Bibring, J.P., Langevin, Y., Michalski, J., Gondet, B., 2008. Abundance of minerals in the phyllosilicate-rich units on Mars. Astronomy & Astrophysics, 487(2), pp.L41-L44.

338. Prasad Rao, G.H.S.V., Murty, Y.G.K., Deekshitulu, M.N., 1964. Stratigraphic relations of precambrian iron formations and associated sedimentary sequences in parts of Keonjhar, Cuttack, Dhenkanal and Sundergarh districts of Orissa, India. In: International Geological Congress, India, 10, pp. 72-87.

339. Preston, L.J., Genge, M.J., 2010. The Rhynie Chert, Scotland, and the search for life on Mars. Astrobiology, 10(5), pp.549-560.

340. Radhakrishna, B.P., Naqvi, S.M., 1986. Precambrian continental crust of India and its evolution. The Journal of Geology, pp.145-166.

341. Raju, D.S.N., Ravindran, C.N., Kalyansundar, R., 1993. Cretaceous cycles of sea level changes in the Cauvery Basin, India e a first revision. Bulletin of the Oil and Natural Gas Commission 30, pp.101-113.

342. Ramanathan, S., 1968. Stratigraphy of Cauvery Basin with reference to its oil prospects. Mem. Geol. Soc. India, 2, pp.153-167.

343. Ramanathan, R.M., 1977. In: Venkatarengan, R. (Ed.), Depositional Systems and Thrust Area for Exploration in Cauvery Basin. ONGC Bulletin 24 (1), 53-69. 1989.

344. Ramasamy, S., Banerji, R.K., 1991. Geology, Petrography and Systematic Stratigraphy of Pre-Ariyalur Sequence in Tiruchirapaui District, Tamil Nadu, India. Geological Society of India, 37(6), pp.577-594.

345. Ramkumar, M., Stuben, D., Berner, Z., 2004. Lithostratigraphy, depositional history and sea level changes of the Cauvery Basin, southern India. Annales Géologiques de la P éninsule Balkanique, 65.

346. Ramkumar, M., 2008a. Cyclic fine-grained deposits with polymict boulders in Olaipadi member of the Dalmiapuram Formation, Cauvery basin, south India: plausible causes and sedimentation model. ICFAI Journal of Earth Sciences 2, 7-27.

347. Ramkumar, M., 2008b. Carbonate diagenesis in the Kallankurichchi Formation, Ariyalur Group, south India and its implications on petroleum prospects. Journal of Geological Society of India 71, 407-418.

348. Ramkumar, M., Stuben, D., Berner, Z., 2011. Barremian-Danian chemostratigraphic sequences of the Cauvery Basin, India: Implications on scales of stratigraphic correlation. Gondwana Research, 19(1), pp.291-309.

349. Rangaraju, M.K., Agarwal, A., Prabhakar, K.N., 1993. Tectono-stratigraphy, structural styles, evolutionary model and hydrocarbon habitat, Cauvery and Palar basins. In Proceedings of 2nd seminar on petroliferous basins of India (Vol. 1, pp. 371-388).

350. Rao, C.P., Gluskoter, H.J., 1973. Occurrence and distribution of minerals in Illinois coals. Urbana: Illinois State Geological Survey.

351. Rao, P.S., 1976. Geology and tectonic history of the Kerala region. Abstract in Seminar on Geomorphology of Kerala, Trivandrum, pp.13-16.

352. Rao, T.G., Naqvi, S.M., 1995. Geochemistry, depositional environment and tectonic setting of the BIF's of the Late Archaean Chitradurga Schist Belt, India. Chemical Geology, 121(1), pp.217-243.

353. Rendon, J.L., Serna, C.J., 1981. IR spectra of powder hematite: effects of particle size and shape. Clay Miner, 16(4), pp.375-384.

354. Richardson, W.A., 1920. The fibrous gypsum of Nottinghamshire. Journal of the Mineralogical Society 19, 77-95.

355. Riding, R., 2000. Microbial carbonates: the geological record of calcified bacterial-algal mats and biofilms. Sedimentology, 47(s1), pp.179-214.

356. Rieder, R., Gellert, R., Anderson, R.C., Bruckner, J., Clark, B.C., Dreibus, G., Economou, T., Klingelhofer, G., Lugmair, G.W., Ming, D.W., Squyres, S.W., 2004. Chemistry of rocks and soils at Meridiani Planum from the Alpha Particle X-ray Spectrometer. Science, 306(5702), pp.1746-1749.

357. Roach, L.H., Mustard, J.F., Murchie, S.L., Bibring, J.P., Arvidson, R.E., Bishop, J.L., Milliken, R.E., Seelos, F., and Team, C.S., 2008. Constraints on the rate of sulphate phase changes in Valles Marineris Interior Layered Deposits. In Lunar Planet. Sci. Conf., XXXIX.

358. Roach, L.H., Mustard, J.F., Murchie, S.L., Bibring, J.P., Forget, F., Lewis, K.W., Aharonson, O., Vincendon, M., Bishop, J.L., 2009. Testing evidence of recent hydration state change in sulphates on Mars. Journal of Geophysical Research: Planets, 114(E2).

359. Roach, L.H., Mustard, J.F., Swayze, G., Milliken, R.E., Bishop, J.L., Murchie, S.L., Lichtenberg, K., 2010. Hydrated mineral stratigraphy of Ius Chasma, Valles Marineris. Icarus, 206(1), pp.253-268.

360. Roberts, S.M., Spencer, R.J., 1995. Paleotemperatures preserved in fluid inclusions in halite. Geochimica et Cosmochimica Acta, 59(19), pp.3929-3942.

361. Roedder, E., 1984. Fluids in salt. Am. Mineral.;(United States), 69.

362. Rothschild, L.J., 1990. Earth analogs for Martian life. Microbes in evaporites, a new model system for life on Mars. Icarus 88, 246-260.

363. Roy, A., Wang, L., Seals, R.K., Metcalf, J.B., 2003. Stabilization Techniques for Reactive Aggregate in Soil-Cement Base Course. Louisiana State University and Louisiana DOTD, Baton Rouge.

364. Roy, S., Venkatesh, A.S., 2009. Mineralogy and geochemistry of banded iron formation and iron ores from eastern India with implications on their genesis. Journal of Earth System Science, 118(6), pp.619-641.

365. Ruan, H.D., Frost, R.L., Kloprogge, J.T., Duong, L., 2002. Infrared spectroscopy of goethite dehydroxylation: III. FT-IR microscopy of in situ study of the thermal transformation of goethite to hematite. Spectrochimica Acta Part A: Molecular and Biomolecular Spectroscopy, 58(5), pp.967-981.

366. Ruff, S.W., Farmer, J.D., Calvin, W.M., Kenneth, E. H., Johnson, J.R., Morris, R.V., Rice, M.S., Arvidson, R. E., Bell , J. F., Christensen, P. R., Squyres, W.S., 2011. Characteristics, distribution, origin, and significance of opaline silica observed by the Spirit rover in Gusev crater, Mars. Journal of Geophysical Research.116, E00F23.

367. Rull, F., Martinez-Frias, J., Rodríguez-Losada, J.A., 2007. Micro-Raman spectroscopic study of El Gasco pumice, western Spain. Journal of Raman Spectroscopy, 38(2), pp.239-244.

368. Sabater, S., Buchaca, T., Cambra, J., Catalan, J., Guasch, H., Ivorra, N., Munoz, I., Navarro, E., Real, M., Romaní, A., 2003. Structure and function of benthic algal communities in an extremely acid river. Journal of Phycology, 39(3), pp.481-489.

369. Saha, A.K., Ray, S.L., 1984. The structural and geochemical evolution of the Singhbhum granite batholithic complex, India. Tectonophysics, 105(1), pp.163-176.

370. Saha, A.K., 1994. Crustal evolution of Singhbhum-North Orissa, eastern India. GSI Publications, 1(1).

371. Sasaki, K., Tanaike, O., Konno, H., 1998. Distinction of jarosite-group compounds by raman spectroscopy. The Canadian Mineralogist, 36, pp.1225-1235.

372. Sass, E., Nathan, Y., Nissenbaum, A., 1965. Mineralogy of certain pyrite concretions from Israel and their alteration products. Mineral. Mag, 35, pp.84-87.

373. Sastry, M.V.A., Mamgain, V.D., Rao, B.J., 1972. Ostracod fauna of the Ariyalur Group (Upper Cretaceous), Tiruchirapalli District, Tamil Nadu. Manager of Publications Civil Lines.

374. Sastri, V.V., Sinha, R.N., Singh, G., Murti, K.V.S., 1973. Stratigraphy and tectonics of sedimentary basins on east coast of peninsular India.

AAPG Bulletin, 57(4), pp.655-678.

375. Satterfield, C.L., Lowenstein, T.K., Vreeland, R.H., Rosenzweig, W.D., 2005a. Paleobrine temperatures, chemistries, and paleoenvironments of Silurian Salina Formation F-1 salt, Michigan Basin, USA, from petrography and fluid inclusions in halite. Journal of Sedimentary Research, 75(4), pp.534-546.

376. Satterfield, C.L., Lowenstein, T.K., Vreeland, R.H., Rosenzweig, W.D., Powers, D.W., 2005b. New evidence for 250 Ma age of halotolerant bacterium from a Permian salt crystal. Geology, 33(4), pp.265-268.

377. Schelble, R.T., Westall, F., Allen, C.C., 2004. ∼1.8 Ga iron-mineralized microbiota from the Gunflint Iron Formation, Ontario, Canada: implications for Mars. Advances in Space Research, 33(8), pp.1268-1273.

378. Schiavon, N., 2007. Kaolinisation of granite in an urban environment. Environmental Geology, 52(2), pp.399-407.

379. Schopf, J.W., 1993. Microfossils of the Early Archean Apex chert: new evidence of the antiquity of life. Science, 260(5108), pp.640-646.

380. Schopf, J.W., Farmer, J.D., Foster, I.S., Kudryavtsev, A.B., Gallardo, V.A., Espinoza, C., 2012. Gypsum-permineralized microfossils and their relevance to the search for life on Mars. Astrobiology, 12(7), pp.619-633.

381. Seidl, V., Knop, O., Falk, M., 1969. Infrared studies of water in crystalline hydrates: gypsum, $CaSO_4 \cdot 2H_2O$. Canadian Journal of Chemistry, 47(8), pp.1361-1368.

382. Serna, C.J., Rendon, J.L., Iglesias, J.E., 1982. Infrared surface modes in corundum-type microcrystalline oxides. Spectrochimica Acta Part A: Molecular Spectroscopy, 38(7), pp.797-802.

383. Sharma, S.K., Angel, S.M., Ghosh, M., Hubble, H.W., Lucey, P.G., 2002. Remote pulsed laser Raman spectroscopy system for mineral analysis on

planetary surfaces to 66 meters. Applied Spectroscopy, 56(6), pp.699-705.

384. Shearman, D.J., Mossop, G., Dunsmore, H., Martin, M., 1972. Origin of gypsum veins by hydraulic fracture. J. Inst. Min. Met., pp.B149-B155.

385. Shebanova, O.N., Lazor, P., 2003. Raman study of magnetite (Fe_3O_4): laser-induced thermal effects and oxidation. Journal of Raman spectroscopy, 34(11), pp.845-852.

386. Sherman, D.M., Waite, T.D., 1985. Electronic spectra of Fe^3+ oxides and oxide hydroxides in the near IR to near UV. American Mineralogist, 70(11-12), pp.1262-1269.

387. Singer, R.B., 1982. Spectral evidence for the mineralogy of high-albedo soils and dust on Mars. Journal of Geophysical Research: Solid Earth, 87(B12), pp.10159-10168.

388. Singh, B., Wilson, M.J., Kuroda, W.J., Fraser, A.R., Merrington, G., 1999. Mineralogy and chemistry of ochre sediments from an acid mine drainage near a disused mine in Cornwall, UK. Clay Minerals, 34(2), pp.301-317.

389. Singh, M., Kannan, B., Rajesh, V.J., 2015. Field and spectral investigation of gypsum deposit,Tamil Nadu, India: A martian analogue site. European Planetary Science Congress, 10, pp. 45

390. Sinha, R., Raymahashay, B.C., 2004. Evaporite mineralogy and geochemical evolution of the Sambhar Salt Lake, Rajasthan, India. Sedimentary Geology, 166(1), pp.59-71.

391. Smith, P.H., and 34 colleagues, 2009. H_2O at the Phoenix landing site. Science 325, 58-61.

392. Solomon, S.C., Aharonson, O., Aurnou, J.M., Banerdt, W.B., Carr, M.H., Dombard, A.J., Frey, H.V., Golombek, M.P., Hauck, S.A., Head,

J.W., Jakosky, B.M., 2005. New perspectives on ancient Mars. Science, 307(5713), pp.1214-1220.

393. Soman, k., 1980. Geology of Kerala. NCESS 8, pp.62.

394. Squyres, S.W., Arvidson, R.E., Bell, J.F., Bruckner, J., Cabrol, N.A., Calvin, W., Carr, M.H., Christensen, P.R., Clark, B.C., Crumpler, L., Des Marais, D.J., 2004a. The Opportunity Rover's Athena science investigation at Meridiani Planum, Mars. Science, 306(5702), pp.1698-1703.

395. Squyres, S.W., Grotzinger, J.P., Arvidson, R.E., Bell, J.F., Calvin, W., Christensen, P.R., Clark, B.C., Crisp, J.A., Farrand, W.H., Herkenhoff, K.E., Johnson, J.R., 2004b. In situ evidence for an ancient aqueous environment at Meridiani Planum, Mars. science, 306(5702), pp.1709-1714.

396. Squyres, S.W., Knoll, A.H., 2005. Sedimentary rocks at Meridiani Planum: Origin, diagenesis, and implications for life on Mars. Earth and Planetary Science Letters, 240(1), pp.1-10.

397. Squyres, S.W., Arvidson, R.E., Bollen, D., Bell, J.F., Brueckner, J., Cabrol, N.A., Calvin, W.M., Carr, M.H., Christensen, P.R., Clark, B.C., Crumpler, L., 2006. Overview of the opportunity mars exploration rover mission to meridiani planum: Eagle crater to purgatory ripple. Journal of Geophysical Research: Planets, 111(E12).

398. Squyres, S.W., Arvidson, R.E., Ruff, S., Gellert, R., Morris, R.V., Ming, D.W., Crumpler, L., Farmer, J.D., Des Marais, D.J., Yen, A., McLennan, S.M., 2008. Detection of silica-rich deposits on Mars. Science, 320(5879), pp.1063-1067.

399. Squyres, S.W., Arvidson, R.E., Bell, J.F., Calef, F., Clark, B.C., Cohen, B.A., Crumpler, L.A., De Souza, P.A., Farrand, W.H., Gellert, R., Grant, J., 2012. Ancient impact and aqueous processes at Endeavour Crater, Mars. Science, 336(6081), pp.570-576.

400. Stanton, R.L., 1972. A preliminary account of chemical relationships between sulphide-lode and 'Banded Iron Formation' at Broken Hill, New South Wales. Economic Geology 67 (8), 1128-1145.

401. Stefov, V., Jovanovski, G., Shoptrajanov, B., Minceva-Sukarova, B., Dimitrovska, S., Boev, B., 2000. Minerals from Macedonia V. Characterization of gypsum, barite and their synthetic analogues by FTIR and RAMAN spectroscopy. Geologica Macedonica, 14, pp.61-66.

402. Stewart, A.J., 1979. A barred-basin marine evaporite in the Upper Proterozoic of the Amadeus Basin, central Australia. Sedimentology, 26(1), pp.33-62.

403. Stoffregen, R.E., 1993. Stability relations of jarosite and natrojarosite at 150-250 C. Geochimica et Cosmochimica Acta, 57(11), pp.2417-2429.

404. Stoffregen, R.E., Alpers, C.N., Jambor, J.L., 2000. Alunite-jarosite crystallography, thermodynamics, and geochronology. Reviews in Mineralogy and Geochemistry, 40(1), pp.453-479.

405. Strother, P.K., Tobin, K., 1987. Observations on the genus Huroniospora Barghoorn: Implications for paleoecology of the Gunflint microbiota. Precambrian Research, 36(3), pp.323-333.

406. Sullivan, W., 1969. Two gases associated with life found on Mars near polar cap. New York Times August 8, 1.

407. Sundaram, R., Rao, P.S., 1986. Lithostratigraphy of Cretaceous and Palaeocene rocks of Tiruchirapalli District, Tamil Nadu, South India. Records of the Geological Survey of India, 115(5), pp.9-23.

408. Sundaram, R., Henderson, R.A., Ayyasami, K., Stilwell, J.D., 2001. A lithostratigraphic revision and palaeoenvironmental assessment of the Cretaceous System exposed in the onshore Cauvery Basin, southern India. Cretaceous Research, 22(6), pp.743-762.

409. Swayze, G.A., Smith, K.S., Clark, R.N., Sutley, S.J., Pearson, R.M., Vance, J.S., Hageman, P.L., Briggs, P.H., Meier, A.L., Singleton, M.J., Roth, S., 2000. Using imaging spectroscopy to map acidic mine waste. Environmental Science & Technology, 34(1), pp.47-54.

410. Taber, S., 1916. The growth of crystals under external pressure. American Journal of Science, (246), pp.532-556.

411. Taber, S., 1918. The origin of veinlets in the Silurian and Devonian strata of central New York. The Journal of Geology, 26(1), pp.56-73.

412. Tassel R.V., 1965. Natrojarosite from the Warkalli Beds, Varkala, Kerala, India. Bulletin- Geological Society of India 2(3), pp.53-56.

413. Tazaki, K., Ferris, F.G., Wiese, R.G., Fyfe, W.S., 1992. Iron and graphite associated with fossil bacteria in chert. Chemical geology, 95(3), pp.313-325.

414. Tewari, A., Hart, M.B., Watkinson, M.P., 1996. A revised lithostratigraphic classification of the Cretaceous rocks of the Trichinopoly district, Cauvery basin, Southeast India. In Contributions to the XV Indian Colloquium on Micropalaeontology and Stratigraphy, 789-800. Dehra Dun: Palaeontological Society of India.

415. Thangavelu, M., Shanmugam, S., Bhattacharya, A.K., 2011. Hyperspectral radiometry to quantify the grades of iron ores of Noamundi and Joda mines, Eastern India. Journal of the Indian Society of Remote Sensing, 39(4), pp.473-483.

416. Tice, M.M., Lowe, D.R., 2004. Photosynthetic microbial mats in the 3,416-Myr-old ocean. Nature, 431(7008), pp.549-552.

417. Tice, M.M., 2009. Environmental controls on photosynthetic microbial mat distribution and morphogenesis on a 3.42 Ga clastic-starved platform. Astrobiology, 9(10), pp.989-1000.

418. Tivey, M.K., Mills, R.A., Teagle, D.A., Herzig, P.M., 1998. Temperature and salinity of fluid inclusions in anhydrite as indicators of seawater entrainment and heating in the TAG active mound. In Proceedings-ocean drilling program scientific results (pp. 179-192). National science foundation.

419. Tosca, N.J., McLennan, S.M., Lindsley, D.H., Schoonen, M.A., 2004. Acid-sulphate weathering of synthetic Martian basalt: The acid fog model revisited. Journal of Geophysical Research: Planets, 109(E5).

420. Tosca, N.J., McLennan, S.M., Clark, B.C., Grotzinger, J.P., Hurowitz, J.A., Knoll, A.H., Schroder, C., Squyres, S.W., 2005. Geochemical modeling of evaporation processes on Mars: Insight from the sedimentary record at Meridiani Planum. Earth and Planetary Science Letters, 240(1), pp.122-148.

421. Tosca, N.J., McLennan, S.M., 2006. Chemical divides and evaporite assemblages on Mars. Earth and Planetary Science Letters, 241(1), pp.21-31.

422. Tosca, N.J., Knoll, A.H., McLennan, S.M., 2008. Water activity and the challenge for life on early Mars. Science, 320(5880), pp.1204-1207.

423. Trendall, A.F., Blockley, J.G., 2004. Precambrian iron-formation. The Precambrian earth: tempos and events. Elsevier, Amsterdam, pp. 403-421.

424. Vail, P.R., Mitchum Jr, R.M., Thompson III, S., 1977. Seismic Stratigraphy and Global Changes of Sea Level: Part 4. Global Cycles of Relative Changes of Sea Level.: Section 2. Application of Seismic Reflection Configuration to Stratigraphic Interpretation.

425. Van Geen, A., Adkins, J.F., Boyle, E.A., Nelson, C.H., Palanques, A., 1997. A 120-yr record of widespread contamination from mining of the Iberian pyrite belt. Geology, 25(4), pp.291-294.

426. Van Kranendonk, M.J., 2006. Volcanic degassing, hydrothermal circulation and the flourishing of early life on Earth: A review of the evidence from c. 3490-3240 Ma rocks of the Pilbara Supergroup, Pilbara Craton, Western Australia. Earth-Science Reviews, 74(3), pp.197-240.

427. Vaniman, D.T., Bish, D.L., Chipera, S.J., Fialips, C.I., Carey, J.W., Feldman, W.C., 2004. Magnesium sulphate salts and the history of water on Mars. Nature, 431(7009), pp.663-665.

428. Vanko, D.A., Bach, W., 2005. Heating and freezing experiments on aqueous fluid inclusions in anhydrite: Recognition and effects of stretching and the low-temperature formation of gypsum. Chemical geology, 223(1), pp.35-45.

429. Varekamp, J.C., Pasternack, G.B., Rowe, G.L., 2000. Volcanic lake systematics II. Chemical constraints. Journal of Volcanology and Geothermal Research, 97(1), pp.161-179.

430. Varnali, T., Edwards, H.G., 2013. A potential new biosignature of life in iron-rich extreme environments: an iron (III) complex of scytonemin and proposal for its identification using Raman spectroscopy. Planetary and Space Science, 82, pp.128-133.

431. Vysotskiy, E.A., Makhnach, A.A., Peryt, T.M., Kruchek, S.A., 2004. Marine and continental lower permian evaporites of the Prypiac'Trough (Belarus). Sedimentary Geology, 172(1), pp.211-222.

432. Wald, G., 1974. Fitness in the universe: Choices and necessities. Origin of life, 5(1-2), pp.7-27.

433. Wang, A., Jolliff, B.L., Haskin, L.A., 1995. Raman spectroscopy as a method for mineral identification on lunar robotic exploration missions.

434. Watkinson, M.P., Hart, M.B., Joshi, A., 2007. Cretaceous tectonostratigraphy and the development of the Cauvery Basin, southeast India. Petroleum Geoscience, 13(2), pp.181-191.

435. Weed, R., Ackert, R.P., 1986. Chemical-weathering of beacon supergroup sandstones and implications for antarctic glacial chronology. South African Journal of Science, 82(9), pp.513-516.

436. Welch, S.A., Christy, A.G., Kirste, D., Beavis, S.G. and Beavis, F., 2007. Jarosite dissolution I–Trace cation flux in acid sulphate soils. Chemical Geology, 245(3), pp.183-197.

437. Wentworth, S.J., Thomas-Keprta, K.L., McKay, D.S., 2002, March. Water on Mars: petrographic evidence. In Lunar and Planetary Science Conference (Vol. 33, p. 1932).

438. Westall, F., 1999. The nature of fossil bacteria: a guide to the search for extraterrestrial life. Journal of Geophysical Research: Planets, 104(E7), pp.16437-16451.

439. Westall, F., Steele, A., Toporski, J., Walsh, M., Allen, C., Guidry, S., McKay, D., Gibson, E., Chafetz, H., 2000. Polymeric substances and biofilms as biomarkers in terrestrial materials: implications for extraterrestrial samples. Journal of Geophysical Research: Planets, 105(E10), pp.24511-24527.

440. Westall, F., Loizeau, D., Foucher, F., Bost, N., Betrand, M., Vago, J., Kminek, G., 2013. Habitability on Mars from a microbial point of view. Astrobiology, 13(9), pp.887-897.

441. White, S.N., 2009. Laser Raman spectroscopy as a technique for identification of seafloor hydrothermal and cold seep minerals. Chemical Geology, 259(3), pp.240-252.

442. Wiltschko D.V., Morse, J.W. 2001. Crystallization pressure versus "crack seal" as the mechanism for banded veins. Geology 29, pp.79-82.

443. Wong, A.S., Atreya, S.K., Encrenaz, T., 2003. Chemical markers of possible hot spots on Mars. Journal of Geophysical Research: Planets, 108(E4).

444. Wray, J.J., Murchie, S.L., Squyres, S.W., Seelos, F.P., Tornabene, L.L., 2009. Diverse aqueous environments on ancient Mars revealed in the southern highlands. Geology, 37(11), pp.1043-1046.

445. Wynn-Williams, D.D. & Edwards, H.G.M., 2000. Proximal analysis of regolith habitats and protective biomolecules in situ by laser Raman spectroscopy: overview of terrestrial Antarctic habitats and Mars analogs. Icarus 144, pp.486-503.

446. Wynn-Williams, D.D., Cabrol, N.A., Grin, E.A., Haberle, R.M., Stoker, C.R., 2001. Brines in seepage channels as eluants for subsurface relict biomolecules on Mars?. Astrobiology, 1(2), pp.165-184.

447. Yung, Y.L., Chen, P., 2015. Methane on Mars. Astrobiol Outreach, 3(125), pp.2332-2519.

448. Zahnle, K., Freedman, R.S., Catling, D.C., 2011. Is there methane on Mars?. Icarus, 212(2), pp.493-503.

449. Zambito IV, J.J., Brett, C.E., Baird, G.C., 2012. The late Middle Devonian (Givetian) Global Taghanic Biocrisis in its type area (northern Appalachian Basin): geologically rapid faunal transitions driven by global and local environmental changes. In Earth and Life (pp. 677-703). Springer Netherlands.

450. Zambito, J.J., Benison, K.C., 2013. Extremely high temperatures and paleoclimate trends recorded in Permian ephemeral lake halite. Geology, 41(5), pp.587-590.

451. Ziegler, A.M., 1990. Phytogeographic patterns and continental configurations during the Permian Period. Geological Society, London, Memoirs, 12(1), pp.363-379.

452. Zolotov, M.Y., Shock, E.L., 2005. Formation of jarosite bearing deposits through aqueous oxidation of pyrite at Meridiani Planum, Mars. Geophys Res Lett 32, doi:10.1029/ 2005GL024253.

453. Zurek, R.W., Chicarro, A., Allen, M.A., Bertaux, J.-L., Clancy, R.T., Daerden, F., Formisano, V., Garvin, J.B., Neukum, G., Smith, M.D., 2010. Assessment of a 2016 mission concept: The search for trace gases in the atmosphere of Mars. Planet. Space Sci. doi:10.1016/j.pss.2010.07.007.

APPENDIX A

Analytical techniques

Preparation of thin sections and wafers

Thin sections of standard thickness i.e. 30 μm of all used samples in the study were prepared using facilities in Centre for Earth Sciences (CEaS), Indian Institute of Sciences, Bangalore, Karnataka for petrographic and electron microprobe analyses. Additionally, doubly-polished wafers were made for fluid inclusion studies of gypsum using the same facilities.

Reflectance spectroscopy

Reflectance spectroscopy makes use of photons of light as a function of wavelength that has been scattered/reflected from the surface. The main principle behind reflectance spectroscopy is that once photons enter into the mineral, some gets reflected from the surface, some gets transmitted through the grain and some gets absorbed. Absorption of photons takes place through several processes: mainly electronic and vibrational processes. The absorption of the photons in the absorbing medium is according to Beers Law and it is expressed as follows:

$$I = I_o \cdot e^{-kx} \tag{A.1}$$

where I is the observed intensity, Io is the original light intensity, k is an absorption coefficient and x is the distance travelled through the medium. The absorption coefficient is traditionally expressed in units of 1/cm (inverse cm) and x in cm.

The most common electronic process responsible for the absorption is unfilled electron shells. Transition elements are the one have unfilled electron shells like iron (Fe), which is most common transition element in minerals. For all transition elements, unfilled d orbitals have identical energies in an isolated ion, but the energy levels split when the atom is located in a crystal field. This splitting of the orbital energy states permits an electron to be moved from a lower level into a higher one by absorption of a photon, having an energy matching the energy difference between the states. Rare earth ions also have unfilled d orbitals, but the deep-lying electrons are well shielded from crystal fields, so the energy levels remain generally unchanged. Vibrational absorption will be seen in the infra-red region of electromagnetic spectrum only if the molecule responsible shows a dipole moment. Water and OH^- (hydroxyl ion) bearing minerals produce diagnostic absorption bands due to vibrational processes. In addition, sulphates, carbonates and phosphates also produce diagnostic vibrational spectra.

The light source used in reflectance spectroscopy can be the Sun or an artificial light source (quartz-tungsten-halogen) emitting wavelengths over a desired range. Orbital spectroscopy is mainly done using light from the Sun. Here, in this study artificial light source i.e. quartz-tungsten-halogen has been used in the dark room environment by focusing on the wavelengths emitted by the Sun. A spectrometer collects the reflected light from the target by breaking or dispersing it into constituent wavelengths, and measuring the intensity as a function of wavelength. The spectra of concerned mineral/material will have diagnostic absorption bands in accordance with the chemical composition and bonding among the atoms/molecules. Mostly the absorption bands can be seen due to vibrations and recognized easily for a mineral. Vibrations mainly occur in the form of translation (smallest amount of energy is required as in longest wavelengths), rotation (moderate amount of energy is required), bending and stretching (large amount of energy is required as in shortest wavelengths). Sometimes the absorption bands are too weak, broad or even similar for the minerals making it difficult to detect and distinguish among them. One of

the most common difficulties faced while identifying the mineral mixtures is overlapping of the absorption bands. The quality of the spectra also depends on grain size. Larger the grains, weaker the absorption bands.

Reflectance spectra of hand-specimens and powdered samples were collected using a FieldSpec Pro HR spectrometer for this study. FieldSpec Pro HR spectrometer was calibrated using the standard Spectralon®. The instrument was operated to collect spectra using a quartz-tungsten-halogen light source in the wavelength range of 0.3-2.5 μm with a viewing angle of i = 10^o. Later, the raw spectra were processed with splice and parabolic corrections.

X-ray diffraction

XRD is common technique used for phase identification of a crystalline material and can provide information on unit cell dimensions. It is based on constructive interference of monochromatic X-rays and crystalline sample. Mostly, X-rays will be generated by a cathode ray tube and filtered to produce monochromatic radiation. After collimation of the X-rays, they will be directed towards the sample. These radiations will interact with the sample and generate a constructive interference when conditions satisfy Bragg's Law. Bragg's Law defines the angles for coherent and incoherent scattering from a crystal lattice and it could be expressed as follow:

$$2dsin(\theta) = n\lambda \tag{A.2}$$

where n is a positive integer, λ is the wavelength of incident wave, θ is the scattering angle (diffraction angle) and d is the lattice spacing.

The diffracted X-rays from the samples will be detected, processed and counted. If the material is well crystallized, there will be well defined X-ray beams leaving the sample in different directions. Mineral identification is usually done by conversion of the diffraction peaks to d-spacings, because each mineral has

a set of unique d-spacings. These d-spacings are compared with the standard reference patterns of the minerals to detect them.

Here, in this study PANalytical X-ray diffractometer is used to obtain the diffractograms of gypsum and clay samples, and the instrument was operated in the conditions: 5-70^o 2θ, step size 0.0840, Cu Kα radiation with the fine powders at National Centre for Earth Science Studies, Thiruvananthapuram, Kerala. Obtained diffractograms were matched with the standards using ICSD/JCPDS software to identify the minerals. For jarosite samples, Bruker D8 ADVANCE X-ray diffractometer was used in the operating conditions of: Copper-alpha radiation, 10^o-80^o 2θ, and step size 0.020305 at a scan step time of 96 sec at University of Kerala, Thiruvananthapuram, Kerala.

Laser Raman Spectroscopy

Raman spectroscopy is one of the most precise, non-destructive and commonly used techniques with minimum sample preparation, to define the molecular composition of the samples. It works on the phenomenon of Raman scattering of monochromatic light from laser in the visible to near infrared range. The laser light interacts with the sample and the energy of laser photons shifts up or down due to molecular vibration or other excitations in the system. In present study, for gypsum and jarosite samples, we have used WiTech alpha 300 Raman system excited with 532 nm (fixed wavelength) laser with 300 mW output in Vikram Sarabhai Space Centre, Kerala. The spectral range of the equipment is 100 to 3600 cm^{-1} shift from the laser line, accomplished with an edge filter. Additionally, Raman studies of fluid inclusions in gypsum were carried out at the National Facility for Geofluids Research and Raman Analysis of NCESS using inVia Raman Microscope (Renishaw, UK, Model No. M-9836-3991-01-A) attached to an inVia Reflex Raman Spectrometer offering automated alignment via the Renishaw WiRE 3.4 software (Fig. A.1). Raman studies are performed using a diode laser exciting at a wavelength of 785 nm (300mW, CW, Model. No. HPNIR 92E371, Class 3B laser product, Renishaw

plc, UK). Instrument calibration performed by measuring Raman spectra of the internal and external silicon sample shows a sharp peak at a full width half maximum (FWHM) of 520±0.5 cm^{-1}. Motorized neutral density filters within the system helps to select desired power levels of 0.05% of the actual laser power. The spectral range of the equipment is from 50 to 4000 cm^{-1} shift from the laser line accomplished with an edge filter. The Raman scattered light is dispersed with a grating having 1200 l/mm. The detection is done by a Peltier cooled CCD detector with 576 × 384 pixels, with spectral resolution of 1 cm^{-1}. The Renishaw inVia Raman system used for this study is fully automated and self-validating with auto aligning and optimization of input laser power. The operation of the equipment is fully software controlled using WiRE 3.4 software. Laser exposure time; 30S, laser power: 15mW, spectrum range: 100-3600 nm.

Figure A.1: InVia Raman Microscope (Renishaw, UK, Model No. M-9836-3991-01-A) attached to an inVia Reflex Raman Spectrometer at the National Facility for Geofluids Research and Raman Analysis of NCESS.

Fourier transform infrared spectroscopy

Fourier transform infrared spectroscopy (FTIR) is used as a modern technique to obtain the absorption, transmission and emission spectrum of any sample. The advantage of using FTIR in mineral identification is that it collects high resolution data over a wide spectral range, enabling us to better differentiate between the minerals. For the study, FTIR spectroscopy was carried out with a PerkinElmer's Infrared (FTIR) spectrometer in Department of Chemistry, Indian Institute of Space Science and Technology, Kerala, using the powder samples. The powders were pressed at 55 to 60 kb to obtain the transmittance spectra of the samples. The infrared (IR) spectra were recorded immediately after the separation of the powder sample from the bulk sample. Spectra were collected in 700-4000 cm^{-1} range with an optical resolution of 0.5 cm^{-1} and wavelength precision of 0.01 cm^{-1} at 220 V, 50 Hz power supply. A baseline correction was made before interpretation of the data.

Microthermometry

Microthermometric studies conducted using a Motorised temperature controlled geology stage (MDSG600) working with Linksys32temperature control and video capture software. The system consists of a MDSG600 stage, aT95-Linkpad system controller, LNP95 liquid nitrogen cooling pump system. The stage is mounted on to a Linkam Imaging station that has been designed to easy access the heating/cooling stage. The temperature of first melting (TFM), temperature of last melting (TLM) and the homogenization temperature (Th) of different inclusions are measured.

Compact Reconnaissance Imaging Spectrometer for Mars

The orbital spectroscopic instrument datasets used for the present study is from MRO-CRISM. Compact Reconnaissance Imaging Spectrometer for Mars

(CRISM) is a hyperspectral imaging spectrometer on-board Mars Reconnaissance Orbiter (MRO), which operates in two modes: (i) 72 channel mapping mode that provide global coverage at 200m/pixel and (ii) full 544 channel targeted mode that provides $10 \times 10 - 20$ km images at resolution of 15-38m/pixel (Murchie, et al., 2007a). It samples the visible to near infrared region of electromagnetic spectrum from 0.36-3.9 μm using two detectors: S detector samples from 0.36 to 1.05 μm and L detector samples from 1.05-3.9 μm. In the present study we have provided the results from the L detector datasets with high resolution target images, which allowed the detection of hydrous and mafic minerals. Datasets were processed by atmospheric and photometric corrections to remove the atmosphere and correct the viewing geometry of CRISM scene. Photometric and atmospheric corrections were applied as defined in Ehlmann et al. (2009); Murchie et al. (2007a, 2009); Arvidson et al. (2006); Mustard et al. (2005). Additionally, in atmospheric correction, a noise removal algorithm was performed that removes the spikes in the spectral and spatial domains without affecting the broader absorptions of mineralogic interest (Parente, 2008). Mostly the spectra were derived through pixel by pixel analysis in the study. For spectral ratioing, pixel spectrum of interest was divided by the flat pixel from the same column of the unprojected image (because denominator taken in the same column reduces detector dependent noise). In this work, CRISM data was downloaded from http://pds-geosciences.wustl.edu/missions/mro/crism.htm and processed using ENVI+IDL 4.7 with CRISM analysis tool (CAT). Spectra derived from different regions of Mars are useful in the identification of the dominant minerals and extracting the broader conclusions. The coarseness of the data results into overshadowing of the absorption bands of the minerals, such as the area with the associated hydrous sulphates and phyllosilicate minerals. Provided with the spatial resolution, minor mineral deposits may go undetected during the analysis. The spectra were compared and matched with the standard inbuilt CRISM spectral library in CAT for ground-truthing, which is a necessary step to be accounted for any results in remote sensing.

APPENDIX B

Additional data

Electron microprobe analysis

Table B.1: Major oxides composition for various samples of clay using EPMA

Point	Na2O	SiO2	MgO	Al2O3	CaO	TiO2	FeO	P2O5	K2O	SO2	Total
1 / 1 .	0.085	34.855	1.743	16.924	1.499	0.277	21.157	0	0.293	0.27	77.103
2 / 1 .	0.103	36.288	1.755	17.546	1.466	0.265	21.058	0	0.231	0.382	79.095
3 / 1 .	0.117	40.711	1.649	19.947	1.526	1.427	15.23	0	0.198	0.353	81.159
4 / 1 .	0.097	46.649	1.568	21.306	1.608	0.03	5.734	0	0.356	0.198	77.546
5 / 1 .	0.124	29.136	1.236	13.752	10.886	0.11	10.928	0.026	0.174	8.78	75.151
6 / 1 .	0.119	49.166	1.829	21.246	1.827	0.068	3.47	0	0.357	0.266	78.347
7 / 1 .	0.435	47.631	0.031	16.281	0.613	0.007	0.539	0	12.887	0.064	78.489
8 / 1 .	0.87	59.804	0.012	13.816	0.145	0.017	0.186	0	14.475	0.25	89.574
9 / 1 .	1.152	60.846	0.01	16.397	0.216	0.059	0.282	0	14.544	0.037	93.544
10 / 1 .	0.853	58.036	0	15.449	0.145	0.014	0.116	0	14.673	0.12	89.407
11 / 1 .	0.085	34.855	1.743	16.924	1.499	0.277	21.157	0	0.293	0.27	77.103
12 / 1 .	0.103	36.288	1.755	17.546	1.466	0.265	21.058	0	0.231	0.382	79.095
13 / 1 .	0.117	40.711	1.649	19.947	1.526	1.427	15.23	0	0.198	0.353	81.159
14 / 1 .	0.097	46.649	1.568	21.306	1.608	0.03	5.734	0	0.356	0.198	77.546
15 / 1 .	0.124	29.136	1.236	13.752	10.886	0.11	10.928	0.026	0.174	8.78	75.151
16 / 1 .	0.119	49.166	1.829	21.246	1.827	0.068	3.47	0	0.357	0.266	78.347
17 / 1 .	0.435	47.631	0.031	16.281	0.613	0.007	0.539	0	12.887	0.064	78.489
18 / 1 .	0.87	59.804	0.012	13.816	0.145	0.017	0.186	0	14.475	0.25	89.574
19 / 1 .	1.152	60.846	0.01	16.397	0.216	0.059	0.282	0	14.544	0.037	93.544
20 / 1 .	0.853	58.036	0	15.449	0.145	0.014	0.116	0	14.673	0.12	89.407

Table B.2: Major oxides composition for various samples of gypsum using EPMA

Point	Na2O	SiO2	MgO	Al2O3	CaO	TiO2	FeO	P2O5	K2O	SO2	Total
1 / 1 .	0	0.048	0.014	0	41	0	0.007	0.492	0.005	35.154	76.72
2 / 1 .	0	0.024	0.012	0	41.403	0	0	0.435	0.006	36.008	77.889
3 / 1 .	0.061	0.044	0	0	40.918	0.025	0.097	0.456	0	35.331	76.932
4 / 1 .	0.037	0.166	0.052	0	41.348	0	0.055	0.43	0	34.669	76.756
5 / 1 .	0	0.184	0.059	0.021	40.881	0.006	0.065	0.423	0.031	34.994	76.664
6 / 1 .	0.035	0.276	0.003	0.018	34.906	0.021	0.012	0.39	0	27.831	63.491
7 / 1 .	0.043	0.291	0.049	0	37.641	0.006	0.153	0.392	0.031	32.536	71.142
11 / 1 .	0	0.059	0	0	40.694	0.041	0.122	0.397	0.003	35.191	76.507
12 / 1 .	0.058	0.186	0.014	0.041	37.581	0.007	0.078	0.388	0.016	31.774	70.142
13 / 1 .	0.026	0.387	0.019	0.148	34.126	0.018	0.039	0.461	0	30.33	65.553
14 / 1 .	0.022	0.904	0.014	0.085	37.181	0.046	0	0.424	0.008	31.426	70.109
15 / 1 .	0.037	0.94	0.025	0.122	39.123	0	0.075	0.418	0.015	29.451	70.205
16 / 1 .	0.028	0.798	0.024	0.055	33.822	0.025	0.167	0.406	0	25.884	61.209
17 / 1 .	0.004	0.263	0.01	0.006	36.376	0.039	0.034	0.406	0.002	28.143	65.285
18 / 1 .	0.062	0.201	0.019	0.01	34.147	0	0.066	0.369	0.02	28.792	63.689
19 / 1 .	0.022	0.666	0.007	0.136	34.046	0.033	0	0.43	0	29.79	65.13
20 / 1 .	0.028	0.21	0.002	0.023	36.842	0.012	0	0.388	0.02	30.896	68.421
21 / 1 .	0.028	0.606	0.031	0	38.02	0.022	0.078	0.48	0.012	32.314	71.59
22 / 1 .	0.05	0.243	0.018	0	36.303	0.01	0.02	0.394	0.024	31.171	68.234
23 / 1 .	0.045	0.174	0	0.032	38.301	0.012	0	0.455	0.015	33.201	72.235
24 / 1 .	0.071	0.284	0.024	0.031	35.964	0	0.067	0.424	0.029	30.967	67.86
25 / 1 .	0.082	0.129	0.027	0.014	38.301	0.011	0	0.404	0.008	33.622	72.597
26 / 1 .	0.063	0.124	0.003	0	41.051	0.032	0.083	0.423	0.019	34.443	76.241
27 / 1 .	0.006	0.184	0.001	0	36.834	0.032	0	0.413	0.017	31.553	69.041
28 / 1 .	0.099	0.469	0.108	0.021	36.593	0.004	0	0.418	0.054	31.86	69.626
29 / 1 .	0.067	0.66	0.055	0.014	33.747	0.037	0	0.409	0.019	28.838	63.847
30 / 1 .	0.052	0.181	0.014	0.18	37.874	0.012	0.442	0.384	0.02	29.278	68.438
31 / 1 .	0.05	0.109	0.032	0.012	28.448	0.008	0	0.379	0.009	26.05	55.097
32 / 1 .	0.06	0.277	0	0.081	30.583	0	0	0.348	0.033	27.867	59.248
33 / 1 .	0.131	0.24	0.008	0.002	37.226	0	0	0.421	0.024	32.404	70.456
34 / 1 .	0.1	0.191	0.008	0	39.805	0.012	0.019	0.456	0.04	31.028	71.658
35 / 1 .	0.054	0.065	0.02	0.009	39.61	0	0.008	0.48	0.005	32.116	72.368
36 / 1 .	0.06	0.265	0.022	0.034	38.895	0	0	0.407	0.031	33.209	72.924
37 / 1 .	0.024	0.384	0.005	0.04	39.428	0.024	0	0.471	0.016	32.75	73.141
38 / 1 .	0.077	0.386	0.028	0.058	34.56	0.019	0.007	0.36	0.029	28.551	64.075
39 / 1 .	0.011	0.039	0.028	0	41.637	0.057	0	0.412	0.017	34.806	77.006
40 / 1 .	0.028	0.069	0	0	41.474	0	0.02	0.431	0	35.424	77.445

Table B.3: Major oxides composition for various samples of gypsum and clay using XRF

	Gypsum					Clay			
Sample	O1*	O2*	ODO8*	KR03*	OD1*	ODO4(1)*	ODO4(2)*	ODO7*	S3*
SiO2	0.51	0.29	1.4	3.3	0.762	31.52	29.42	29.87	38.06
TiO2	ND	ND	ND	0.053	ND	0.499	0.451	0.575	0.746
Al2O3	0.22	0.14	0.676	1.526	0.3	13.22	14.93	15.75	18.63
MnO	ND	ND	0.0309	ND	ND	0.421	0.325	ND	ND
Fe2O3	0.08	0.05	0.547	1.38	0.109	24.21	36.47	1.545	4.807
CaO	34.58	36.96	36.58	41.34	36.96	7.424	3.633	13.76	10.01
MgO	ND	ND	0.059	0.168	0.042	0.746	0.786	0.325	0.683
Na2O	ND	ND	ND	ND	ND	0.598	0.304	0.689	0.585
K2O	ND	ND	0.027	0.0591	0.013	0.511	0.445	0.539	0.525
P2O5	ND	ND	ND	ND	ND	ND	ND	0.068	ND
SO3	51.03	53.77	53.34	49.19	54.14	10.3	5.6	23.35	17.96
SrO	0.03	0.03	0.0289	0.029	0.0423	0.0248	0.0253	0.0636	0.0285
LOI	13.6	8.76	7.31	2.95	7.63	10.3	7.32	13.2	7.84
Total	100.04	100	100	100	100	99.77	99.71	99.73	99.87

Table B.4: Major oxides composition for hematite and silica components of banded iron formations using EPMA

Point	SiO2	MgO	Al2O3	CaO	TiO2	FeO	Total
1 / 1 .	0.786	0.072	0	0.021	0	90.853	91.732
2 / 1 .	1.034	0.067	0	0.018	0.012	90.149	91.28
3 / 1 .	1.12	0.038	0	0.007	0	90.816	91.981
4 / 1 .	1.156	0.057	0.005	0.036	0	90.521	91.776
5 / 1 .	1.003	0.014	0	0	0.015	89.934	90.965
6 / 1 .	1.138	0.011	0	0.011	0	90.314	91.473
7 / 1 .	0.668	0.025	0.052	0.009	0	92.505	93.26
8 / 1 .	0.975	0	0	0	0	89.31	90.284
9 / 1 .	0.956	0.028	0	0	0.029	91.803	92.816
10 / 1 .	0.777	0.005	0	10.777	0.023	70.517	82.099
11 / 1 .	95.176	0.208	0.062	0.054	0	2.987	98.488
12 / 1 .	94.835	0.221	0.096	0.026	0.018	2.719	97.915
13 / 1 .	94.581	0.054	0.04	0.026	0.025	0.622	95.348
14 / 1 .	90.721	0.02	0.091	0.064	0	0.4	91.296
15 / 1 .	95.898	0.001	0.003	0.014	0	0.361	96.277
16 / 1 .	97	0.007	0	0.035	0	0.233	97.276
17 / 1 .	98.066	0.08	0.035	0.039	0	1.229	99.449
18 / 1 .	95.489	0.081	0.059	0.019	0	2.397	98.045
19 / 1 .	96.842	0.08	0.088	0.02	0	2.081	99.111
20 / 1 .	96.586	0.072	0.021	0.026	0.028	1.513	98.246
21 / 1 .	97.344	0.019	0.007	0.033	0	0.285	97.688
22 / 1 .	98.177	0.036	0.049	0.018	0.005	0.321	98.604
23 / 1 .	99.372	0.024	0.025	0.016	0.011	0.777	100.224
24 / 1 .	98.741	0.008	0	0.011	0	0.19	98.949
25 / 1 .	97.542	0	0	0	0.028	0.275	97.844
26 / 1 .	98.307	0.014	0.018	0.008	0	0.312	98.658
27 / 1 .	97.172	0.111	0.031	0.05	0.037	1.335	98.735
28 / 1 .	98.04	0.06	0.004	0	0.006	0.453	98.563
29 / 1 .	96.256	0.156	0.035	0.018	0	2.374	98.84
30 / 1 .	98.539	0.019	0	0.038	0	0.273	98.869

Table B.5: Major oxides composition for hematite and silica components of banded iron formations using EPMA

Point	Na2O	SiO2	MgO	Al2O3	CaO	TiO2	FeO	K2O	Total
1 / 1 .	0.554	21.92	4.081	19.084	0.054	0	42.189	0.272	88.154
2 / 1 .	0.383	22.207	4.183	18.954	0.072	0.008	41.869	0.267	87.943
3 / 1 .	0.392	21.944	4.345	18.829	0.065	0	41.834	0.229	87.639
4 / 1 .	0.544	24.148	4.466	20.32	0.124	0	38.873	0.34	88.814
5 / 1 .	0.696	23.756	4.749	20.17	0.121	0	39.228	0.318	89.038
6 / 1 .	0.879	23.693	4.557	19.831	0.117	0.004	40.603	0.403	90.087
7 / 1 .	0.104	100.318	0.01	0.049	0.013	0	0.758	0.025	101.277
8 / 1 .	0.134	97.303	0.019	0.137	0.045	0.002	0.896	0.047	98.582
9 / 1 .	1.117	96.174	0.055	0.109	0.051	0	1.803	0.112	99.42
10 / 1 .	0.072	97.967	0.088	0.365	0.015	0.017	1.565	0.031	100.119
11 / 1 .	0.098	96.722	0	0.035	0.029	0	0.406	0.041	97.331
12 / 1 .	0.047	97.852	0.048	0.12	0.011	0.004	1.593	0.019	99.694
13 / 1 .	0.095	96.206	0.18	0.806	0.02	0.009	4.231	0.057	101.605
14 / 1 .	0.887	21.477	4.154	17.927	0.166	0	39.97	0.387	84.968
15 / 1 .	0.755	22.08	4.007	18.335	0.179	0.001	40.989	0.504	86.851
16 / 1 .	1.054	18.527	2.317	16.806	0.193	0	40.861	0.868	80.626
17 / 1 .	0.92	14.184	1.545	12.966	0.184	0	47.497	0.655	77.951
18 / 1 .	0.64	21.937	4.233	18.23	0.126	0.031	41.079	0.178	86.454
19 / 1 .	0.162	98.928	0.005	0.021	0.016	0.005	0.407	0.044	99.589
20 / 1 .	0.063	99.14	0.018	0.031	0.008	0.026	0.264	0.002	99.551
21 / 1 .	0.07	92.36	0	0.193	0.017	0.016	7.894	0.027	100.577
22 / 1 .	0.081	97.909	0	0.073	0.024	0	0.546	0.049	98.682
23 / 1 .	0.014	0.377	0.013	0.174	0	0.014	89.637	0.001	90.23
24 / 1 .	0.031	0.426	0.008	0.251	0.013	0.039	90.668	0.002	91.438
25 / 1 .	0	0.413	0.009	0.362	0.023	0.008	90.244	0	91.059
26 / 1 .	0.038	0.495	0	0.32	0.013	0.04	89.548	0	90.455
27 / 1 .	0.073	0.298	0.01	0.1	0	0.047	90.511	0.013	91.051
28 / 1 .	0.038	0.372	0	0.17	0.002	0.028	92.154	0.025	92.79
29 / 1 .	0.021	0.602	0.001	0.39	0	0.012	90.53	0	91.555
30 / 1 .	0.038	0.596	0.027	0.211	0	0.005	90.496	0	91.373

Table B.6: Major oxides and elemental composition for jarosite using EPMA

Oxides	FeO	SiO2	K2O	SO3	Na2O	Total
JAR/Pos 1	32.012	2.879	0.138	29.426	1.623	66.078
JAR/Pos 2	32.859	4.324	0.13	30.11	2.68	70.103
JAR/Pos 3	36.1	6.889	0.144	30.286	2.643	76.062
JAR/Pos 6	32.641	6.421	0.341	29.791	2.578	71.772
JAR/Pos 7	26.805	6.367	0.395	24.146	1.884	59.597
JAR/Pos 13	29.981	6.116	0.168	28.858	2.069	67.192
JAR/Pos 14	30.438	6.401	0.173	27.719	2.806	67.537
JAR/Pos 24	14.484	6.391	0.075	13.994	1.273	36.217
JAR/Pos 25	5.323	4.832	0.055	6.834	0.414	17.458
JAR/Pos 26	6.938	6.186	0.044	6.719	0.823	20.71
JAR/Pos 37	10.512	2.1	0.073	9.097	0.925	22.707
JAR/Pos 41	0.728	3.277	0.015	1.139	0.108	5.267

Elements	Fe	Si	K	S	Na	Total
JAR/Pos 1	6.3966	0.6878	0.0421	5.2769	0.752	13.1554
JAR/Pos 2	6.1865	0.9735	0.0373	5.0876	1.1697	13.4547
JAR/Pos 3	6.3108	1.4401	0.0384	4.7514	1.0712	13.6119
JAR/Pos 6	5.9594	1.4018	0.0949	4.8813	1.0911	13.4285
JAR/Pos 7	5.8736	1.6683	0.1321	4.7484	0.957	13.3795
JAR/Pos 13	5.7643	1.406	0.0491	4.9793	0.9222	13.121
JAR/Pos 14	5.9027	1.4842	0.0511	4.8242	1.2616	13.5238
JAR/Pos 24	5.0396	2.6589	0.0399	4.3698	1.0269	13.135
JAR/Pos 25	3.5687	3.873	0.0567	4.1118	0.6431	12.2533
JAR/Pos 26	4.0801	4.3503	0.0396	3.5462	1.1217	13.138
JAR/Pos 37	6.1303	1.4641	0.0648	4.7612	1.2511	13.6715
JAR/Pos 41	1.4852	7.9921	0.0455	2.0843	0.51	12.1171

Table B.7: Major oxides and elemental composition for various samples of jarosite and mixed components using EPMA

	Oxides	FeO	SiO2	K2O	SO3	Na2O	Total
Grain 1	MC/Pos 1	30.937	9.266	0.342	27.869	3.239	71.653
Grain 2	MC/Pos 1	28.692	10.383	0.356	26.703	2.895	69.029
	MC/Pos 2	3.7	21.843	0.095	1.927	8.019	35.584
Grain 3	MC/Pos 3	28.713	10.37	0.356	27.733	2.888	70.06
	MC/Pos 4	13.464	24.195	0.176	14.37	1.737	53.942
	MC/Pos 5	29.178	7.211	0.4	26.082	2.293	65.164
	MC/Pos 8	26.169	15.864	0.19	23.918	2.791	68.932
	MC/Pos 9	25.453	10.887	0.283	22.518	2.785	61.926
	MC/Pos 10	17.041	18.564	0.171	15.321	2.052	53.149
	MC/Pos 11	15.044	20.144	0.174	14.381	1.774	51.517
	MC/Pos 12	11.626	22.664	0.154	10.749	1.367	46.56
	MC/Pos 15	28.105	10.489	0.171	25.804	2.79	67.359
	MC/Pos 16	28.135	10.52	0.185	25.482	2.484	66.806
	MC/Pos 17	29.193	7.983	0.182	26.963	2.329	66.65
	MC/Pos 18	27.342	11.444	0.153	25.191	2.544	66.674
	MC/Pos 19	21.953	21.401	0.479	18.541	2.551	64.925
	MC/Pos 20	23.428	23.304	0.454	19.5	1.705	68.391
	MC/Pos 21	22.611	22.112	0.412	19.474	2.084	66.693
Grain 4	MC/Pos 22	22.232	21.331	0.261	19.267	2.375	65.466
	MC/Pos 23	20.852	17.358	0.197	17.247	2.087	57.741
	MC/Pos 27	20.682	23.943	0.296	18.209	2.163	65.293
	MC/Pos 28	18.301	25.01	0.278	16.41	2.071	62.07
	MC/Pos 29	23.001	18.784	0.241	20.142	2.276	64.444
	MC/Pos 30	22.472	21.058	0.313	19.987	2.465	66.295
	MC/Pos 31	31.112	9.826	0.286	27.656	2.528	71.408
	MC/Pos 32	21.228	21.79	0.339	18.225	2.46	64.042
	MC/Pos 33	24.563	19.257	0.285	21.434	2.7	68.239
	MC/Pos 34	20.266	22.524	0.194	18.311	2.124	63.419
	MC/Pos 35	20.149	23.041	0.291	17.764	2.266	63.511
	MC/Pos 36	15.424	24.949	0.177	12.724	1.645	54.919
	MC/Pos 38	23.256	21.329	0.267	20.84	2.308	68
	MC/Pos 39	27.374	18.754	0.261	24.949	3.005	74.343
	MC/Pos 40	13.282	33.806	0.201	11.255	1.04	59.584

Continued...

	Elements	Fe	Si	K	S	Na	Total
Grain 1	MC/Pos 1	5.6187	2.0123	0.0946	4.5424	1.364	13.6321
Grain 2	MC/Pos 1	5.3362	2.309	0.1009	4.4571	1.2482	13.4514
	MC/Pos 2	1.2598	8.892	0.0493	0.5889	6.3299	17.1198
Grain 3	MC/Pos 3	5.2285	2.2579	0.0989	4.5322	1.2192	13.3368
	MC/Pos 4	2.881	6.1903	0.0575	2.7595	0.8619	12.7503
	MC/Pos 5	5.8546	1.7302	0.1226	4.6968	1.067	13.4711
	MC/Pos 8	4.7622	3.4519	0.0527	3.9063	1.1778	13.3508
	MC/Pos 9	5.2862	2.7036	0.0897	4.1971	1.3412	13.6177
	MC/Pos 10	3.8879	5.0642	0.0596	3.1371	1.0854	13.2342
	MC/Pos 11	3.4677	5.5518	0.0611	2.9747	0.9479	13.0032
	MC/Pos 12	2.8924	6.7421	0.0585	2.3999	0.7886	12.8815
	MC/Pos 15	5.3523	2.3884	0.0497	4.4101	1.2317	13.4322
	MC/Pos 16	5.4053	2.4167	0.0543	4.3936	1.1065	13.3765
	MC/Pos 17	5.6632	1.8517	0.054	4.6942	1.0477	13.3108
	MC/Pos 18	5.2246	2.6147	0.0447	4.32	1.1273	13.3312
	MC/Pos 19	4.1691	4.8598	0.1389	3.1601	1.1234	13.4512
	MC/Pos 20	4.1967	4.9914	0.124	3.1348	0.7083	13.1551
	MC/Pos 21	4.1535	4.8569	0.1156	3.2104	0.8874	13.2238
Grain 4	MC/Pos 22	4.1662	4.7798	0.0745	3.2403	1.0319	13.2927
	MC/Pos 23	4.4936	4.4728	0.0649	3.3356	1.043	13.4099
	MC/Pos 27	3.8271	5.2976	0.0835	3.024	0.9278	13.1601
	MC/Pos 28	3.5165	5.7461	0.0814	2.8298	0.9228	13.0965
	MC/Pos 29	4.417	4.3133	0.0706	3.4714	1.0135	13.2859
	MC/Pos 30	4.157	4.6579	0.0883	3.3182	1.0571	13.2784
	MC/Pos 31	5.6474	2.1326	0.0792	4.5053	1.0639	13.4284
	MC/Pos 32	4.059	4.982	0.0989	3.1274	1.0905	13.3579
	MC/Pos 33	4.4772	4.197	0.0793	3.5062	1.1412	13.4008
	MC/Pos 34	3.859	5.1283	0.0563	3.1291	0.9377	13.1104
	MC/Pos 35	3.8401	5.2508	0.0847	3.0384	1.0013	13.2153
	MC/Pos 36	3.3234	6.4275	0.0581	2.4605	0.8219	13.0915
	MC/Pos 38	4.1886	4.5934	0.0734	3.3687	0.9638	13.1878
	MC/Pos 39	4.5917	3.7615	0.0669	3.7558	1.1688	13.3447
	MC/Pos 40	2.5341	7.7124	0.0586	1.9273	0.4598	12.6923

LIST OF PAPERS BASED ON THESIS

Papers in Refereed Journals

1. **Singh, M.**, Singhal, J., Prasad, K.A., Rajesh, V.J., Ray, D., Sahoo, P., 2016. Spectral characteristics of banded iron formations in Singhbhum craton, eastern India: Implications for hematite deposits on Mars. Geoscience Frontiers, 7(6), pp.927-936.

2. **Singh, M.**, Rajesh, V.J., Sajinkumar, K.S., Sajeev, K., Kumar, S.N., 2016. Spectral and chemical characterization of jarosite in a palaeolacustrine depositional environment in Warkalli Formation in Kerala, South India and its implications. Spectrochimica Acta Part A: Molecular and Biomolecular Spectroscopy, 168, pp.86-97.

3. **Singh, M.**, Rajesh, V.J., Kannan, B., Bhattacharya, S., 2017. Chemical and spectral characterization of gypsum-phyllosilicate association in Tiruchirapalli, South India and its implications. Geological Journal (*Accepted*).

Presentations in International Conferences

1. **Mahima Singh**, V.J. Rajesh, 2014. Mineralogical characterization of Juventae Chasma, Mars: Evidences from MRO-CRISM. ISPRS-2014.

2. **Mahima Singh** et al., 2015. Hyperspectral characterization of jarosite of Warkalli Formation, Varakalai, Southern India: Implications to Mars. Lunar and Planetary Science Conference.

3. **Mahima Singh**, Bharathi Kannan, V.J. Rajesh, 2015. Field and spectral investigation of gypsum deposit, Tamil Nadu, India: A martian analogue site. European Planetary Science Congress 2015, 10 (EPSC 2015-45).

4. **Mahima Singh** et al., 2015. Field investigation and spectral characterization of Banded Iron Formation, Odisha, India: Implications to hydration processes on Mars. European Planetary Science Congress 2015, 10 (EPSC 2015-155).

5. **Mahima Singh**, V.J. Rajesh, 2016. Mineralogical investigations in East Candor Chasma, Valles Marineris, Mars and Implications. Lunar and Planetary Science Conference.

Presentations in National Conferences

1. **Mahima Singh** et al., 2013. Spectral and Chemical Characteristics of Gypsum from Peramballur, Tamil Nadu: Implications for Hydration Processes on Mars. Workshop on Mars Orbiter Mission, PRL, Ahmedabad, pp 13, (July 26-27, 2013).

2. V.J. Rajesh, **Mahima Singh**, Bharathi Kannan, Satadru Bhattacharya, Dwijesh Ray, Prakash Chauhan, L. Gnanappazham, 2013. Spectral and chemical characteristics of gypsum from Permballur, Tamil Nadu: Implications for hydrations processes on Mars. Paper presented at workshop on Mars Orbiter Mission, 26-27 July 2013, PRL, Ahmedabad.

3. **Mahima Singh** et al., 2013. Spectral characterization of hematite from banded iron formation, Singhbhum craton: Astrobiological Implications to Mars. Abstract submitted to National Symposium on Remote Sensing and GIS for environment, Andhra University, Visakhapatnam.

4. **Mahima Singh** et al., 2014. Hyperspectral and Geological characteristics of Jarosite in Warkalli Formation, Varkalai, South India: A Probable Terrestrial Analogue to Mars. Abstract submitted to "Workshop on Mars Orbiter Mission-Data Analysis and Science Plans" PRL, Ahmedabad.

5. **Mahima Singh** et al., 2014. Spectral Characteristics of Hydrous sulphate-Phyllosilicate association in Tiruchirapalli, India: Implications to Mars. 18th National Space Science Symposium (NSSS - 2014), Dibrugarh University, Dibrugarh, Assam (Jan 29-Feb 1, 2014).

6. **Mahima Singh**, Rajesh V.J., Prakash Chauhan, 2015. Mineralogy of East Candor Chasma, Valles Marineris, Mars: Evidences from MRO-CRISM Datasets. MOM Workshop, PRL, Ahmedabad.

7. **Mahima Singh**, Rajesh V.J., 2015. Mineral detection in banded iron formations of Singhbhum craton, eastern India using laser Raman and FTIR spectroscopic techniques: implications to Mars. NSSS-2016.

8. Thejashree G., **Mahima Singh**, Rajesh V.J., 2015. Mineralogical investigation in Melas Chasma, Valles Marineris, Mars. NSSS-2016.